

**Centre for Marine Science and Technology
School of Applied Physics
Department of Imaging and Applied Physics**

**Characterisation of long-range horizontal performance of
underwater acoustic communication**

Grant Mark Pusey

**This thesis is presented for the Degree of
Doctor of Philosophy
of
Curtin University of Technology**

May 2011

Declaration

To the best of my knowledge and belief this thesis contains no material previously published by another person except where due acknowledgement has been made.

This thesis contains no material which has been accepted for the award of any other degree or diploma in any university.

Signature: _____

Date: _____

Abstract

Underwater acoustic communication is a rapidly progressing field of technology, largely due to recent advances in low cost and power efficient digital signal processors. Unfortunately, the unpredictable and time varying physical properties of the underwater acoustic channel reduce communication reliability over long ranges. This study sought to characterise the performance of horizontal underwater acoustic data communication in various scenarios with particular application to subsea monitoring and control systems.

To fulfil the experimental needs, two custom-built high frequency ambient noise recorder and modem control units were developed to operate with commercial underwater acoustic modems. Additionally, an underwater acoustic communication simulator based on the Bellhop propagation model was developed for Matlab, capable of producing performance predictions in both spatial and temporal studies. A series of short-term trials were conducted to determine the limitations of modem performance over different ranges. These trials included shallow water studies off the coast of Perth, Western Australia ($D < 30$ m), and a French deep water trial ($D \leq 1000$ m) which used stand-alone modems. Experimental findings were compared to predictions obtained using two-dimensional range-depth performance simulations. Performance predictions for the second shallow water trial produced very similar statistics to those found during the experiment. Simulations of the French trial produced a similar overall trend but with a spatial discrepancy, possibly caused by inaccurate knowledge of the environment. From two-dimensional simulations, the optimum modem positioning in a deep underwater channel was found to be highly dependant on the sound speed profile, particularly the location of the sound speed minimum. In shallow water simulations and trials, communication reliability was found to increase when nodes were located at mid-depth.

A long-term investigation of the environmental influences on modem reliability was carried out off the coast of Perth in approximately 100 m of water. This involved simultaneously collecting environmental and modem performance data for over

16 days. The signal to noise ratio remained high for the duration of the trial so modem performance fluctuations could be attributed to changes in channel propagation. Using multiple linear regression, the measured environmental parameters were correlated with the observed modem performance and their contributions to an overall fitting curve were calculated. It was determined that the sound speed profile, in addition to the sea surface roughness, contributed strongly to the fitting curve, with a weaker contribution from the measured signal to noise ratio. This result was confirmed by performing temporal simulations which incorporated more detailed time-dependant environmental parameters. By progressively adding more parameters to the simulator including ambient noise, wave height and the sound speed profile, simulations provided more accurate predictions of the observed performance

Overall, the horizontal performance of underwater acoustic communication was characterised in several scenarios from a series of experimental and numerical investigations. Additionally, the developed simulator was shown to be an effective and flexible tool for predicting the performance of an underwater acoustic communication system. The results and tools discussed in this thesis provide an extensive investigation into the factors influencing horizontal underwater acoustic communication. The analysis demonstrates that whilst underwater acoustic communication can be effective, it is not yet a viable alternative to cabled telemetry for long-range subsea monitoring and control applications, where reliability is crucial. Underwater acoustic communication would best be suited as a non-critical or backup method for continuous monitoring systems until channel prediction and equalisation techniques are further refined.

Acknowledgements

The primary funding for this project has been through the CSIRO National Research Flagship Cluster on Pipelines and the Centre for Marine Science and Technology (CMST), Curtin University. Curtin University in conjunction with CMST also provided a scholarship stipend. The IEEE committee provided financial assistance to attend OCEANS '09 in Bremen. The research conducted internationally was part of the DAMOCLES (2005-2010) and ACOBAR (2008-2012) projects funded by EU.

The incomparable depth of knowledge and experience offered by my supervisor, Dr Alec Duncan, is surpassed only by his patience. Dr. Duncan's guidance and support in all areas of this program was crucial to its completion. This program was co-supervised by Dr Alexander Gavrilov who provided innovative ideas throughout the program and helped establish research contacts with other scientists and engineers in the field. My associate supervisor, Dr Matthew Dunbabin was crucial for commencing experimental work, providing the initial background knowledge and equipment, in addition to ongoing support and ideas throughout the program.

The staff at the Centre for Marine Science and Technology provided an abundance of assistance in the technical aspects of my program, as well as providing a friendly and engaging professional atmosphere to work in. Specifically, I acknowledge Frank Thomas and Mal Perry for their tremendous technical support in the development of the electronics, equipment and techniques used in the deployments. Dr Rob McCauley was also essential to the conduction of the experiments, sharing his wealth of on-deck experience in field trials to ensure success. Ann Smith is also acknowledged as the glue that holds CMST together with her hard work as office administrator.

Thanks are extended to Rod Marton from Anchor Boat Charters as well as Paul Pittorini and the crew aboard Reliance II for their professional assistance in the safe and comfortable execution of the Perth trials. Jason How and the Department of Fisheries are also acknowledged for facilitating the acoustic tag trials.

Aquatec Group Limited provided enormous amounts of technical assistance for this project, above and beyond what was expected. I'd like to acknowledge the director, Andy Smerdon for providing additional opportunities and industry experience including a rare chance to conduct field trials in the Arctic. Acknowledgement is extended for the assistance provided by the Observatoire Océanologique de Villefranche-sur-Mer, Université Pierre et Marie Curie in facilitating the French trials. Additionally, the professional and friendly Norwegian Coastguard crew aboard KV Svalbard made the Arctic cruise an unforgettable experience.

My fellow PhD students, past and present, have been of excellent support, collectively providing a fun and relaxed atmosphere to work in. Kevin Jarrett, Daniel Veen and recent graduates Dr Iain Parnum, Dr Miles Parsons and Dr Binghui Li each ensured that time spent not working was time well spent.

I especially acknowledge the support of my parents, Garry and Rona Pusey, whose hard work and dedication over the years has always inspired me to take the same positive attitude to all tasks. Finally, my sincere gratitude goes to my fiancée, Megan, for her unmatched patience, understanding, and encouragement throughout the program.

Table of Contents

List of Figures	xii
List of Tables	xxi
List of Abbreviations.....	xxiii
1 Introduction	1
1.1 Motivation.....	1
1.2 Thesis Aims	3
1.3 Thesis Outline	4
1.4 The Original Contributions of the Thesis	6
2 Review of Literature	8
2.1 Modulation Techniques	9
2.2 Equalisation and Beamforming Techniques	16
2.3 Simulation Methods and Analytical Performance	21
2.4 Networking and Protocol Standardisation	25
2.5 The Kauai Experiment.....	30
3 Methodology	34
3.1 Experimental Hardware	34
3.1.1 Ambient Noise Recorder.....	35
3.1.2 Modem Control Stack.....	38
3.2 Embedded Software Development.....	40
3.2.1 C8051F120: ModCon	40
3.2.2 SoMo650: PDALogger	42
3.2.3 SoMo650: PDALogger Skinny	44
3.3 Underwater Acoustic Communication Simulator	46
3.3.1 Data and Signal Generation	47
3.3.2 Received Signal Simulation	48
3.3.3 Noise Generation	50
3.3.4 Data Analysis and Verification	52
4 Spatial Investigation of Communication Performance in Short-term Trials	55

4.1	<i>Perth Initial Communication and Localisation Trial</i>	55
4.1.1	Experimental Setup.....	55
4.1.2	Preliminary Observations.....	59
4.1.3	Localisation of the Seabed Acoustic Package.....	60
4.1.4	Ambient Noise Measurements	61
4.1.5	Signal Strength Measurements.....	63
4.1.6	Modem Reception.....	65
4.1.7	Summary	66
4.2	<i>Perth Long Range Shallow Water Trial</i>	68
4.2.1	Experimental Setup.....	68
4.2.2	Modem Performance.....	72
4.2.3	Ambient Noise Analysis	73
4.2.4	Acoustic Signal Analysis	74
4.2.5	Spatial Simulation of Shallow Water Perth Trial	77
4.2.6	Summary	82
4.3	<i>French Long Range Deep Water Trial</i>	84
4.3.1	Experimental Setup.....	84
4.3.2	Modem Performance.....	85
4.3.3	Signal to Noise Ratio	86
4.3.4	Signal Power Fluctuations	89
4.3.5	Spatial Simulation of Deep Water French Trial.....	90
4.3.6	Summary	98
5	Long-term Investigation of Environmental Parameters Affecting Communication.....	100
5.1	<i>Experimental Setup</i>	100
5.2	<i>Recovery and Initial Analysis</i>	106
5.3	<i>Experimental Data</i>	108
5.3.1	Temperature Measurements and Sound Speed Profile.....	108
5.3.2	Wind and Waves.....	113
5.3.3	Modem Performance: Standard Communication	114
5.3.4	Modem Performance: Interrogations	116
5.3.5	Acoustic Noise Analysis	121
5.3.6	Acoustic Signal Analysis	126

5.3.7	Statistical Analysis using Acoustic Data	130
5.4	<i>Temporal Simulation of Long-term Perth Trial</i>	132
5.5	<i>Assessment of the Predictability of Long-term Communication Performance</i>	141
5.5.1	Environmental Contributions to Ambient Noise.....	141
5.5.2	Factors Affecting Acoustic Modem Performance in the Perth Trial	145
5.5.3	Comparison with Long-term Simulation Results	149
5.5.4	Interpretation and Discussion.....	151
5.6	<i>Summary of Findings</i>	153
6	Discussion	155
6.1	<i>Evaluation of Methods</i>	155
6.2	<i>Considerations for the use of Underwater Acoustic Communication</i>	158
6.2.1	Modem Positioning.....	158
6.2.2	Effects of Received Signal Strength	161
6.2.3	Noise Sources	162
6.3	<i>Predictability of Modem Performance</i>	164
6.4	<i>Underwater Acoustic Communication for Real-time Monitoring and Control Systems</i>	168
7	Conclusions and Opportunities for Future Research	172
7.1	<i>Conclusions</i>	172
7.2	<i>Opportunities for Future Research</i>	174
8	References	177
Appendix A	Background Information and Theory	189
A.1	<i>Subsea Pipelines</i>	189
A.1.1	Distribution and Hazards	189
A.1.2	Monitoring of Pipelines and Repair Techniques	191
A.2	<i>Underwater Acoustic Propagation</i>	195
A.2.1	Signal Power and Signal to Noise Ratio	196
A.2.2	Spreading Loss	197
A.2.3	Absorption Loss.....	198
A.2.4	Acoustic Noise	201
A.2.5	Scattering and Boundary Reflections	203
A.2.6	Refraction of Acoustic Paths.....	207

A.2.7	Time-variability of an Underwater Acoustic Channel.....	212
A.2.8	Ray Modelling Methods	214
A.3	<i>Communication and Signal Processing</i>	216
A.3.1	Introduction	216
A.3.2	Signal Modulation Techniques.....	218
A.3.3	Channel Capacity.....	220
A.3.4	Error Correction Algorithms	221
A.3.5	Multiple Node Access to the Underwater Channel	222
Appendix B	Modem Performance Measurements in the Arctic.....	223
B.1	<i>Experimental Setup</i>	224
B.2	<i>Trial 1: Initial Communication and Acoustic Recordings</i>	227
B.3	<i>Trial 2: Vertical Communication Test</i>	232
B.4	<i>Trial 3: Fjord Testing and High Speed Communication</i>	234
B.5	<i>Summary</i>	237
Appendix C	Acoustic Tag Performance and Noise Measurements at Cockburn Sound.....	239
C.1	<i>Introduction</i>	239
C.2	<i>Receiver Ping Detection</i>	242
C.3	<i>Acoustic Noise Analysis</i>	246
C.4	<i>Acoustic Ping Detection</i>	250
C.5	<i>Reception Trends and Comparisons</i>	260
C.6	<i>Summary</i>	264
Appendix D	Additional Equipment Information	265
D.1	<i>Trialled Underwater Acoustic Modems</i>	265
D.1.1	DSPComm: The AquaComm.....	265
D.1.2	Aquatec Group Limited: The AQUAmodem.....	266
D.2	<i>MCS Stackable Board Schematics</i>	267
D.3	<i>MCS PCB Designs</i>	269
D.3.1	Power Control PCB Design	269
D.3.2	Communications and RTC PCB Design.....	269
D.4	<i>ModCon Routines</i>	270
D.5	<i>PDALogger Routines</i>	277
D.6	<i>PDALogger Skinny Routines</i>	281

Appendix E	List of Publications	284
Appendix F	Copyright Licenses	286

List of Figures

Figure 2.5.1. Illustration of the experimental setup for one of the KauaiEx deployments in 2003.	31
Figure 2.5.2. Sound speed variations observed on July 1, 2003 (left). Evolution of the temperature profile obtained from one of the thermistor strings over the duration of the experiment (right). (Siderius, 2007).....	32
Figure 2.5.3. Effect of environmental characteristics on communication performance	33
Figure 3.1.1. Block diagram of equipment developed for the analysis of underwater acoustic communication.....	35
Figure 3.1.2. The primary components of the underwater recording system.	36
Figure 3.1.3. Free field sensitivity frequency response of the Marconi SH101X spherical hydrophone, digitised from the specification sheet.	37
Figure 3.1.4. Photo showing spread view of Modem Control Stack components	38
Figure 3.1.5. Photo of assembled Modem Control Stack.	39
Figure 3.2.1. Flow Diagram of ModCon.	40
Figure 3.2.2. Screenshot of <i>PDALogger</i>	43
Figure 3.2.3. Basic flow diagram of <i>PDALogger</i>	44
Figure 3.2.4. Basic flow diagram of <i>PDALogger Skinny</i>	45
Figure 3.3.1. Block diagram of the underwater acoustic communications simulator	46
Figure 3.3.2. Spectrogram of the generated signal obtained from a test input hexadecimal character string.....	48
Figure 3.3.3. Impulse response as calculated from the arrival amplitude and delay result from the Bellhop propagation model	49
Figure 3.3.4. Spectrogram of the simulated received signal for the corresponding positions shown in Figure 3.3.3.....	50
Figure 3.3.5. Amplitude distributions for noise collected during the trials off the coast of Perth, Western Australia.	51

Figure 3.3.6. Output of the band-pass filters for each carrier component, f for the source (top) and simulated received (bottom) waveforms.....	53
Figure 3.3.7. Comparison result for the example simulation with a range of 1 km ...	54
Figure 4.1.1. Photograph of the seabed modem receiver and ambient noise recorder extracted from the underwater housing.....	56
Figure 4.1.2. Photo of transmitter bundle including CTD probe (left) and underwater acoustic modem (right).	57
Figure 4.1.3. Positions of the transmitter casts occurring during southerly vessel drift.	58
Figure 4.1.4. Localisation of the ambient noise recorder.....	61
Figure 4.1.5. Ambient noise power spectrum calculated using the ambient noise recordings during a period of minimal activity in the trial	62
Figure 4.1.6. Spectrogram calculated from 260 minutes of ambient noise data recorded during the trial.....	62
Figure 4.1.7. Spectrogram of various stages of modem communication.....	63
Figure 4.1.8. Signal strength as measured by the ambient noise recorder following use of the signal detection algorithm.	64
Figure 4.1.9. Signal strength as observed by each of the deployed modems, confirming lack of reception beyond approximately 500m.	65
Figure 4.1.10. Relative success rate versus distance obtained by binning the success rate over 40 m blocks.....	66
Figure 4.2.1. Bathymetry and locations of test positions used for the trial.	69
Figure 4.2.2. Two-dimensional bathymetry for two distinct propagation paths extracted from Figure 4.2.1.	69
Figure 4.2.3. Photo of deployment gear.....	70
Figure 4.2.4. Photo of end cap of the plastic transmitter housing, showing the attachment of the LCD module.	71
Figure 4.2.5. Success rate versus range for the transmission of data from the research vessel to the remote modem.	72
Figure 4.2.6. Power density spectrogram of the entire deployment, calculated using 20 s blocks of recordings.....	73
Figure 4.2.7. Noise power spectrum obtained using quiet periods of the deployment when vessel noise was minimised.	74

Figure 4.2.8. Summary of the received signal and noise powers as observed by the seabed underwater acoustic recorder.	75
Figure 4.2.9. Comparing the ambient noise to the average signal power received for TP7.	76
Figure 4.2.10. Simulator performance summary for a sample position ($D = 15$ m, $r = 4$ km) during the Perth long range trial.	77
Figure 4.2.11. Two-dimensional predicted word error probability for the shallow water Perth trial for each modem depth at the recorder location, without the addition of ambient noise	78
Figure 4.2.12. Two-dimensional predicted word error probability for shallow water Perth trial for two modem depths, with the inclusion of 75 dB re $1\mu\text{Pa}^2/\text{Hz}$ noise	79
Figure 4.2.13. Smoothed depth-averaged word error probability for receivers centred at a depth of 15 m acquired from a high resolution focussed simulation.	80
Figure 4.2.14. Nominal mapping function to obtain transmission error probability based on word error probability, using a Binomial distribution.....	81
Figure 4.2.15. Smoothed depth-averaged transmission failure probability for receivers centred at a depth of 15 m	81
Figure 4.3.1. Vessel locations during trials off the coast of Nice, France. The stationary transmitter was located within 150 m of Test Position 1 for the duration of the trial.....	85
Figure 4.3.2. Summary of bit error rates versus range measured during the French trial.	86
Figure 4.3.3. Calculated signal to noise ratio (SNR) based on modem recordings, showing the relative strength for each frequency component used in telemetry.....	87
Figure 4.3.4. Averaged transmission loss versus range obtained from trials overlaid with predictions from the model.....	88
Figure 4.3.5. Smoothed signal power over the four adjacent frequency bands each with a bandwidth of 500 Hz.	89
Figure 4.3.6. Sound speed profile and ray path diagram for declining bathymetry modelled to simulate trial data from the Villefranche-sur-Mer coast....	90
Figure 4.3.7. Word error probability over a depth-range grid predicted from simulations of the French trial using an upwardly refracting SSP and without adding noise.	91

Figure 4.3.8. Simulation result for the French modem trial using an upwardly refracting SSP, including noise.	92
Figure 4.3.9. Results from high resolution range simulation of the French trials with a centre depth of 25 m.....	93
Figure 4.3.10. Summer SSP for the French modem trial showing a thermocline giving both downward and upward bending rays.....	95
Figure 4.3.11. Simulation result obtained for the French trial using a summer SSP with noise.	96
Figure 4.3.12. Simulation of the French trials during summer using the ‘max’ algorithm which synchronises the receiver to the maximum amplitude arrival	97
Figure 4.3.13. Summary from high resolution range simulations of the French trials, showing the differences between obtained results using a summer and winter SSP.	98
Figure 5.1.1. Locations of the two acoustic packages (AP1 and AP2) and other sensors used for the long-term deployment off the coast of Western Australia.	101
Figure 5.1.2. Experimental setup for the long-term trial showing all equipment used in the deployment.	102
Figure 5.1.3. Configuration of some of the equipment unique to the Perth long-term modem deployment.....	103
Figure 5.1.4. Software cycle for the long-term trial, showing the various phases of recording and communication.	105
Figure 5.2.1. Photos of the underwater acoustic modems following recovery after three weeks of operation.	106
Figure 5.3.1. Temperature profile as recorded by the eight-element thermistor string deployed with Acoustic Package (AP) 1.....	108
Figure 5.3.2. Measured tide at Fremantle Harbour (Perth) during the deployment period.	109
Figure 5.3.3. Calculated depths for PT1 and PT4 (See Table 5.1.1) along the thermistor string using the measurements from the pressure sensors..	110
Figure 5.3.4. Sound speed profile as calculated using data from the eight-element thermistor string deployed with acoustic package (AP) 1 and corrected for changes in sensor depth.	110
Figure 5.3.5. Plot of temperature gradient vs. time using the least squares linear fit over eight elements in the bottom 50 m of the water column.	111

Figure 5.3.6. Sea surface temperature measured at the deployment location via satellite.	112
Figure 5.3.7. Sound speed profile for Perth long-term deployment following the inclusion of SST measurements.	112
Figure 5.3.8. Wind speed as observed during the deployment period by a weather station at Rottnest Island.	113
Figure 5.3.9. Total wave height and sea contribution as observed during the deployment period by the Rottnest Waverider buoy.	114
Figure 5.3.10. Proportion of successful transmissions for both modems based on one way individual short transmissions.....	115
Figure 5.3.11. Proportion of successful transmissions averaged for both modems based on one way individual short transmissions.....	116
Figure 5.3.12. Success rate for modem interrogations originating from AP1 (top) and AP2 (bottom).	118
Figure 5.3.13. Mean proportion of interrogation success for both modems versus time, for each requested packet size.	119
Figure 5.3.14. Memory interrogation success probability, averaged over all transmission lengths.....	120
Figure 5.3.15. Overall modem performance versus time utilising both the one way transmissions and memory interrogations.....	121
Figure 5.3.16. Spectrogram of one sample recording showing perfect modem performance in both directions.	122
Figure 5.3.17. Sample ambient noise spectrum as measured by AP1 and AP2, using 10 s of noise from the point denoted by N3 in Figure 5.3.20.....	123
Figure 5.3.18. Overall spectral power versus time for the deployment duration as recorded by AP1.	124
Figure 5.3.19. Overall spectral power versus time for the deployment duration as recorded by AP2.	125
Figure 5.3.20. Extracted spectral power present in the 9600 Hz carrier frequency band.....	126
Figure 5.3.21. Spectral power versus time for each frequency component utilised by the modems.....	128
Figure 5.3.22. Averaged spectral power for both the signal and noise components from the acoustic analysis.	129

Figure 5.3.23. Probability of transmitted memory requests being successfully interpreted by the remote modem.	130
Figure 5.4.1. Sample spatial simulation (t = 13 hours) showing typical predicted performance.	133
Figure 5.4.2. Simulated time dependant performance for Perth trial, calculated using various Bellhop model parameters to assess the impact of ray count and launch angle.	134
Figure 5.4.3. Overlaid simulated performance using the basic ‘first’ and the later added ‘max’ method, showing the overall increase in performance ...	135
Figure 5.4.4. Simulated time dependant performance for Perth trial using ‘max’ synchronisation method, calculated using various levels of ambient noise	136
Figure 5.4.5. Scatter plot of predicted word success rates with various amounts of noise compared to the noise-less simulation.	137
Figure 5.4.6. Ray amplitude distribution with respect to launch angle, showing the effect of introducing significant wave height into the simulator.	138
Figure 5.4.7. Simulated performance using the ‘max’ synchronisation method during the long-term Perth trial, with and without considerations of surface roughness.	139
Figure 5.4.8. Scatter plot of performance increase with wave height, demonstrating a positive effect of surface roughness.	139
Figure 5.4.9. Standard deviation of simulated performance within each area of interest as a function of the average calculated performance.	140
Figure 5.5.1. Trend comparisons for the wind and wave data collected during the long-term Perth trial.	142
Figure 5.5.2. Cross correlation between wind speed and wave height showing the correlation between measurements from the Perth long-term trial.	143
Figure 5.5.3. Cross correlation of measured ambient noise levels with those using the linear combination of sea wave height, sea surface temperature and seabed temperature (Table 5.5.1).	144
Figure 5.5.4. Plot of cross correlation between the linear regression prediction for acoustic modem performance and the statistics obtained from the long-term Perth trial.	147
Figure 5.5.5. Direct comparison of measured performance trends with predictions using linear models.	148
Figure 5.5.6. Comparison of performance trends from simulations and measured data from the long-term Perth trial.	150

Figure 5.5.7. Cross correlation of performance trends from simulations and data obtained from the long-term Perth trial.....	151
Figure 6.1.1. Remaining disk space as a function of time as received acoustically by one of the remote modems in the long-term Perth trial	157

List of Figures (Appendices)

Figure A.1. Illustration of a typical free-span (top). Image of a free-span, captured by a ROV mounted inspection system (middle). An image depicting a cracked concrete coating (bottom).....	190
Figure A.2. Demonstration piece of the Trans Alaskan Oil Pipeline showing the integration of a pipeline inspection gauge (pig).	191
Figure A.3. Absorption coefficient of seawater as calculated in laboratory measurements.	199
Figure A.4. Attenuation loss due to the combination of spherical spreading and absorption for different frequencies, calculated by combining Equation A.4 and Equation A.6.....	200
Figure A.5. Latest ambient noise prediction curves in the Australian region showing wind dependant noise sources as well as typical marine and traffic contributions. (Cato, 2009).....	202
Figure A.6. A typical sound speed profile highlighting the various depth-dependent regions that can occur in the ocean. Adapted from Urick (1983).	209
Figure A.7. Illustrative ray trace of acoustic energy propagating through the SOFAR deep underwater sound channel. (Duncan, 2006).....	210
Figure A.8. Ray trace for a notional environment where transmissions originating near the surface propagate through the surface duct. (Duncan, 2006)	210
Figure A.9. Open System Interconnection (OSI) layer model for networking systems.	217
Figure B.1. Location of the Fram Strait where the majority of the Arctic Cruise took place aboard the KV Svalbard.	223
Figure B.2. Deployment plan showing the orientation of equipment to be tested. ...	224
Figure B.3. Photographs taken during the deployment showing deployment in ice (left) and small boat operations with KVS mobile in the Fjord (right).....	225
Figure B.4. Preparation in the wet lab on KV Svalbard.	225
Figure B.5. Spectrogram of two recordings depicting identical transmissions originating from the KVS deck modem.	229

Figure B.6. Spectrograms of recordings of the wake-up sequence transmitted by the modems.	230
Figure B.7. Simple ray trace geometry depicting the predicted path length for the first two eigenrays received at the hydrophone.	231
Figure B.8. Noise power spectrum measured during silence between modem communications.....	235
Figure C.1. Equipment layout used for the long-term deployment of acoustic tags and high frequency ambient noise recorders.	240
Figure C.2. Diagram depicting the duty cycles used for the high frequency underwater acoustic recordings in the Cockburn Sound range trial....	241
Figure C.3. Probability of ping detection versus range for the three acoustic tags deployed over the two week period.	242
Figure C.4. Probability of ping detection versus time for the three acoustic tags deployed over the trial period.....	244
Figure C.5. Spectrogram (bottom) demonstrating the ambient noise over a period of approximately 5 days as observed by the acoustic recorder with the 69 kHz band extracted	247
Figure C.6. Ambient noise power spectral density for a quiet period of the deployment (approximately 2 days elapsed) as observed by each acoustic recorder.....	248
Figure C.7. Spectrogram (bottom) demonstrating the ambient noise over a period of approximately 5 days with the 69 kHz band extracted.....	249
Figure C.8. Spectrogram of one recording using the recorder located at the source, demonstrating the reception of three separate and unique ping codes	250
Figure C.9. Spectrogram of one recording using the recorder located 98 m from the acoustic tags, demonstrating the reception of three separate and unique ping codes.....	251
Figure C.10. Step-by-step construction of the matched filters used in the Cockburn Sound study.	252
Figure C.11. Matched filter output showing pulses representing successful detection of the three unique tags in a single recording.....	253
Figure C.12. Matched filter output showing pulses representing successful detection of two tags where pulse codes have overlapped.....	254
Figure C.13. Detection algorithm output (SNR of minimum amplitude pulse) which operated on each maximum of the matched filter (cross correlation) output.	255

Figure C.14. Results of the improved detection algorithm which operated on each maximum of the matched filter (cross correlation) output.....	257
Figure C.15. Noise trends as measured by both ambient noise recorders showing measured narrowband and broadband energy.	260
Figure C.16. Recorded signal power for ping detections made by the ambient noise recorders.	261
Figure C.17. Comparison and cross correlation of ambient noise power measured by the ambient noise recorder located at the source and the ping detection failure rate of the receiver located 49 m from the source.	263
Figure D.1. Photo of assembled Modem Control Stack with attached AquaComm boards mounted as the two upper PCBs.....	265
Figure D.2. Photo of the AQUAmodem fitted to the deep water housing for one of the experiments. A protective cage was attached to the transducer. ...	266

List of Tables

Table 2.3.1. Summary table of communication simulators (incorporating physical channel characteristics) presented in literature review, compared to the simulator presented in this thesis.....	25
Table 4.1.1. Deployment times for each Test Point (TP) location, relative to the first recording. Times are given as the number of minutes from the first recording synchronised at 10:00:00 AM WST.....	58
Table 4.2.1. Deployment Times for each Test Point (TP) location.....	68
Table 4.3.1. Deployment positions for the Nice trials. Approximate water depth at each modem position is also given.	85
Table 5.1.1. Summary of temperature and pressure sensor positions along the riser for Acoustic Package (AP) 1.	103
Table 5.3.1. Table summarising the results of memory interrogations conducted throughout the deployments.	117
Table 5.3.2. Summary of analysis of the acoustic recordings showing measured signal and noise levels during the deployment.....	127
Table 5.3.3. Table summarising the results of memory interrogations conducted throughout the deployments	131
Table 5.5.1. Best prediction curves for ambient noise, obtained using multiple linear regression	144
Table 5.5.2. Contributions of each environmental parameter following the use of multiple linear regression to obtain the best prediction curve for the communication success rate during the long-term Perth trial.	146
Table 5.5.3. Coefficients from a simplified multiple linear regression analysis, utilising only wind speed and SSP gradient.....	148

List of Tables (Appendices)

Table A.1. Examples of methods used to transmit digital communication. A variant of one or more these methods is generally utilised for underwater acoustic telemetry.	219
Table B.1. Separation distances for ambient noise recordings during the Arctic trials, as radioed by control aboard the mother ship.....	228

Table B.2. Statistics acquired during a vertical transmission test aboard KV Svalbard.	232
Table B.3. Detections statistics acquired during trials conducted in the Fjord nearby Longyearbyen.	236
Table B.4. BER for high speed data packets following detection from KVS mobile to KVS deep.	237
Table C.1. Various configurations for the acoustic tags (pingers) used for the Cockburn Sound range trials.	240
Table C.2. Number of detections as observed by each recorder compared to the actual amount of pings transmitted by the tags.	258
Table C.3. Recorded signal levels for each acoustic tag compared to the source level given in their description. (100 Hz Bandwidth)	258

List of Abbreviations

AcTUP	Acoustic Toolbox User interface and Post processor
ADC	Analogue to Digital Converter
ADCP	Acoustic Doppler Current Profiler
AUV	Autonomous Underwater Vehicle
AWGN	Additive White Gaussian Noise
BER	Bit Error Rate
BFSK	Binary Frequency Shift Keying
BPSK	Binary Phase Shift Keying
CCK	Complimentary Code Keying
CDMA	Code Division Multiple Access
CF	Compact Flash
CSMA	Carrier Sense Multiple Access
CT(D)	Conductivity, Temperature, (Depth)
DADS	Deployable Autonomous Distributed System
dB	Decibels
DFE	Decision Feedback Equaliser
DPSK	Differential Phase Shift Keying
DS-CDMA	Direct Sequence Code Division Multiple Access
DSP	Digital Signal Processor
DSSS	Direct Sequence Spread Spectrum
ELF	Extremely Low Frequency
FAT	File Allocation Table
FDM	Frequency Division Multiplexing
FDMA	Frequency Division Multiple Access
FEC	Forward Error Correction
FHSS	Frequency Hopping Spread Spectrum

FSK	Frequency Shift Keying
GPRS	General Packet Radio Service (mobile phones)
ISI	Inter-Symbol Interference
KauaiEx	Kauai Experiment
KVS	KV Svalbard (vessel)
LCD	Liquid Crystal Display
m	Metres
MAC	Medium Access Control
MCS	Modem Control Stack
MFSK	Multiple Frequency Shift Keying
Modem	Modulator / Demodulator
MPSK	Multiple Phase Shift Keying
OFDM	Orthogonal Frequency Division Multiplexing
OSI	Open System Interconnection (Model)
Pa	Pascals
PC	Personal Computer
PDA	Portable Digital Assistant
pig	Pipeline Inspection Gauge
PLL	Phase-locked Loop
PPC	Passive Phase Conjugation
PPM	Pulse Position Modulation
PSD	Power Spectral Density
PSK	Phase Shift Keying
psu	Practical Salinity Units
QPSK	Quadrature Phase Shift Keying
RF	Radio Frequency
RMS	Root Mean Square
ROV	Remotely Operated Vehicle
RS	Reed-Solomon (code)
RTC	Real Time Clock

s	Seconds
S/PDIF	Sony/Philips Digital Interconnect Format
S2C	Sweep Spread Carrier
SD	Secure Digital (card)
SD	Standard Deviation (statistics)
SNR	Signal-to-Noise Ratio
SOFAR	Sound Fixing and Ranging (Channel)
SS	Spread Spectrum
SSP	Sound Speed Profile
TDMA	Time Division Multiple Access
TL	Transmission Loss
TOSLINK	Toshiba-Link (optic fibre link)
TP	Test Point
UART	Universal Asynchronous Receiver/Transmitter
USB	Universal Serial Bus
UUV	Unmanned Underwater Vehicles
VLA	Vertical Linear Receive Arrays
WHOI	Woods Hole Oceanographic Institution
WLAN	Wireless Local Area Networking
XBT	Expendable Bathythermograph

1 Introduction

1.1 Motivation

Underwater pipelines have become commonplace for the efficient transport of offshore oil and gas resources. However, the chance of failure in such pipelines brings great environmental and financial risk. It is therefore vital to develop and implement effective methods for regular monitoring and maintenance of these structures. An appropriate approach to the real-time monitoring of pipeline conditions is the use of internal and external sensors. Networks of different sensors can relay information via an underwater data link to a central station, allowing an immediate response if necessary and limiting any potential damage. Additionally, an underwater communication link provides the capability to remotely control instrumentation should preventative action be required.

The challenge for subsea monitoring is achieving reliable data transmission between individual sensor nodes and onward to land-based stations. Umbilicals carrying electrical or fibre optic cabling are a favourable option for high-bandwidth applications. However, their weakness is the significant cost in deploying and maintaining the infrastructure. Additionally, should an umbilical become severed, all contact and control would be immediately lost. For this reason, wireless telemetry methods are preferred, at least as a backup form of communication.

The partial conductivity of seawater inhibits the transmission of radio waves, limiting most conventional forms of wireless technology. Electromagnetic transmissions at optical wavelengths also have restricted range capabilities. The most appropriate wireless technology for long range subsea telemetry emerges as acoustic communication. This is not surprising given the extensive use of acoustics for underwater applications including sonar operation and acoustic tracking. Advantages

of using acoustics include the relatively small size and low cost of transducers and recent dramatic increases in microprocessor capabilities.

The infamous BP Deepwater Horizon oil spill in 2010 is one disaster where questions have been raised regarding the usefulness of acoustic communication in the offshore oil and gas industry. It was revealed in an article in *The Wall Street Journal* (2010) that a backup acoustic switch already used in other nations as a last resort to seal an oil-well was not employed in the rig. It is debatable whether or not a backup acoustic switch would have been beneficial given the damage to the well-head. However, the magnitude of the spill into the Gulf of Mexico highlights the need for more wireless backup communication systems to help prevent such disasters.

Acoustic data communication remains a computationally demanding field, particularly when considering increased data rates and networking applications. The transfer of current wireless protocols used in Radio Frequency (RF) communications to underwater acoustics is not always effective due to differences between the physical media. These include an inherent delay five orders of magnitude higher than RF transmission and time-varying physical conditions which alter the propagation characteristics of the underwater channel. These problems are combined with difficulty in controlling and predicting the ambient noise at a receiver location. In particular, interference from shipping and biological noise can be detrimental to an acoustic telemetry system.

When considering the several variable characteristics of the ocean, the effect of the environment on subsea telemetry becomes complicated and can be hard to accurately predict. Much effort has been spent predicting acoustic communication performance, ranging from basic propagation modelling to developing complex simulations for high speed underwater networks. Unfortunately, the communication and simulation methods utilised by modem manufacturers are generally tailored to suit an individual application. Consequentially, channel simulators tend to focus on the variables that would affect specific equipment in a unique scenario rather than offering a broader prediction.

1.2 Thesis Aims

The primary aim of this thesis is to characterise the performance of horizontal underwater acoustic data communication in various scenarios, with particular application to subsea monitoring and control systems. This involves a comprehensive review of the current technology found in literature, carrying out acoustic modem experiments designed specifically for this study, and performing simulations for comparison with measured data.

Specifically the following aims are to be achieved:

- Review the theory, current progress and challenges involved with underwater acoustic communication.
- Design and build the appropriate electronics and software for *in situ* performance characterisation of underwater acoustic communication
- Design and conduct experiments to obtain data relating the performance of acoustic communication to the surrounding environmental conditions in both short-term and long-term scenarios.
- Develop and implement appropriate data analysis techniques to characterise acoustic communication performance with respect to environmental conditions.
- Design and construct an advanced underwater acoustic communication simulator which utilises pre-existing channel models to predict modem performance in similar scenarios to those found during experimentation, and compare the results with those obtained from field measurements.
- Establish a foundation for predicting the performance of underwater acoustic communication for long range horizontal transmission in new environments.

This research was designed to help determine the feasibility of utilising acoustic modems for real-time monitoring and control for subsea pipeline networks, either as a primary or secondary means of long range communication.

1.3 Thesis Outline

This thesis divides the steps taken to achieve the aims outlined above into individual chapters. A comprehensive review of current research is followed by information regarding the custom-built deployment equipment and underwater acoustic communication simulator. Details of short-term and long-term field trials are then discussed in chronological order to best demonstrate the evolution of data collection and analysis techniques. Finally, the literature review, results from the trials and their related simulations are linked and discussed regarding their application to implementing underwater acoustic communication for subsea monitoring and control.

The main thesis chapters are organised as follows:

- Chapter 2 conveys a comprehensive literature review of the history and latest developments in all areas of underwater acoustic communication. These include the current state of the art in digital modulation methods, effective signal processing algorithms for receivers, protocols for distributed networks and channel simulators.
- Chapter 3 gives a brief overview of the hardware and software that was used to collect most of the data discussed in this thesis. This includes the custom hardware developed for independent ambient noise recording and flexible modem control. The chapter also outlines the Matlab-based underwater acoustic communication simulator which was designed to predict the performance of acoustic communication based on environmental parameters utilising the Bellhop propagation model. The simulator was used to predict the telemetry performance for three trials presented in later chapters.
- Chapter 4 introduces field experimentation with two short-term trials which were performed off the coast of Perth, Western Australia. These deployments were conducted in shallow water ($D < 30$ m) highlighting issues regarding multipath propagation. The trials introduce the methods used to acquire performance and environmental data simultaneously. The location varied slightly between trials, illustrating both differences in environmental

conditions as well as modem performance. An additional deep-water study ($D \leq 1000$ m) conducted off the coast of France highlights the effects of the sound speed profile on communication. Simulations were conducted using the environmental parameters from two trials presented in this chapter. Spatial simulations are presented, providing two-dimensional performance estimate grids for comparison with field data.

- Chapter 5 investigates time-dependant environmental conditions and their effect on underwater communication, examined in a final long-term experiment. This trial was designed specifically to collect the maximum amount of data for this study, including modem performance, sound speed profiles and sea surface conditions over a 21 day period. This chapter analyses the environmental changes that occurred and their subsequent effects on acoustic telemetry. The communication simulator was also utilised for the long-term deployment, predicting the temporal variation in performance over an area of interest related to the location of a receiving modem. The measured fluctuations in the sound speed profile, ambient noise and wave height were included in the simulation and the results compared to the trial data. Chapter 5 outlines the comparisons made between the simulated results and the obtained statistics, in addition to determining the effects of each environmental parameter on the measured performance.
- Chapter 6 discusses the major results from the studies presented in the preceding chapters and presents strategies for the use of underwater acoustic communication for monitoring and control systems. The discussed topics include predictability of communication, major considerations for utilising acoustic communication and application of the technology for a real-time monitoring system.
- Chapter 7 concludes the thesis with final comments and recommendations for future work in the field of horizontal underwater acoustic communication for real-time monitoring and control.

The appendices supplement the information held within the body of the thesis, should it be required. These include a comprehensive review of the theory behind

acoustic telemetry, information regarding the developed equipment and detailed reports regarding two additional studies. The first of these studies involves a series of Arctic trials performed aboard an icebreaking vessel. The second study involves a long-term experiment performed in Cockburn Sound, off the coast of Western Australia using acoustic identification tags and ambient noise recorders.

1.4 The Original Contributions of the Thesis

All of the work described in this thesis was performed by the candidate, with the exception of participating in data acquisition for the French Trial (Section 4.3.1).

The contributions of this thesis stem from a comprehensive experimental and computational investigation into the performance of underwater acoustic communication in several unique environments. This is divided into five main chapters of original work.

Chapter 2 presents a new comprehensive review of the latest advancements in underwater acoustic communication. This provides an overview of the current state of the art in modulation techniques, signal processing, and results from the latest experimental and simulation work.

In Chapter 3, the methods used to achieve the forthcoming results are described. The custom-built electronics and software establish an original flexible instrument package that allows for a diverse range of subsea functionality. Similarly, the simulator represents an original design, which built onto an existing open-source propagation model, allows for the direct analysis of acoustic communication performance for any two-dimensional scenario. In addition to facilitating depth and range dependant acoustic environments, the simulator provides the flexibility to be modified for testing of any specific protocol and signal processing method.

Chapter 4 characterises the performance of underwater acoustic communication in three unique environments from various short-term, range dependant trials. Most of the trials utilised the same hardware which provided an original opportunity to compare the performance of a single communication system under different challenging scenarios. The data obtained from the simulator described in Chapter 3 provides two-dimensional spatial performance estimates and evaluates the predictability of acoustic communication for short-term studies.

In Chapter 5, an original study of the impact of temporal environmental fluctuations on communication is presented, supplemented by an additional unique trial using acoustic tags (Appendix C). This chapter provides a detailed analysis of the performance affecting parameters in underwater communication over a 16 day period. This is done by relating the observed modem performance to fluctuations in wind speed, wave height, ambient noise and temperature profile. Chapter 5 also demonstrates further flexibility of the simulator which allows for the innovative automatic reconfiguration of parameters in time dependant simulations. A comparison between simulated and measured performance data assesses the predictability of underwater communication during the long-term deployment. Additionally, the comprehensive amount of collected data shows the effectiveness of the hardware described in Chapter 3 for long-term deployments.

Finally, Chapter 6 combines the newly obtained knowledge from the preceding chapters to establish an original point of view of the effectiveness of acoustic communication for subsea monitoring and control.

Much of the research presented in this thesis has generated technical papers, some of which have been peer reviewed. Details of current published articles can be found in Appendix E.

2 Review of Literature

The following is a review of the current literature discussing the various elements of underwater acoustic communication. This summary is focussed primarily on developments over the last two decades, although some notable older literature is presented. Prominent summaries on acoustic communication development prior to this period include those produced by Stojanovic (1998) and Kilfoyle and Baggeroer (2000). Additionally, a comprehensive review of phase-coherent modulation techniques has been produced by Freitag *et al.* (2004).

Described in a recent summary paper by Chitre *et al.* (2008), the historical development of underwater acoustic communication has stemmed from the initial primitive use of sonar as a means to signal by using pings. From further understanding of the underwater acoustic channel and refinement of digital communication techniques, underwater telemetry has become applicable to more challenging scenarios. Significant milestones came from multipath compensation and the development of channel equalisers which gave rise to dramatic increases in data rates. Subsequently, the applicability of underwater communication has advanced from incoherent digital modulation which was restricted to mostly vertical channels, to sophisticated coherent techniques employed over challenging multipath environments. The overall development of the field of underwater acoustic communication has been driven by a perpetual need for faster and more robust digital signalling techniques, which have been facilitated largely by increases in portable computational technology. However, it will become evident throughout this literature review that the capabilities of each individual system are highly dependant on both the applied environment and the technology available to the researcher.

This chapter is structured to best represent the processes involved in establishing an underwater acoustic link. The first section outlines the various modulation schemes and their effectiveness in different scenarios, with detail regarding the receiving algorithms and signal processing located in the second section. The current state-of-

the-art in communication simulators is then presented, followed by a case study relevant to the long-term trial presented in the experimental chapters. Although prior knowledge regarding underwater acoustic communication is assumed, a comprehensive introduction to the background theory including underwater acoustics and data communication techniques is located in Appendix A should it be required.

2.1 Modulation Techniques

The first underwater acoustic communication systems typically relied on non-coherent modulation techniques where transmitting and receiving systems are not phase synchronised. Frequency modulation was typically used due to the relative stability of frequency in an underwater channel, where phase and amplitude are subject to more distortion. The most popular methods included the adaption of Frequency Shift Keying (FSK) based techniques which relied mostly on guard intervals between successive symbols to ensure the impact of Inter-Symbol Interference (ISI) was minimised (Stojanovic, 1998).

Despite the surge in phase-coherent techniques over the past couple of decades, FSK is still widely used in systems where reliability is preferred over throughput such as the acoustic release (Kilfoyle and Baggeroer, 2000). One notable example of an early FSK system was developed by Woods Hole Oceanographic Institution (WHOI). The developed technology was capable of transmitting up to 1200 bps over a 3 km vertical channel (Catipovic *et al.*, 1989). The presented acoustic modem operated with relatively high carrier frequencies of 15-20 kHz. A Multiple Frequency Shift Keying (MFSK) technique was implemented where up to 16 carrier frequencies were modulated in parallel. By utilising frequency diversity, selective fading at the receiver was managed. The use of an onboard Digital Signal Processor (DSP) chip in the WHOI modem also demonstrated its effectiveness in receiving and demodulating acoustic communication signals.

Non-coherent methods of data transfer continued their popularity in underwater modems as highlighted by Coates *et al.* (1994) who demonstrated the “BASS 600” communication link. Both FSK as well as introductory phase coherent techniques were shown to work effectively in two trials over much shorter distances of hundreds of metres. Data rates up to 200 kbps were obtained, highlighting the effectiveness of the 600 kHz carrier frequency. This technology also began to demonstrate the possibilities of coherent methods of communication. However, for this particular trial the phase coherent techniques performed less effectively due to inadequate detection techniques at the receiver.

Scussel *et al.* (1997) presented a MFSK-based modem capable of operating at up to 2400 bps. New methods of coding were utilised by the modem; Hadamard coding and 1-of-4 MFSK modulation. Frequency bands were selectable between 1-25 kHz to accommodate different scenarios. Some applications were presented by Green *et al.* (1998). These examples included a trial performed in a depth of 200 m which established effective communication over 5 km. Other deployments involved vertical distances of over 1000 m as well as introducing underwater networking. This paper also discusses the use of the modems for a notable subsea network, Seaweb. More information on Seaweb and underwater networking is given in Section 2.4.

Another FSK based acoustic communication system developed around the same time was presented by Kuchpil *et al.* (1997). A carrier frequency of 10 kHz was used with the modems operating at 16 bps. Trials were conducted in the Brazilian Campos Basin with communication achieved in depths of 600 m and ranges up to 4 km. The results also highlighted the detrimental characteristics of an underwater acoustic communication channel including frequency spreading. Overall the paper demonstrated strong feasibility for acoustic modems as a simple communication system for subsea control and monitoring. Such a concept was not entirely new. A study by Garrood and Miller (1982) demonstrated the use of underwater acoustic communication for transmission of control commands. This involved FSK techniques implemented at data rates of up to 40 bps. Additionally, post-experimental analysis suggested higher data rates were achievable as the guard times were longer than necessary.

Chirp FSK techniques (modulation of frequency sweeps) are becoming widely adopted in underwater acoustic communication as described by LeBlanc *et al.* (1999). Utilising a frequency range of 20-30 kHz, data transfer was achieved in depths of less than 10 m over a range of approximately 100 m. Four modes of operation were trialled with the fastest data rate of 2400 bps reliably achieved. This was further optimised for the frequency range of 16-32 kHz and results are presented by LeBlanc *et al.* (2000). In a paper by Courmontagne *et al.* (2008), simulations of a chirp scheme were shown to achieve data rates of up to 7000 bps. Additionally, low error rates observed at low SNR indicated the scheme could be useful in long-range applications.

Non-coherent techniques based on FSK are still widely used in the most recent applications of underwater communication. For example, Iitis *et al.* (2005) presented the development of a MFSK technique for use with an underwater network. An acoustic modem based on a DSP was developed with a target data rate of 133 bps. The specific aim of the new protocols was to establish a robust method of communication with adaptive signalling techniques and synchronisation measures. At the time of publication, modem hardware was still in development; however, simulations showed the potential of the techniques being developed.

Phase coherent signalling schemes in underwater communication are growing in popularity as the high-end computational demands for synchronisation and acquisition are being met with low powered and highly efficient DSP technology. Phase coherence in an acoustic channel places significant demand on signal processing at the receiver for communication systems to operate effectively (Stojanovic *et al.*, 1994). These techniques are generally accompanied by customised equalisers (Section 2.2) to handle the difficulties associated with multipath propagation. One of the simpler methods of coherent telemetry is the use of Differential Phase Shift Keying (DPSK) where the bit stream is encoded into the difference of phase between adjacent symbols rather than relative to a fixed reference. DPSK was the phase coherent technique used in the previously mentioned “BASS 600” link (Coates *et al.*, 1994). This scheme was a common first step before moving to fully coherent communication systems that utilised complex receiver

processing techniques such as Decision Feedback Equalisation (DFE) and Phase-Locked Loops (PLLs) (Kilfoyle and Baggeroer, 2000).

A range of modulation schemes have recently been developed that occupy the maximum possible bandwidth of the underwater acoustic channel. Frequency diversity helps overcome signal fading, lowering error rates and providing a more reliable method of telemetry. One popular example is the implementation of Orthogonal Frequency-Division Multiplexing (OFDM). In OFDM, the transmitted bit stream is divided into a number of subcarrier frequencies and transmitted at modest data rates. The basic operation of the receiver is to de-spread these signals and recombine them into the original bit stream (Van Nee, 2000). This is particularly useful for robust performance in long-range communication where signal fading due to multipath is severe.

An OFDM technique was proposed and tested by Leus and van Walree (2008) for use with Unmanned Underwater Vehicles (UUVs). With covert communication in mind, low SNRs were considered and two low transmission rates (4.2 bps and 78 bps) were trialled with a total bandwidth of 3.6 kHz. The system was tested in northern Europe between August and September 2007. The paper discusses three experiments in different conditions. Two of these trials were conducted in the Baltic Sea with a centre frequency of 3.3 kHz. The main difference between the two experiments was the transmission range, being 8 km and 52 km respectively. The transmitter was located at a depth of 40 m and a string of hydrophones was used to receive the signal. A single hydrophone at 50m was analysed for both experiments. The third experiment was conducted on the Norwegian continental shelf. This operated with a centre frequency of 5 kHz and used a different modem transducer to previous experiments located 60 m below the ocean surface. In this experiment, the transmitter was towed from the receiver array at approximately 2.5 ms^{-1} to a range of 38 km.

The OFDM system worked effectively during the field trials with regards to covert communication. In particular, the low SNR waveforms that were successfully

decoded by the receiver were found to be inaudible and indistinguishable from the background noise in energy spectrograms. The high data rate communication was found to be limited by the large range causing spread of the arrival times. For the lower data rate, the SNR limit was due to the inability of the detection algorithm to acquire the signal for processing and not related to the OFDM communication scheme.

In addition to working with OFDM, van Walree and Leus (2009) analysed more data obtained in the Baltic Sea experiments. However, instead of using OFDM waveforms, regular Frequency-Division Multiplexing (FDM) transmission was investigated with a fewer number of sub-bands. Each sub-band contained the same stream of data, however, interleaved training bits allowed a multiband equalisation approach at the receiver. More information about the use of training bits and equalisation for receiver processing is located in Section 2.2. During the trial, communication was adequately achieved at 75 bps with SNRs as low as -12 dB.

A shallow water case study for OFDM communications was conducted in Singapore and was presented by Chitre *et al.* (2005). In depths of approximately 20 m, an OFDM DPSK signal with a centre frequency of 51 kHz and a bandwidth of 24 kHz was transmitted up to 350 m in range. Interestingly, the impact of snapping shrimp on the performance of underwater telemetry was included in this study. Error free data rates at up to 5.3 kbps were obtained in the experiments and the importance of corrective coding techniques was highlighted.

Spread spectrum technologies have been widely adopted for both the bandwidth utilisation and applications in underwater acoustic networks. An introduction to the use of spread spectrum techniques in underwater communication as well as experimental results was given by Freitag *et al.* (2001). The results highlight comparatively better overall performance of the advanced Direct Sequence Spread Spectrum (DSSS) method as well as the simplicity in implementing non-coherent Frequency Hopping Spread Spectrum (FHSS) in some applications.

Sozer *et al.* (1999) proposed transmitter and receiver designs for a DSSS underwater acoustic communication system. The paper discussed the limitations on bandwidth and intended range capabilities of such a system. Data from an experiment in the Baltic Sea was presented, showing error free communication at low SNR. Similarly, shallow water trials were presented by Freitag *et al.* (2001) which highlighted the suitability of DSSS for Code Division Multiple Access (CDMA) implementations in networking. Trialled data rates varied from 19 bps to 320 bps with a centre frequency of 13.5 kHz and a bandwidth of 4.8 kHz. The results also demonstrated the effectiveness of increasing the number of chips per symbol (subsequently decreasing the data rate) on the performance of spread spectrum modulation.

Yang and Yang (2008) presented the performance of DSSS in low SNR environments. Additionally, the use of Passive Phase Conjugation (PPC) was described. A channel estimate was used to filter the received signal in order to remove multipath components. The study utilised just one receiving hydrophone while many other trials of this type typically used more to take advantage of spatial diversity (Section 2.2). In-depth analysis of the channel characteristics and its effects on the Bit Error Rate (BER) are discussed. Data from the TREX04 experiment off the coast of New Jersey were compared with performance models. A major finding of the experiment was that the code length for DSSS systems need to be long enough to allow for multipath arrivals to fade before a spectral component is reused. The use of training sequences was avoided so channel estimation was somewhat inaccurate. However, with several methods trialled and the results analysed, the system was able to provide good performance at SNR as low as -8dB.

A recent development of DSSS communication systems was presented by Chengbing *et al.* (2009), demonstrating a variable rate spread spectrum system. This system was tailored for shallow water communication, implementing complex coding systems to allow for accurate receiver performance. The paper introduces Complementary Code Keying (CCK) which is also utilised in Wireless Local Area Networking (WLAN) to support the variable Wi-Fi throughput rates. In CCK, code words of fixed length are transmitted with the number of bits each word represents being dependant on the target bit rate. Modifying the bit rate was performed by adding or removing this

redundancy to a fixed payload. The adaption of such a technique to underwater acoustics was presented and the performance compared using several simulations. The results were promising for increasing the range capabilities, data rates and reliability of communications by using DSSS-CCK.

Another emerging example of adaptive techniques applied to modulation schemes in underwater modems was presented by Kebkal and Bannasch (2002). The Sweep Spread Carrier (S2C) technique involves transmitting a succession of sweeps, spreading over a broad bandwidth of the signal spectrum. For experiments conducted in August 2001, differential Binary Phase Shift Keying (BPSK) modulation was encoded in sweeps utilising a bandwidth of 40 - 80 kHz (Kebkal, 2004). Various sweep durations were trialled with obtained data rates ranging from 2 - 12 kbps. Further work reported by Kebkal *et al.*, (2004, 2005) evaluated the performance limits of different transmission characteristics by using both simulations and experimental data.

In most cases, the modulation schemes adopted by underwater acoustic communication systems are based on techniques already utilised for radio wireless systems. Jones (2007) discussed this adaption of techniques and demonstrated acoustic technology's increasing ability to provide fast and reliable subsea communications. Cheaper and more computationally efficient hardware continues to expand into the future. With this technological growth, modulation techniques for acoustic data transmission will help provide faster and more reliable digital communication in the most unforgiving subsea conditions.

It is important to understand that the results for the modulation schemes presented in the preceding studies can not be directly compared due to the differences in how they were obtained. These differences may include the physical environment surrounding a specific field trial or the use of advanced receivers or transducer arrays. The study presented in this thesis seeks to highlight the environmental impacts on telemetry by using the same underwater acoustic modems in the majority of the trials as well as implementing the same algorithms for different communication simulations.

2.2 Equalisation and Beamforming Techniques

To deal with the unpredictable and time dependant distortions inherent in the underwater acoustic channel, there have been significant advances in signal processing techniques and modem receiver design. Over the last several years, adaptive equalisers have been developed to attempt to adequately reconstruct a received signal based on the instantaneous channel parameters. The advanced signal processing capabilities of DSPs combined with the use of transducer arrays have opened the door for time-reversal signal processing to be performed in real time in acoustic modems. In order to adequately synchronise a signal and remove ISI, the response of an underwater channel can be used to refocus the distorted signal to its intended waveform. This is typically done by transmitting probe signals or training sequences before an acoustic data packet is sent.

Higher decision accuracy and data rates can be obtained by accounting for the temporal changes in the underwater acoustic channel on a symbol-by-symbol basis by using adaptive filtering. Continuous updating of channel filters can be provided by using decision feedback equalisation (DFE). This iterates the channel estimate with each symbol decision and reconfigures the channel filter in real-time, and is described early by Stojanovic *et al.* (1993, 1994, 1995). These techniques introduced capabilities to achieve relatively high data rates and transmission ranges. Several trials were performed with 4- and 8-Phase Shift Keying (PSK) modulation techniques in shallow and deep water. Some of these trials also involved the use of a receiver array to determine the optimal receiver depth. However, the full spatial diversity was not always exploited for refocussing in these studies. The trial results presented in the studies showed promise for both long and short range PSK communication. For example, a deep underwater link of over 200 km was achieved with data rates of up to 660 bps. Also, a shallow water link of 4 km achieved a data rate of 10 kbps without error.

Time-reversal applied at the receiver in the frequency domain, known as Passive Phase Conjugation (PPC), has been discussed by Hursky *et al.* (2001). The study

included analysis of experimental data from SignalEx, conducted on the American coast. The feasibility of using the time domain equivalent to MFSK, Pulse Position Modulation (PPM) was investigated. The impulse response of various channels was presented, showing strong time variation with drifting nodes. Whilst PPM by itself was vulnerable to multipath interference, results demonstrated feasibility in using PPC with lower data rates from 25 – 32 bps achieved.

An early description of developing robust coherent signal processing at the receiver was given by van Gijzen and van Walree (2000) regarding the ROBLINKS experiment conducted in the Netherlands. A BPSK modulation scheme was used with two displaced carriers. These carriers compensated for Doppler spread caused by vessel movement by guiding the receiver to the carrier frequency. Transmissions began with a training sequence followed by silence. This ensured a 20 element receiver array could correct for multipath propagation before the data, preceded by header information, was demodulated. The water depth was approximately 13 m with the receiver array spanning the water column. Ranges varied from 1 – 10 km. Impulses, tones and sweeps were also transmitted to the receiver periodically to record the overall variations in the acoustic channel over the seven day trial.

The results from the ROBLINKS experiment (Gijzen and van Walree, 2000) demonstrated the usefulness of a receiver array for compensating for signal fading. DFE was also used to compensate for the time variation of the physical channel. Using up to four hydrophones, a zero error rate was established at 4 kbps. However, the system was unable to successfully decode the data when making use of just one array element, including the one with strongest signal clarity. Experiments discovered that environmental impacts were more severe with carrier frequencies greater than 6 kHz. These included significant temporal variation in multipath characteristics. The usefulness of the displaced carriers for receiver guidance was also shown to be limited when one or of the carriers was subject to fading.

A notable study on time reversal has been presented by Rouseff *et al.* (2004). Decision-directed passive phase conjugation was first analysed. Instead of emitting

an initial probing pulse as with other studies, a known data sequence was transmitted to the receiver first. By comparing the received training signal with what was expected, the matched filter was continuously updated, iterating and adapting to the changes in the acoustic channel as a DFE. Spatial diversity was also studied. The achieved BER was used as a performance indicator, measured using different combinations of the array elements. Whilst using the full 14 element array provided a zero BER, it was determined that performance was significantly poorer when less than 5 elements were used. Importantly, the paper highlights that the overall number of elements used in the process was a greater contributor to performance than their relative positions in the array. Frequency diversity was finally presented and the BER in simulations was found to increase as the ratio of the bandwidth to data rate was decreased. Further work on this is demonstrated later (Rouseff, 2005). Numerical models helped characterise the effects of the number of array elements, transmission bandwidth and oceanographic parameters. It was also discovered that only a weak correlation existed between the array geometry and the reception quality. This further suggested that compact arrays of more elements could be used in place of those that spanned the entire water column.

Recent work by Stojanovic (2005) demonstrated more complex methods for simultaneous focussing and removal of residual ISI in acoustic communication signals. This included determining the appropriate techniques applied at both the transmitter and receiver to ensure optimum SNR, bandwidth utilisation and data rates. Additionally, Guosong (2009) investigated simple methods for the synchronisation of signals used in underwater communication. This was done in the frequency domain with PPC communications in mind and utilised the transmission of two pulses separated by a coherence time for synchronisation.

Notable work has been performed with active phase conjugation such as the experiments presented by Kuperman *et al.* (1998). These involved transmitting a probe signal to a receiver array located several kilometres away. The received signal was subsequently time reversed and retransmitted back through the same channel. It was found that the reciprocal transmission focussed back to the original source both spatially and temporally. Expanding on this experiment, an example of a time

reversal mirror was demonstrated by Edelmann *et al.* (2002). Here, a BPSK signal was encoded using the reciprocal of the channel impulse response to refocus at the receiver. A further study of phase conjugated array transmission was presented by Smith *et al.* (2003). Modelling of the underwater channel was used to examine and verify the performance of various design parameters of time-reversal systems in a water depth of 200 m. Several aspects of phase conjugation were investigated and the study demonstrated the focussing technique's usefulness for underwater communication methods. Specifically, the ability of a phase conjugated array to focus transmissions to the positions of underwater nodes was observed and discussed.

An additional technique applied at a transmitter which is suitable for long range propagation is parametric transduction. In parametric arrays, the non-linear properties of underwater acoustics are used to create highly directive acoustic waves which significantly reduce multipath propagation. This is done by emitting signals of high amplitude at two high and slightly different primary frequencies. A highly directional difference (secondary) frequency component is also emitted as a result. This secondary component of much lower frequency and high directionality is of great interest in many applications including sonar and communications. An early study of parametric transduction is presented by Muir (1974), demonstrating its effects in underwater propagation. This includes analysis of the beamwidth and power efficiency in several scenarios.

An early investigation of parametric transduction for long range shallow water communication was presented by Coates *et al.* (1996). Here, the "BASS 300 PARACOM" link was developed with a primary frequency of 300 kHz and a difference frequency of 50 kHz. However, the system was described as a precursor for a much lower frequency version. A further development was described by Zheng *et al.* (1996), demonstrating the use of parametric transduction with the "BASS 50 PARACOM" link. This system utilised 2, 4 and 8 DPSK methods with a 50 kHz primary frequency and 5 kHz secondary frequency. Transmission was performed using two different types of transmit arrays with a single line receiver array tuned to the reception of the differential frequency. Two trials are discussed in the paper. Both

experiments used one-way transmissions of text and an image of the Birmingham University logo. Trials were performed for long-range scenarios ($r > 10$ km) with the transmitter located below the thermocline to ensure a direct path to the receiver.

It was found during the BASS 50 PARACOM trials that the Signal-to-Noise Ratio (SNR) fluctuated with both weather and nearby shipping noise, consequently affecting the error rates. It would also be expected that a system utilising parametric transduction would consume much more power than a typical communication system given the higher output levels at the source. However, reliable and long range communication at a relatively low cost of physical transmitter size was provided, reducing the multipath inherent in all long range and shallow water communications. Further work with the PARACOM project was presented by Loubet *et al.* (1996) demonstrating the signal transformations for various modulation types. Overall, the BASS 50 PARACOM system was demonstrated to be effective for long range communication in adverse water conditions, despite a setback in power efficiency (Zheng *et al.*, 1999). An overview of the use of parametric transduction in underwater communications can also be found by Kopp *et al.* (2000).

The signal processing techniques used to increase the clarity of acoustic communication signals have significantly improved telemetry performance over recent years. Particularly for the larger studies, many of the experiments have involved the use of testing platforms including acoustic receive arrays and vessel support. It is evident that the use of transducer arrays has a significant effect on telemetry performance. Also, the applied receiving techniques have typically been performed following data collection. These methods are an excellent way to develop the signal processing techniques required for underwater communication by providing real data for investigation. However, transplanting the spatial, computational and power capabilities expressed in the aforementioned studies to an individual device may prove difficult in the near future. It is therefore expected that most compact underwater acoustic modems utilising a single transducer would need emphasis on effective signal processing techniques and power efficient design. Additionally, the results involving spatial diversity suggest that an investigation into using compact receive arrays with commercial packages may be useful.

2.3 Simulation Methods and Analytical Performance

The most accurate way to evaluate the performance of underwater telemetry is through field experimentation. However, the considerable expense of conducting a field trial places an importance on developing modelling techniques to complement experimental data. Simulation of underwater acoustic communication provides a cost effective alternative to field trials. Channel simulators estimate the output of an underwater channel by applying a relevant model to the transmitted signal. The predictions from different models can vary significantly, each having merits in various areas. These areas include transmission loss studies, multipath prediction and noise prediction. A useful introduction to characterisation of a time-varying underwater acoustic channel for modelling subsea communication links can be found in Stojanovic and Preisig (2009).

An early notable discussion on acoustic communication simulations has been produced by Essebbar *et al.* (1994). The study consisted of two main elements. The first of these was the variations in the sound speed profile measured in the Mediterranean, which dramatically affected the propagation characteristics of the underwater channel. A distinction between the summer and winter periods was highlighted, with the winter period shown to produce a relatively uniform temperature profile. A channel simulator was then presented. Firstly this involved characterising the underwater channel by modelling the impulse response using a basic ray trace. The study demonstrated the suitability of considering discrete eigenrays incident on the receiver for performance simulations. Additionally, trials data were compared to the simulation results and showed that frequency spreading within a channel could be neglected for simulations. However, the Doppler shift would need to be considered for certain scenarios such as moving nodes.

Communication performance was also examined in the study by Essebbar *et al.* (1994) by counting the number of eigenrays incident on the receiver. The importance of the position of the transmitter and receiver relative to the thermocline was emphasised. Interestingly, it was found that amplitude fluctuations were evident

when there was a slight amount of transmitter/receiver motion. This may prove difficult for an equaliser to detect and compensate for. Furthermore, whilst a strong signal may be present at the depth of minimum sound velocity, it was indicated that the signals arriving via different paths would destructively interfere with each other causing fading. In this case, the receiving modem would be best located slightly below the sound speed minimum to provide a clear timing offset for the arrivals.

In addition to physical models such as ray tracing using geometric and oceanographic parameters, some studies utilise statistical methods to simulate the effects of an underwater channel, sometimes incorporating a time-varying transfer function. As there is still no standardised model to address short-term channel fluctuations, statistical models are typically estimated or obtained from field measurements and are incorporated into existing simulations. One example of incorporating short-term fluctuations has been presented by Viala *et al.* (2002) which demonstrated the potential of RAYSON software, a simulator capable of incorporating a time-varying impulse response. However, no implementation of the methods was demonstrated. As simulators became capable of incorporating time-variability to a channel model, various statistical methods were adopted and evaluated to determine the best fit to experimental results.

Demonstration of various simulation methods has been presented by Green and Rice (2004). This investigation used the properties of an underwater acoustic channel obtained from at-sea experiments as well as models such as ray traces from Bellhop (Appendix A.2.8). The impulse response was obtained using known channel details and applied to simulate the signal obtained at the receiver. Conversely, the use of a matched filter to estimate the impulse response given knowledge of the transmitted signal was discussed. Rate range, the time variation of symbol arrivals due to the relative node velocities was also introduced. In these experiments, noise obtained from artificial and recorded sources was introduced into the simulator. This included varying the amplitude of the induced noise according to the characteristics of the location. The simulator was run using Matlab. A simulated signal originating from an interfaced modem was fed to the input of a receiving modem in real-time. This allowed the simulation of an underwater channel without the need of repetitive and

expensive sea-trials. This method provided a good benchmark for predicting the performance of modems, provided the characteristics of the channel were already well known.

A simple simulator focusing on multipath propagation was described by Kraus and Kalangi (2004). This paper illustrated a scheme for channel simulation which accounted for reflections from the seabed and sea surface. Scattering and attenuation were considered at each boundary interaction in addition to a basic inclusion of sea noise. However, because the model assumed an isovelocity underwater channel, this simulator can only be considered a basic approach, useful for shallow water environments where multipath propagation is a more important consideration.

Munoz Gutierrez *et al.* (2005) investigated developing a simulator for channels suitable for 4800 bps QPSK transmission. The simulation focused on the effects of signal fading due to Doppler frequency spread and presented a simple simulation to predict the expected BER. In this experiment, refraction in the water column was not considered. Results show that as the number of eigenpaths increased, so did the bit error rate. This correlates with the expectation that multipath arrivals have a detrimental effect on signal reception.

A brief discussion by Hayward (2004) provided an overview of channel capacity estimation techniques based on Bellhop modelling. This study used experimental oceanographic data from previous measurements in 60 m of water including sound speed information reaching 100 m from the sea surface (into the seabed). It also assumed knowledge of the transfer function was perfect. The results demonstrated relatively high data rates (>100 kbps) for a 193 dB re 1 μ Pa @ 1 m source level from a 1 km to 20 km range. When compared to the actual data rates achieved in typical subsea communications, these unrealistic values highlight the poor predictability of a real underwater channel. Further work with estimating channel capacity of an underwater communications channel have been produced by Stojanovic (2006) and Socheleau *et al.* (2009, 2010), showing specific attention to statistical models. Evaluations of channel capacity estimations for typical shallow water scenarios have

been shown in a recent paper by Passerieux (2010), which also highlights the complicated nature of a subsea communications channel.

Experimental results of MFSK communication have been compared to simulations as carried out by Yang and Yang (2006). The 2, 4 and 8-FSK based signalling schemes were trialled in a depth of approximately 70 m with both array and single transducer deployments. Symbol separation was 12.5 ms with communication tested at ranges of up to approximately 4 km. The statistical simulations of BER were based on Rayleigh distribution and K distribution curves with predictions calculated as a function of the observed SNR. It was found that a significantly higher BER was measured than predicted by the Rayleigh curve. However, by using the experimental data to improve a K -distribution estimate, a good overall correlation was found. Similarly, Zhou and Shim (2008, 2009) used the Rayleigh fading channel in simulations and mapped the theoretical channel capacity based on the expected SNR.

A recent development for simulations tailored for underwater acoustic networks has been presented by King *et al.* (2009). This study used the latest Bellhop propagation model for determining the channel characteristics based on the geometry of the network and surrounding environment. The treatment of eigenrays provided for the transfer function of the channel which presented an understanding of the expected SNR and impact of ISI. The model also included the addition of wind dependant noise based on real data. It was anticipated that such a model would be included for current network simulators to provide a more accurate simulation based on environmental parameters rather than statistical channels.

The underwater communication simulator presented in this thesis (described in Section 3.3) builds onto the existing methods discussed in the aforementioned studies which utilised physical models, shown in Table 2.3.1. Specifically, the simulator incorporates a sophisticated physical channel model and compares the results to experiments where, in some cases, a substantial amount of environmental data was collected. This provided validation of the simulator in contrasting scenarios.

Table 2.3.1. Summary table of communication simulators (incorporating physical channel characteristics) presented in literature review, compared to the simulator presented in this thesis.

Publication	Factors in SSP	Factors in bathymetry	Factors in seabed type	Surface roughness	Time variation	Results / Experiments
Essebbbar et al (1994)	Yes	No	No	No	Transducer motion. Long-term SSP	Demonstrates effects of motion, seasonal variations
Kraus and Kalangi (2004)	Isovelocity	No	Yes – Single Layer	Yes	No	QPSK performance, no validation with experiment
Viala et al. (2002)	Yes – Range dependant	Yes – range dependant	Yes – Range dependant	No	Rayleigh, Rice channels	None
Hayward (2004)	Yes – Range dependent	No	Yes – Single Layer	No	Unknown	Theoretical channel capacity only, effect of internal waves studied
Munoz Gutierrez et al. (2005)	Proposed	Proposed	No	No	Rayleigh, Rice channels, Doppler spread	QPSK performance, no validation with experiment
Simulator presented in this thesis	Yes – Range independent	Yes – Range dependant	Yes – Multi-layer	Yes	Long-term - SSP, Wave height, Noise	FSK performance - Compared to experiments: deep, shallow, time-evolving

2.4 Networking and Protocol Standardisation

The use of underwater acoustic communication in subsea networking facilitates the unassisted retrieval of oceanographic data that is traditionally obtained using the deployment and recovery of data recording devices. In addition to providing a method to receive data in real-time, underwater networks provide the ability to react to changes in the environment as they occur. For example, the duty cycle of an underwater current profiler may be increased following a command originating from a nearby beacon that detects unusual wave movement at the surface. This would provide higher efficiency in all monitoring systems, particularly where there is a high cost associated with their deployment and recovery.

An introduction to the problems faced when developing an underwater acoustic network has been given by Proakis *et al.* (2001). Substantial papers with similar

themes have been produced by Akyildiz (2004), Heidemann *et al.* (2006) and Cui (2006), highlighting the additional constraints on underwater acoustic communication systems if they are to be utilised for networking. These restrictions include the low bandwidth limiting the frequency bands available for protocols, as well as high levels of signal delay due to the relatively slow speed of sound propagation. Additionally, Chitre *et al.* (2008) gives a recent overview of the factors of underwater acoustic communication relevant to subsea networking, including examples of their implementation.

One step towards adapting to the delays experienced in underwater networks was presented by Syed and Heidemann (2006). This paper demonstrates a new method of time synchronisation between nodes. Accurate clock synchronisation becomes particularly important for surveillance networks and long-term deployments where constant resynchronisation may be necessary. Additionally, the long-term deployments of underwater nodes increase the importance of modem power efficiency. Low power acoustic modems for use with short-range networks have been presented by Wills *et al.* (2006). The presented modems utilised non-coherent FSK modulation and priority was placed on minimising the power consumption for a predominantly idle sensor node.

The topology of a subsea network is dependant on the structure of the nodes as well as the priority of information flow. A centralised system provides a central station for all nodes to communicate through whereas distributed networks utilise individual connections between nodes. Multi-hop topology has been found to be the most energy efficient method (Sozer, 2000). This finding is expected as the multi-hop topology utilises connections between neighbouring nodes to transmit over the shortest distance towards the final destination. This method also minimises any possible network collisions, provided adequate packet routing systems are in place. For a subsea pipeline network, this would be the appropriate topology to use; however, additional redundancy would need to be implemented. These measures would allow for the possible recovery of a link using an ad-hoc connection should one or more modems fail.

Media Access Control (MAC) methods for undersea networks have widely been focussed on CDMA based systems, in conjunction with spread spectrum modulation techniques. A model Direct Sequence CDMA (DS-CDMA) system developed by Voudouri-Maniati (2002) showed promising results. This study involved multiple user access in simulations including scenarios with high noise levels. A similar study was presented by Mar and Seah (2006) for multi-hop networks under highly impulsive snapping shrimp noise, using a Rayleigh fading channel.

Experimental analysis of DS-CDMA performance was presented by Stojanovic and Freitag (2006). In the investigation, Quadrature Phase Shift Keying (QPSK) was utilised with DSSS achieving combined data rates of up to 10 kbps. The experiment utilised signals for four users, transmitted over a 2.3 km range off Italy in a water depth of approximately 100 m. Simulation of multiple users was achieved by adding each user's signal component to the transmitter output. Spatial diversity was implemented with an array of 12 hydrophones used to receive the signal, as well as coherent receiver algorithms including a DFE. Results demonstrated effective communication at high data rates in complex underwater channels with up to four users.

A milestone in subsea networking is represented by the Seaweb underwater networks, first deployed by the US Navy in the late 1990s (Rice *et al.*, 2000). This ongoing program aims to establish wide-area undersea surveillance systems by using a Deployable Autonomous Distributed System (DADS). This includes a backbone of stationary nodes as well as peripheral nodes involving mobile vehicles such as Autonomous Underwater Vehicles (AUVs). These sensors are linked to shore using gateway nodes acting as an interface to the sea surface for ongoing radio communications with land based control centres.

As the hardware used by the Seaweb program progresses, the modulation schemes vary; however, spread spectrum techniques (FHSS and DSSS) are typically utilised. The MAC protocols implemented on Seaweb deployments do not exclude the use of Time and Frequency Division Multiple Access (TDMA and FDMA) methods, but

instead attempt to use them in conjunction with the natively appropriate CDMA method. In addition to a sophisticated MAC layer, handshake and repeat request methods have also been established for the network as described by Creber *et al.* (2001).

The Seaweb program has since evolved into a fully integrated subsea network with server-side access to subsea communications (Fletcher *et al.*, 2003). Recent progress has allowed the deployed subsea network to configure itself using server-located neighbour tables. This measure ensures collisions are minimised and the status of neighbouring nodes are known for effective network management.

Underwater networks have become a popular method for real-time data delivery in many distributed subsea sensor networks. An example of an integrated system delivering oceanographic data from seabed sensors was presented by Codiga *et al.* (2004). Several nodes were deployed within a range of approximately 3 - 4 km with a depth ranging from 25 - 50 m. Existing infrastructure allowed for the easy integration of a gateway buoy for land-based access to the network using radio waves. As with Seaweb, the program utilised its own unique methods of signal conditioning and packet routing to obtain optimum results for the environment.

The integration of vehicles into subsea networks has been explored and demonstrated by Dunbabin *et al.* (2006). In the study, a series of eight underwater sensor nodes, “Aquaflecks” were distributed throughout a water column in an Olympic sized swimming pool. Each node encompassed integrated systems including a low-power and low-range non-coherent acoustic modem operating at 50 bps with a centre frequency of 30 kHz and an intended range of 20 m. Additionally, an optical communication system was used with a range of 2 - 8 m depending on conditions. This optical transfer system was capable of operating at a maximum rate of 320 kbps. By incorporating both methods of transfer an AUV was demonstrated to act as a data mule by collecting information systematically from each stationary node. This was done by first utilising low rate acoustic communication to achieve close proximity to the desired node, followed by optical methods to align and download data at much

higher speeds. The current progress of the program indicates the possibility of using a hybrid of communication techniques for the retrieval of substantial amounts of data. Furthermore, the navigation and operation of the AUV gives rise to the possibility of its use as a maintenance tool for an underwater sensor network.

It is evident from the literature that standards for modulation schemes and network protocols have not been established for underwater telemetry. Otnes *et al.* (2009) discussed the possible standardisation of underwater acoustic communications given the foreseen interference that will occur between acoustic devices as they become implemented more often. The key component in the presented description is a roadmap which requires the ordered implementation of standards. This begins with the standardisation of channel simulators to cater for the various implementations of acoustic modems. From here, the application of flexible modem software needs to be developed, so modems from different vendors can communicate with one another. A standard plan for frequency band usage would then follow. This would involve the allocation of specific bands for various acoustic devices, not just modems. Finally, a standard protocol simulator can be developed. Overall, such an implementation would take a considerable amount of time and effort but would be highly useful as has been shown with the standardisation of radio communications.

The simulation of acoustic communication for subsea networking has been developed in recent years. The ns2 network simulator is widely used for the simulation of network protocols in development. However, its use for high latency underwater acoustic applications is a relatively new achievement. A description of this use was presented by Harris and Zorzi (2007). The major aspects of the simulator were verified using other analytical methods where it was found to be accurate in comparison. As a result, ns2 modified for underwater acoustic telemetry may be suitable for the development of subsea network protocols.

2.5 The Kauai Experiment

A recent example of a comprehensive long-term performance study of underwater acoustic communication systems is the Kauai Experiment (KauaiEx). This was conducted between June and July 2003 off the coast of the Hawaiian island of Kauai. The aim of KauaiEx was to offer a detailed view of acoustic propagation in the frequency range of 8 - 50 kHz used for various subsea applications (Porter *et al.*, 2004). The most relevant purpose of the experiments was to relate underwater acoustic communication performance to changes in the environmental conditions. This goal included the consideration of a variety of modulation schemes. This study is most relevant to this thesis given the similarities in attempting to investigate the long-term variability of acoustic communication performance with changing environmental conditions.

The experimental setup for KauaiEx involved several pieces of subsea instrumentation being deployed between sophisticated and reconfigurable transmitting and receiving test beds. This is shown in Figure 2.5.1. The setup included two 16 element Vertical Linear Receive Arrays (VLAs), thermistor strings, waverider buoys, conductivity and temperature (CT) sensors and an Acoustic Doppler Current Profiler (ADCP) which were all deployed in line with the propagation path. The comprehensive sensor deployment provided monitoring of several environmental parameters. During the trial, the performance of modulation methods including FSK, PSK and Spread Spectrum signalling was measured.

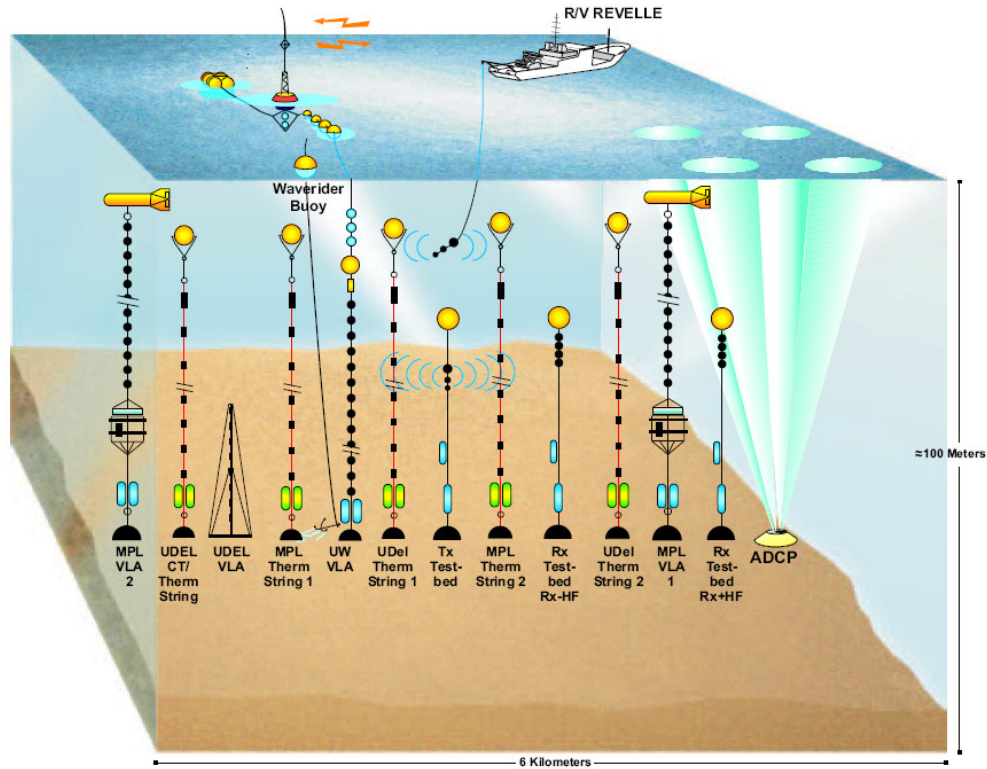


Figure 2.5.1. Illustration of the experimental setup for one of the KauaiEx deployments in 2003. This shows the various instruments deployed in addition to a sophisticated acoustic communications test bed. (Siderius, 2007)

A significant study of the area was performed using only data from the deployed thermistor strings. The arrays of 13 thermistors at depths ranging between 4 – 82 m collected the temperature of the water column over the deployment period. The sound speed was highly dependant on temperature for the depths considered in this study. Therefore, the temperature measurements spanning the water column can be considered an important factor when predicting the horizontal propagation of sound. Data from KauaiEx showed a relatively uniform mixed layer below the surface and a thermocline that typically occurred below 50 m. Furthermore, daily variations were evident when investigating the long-term trends of the temperature profile.

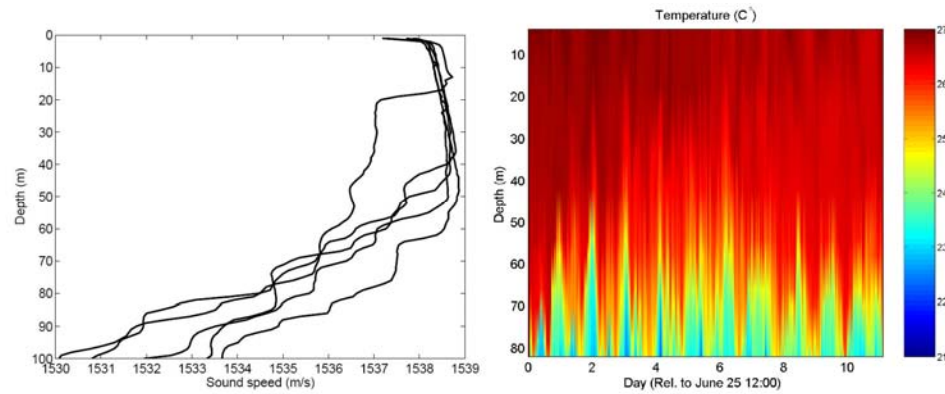


Figure 2.5.2. Sound speed variations observed on July 1, 2003 (left). Evolution of the temperature profile obtained from one of the thermistor strings over the duration of the experiment (right). (Siderius, 2007)

The performance of non-coherent communication techniques during KauaiEx has been investigated by Siderius (2004, 2007). Two separate bands of MFSK with 128 frequency components each and a spacing of 40 Hz were considered for transmission. The scheme utilised 4 frequencies to determine two bits of data, known as 1 of 4 coding. The scheme resulted in 30 sets of 2 determinant bits, giving 60 total bits. A symbol duration of 25 ms resulted in the overall data rate of 2400 bps for each transmission band. This relatively high data rate with no error correction algorithms was chosen deliberately to ensure the communication system was prone to errors. This enabled the performance to be quantified using the received BER.

Results obtained when operating in a frequency range of 8.0 – 13.2 kHz over 3 km showed the SNR to be sufficient for effective detection of the signal. After investigating signals received at different depths of the VLA, receivers at mid-depth performed in close comparison to those in a Rayleigh fading channel. Overall performance was found to improve with depth. This is consistent with the depth dependant speed of sound refracting the bulk of the energy toward the seabed. Additionally, a correlation was found between the measured temperature and performance over depth. Whilst this correlation could indicate a direct relationship, a more appropriate explanation would be the reduction of the thermocline steepness, promoting a more even distribution of ray paths. This explanation was confirmed during a period of a relative isovelocity channel, where receivers at deeper positions performed as poorly as those located throughout the rest of the water column.

A similar study with coherent BPSK was also conducted using the 3 km path during KauaiEx (Song *et al.*, 2008). Time reversal and DFE were implemented with spatial diversity exploited using two portions of the VLA; the top and bottom four receivers. Transmission involved a 10 s long BPSK signal with a carrier frequency of 12 kHz at 4000 symbols per second. The output SNR of the receiving processor (DFE, etc) was investigated to quantify communication performance.

The output SNR was found to fluctuate dramatically during the trial. In addition, performance measured in two different environmental scenarios (Figure 2.5.3) demonstrated results similar to those obtained for non-coherent communication. Specifically, periods where the thermocline was well defined resulted in better performance and vice versa. Rough seas were also found to negatively affect the performance in the mixed layer, whereas the performance of a deeper receiver was only slightly influenced.

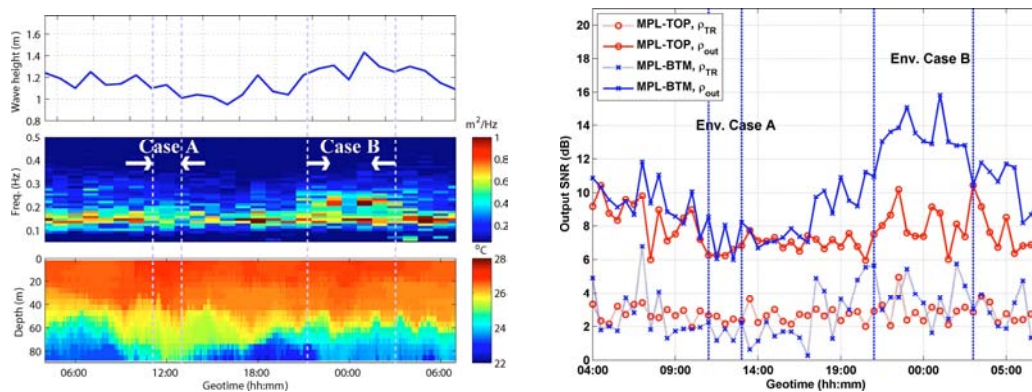


Figure 2.5.3. Effect of environmental characteristics on communication performance. Wave height, surface wave spectrum and evolution of the temperature profile (left). SNR (Final output and time reversal only), showing performance changes for each receiver set (top and bottom portions of the water column) over the trial period (right). (Song, 2008)

Overall, the KauaiEx program achieved several outcomes related to the long-term performance of acoustic modems. The performance of both coherent and non-coherent techniques was shown to fluctuate with environmental parameters including wave height as well as the temperature variations in the water column. This provides valuable information relating to performance expectations of underwater telemetry over long ranges on subsea pipelines, providing a promising outlook given that near-bottom communication in this case was most effective.

3 Methodology

3.1 Experimental Hardware

Two pairs of commercially available acoustic modems were acquired from different manufacturers for communication performance measurements. The DSSS-based AquaComm modem (Appendix D.1.1) was used for a preliminary study in a shallow water investigation. Operating at a frequency band of 16 - 30 kHz, the modems were expected to be limited in range when compared to lower frequency modems due to the absorption characteristics of the underwater channel. For the remainder of the trials, the FSK-based AQUAmodem (Appendix D.1.2) was used. This modem operated at lower frequencies of 7 – 11 kHz using a transducer with a hemispherical beam pattern and was intended for long range communication. Communication using these modems was expected to be more susceptible to channel fluctuations given the simplistic communication techniques employed by the devices. For example, the modems were expected to perform poorly in shallow water scenarios where high levels of multipath interference were likely. This susceptibility was considered a benefit for the study, providing performance data that was independent of advanced modulation or equalisation algorithms (described in Chapter 2) which allowed for a broader application of the results.

Two identical equipment packages were developed for modem integration. Each package included an ambient noise recorder and modem control unit to simultaneously collect environmental and communication performance data. A block diagram of this equipment is shown in Figure 3.1.1. The design and operation of the devices are described in the sections that follow.

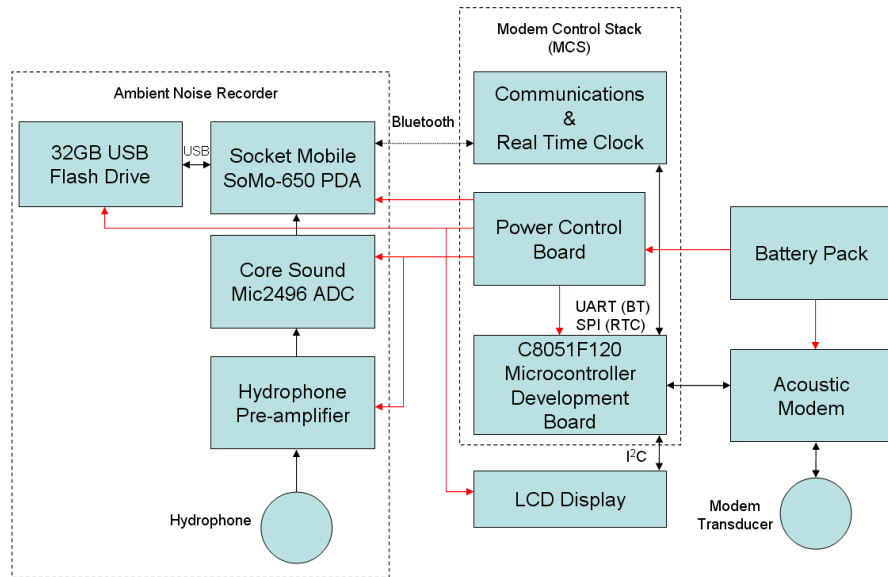


Figure 3.1.1. Block diagram of equipment developed for the analysis of underwater acoustic communication. Major components include a high frequency acoustic noise recorder, modem interface and advanced power control.

3.1.1 Ambient Noise Recorder

Ambient noise recordings needed to be carried out in the operating areas to understand the mechanisms affecting acoustic modem performance. The modem used in the majority of experiments (AQUAmodem) was able to record both the ambient noise levels and the received waveforms. Additionally, information about internal errors was available without requiring an interfaced logger. To compliment this data, an additional high frequency acoustic recording device was deployed to help independently assess modem performance. The overall collection of data helped establish the possible causes of performance issues such as anomalies in the physical channel and any technological problems faced by the modem units.

The recording component of the hardware (pictured in Figure 3.1.2) was built around the Mic2496 Analogue to Digital Converter (ADC) developed by Core Sound. Two hardware versions of the ADC were used, both capable of sample rates up to 192 kSamples/s with 16 bit resolution. The major differences between the two versions included a modified gain control mechanism and various interface improvements. The output from the ADC via either a fibre optic (TOSLINK) or

coaxial link was in a digital audio format: Sony/Philips Digital Interconnect Format (S/PDIF). When power was applied to the ADC, a digital audio stream was fed to a custom Compact Flash (CF) card designed to interface with computer hardware.

A Portable Digital Assistant (PDA) was used to receive the digital audio stream via its CF slot for processing. The Socket Mobile SoMo-650 supported all three interfaces critical to the operation of the recorder: CF slot for reception of the audio stream, Secure Digital (SD) card slot for temporary high-speed storage of the data and Universal Serial Bus (USB) host functionality, needed for high capacity external storage. Any external storage device formatted in FAT32 could be utilised by the USB host function. However, conventional hard disk drives were found to consume significant amounts of power, particularly during power-up. This was a concern as long-term deployments required the device to be regularly cycled on and off. USB flash drives were found to consume significantly less power and provided capacities up to 32 GB with very little physical space requirement. Consequently, USB drives were used in the deployments presented here, along with SD card access for intermediate storage.



Figure 3.1.2. The primary components of the underwater recording system. The SoMo650 (left), PDAudio CF interface (top) and Mic2496 ADC (right) were all integrated to function as a high frequency underwater acoustic recorder.

A Marconi SH101X spherical hydrophone was used in all the deployments by both recorders, yielding an upper frequency limit of 100 kHz (see Figure 3.1.3 for the calibration curve). The hydrophone output was passed through a pre-amplifier located directly beneath the end-cap of the underwater housing to maximise shielding from the recorder components. Two 20 dB pre-amplifiers were aligned in series to provide an expected total gain of 40 dB, with any additional gain from the ADC minimised. Following calibration, the total system gain was found to be 40.25 dB.

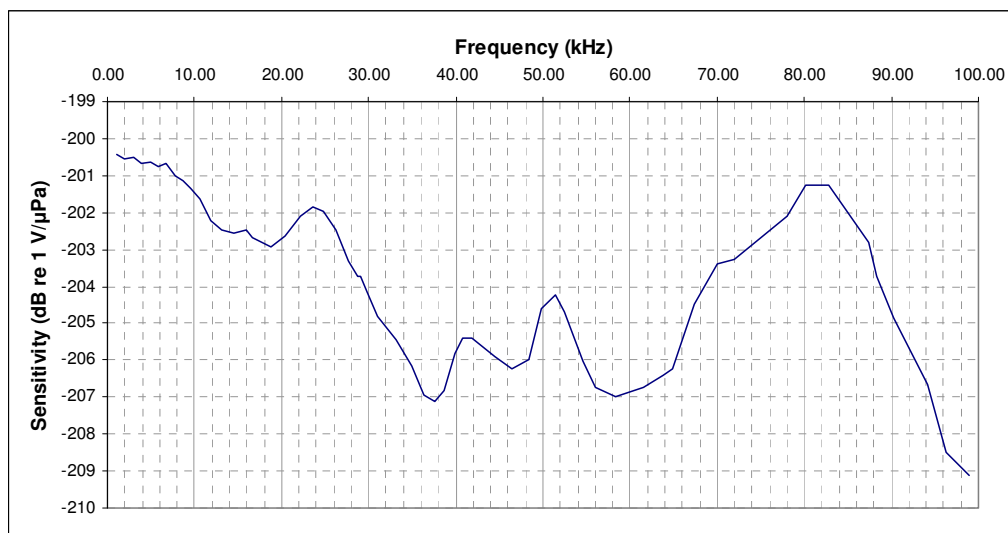


Figure 3.1.3. Free field sensitivity frequency response of the Marconi SH101X spherical hydrophone, digitised from the specification sheet.

3.1.2 Modem Control Stack

All subsea components were controlled by a set of electronics later named the Modem Control Stack (MCS). These components included a Silicon Laboratories C8051F120 microcontroller, operating at a clock speed of 100 MHz. The microcontroller provided two Universal Asynchronous Receiver / Transmitters (UARTs) for simultaneous serial communication with the recording device and any interfaced underwater acoustic modem.

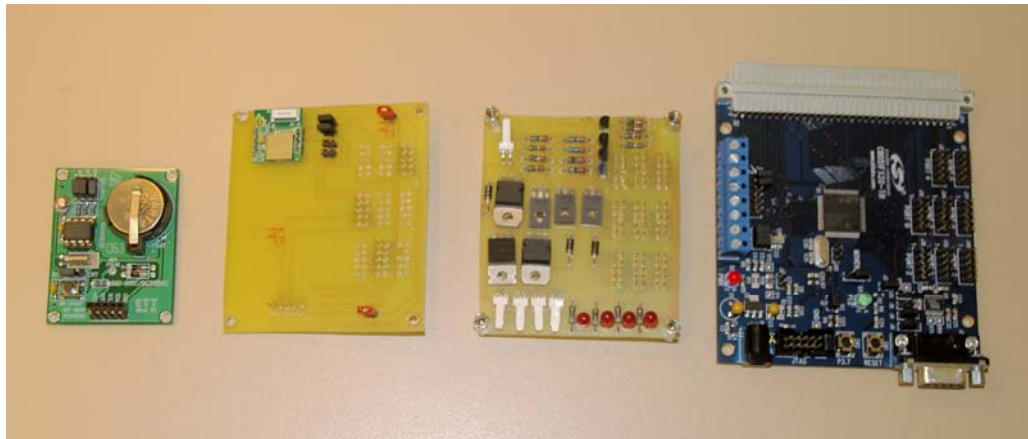


Figure 3.1.4. Photo showing spread view of Modem Control Stack components including (left to right) Real Time Clock Module, Communication Board, Power Control Board and Silicon Laboratories C8051F120 Development Board.

Two additional electronic boards were built specifically to interface with the C8051F120 development board via stackable pin-out connectors. The schematics and PCB designs of these can be found in Appendices D.2 and D.3. The first of the boards was designed primarily to control the power consumption of the entire unit. This involved 4 controllable solid state switches each with an output connector for its intended application. Three of these controllable outputs were 5 V supplies for logical devices including the PDA, Flash Disk and the Liquid Crystal Display (LCD) module used in some deployments. The other power output was a generic route of the input voltage to be directed externally to devices such as the recording ADC and pre-amp. The power control board provided comprehensive control of the power routed throughout the MCS. Other debugging tools were added to this board such as LED indicators; however, these were not used during deployment to conserve power.

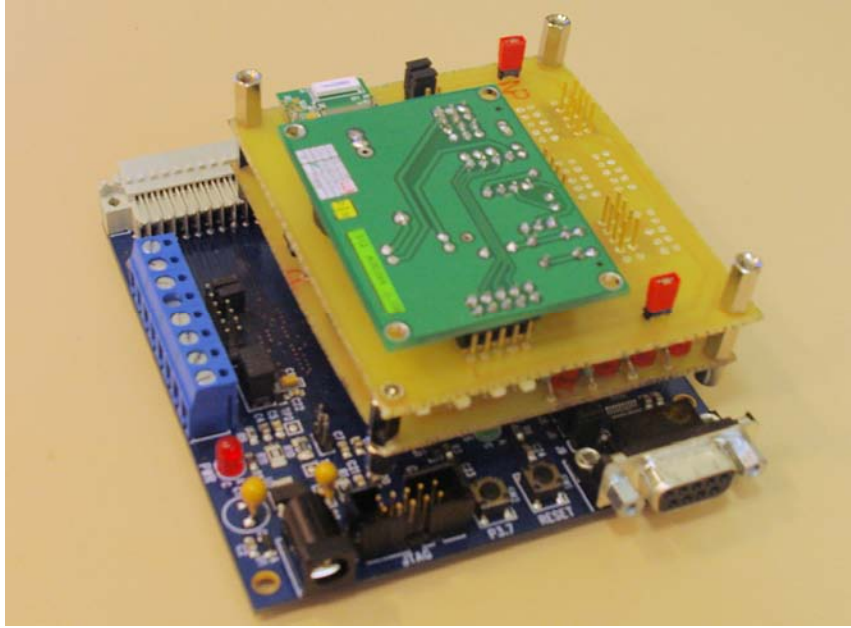


Figure 3.1.5. Photo of assembled Modem Control Stack. This included (top to bottom) the Real Time Clock, Communications Board, Power Control Board and finally the commercially available C8051F120 development board.

A communications board allowed for the integration of all components used in the experiments. This provided a gateway to the PDA and all other devices attached to the instrument. A Bluetooth module (Promi-ESD-02) was interfaced to one of the UARTs of the microcontroller providing a seamless low power serial communications link which compensated for the lack of RS232 support on the PDA. Additionally, the communications board was interfaced to a Real Time Clock (RTC) unit. The onboard RTC chip was the Philips PCF8583 and the onboard crystal was replaced with a more accurate version to minimise clock drift. The RTC provided the microcontroller with the ability to accurately keep track of time without the use of the PDA, which was crucial to the scheduling of the system.

For most of the shallow water experiments, a plastic housing was used for non-recording hardware. To take advantage of the transparent end-cap, a 20 x 4 character LCD Module was attached and interfaced with the MCS which provided detailed data to the user. Output information included recording status as well as modem success rates. This feedback greatly improved deployment efficiency, providing information to the user while field trials were ongoing.

3.2 Embedded Software Development

3.2.1 C8051F120: ModCon

Low-level control of the experimental hardware was provided by a software package developed for the MCS, named *ModCon*. A basic outline of the flow of this software is shown in Figure 3.2.1. For a comprehensive description of *ModCon* functions, refer to Appendix D.4. For access to the source code, please contact the author.

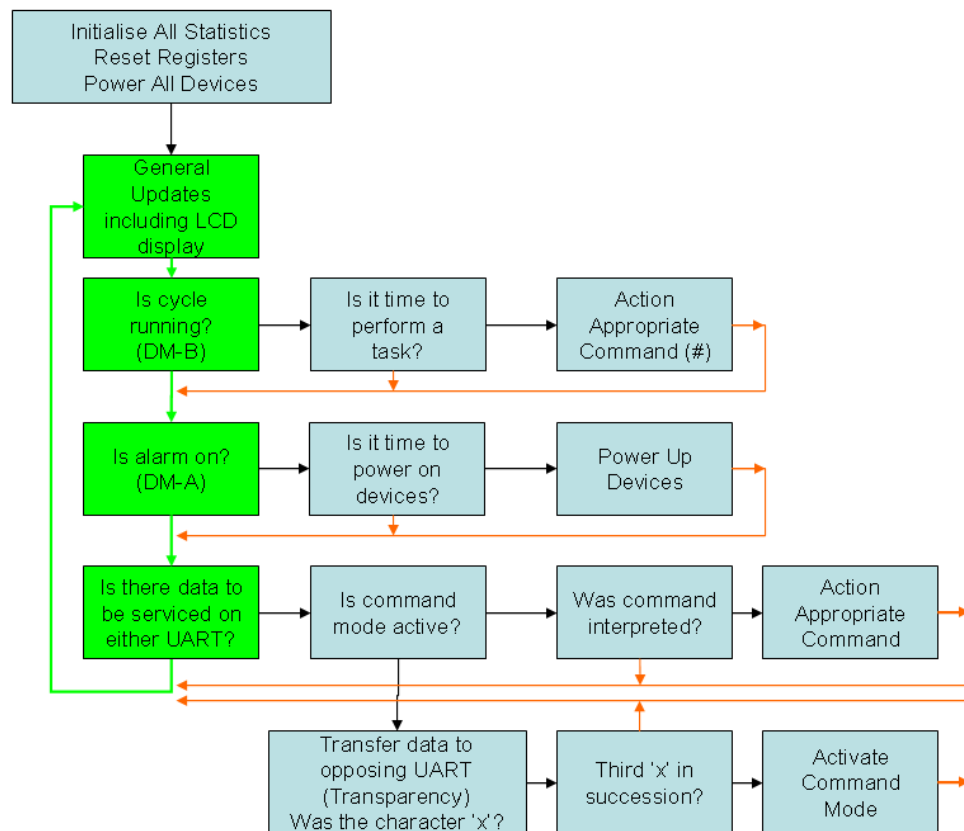


Figure 3.2.1. Flow Diagram of ModCon. The majority of the flow is dependant on the initiation of commands from either the scheduling system or a command transmitted via a UART. Additional information about the individual commands can be found in Appendix D.4

Developed in C, *ModCon* was based on command interpretation to handle communication with all hardware connected via both UARTs of the C8051F120. Additionally, routines were developed to translate commands from the PDA to a format recognised by the attached modem. A function was also implemented to

provide seamless communication between the two UARTs. This was useful for many aspects of the development by allowing the debugging of modem equipment without the need to dismantle the connection to the MCS.

Power routines were developed that allowed the MCS to route power to individual devices by toggling the output pins of the power control board. In addition, the power routing functions were fully accessible via the command interpreter. The MCS was able to preserve battery life by utilising these routines. RTC commands also provided easy access to date and time information. The RTC was fully customisable via the command interpreter, allowing the writing and reading of clock information during deployment. LCD routines were also developed to provide access to the display module fitted to the plastic housing. This allowed external devices such as the PDA to provide additional feedback to the LCD screen via the MCS.

Scheduling was provided using two methods. Deployment mode A utilised a comparison of the RTC with a given alarm time. As the MCS cycled through service routines, the RTC was regularly monitored until the required date and time was reached. At this point, power was applied to the PDA which handled the rest of the high level scheduling using software developed specifically for the deployments (*PDALogger*, Section 3.2.2). Following execution of the wake-up procedure, the MCS alarm was disabled until another schedule was initiated, dependant on higher level control. Deployment mode B provided a scheduling system independent of other software or external input, providing a schedule based solely on duty cycles of the microcontroller. This was hardcoded into *ModCon* before deployment, executing particular routines at given minute intervals. This scheme was a more robust method of scheduling, independent of other devices or user interaction. Furthermore, this made the system mostly unaffected by any reset should a short-term power failure have occurred in the field.

3.2.2 SoMo650: PDALogger

The majority of user input/output was performed via the PDA when the device was operational. This was done using software developed for the PDA, utilising the touch screen display. The main package running on the SoMo650 was named *PDALogger* and was initially designed only for the noise recording component of the trials. However, it became increasingly useful in the high level control of the deployment, particularly due to the simplicity in executing functions at set time intervals. In addition, the large memory capability in the SoMo650 was taken advantage of, capable of storing hundreds of scheduled tasks for the *PDALogger* software.

The primary purpose of the PDA system was to utilise the CF slot input for a digital data stream and to store it direct to flash disk. This task was performed by bundled software, *Live2496* developed by Gordon Gidluck. With the recordings configured to commence upon start-up of *Live2496*, the *PDALogger* software was able to directly control the starting and stopping of the ambient noise recordings by calling and terminating the *Live2496* process.

The advantage of using *PDALogger* to perform higher level control of the recording and modem commands was the ease in customising the system on-the-fly. In contrast to hard coding the ModCon schedule, *PDALogger* provided a detailed user interface, allowing essentially all variables of a deployment to be customised following code compilation. This included the times, dates and actions of the recorder. The user interface also provided immediate diagnostic updates should any problems regarding the attached hardware occur. The ability of the software to write to files also proved useful, allowing the logging of all tasks and trial results to non-volatile memory in real-time. A screenshot of *PDALogger* in operation is presented in Figure 3.2.2

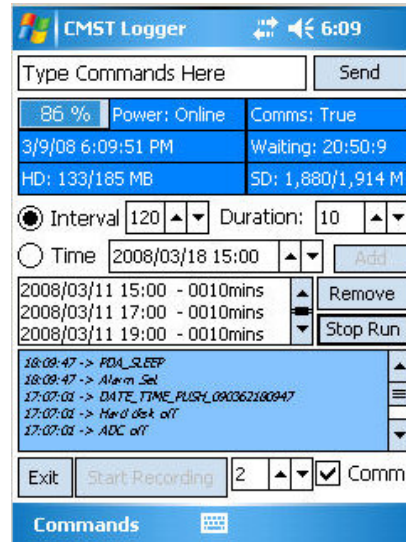


Figure 3.2.2. Screenshot of *PDALogger*, showing the user interface and example of scheduled recordings. The bottom panel also provided a preview of the latest logged events.

For high speed recordings of 176.6 kSamples/s or more, recording directly to USB was an unstable procedure. A watchdog service was implemented to monitor the recording process which would restart Live2496 should a recording fail. In addition, writing to high capacity USB devices including mechanical hard disks produced high amounts of electronic noise and power loss. To combat these problems, the software was able to utilise the SD slot in the SoMo650 to buffer up to 2GB of recording data to the SD card. During recording, *PDALogger* monitored the SD card capacity to determine when a data transfer to the hard disk was required. By taking advantage of the power features on the MCS, all unnecessary devices were turned off during this procedure. Overall, however, this method consumed more power than writing directly to disk. Consequently, the SD routines were only utilised for high speed recordings and when a mechanical hard disk was used.

As with *ModCon*, the software flow of *PDALogger* was controlled by both the schedule set internally as well as a command interpreter designed to handle inputs from the Bluetooth serial port. This flow is outlined in Figure 3.2.3. The serial inputs comprised mostly data deliberately transmitted by *ModCon* to be logged to PDA memory. However several commands were also available to perform tasks such as clock synchronisation, remote scheduling and power control. For a comprehensive description of *PDALogger* routines, refer to Appendix D.5.

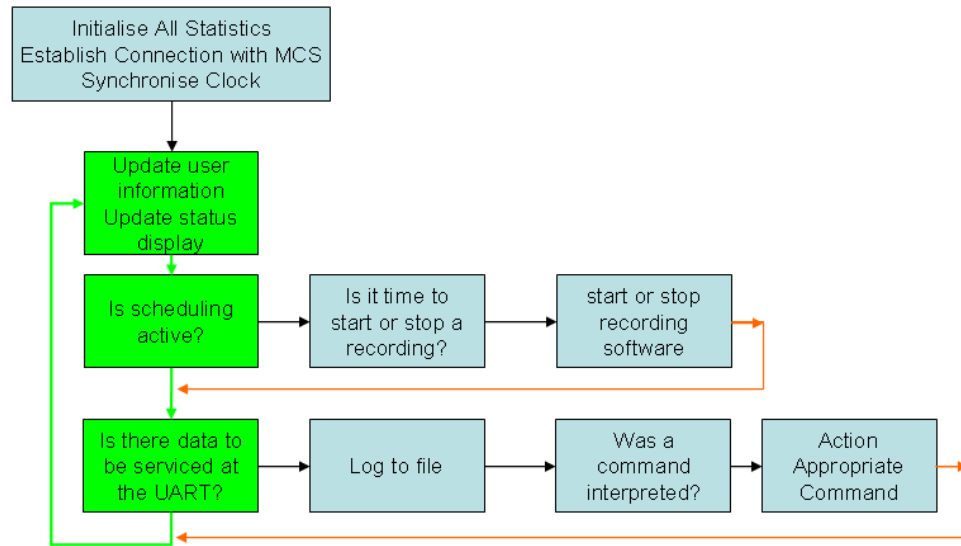


Figure 3.2.3. Basic flow diagram of *PDALogger* showing basic outline of program cycle. Additional information about the individual commands can be found in Appendix D.5

PDALogger was developed with the power saving qualities of the PDA integrated into the schedule routine. By using the alarm function of *ModCon*, the software placed the PDA into a sleep state when a recording was complete to be woken up a minute before the next schedule began. When the device was brought out of sleep, *PDALogger* continued to function from its original program state, retaining saved schedules and re-establishing Bluetooth connectivity with the MCS. The software was developed to fully compliment *ModCon* in Deployment Mode A.

3.2.3 SoMo650: PDALogger Skinny

Following the development of Deployment Mode B on *ModCon*, much of *PDALogger* was redundant. This included the scheduling functions which, in Deployment Mode B were controlled by the MCS. To streamline functionality, a separate item of PDA software was used to perform core functions. *PDALogger Skinny* was designed to synchronise with the MCS and start recording upon start-up. This mode of operation meant the PDA was no longer placed in sleep mode, but rather completely turned off. A flow diagram of the package can be seen in Figure 3.2.4. A comprehensive list of the functions can be located in Appendix D.6.

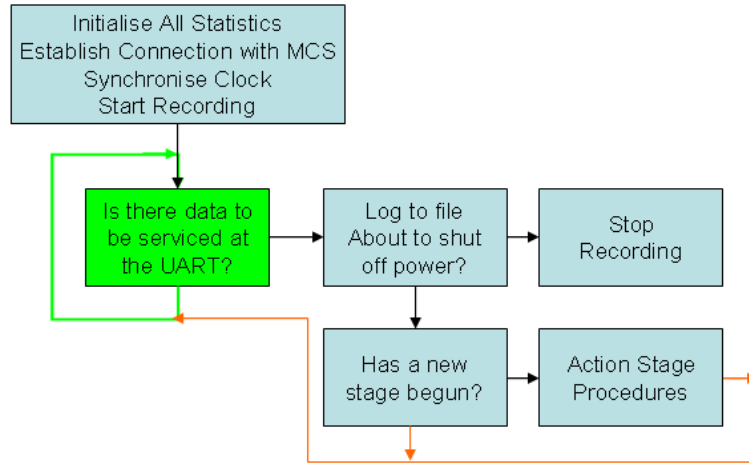


Figure 3.2.4. Basic flow diagram of *PDALogger Skinny*, demonstrating a much more simple cycle designed to complement deployment mode B. Additional information about the individual commands can be found in Appendix D.6

Unlike the original version of *PDALogger*, there was no user interface for *PDALogger Skinny*, apart from a range of functions intended for administrative and debugging use. The MCS relayed all information regarding modem communication deployment to the PDA software allowing the logging of all events for later analysis. Redundancy built into the software ensured that recording occurred regardless of whether or not a Bluetooth connection or time synchronisation was successful.

For high speed recordings requiring the use of the SD card, *PDALogger Skinny* was set up much the same as the original version. However, transfer of the recordings to the hard disk occurred immediately after each recording, rather than only when the SD card was nearly full. This ensured that recordings were not interrupted in the event of a full SD card. Also, whilst power to the PDA was removed after a predetermined interval as a precaution, regular operation involved *PDALogger Skinny* sending a completion code to ModCon via Bluetooth when data transfer was complete. Power was then removed from the devices before the next cycle began, ensuring maximum power saving.

3.3 Underwater Acoustic Communication Simulator

Considerable time and expense is involved in conducting field trials to assess the performance of underwater acoustic communication protocols. As a result, underwater acoustic communication simulators are becoming widely adopted for use in developing protocols and testing them in various environments. As part of this program, various trial environments were modelled to simulate the deployments presented in the experimental sections. In addition to acoustic propagation models, an acoustic communication simulator was constructed to assess the performance of the FSK modulation techniques employed by the AQUAmodem. This section presents the design of the acoustic communication simulator which is based on the Bellhop beam tracing code (Appendix A.2.8). Results of acoustic propagation modelling and the subsequent communication performance simulations are shown later, accompanying the related experimental sections.

The underwater acoustic communication simulator comprised several layered functions which were divided into modules. The structure of these modules is shown in Figure 3.3.1, depicting the stages of predicting modem performance.

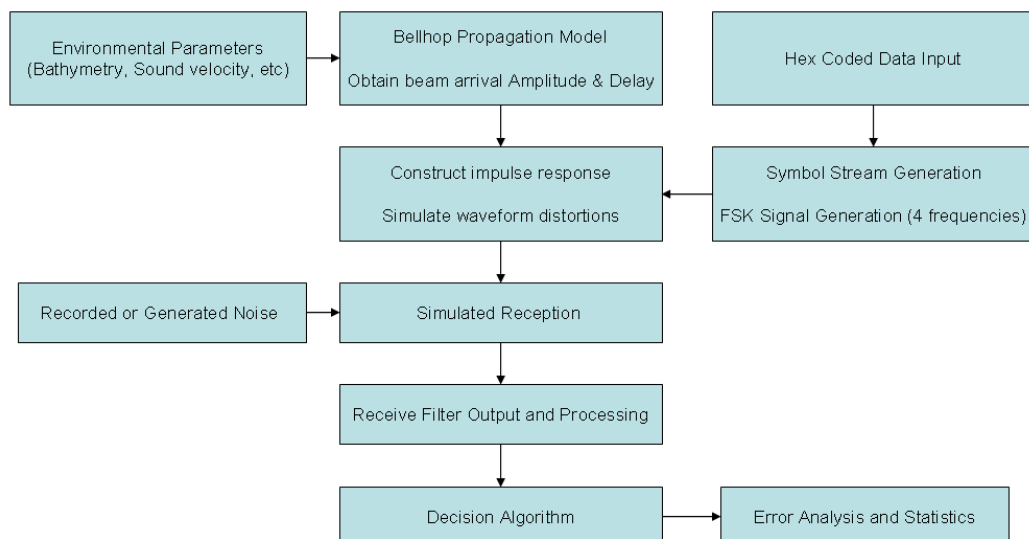


Figure 3.3.1. Block diagram of the underwater acoustic communications simulator. The simulator used environmental information with Bellhop propagation code to produce and analyse a simulated received waveform which was then compared to the input.

3.3.1 Data and Signal Generation

The AQUAmodem processes each byte as two nibbles (4-bit words). Each nibble is represented by a hexadecimal character and a unique four-tone sequence. Similarly, the simulator developed for this study first processed an input stream of hexadecimal characters for transmission. Following generation of the character stream, a tone sequence was encoded using a look-up table. Each individual tone lasted 10 ms. This timing equated to 8 tones (80 ms) for each byte which resulted in a total data rate of 12.5 bytes per second or 100 bits per second.

Error correction codes were not added to the input stream. However, the modulation scheme utilised each of four possible tones only once for each nibble. This resulted in 24 usable tone combinations out of a possible 256 in each sequence. Of these, 16 combinations represented data symbols, while the others were likely used by the modem manufacturer for other functions such as synchronisation and testing. This redundancy was taken into account at the simulator receiver and is discussed later. A source level of 180 dB re 1 μ Pa @ 1 m was used for the simulations presented here, representing the maximum capabilities of the acoustic modem. However, the source levels used by the modems during each field trial were not calibrated, likely to have been between 168 – 180 dB re 1 μ Pa @ 1 m. Consequently, the noise input level in simulations was offset to obtain the SNR measured during experimentation.

Figure 3.3.2 shows the spectrogram of an example transmission which was used as the test transmission for all presented simulations. The corresponding hexadecimal code was:

01234567890ABCDEF44724772616E745075736579F

The code utilised all possible hexadecimal characters with an additional character string of the author's hopeful name following examination. To add a random element to the transmission, the order was slightly skewed and the characters '0' and 'F' were utilised twice, given their more likely occurrence in real data. At 21 bytes the transmission of the simulated signal encoded with the test string lasted 1.66 s.

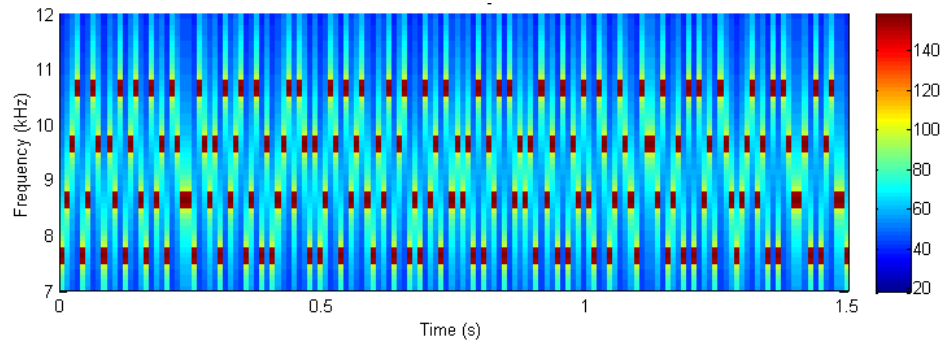


Figure 3.3.2. Spectrogram of the generated signal obtained from a test input hexadecimal character string (01234567890ABCDEF44724772616E745075736579F). The modulation scheme mimicked that of the AQUAmodem for comparison with trial data.

3.3.2 Received Signal Simulation

The simulator utilised Bellhop for the acoustic propagation modelling. Developed by Mike Porter from HLS Laboratories, Bellhop utilises Gaussian beam tracing, an adaption of ray tracing code, to model transmission loss throughout the water column. More on ray tracing theory and Bellhop can be found in Appendix A.2.8. In addition to ray trace diagrams and transmission loss calculations, the model calculates arrival delays and amplitudes for each ray path.

The Bellhop propagation modelling was executed via the Centre for Marine Science and Technology (CMST) Underwater Acoustic Propagation Modelling Software (AcTUP). For the simulator presented here, AcTUP was called to run the propagation model with parameters specific to the simulation. These variables included environmental conditions such as the sound speed profile and bathymetry, as well as model parameters including the number of rays for the simulation and receiver locations. As shown later, some simulations involved receivers spanning the entire water column, whilst others focussed on a specific region of interest.

The output from the Bellhop model provided amplitude, phase and delay information for each ray connecting the source and receiver. This information was used to calculate the transfer function of the underwater channel as the temporal impulse response. As an example, consider a downward sloping bathymetry with a Sound

Speed Profile (SSP) exhibiting a thermocline (Figure 4.3.10) which is investigated later in Section 4.3.5. Figure 3.3.3 shows the resulting absolute value of the impulse response and phase inversions for a receiver located at a depth of 25 m, approximately 1000 m from a similarly deployed transmitter. The arrivals shown in the calculated impulse response were consistent with the reflected arrivals shown in the ray trace (Figure 4.3.10). To illustrate the absence of a direct path at longer range, the impulse response for a receiver placed 4000 m from the transmitter is also shown in Figure 3.3.3. At close range, the two closely spaced arrivals of opposing phase (inverted amplitude) represented the direct path and the reflection from the sea surface. At 4000 m, the first arrivals involved a cluster of reflected rays, likely to cause interference with one another.

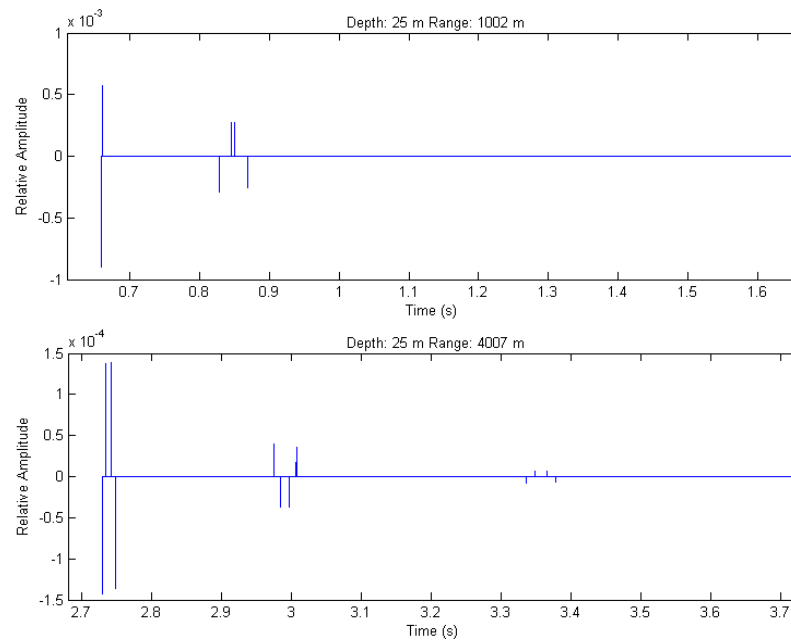


Figure 3.3.3. Impulse response as calculated from the arrival amplitude and delay result from the Bellhop propagation model. Two ranges are shown: At 1 km, the first arrivals comprised the direct path and the reflection (top), at 4 km the direct path was not present with reflections constituting the first ‘set’ of arrivals (bottom).

The communication simulator was capable of adjusting the impulse response to account for sea surface roughness before producing the final signal for analysis. This was done by multiplying the amplitude of each ray arrival by \check{R}^N , where \check{R} was obtained from Equation A.9 and N was the number of surface reflections. The use of this feature was limited to only one simulation in this thesis where wave height data was available. This wave height adjustment is shown in more detail in Section 5.4.

The generated signal was convolved with the impulse response to produce the received waveform. Although the impulse response diagrams only illustrated phase inversion, the convolution method used in this simulator involved multiplying the complex amplitude of each arrival by the generated waveform to incorporate phase. The resulting signals for each arrival were then added to produce the output of the simulator. The spectrogram of the simulated signals following processing is shown in Figure 3.3.4, demonstrating the effect of the impulse responses in Figure 3.3.3.

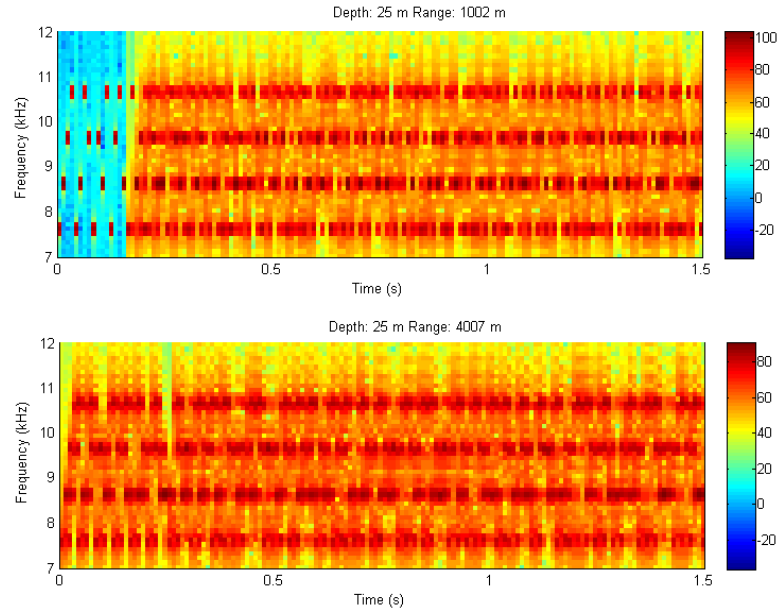


Figure 3.3.4. Spectrogram of the simulated received signal for the corresponding positions shown in Figure 3.3.3.

3.3.3 Noise Generation

The generated noise in the simulator was designed to replicate the noise as characterised at each deployment location. As the carrier frequencies were close together with little disparity in the spectral power, the primary issue for noise generation was estimation of the amplitude distribution. To investigate the appropriate type of noise to generate, the amplitude statistics were obtained from ambient noise data from the previous experiments. An amplitude histogram was calculated for ambient noise data collected from the three Australian trials (Sections 4.1, 4.2 and 5). The distributions were compared to the equivalent normal (Gaussian) distribution. This comparison is shown in Figure 3.3.5.

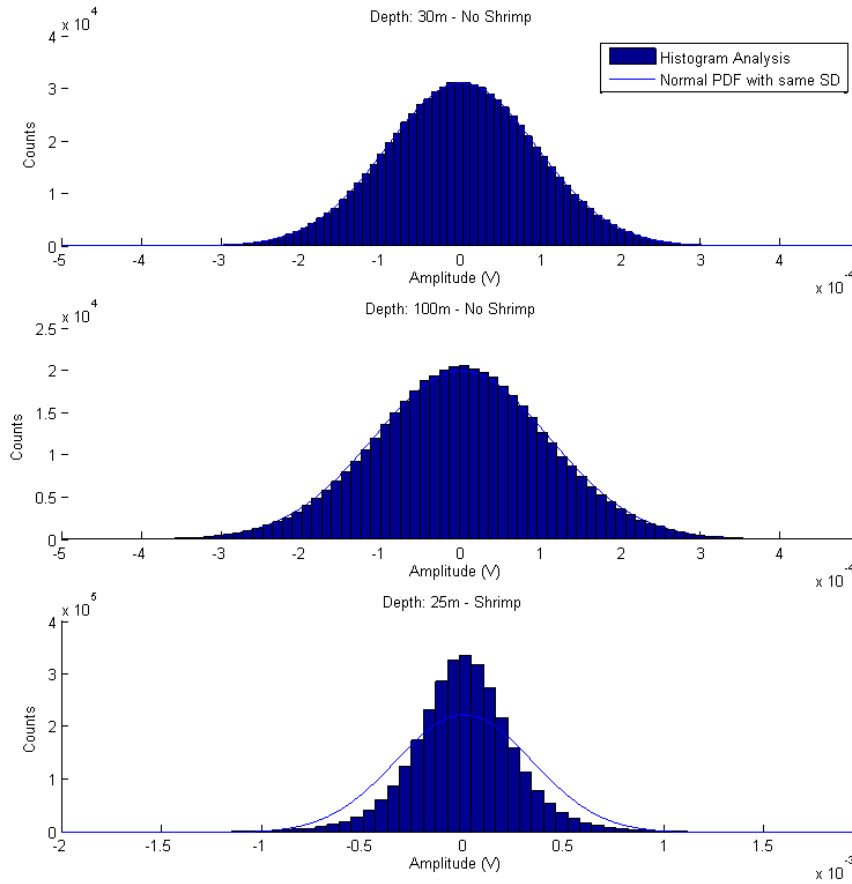


Figure 3.3.5. Amplitude distributions for noise collected during the trials off the coast of Perth, Western Australia. Noise from trials discussed in Section 4.2 (top) and Section 5 (middle) were found to exhibit Gaussian amplitude statistics. The shallow trial discussed in Section 4.1 revealed a non-Gaussian amplitude distribution (bottom) due to the occurrence of snapping shrimp near the receiver.

Statistics acquired from the shallow deployment off the coast of Hillarys demonstrated non-Gaussian noise distribution. This finding was attributed to the existence of snapping shrimp in the environment which has been found by Legg (2009) to complicate amplitude statistics. Conversely, data from the deeper water deployments demonstrated a good agreement with a normal distribution. This result justified applying Gaussian noise to the simulated waveform before feeding the signal to the receiver algorithm. However, when consideration of the effects of snapping shrimp is required (particularly for shallower environments) the noise statistics would require a different statistical model.

3.3.4 Data Analysis and Verification

The signal acquisition method used by the AQUAmodems was unknown and could not be replicated in the simulator. Therefore, the default method of signal synchronisation ('first' method) involved acquisition of the signal from the point of first ray arrival. However, in some of the trials this method was unrealistic in terms of predicting realistic modem behaviour, particularly where Bellhop predicted a first arrival of very low amplitude. As an alternative method, the 'max' method of synchronisation acquired the signal at the point of arrival of the ray with maximum amplitude. It is noted in the thesis where the use of the 'max' synchronisation method is used as an alternative algorithm.

Following signal acquisition using one of the two described methods, the signal was fed through to the receiver module of the simulator. This module consisted of various levels of processing. The first stage involved separating the simulated signal into four filtered outputs using Butterworth filters with a bandwidth of 400 Hz, centred at each of the carrier frequencies. As the experiments and simulations involved stationary nodes, it was assumed that the Doppler Effect could be ignored. Each filter output was processed to obtain the mean squared pressure levels for comparison. Figure 3.3.6 shows the output at this stage for both the source and simulated received waveforms.

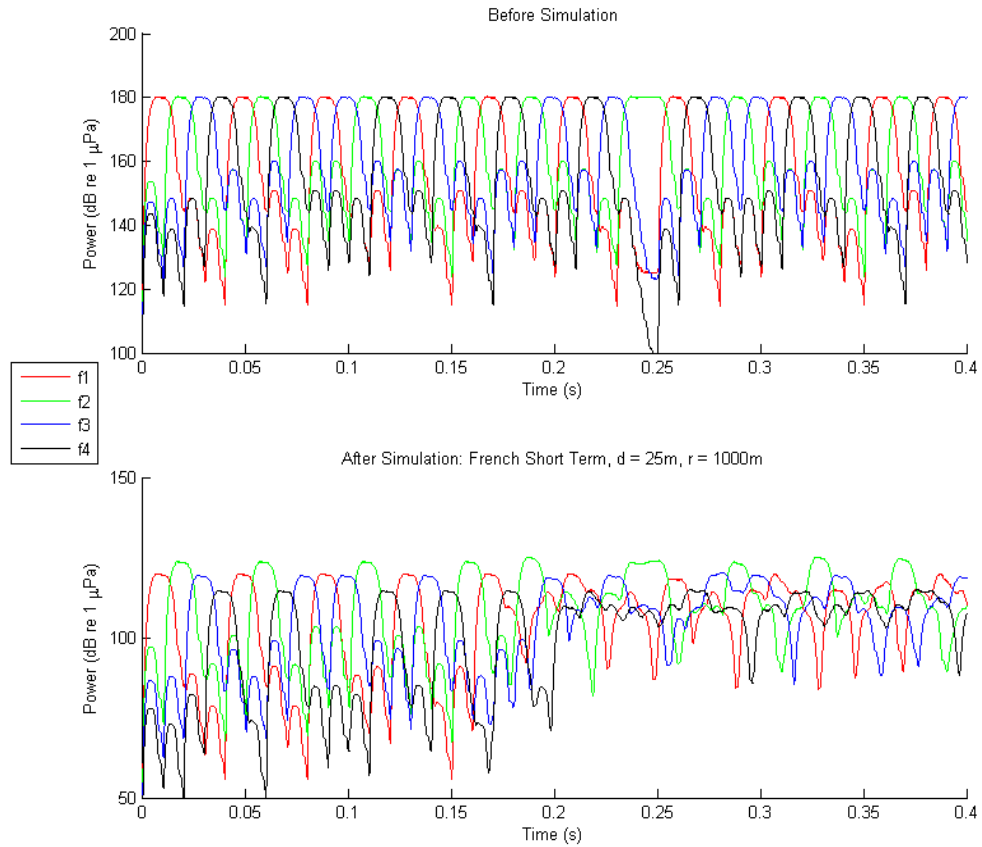


Figure 3.3.6. Output of the band-pass filters for each carrier component, f for the source (top) and simulated received (bottom) waveforms. The signal was generated from the hexadecimal string: 01234567890ABCDEF44724772616E745075736579F.

The average power present in each filter output within each tone period was stored to memory for comparison. The filter output yielding the highest power represented the most likely transmitted tone. The receiver accounted for the redundancy provided by the modulation scheme, given the finite number of tone combinations needed to form each 4-bit word. Each symbol decision was made in chronological order, comparing the symbol stream with a look-up table of known combinations. Each subsequent decision was based on the remaining possibilities. Due to the method used in the decision algorithm, one incorrect symbol decision resulted in errors for any that followed within the same nibble. Figure 3.3.7 shows the symbol success over time for the test transmission using the algorithm with and without including the redundancy. In this simulation, the redundancy was shown to dramatically improve overall performance.

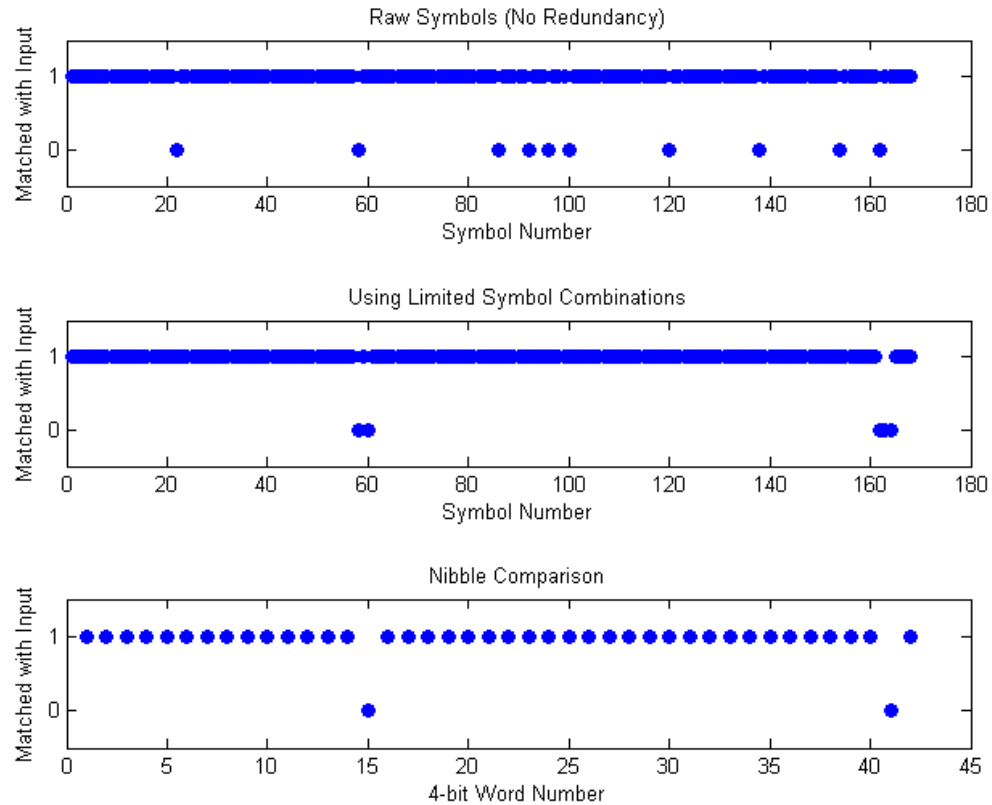


Figure 3.3.7. Comparison result for the example simulation with a range of 1 km. The raw decisions (top) were processed using the modulation scheme redundancy to produce a symbol stream estimate (middle). After converting back into a series of 4-bit words, two were found to be incorrectly resolved by the receiver (bottom).

Following the symbol decision process, each 4-bit word was determined using the same look-up table as utilised at the transmitter, and the hexadecimal character string was reconstructed for comparison and evaluation. The raw BER was established at the nibble level by comparing the received hex string with the original input. For the example simulation presented in this section (based on the summer simulation presented in Section 4.3.5), the raw BER was found to be 4.8 % at a receiver depth of 25 m and range of 1 km.

4 Spatial Investigation of Communication Performance in Short-term Trials

This chapter describes three short-term field trials carried out both locally and internationally to collect information regarding acoustic modem performance in contrasting environments. The first two trials were performed off the coast of Perth, Western Australia, conducted in shallow water using the equipment described in Section 3.1. A deeper water trial was conducted off the coast of Nice, France using stand-alone modems. An additional set of trials performed in the Arctic determined the effects of vessel noise and increased data rates on performance. However, a lack of environmental data limited the analysis so a detailed report has been consigned to Appendix B. The simulator described in Section 3.3 was implemented to provide two-dimensional (range-depth) performance prediction grids for two trials presented in this chapter. The results of these simulations and comparisons with field data are also presented in the relevant sections.

4.1 Perth Initial Communication and Localisation Trial

4.1.1 Experimental Setup

Following controlled testing of the high frequency recorders a short-term field trial was performed approximately 7 km off the coast of Perth, Western Australia. This deployment took place on 14th July 2008 and was carried out over approximately 5 hours. The aims of the experiment were to assess the field performance of the underwater acoustic recorder and MCS in the early stages of development. However, the adequate performance of the hardware during this test resulted in the acquisition of acoustic and communication performance data which were subsequently analysed. In this trial the DSPComm AquaComm modems were used, operating with a DSSS modulation scheme at 100 bps with the default settings.

For the short range trial a single high frequency recorder was used in conjunction with a primarily receiving modem. A sampling rate of 96 kHz was chosen to ensure stability and acquisition within the frequency bands used for communication. This acoustic package was deployed in a deep-water housing on the seabed in a water depth of approximately 22 m. Both the recorder hydrophone and modem transducer were located at the top of the housing, facing upwards, approximately 25 cm from the seabed. This configuration was expected to help reduce the impact of noise from seabed sources such as snapping shrimp. A T-bar was used to ensure the housing orientation remained the same for the duration of the deployment. Figure 4.1.1 is a photograph of the housing shortly before one of the test deployments and also shows the transducers and electronic components.

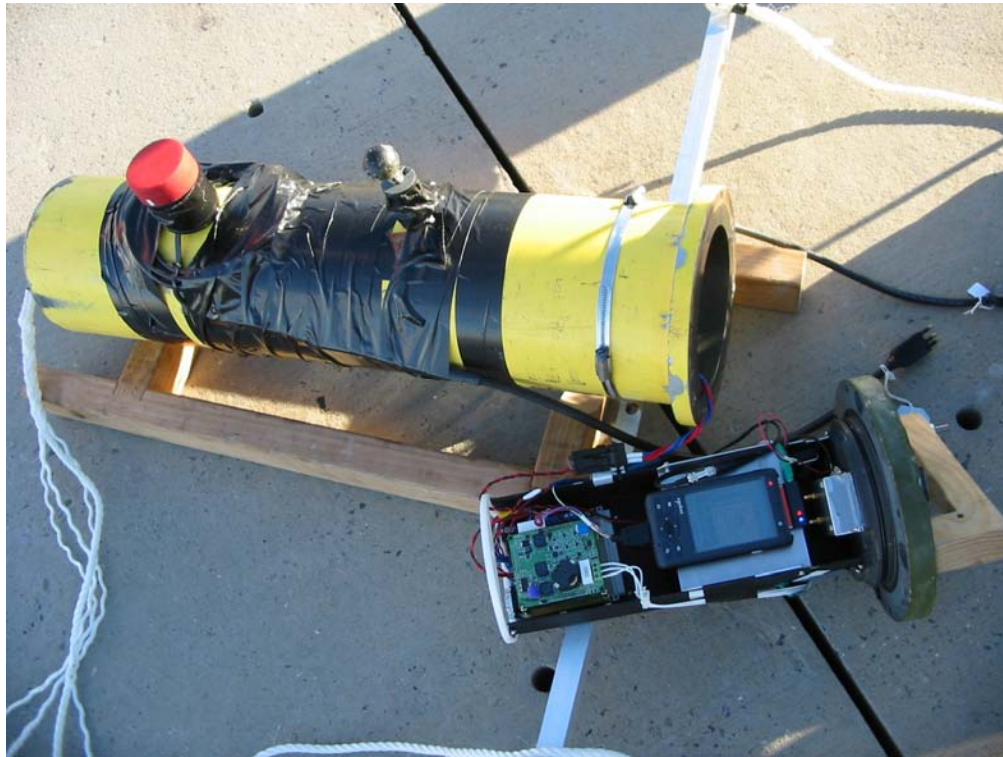


Figure 4.1.1. Photograph of the seabed modem receiver and ambient noise recorder extracted from the underwater housing. The upper OEM board of the AquaModem and recording PDA are visible. The housing was supported by a T-bar to ensure the hydrophone (black and spherical) and modem transducer (red and cylindrical) remained facing upwards.

The interrogation of the receiving modem was performed using a transmitter with largely the same hardware. The primary difference between the two acoustic packages was that the transmitting modem was not accompanied by an ambient noise recorder. The transmitting package comprised the MCS with an attached AquaComm modem and PDA for schedule control with no recording components present. The equipment was positioned within a plastic underwater housing and the modem transmitter was oriented downwards as shown in Figure 4.1.2. The subsea housing was attached to a Conductivity, Temperature and Depth (CTD) probe used to measure the Sound Speed Profile (SSP) at each interrogation location.



Figure 4.1.2. Photo of transmitter bundle including CTD probe (left) and underwater acoustic modem (right). The modem transducer was suspended approximately 30 cm below the plastic electronics housing which was lowered periodically from the research vessel.

The trial involved lowering the transmitting modem from the research vessel at various positions to interrogate the remote acoustic package. Upon arrival at each cast site the vessel's engines were switched off, allowing it to drift in a southerly direction during each cast. The transmitting bundle was lowered in 5 m increments starting approximately 10 cm below the sea surface. Cast locations are marked in Figure 4.1.3. The time that each cast took place, relative to the start of the recording is provided in Table 4.1.1

Table 4.1.1. Deployment times for each Test Point (TP) location, relative to the first recording. Times are given as the number of minutes from the first recording synchronised at 10:00:00 AM WST.

TP	Start Min	End Min	TP	Start Min	End Min	TP	Start Min	End Min
1	82.15	104.15	4	128.55	149.55	7	185.28	200.28
2	52.73	70.73	5	266.83	282.83	8	212.45	224.45
3	26.35	42.35	6	163.58	178.58	9		

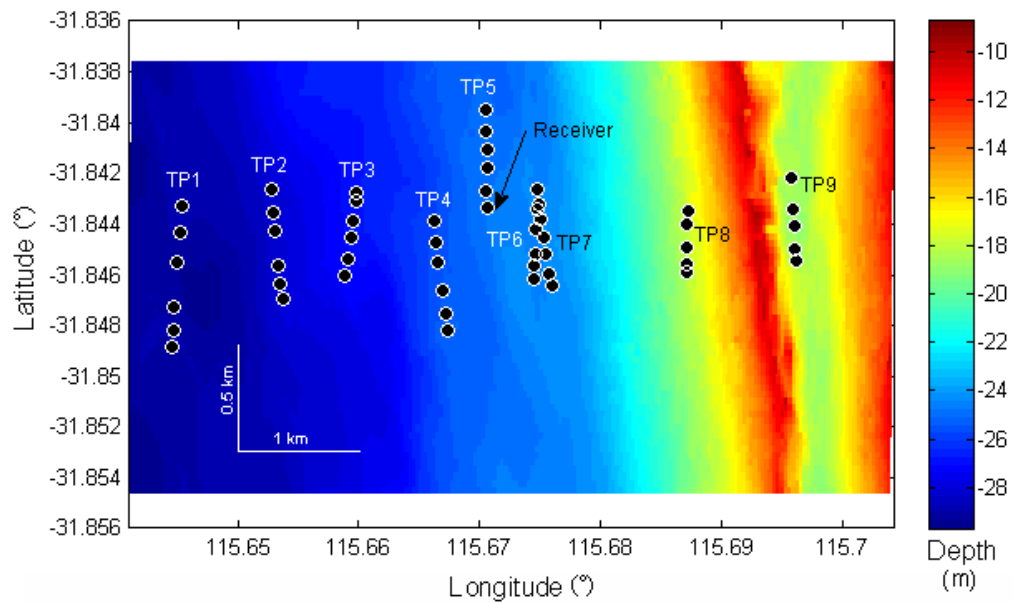


Figure 4.1.3. Positions of the transmitter casts occurring during southerly vessel drift. Each test point (TP) was accompanied by sub-locations denoting each 5m depth increment. Bathymetry data was obtained courtesy of the Department of Transport, Western Australia (www.transport.wa.gov.au), modified by Dirk Slawinski and Jason Waring.

The receiving modem was configured to remain passive unless a query was made by the interrogating modem. The on-board PDA was running *PDALogger* on a schedule that restarted recording every 20 minutes with no power management in place on the MCS. Modem transactions were recorded to non-volatile memory. The transmitting bundle used aboard the research vessel also operated with *PDALogger* and the MCS on the same schedule with the onboard RTCs synchronised across all devices.

Modem interrogations were scheduled using *PDALogger* at the transmitter. The interrogator was configured to transmit two separate ASCII strings to the receiver approximately every 30 seconds. The first transmission was a test string of the maximum length of 99 bytes. The second string was a command interpretable by *PDALogger* located on the remote bundle. This command, 'GETINFO', prompted a response transmission which included the remaining disk space in the recorder. The time taken for the remote acoustic package to respond was typically limited only by the 0.25 second delay inherent in the modem transmitter. However, in some cases a communication bottleneck between the PDA and MCS resulted in delay times of up to one second.

When a successful modem transmission was received, both modems were configured to respond initially with an acknowledgement packet. In this experiment the acknowledgement did not affect the behaviour of the equipment during the trial, but was recorded to aid in post-deployment analysis. Furthermore, it was possible that whilst the reception of a packet may have been successful, the corresponding acknowledgement signal was not decoded by the transmitter. However, in the analysis presented here the success rate of acknowledgement packets was assumed to correlate with the success of the original transmissions.

4.1.2 Preliminary Observations

Following the trial, initial data analysis showed that the hardware operated as expected. However, the transmission range of the modems was found to be much less than the anticipated 3 km. Successful modem connectivity was only observed during transects originating at TP4, TP5, TP6 and TP7. These locations were the four closest to the position of the deployed seabed receiver package. Apart from signal strength information, internal data such as recorded signals and error information was not accessible from the modems used in this deployment. This constraint restricted the determination of whether the range capability was limited by either SNR or multipath effects.

4.1.3 Localisation of the Seabed Acoustic Package

During the initial deployment of the recorder the GPS co-ordinates of the vessel were documented by hand. After completing the final transect the position of the marker buoy was discovered further south than originally recorded. This discrepancy included the consideration of vessel drift and was supported by a slight disparity in the vessel location during recovery. Such a difference presented an opportunity to utilise the modem data for localisation of the receiving seabed modem. Positioning was performed by determining the time delay between the successful transmission of a packet and the acknowledgement response.

Localisation involved assuming a homogenous horizontal channel at relatively long ranges to eliminate inclusion of depth. Considering only the initial direct acoustic path between the transmitter and receiver, the distance between the recorder and the position of the vessel r could be determined as:

$$r = \frac{(t_w - t_d) \cdot c_w}{2} \quad \text{Equation 4.1.1}$$

Here, t_w is the time between the falling edge of the transmitted packet and the rising edge of the received acknowledgement. The internal modem delay t_d was measured to be approximately 0.25 s and speed of sound in water c_w was assumed to be approximately 1500 ms^{-1} .

The vessel's internal GPS was used to record the waypoints during the casting of the transmitter. The position of the vessel was interpolated for each transmission by using the associated timestamps which were previously synchronised to GPS time. By measuring the time delay at these positions an estimation of range was acquired using Equation 4.1.1. To obtain direction the surrounding interrogation positions were used and circles of radius, r converged at the location of the receiver. Figure 4.1.4 demonstrates how circles of known radius confirm the location of the recorder to be approximately 300 m south of the originally documented position.

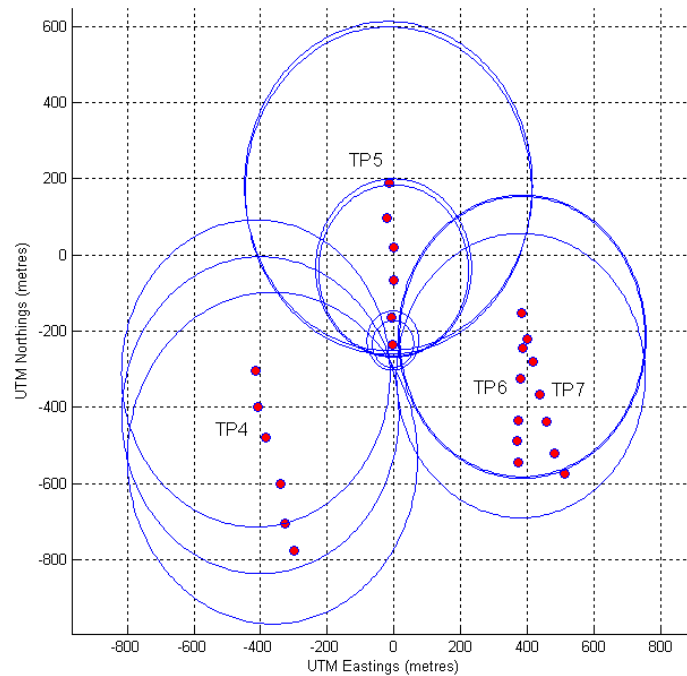


Figure 4.1.4. Localisation of the ambient noise recorder. By determining the time delay of the modems at various points, circles of known radius successively approximate the position of the recorder using the point of convergence.

4.1.4 Ambient Noise Measurements

Data from the ambient noise recorder located on the seabed provided approximately 5 hours of sound recordings at the receiver. The data was found to contain high levels of snapping shrimp noise. To obtain the noise power spectrum, a power spectral density curve was calculated using the recordings taken while the vessel was positioned at TP1, TP2 and TP3. At these locations no modem communication was successful or detected by the recorder and any shipping noise was overpowered by shrimp noise. Figure 4.1.5 shows the noise power spectrum obtained corrected for system gain and hydrophone sensitivity.

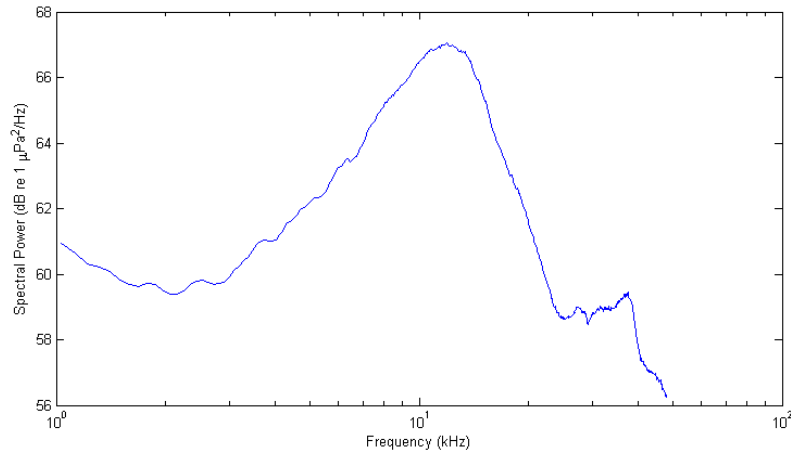


Figure 4.1.5. Ambient noise power spectrum calculated using the ambient noise recordings during a period of minimal activity in the trial (first 100 minutes of recordings). A log scale has been used for comparison with noise prediction curves in Figure A.5.

The measured noise data had some similarities with the prediction curves for snapping shrimp shown in Figure A.5 but with a discrepancy in the location of the peak frequency. Further analysis shown in Figure 3.3.5 demonstrated a non-Gaussian amplitude distribution which is also consistent with the presence of snapping shrimp (Legg, 2009). There were no other obvious sources of noise in the ambient noise data. Vessel noise was rarely present and typically observed at lower frequencies. The ambient noise did not fluctuate significantly. Figure 4.1.6 shows the recorded power density spectrogram over the duration of the deployment.

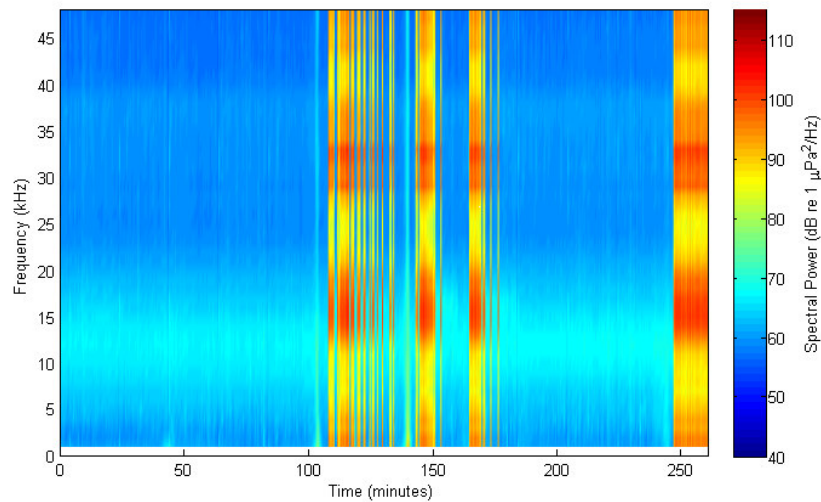


Figure 4.1.6. Spectrogram calculated from 260 minutes of ambient noise data recorded during the trial. The first 20 minutes of the recording was omitted, as it contained only noise from the deployment of the recorder itself. The periods of saturation are due to modem connectivity where local acknowledgement packets were transmitted.

4.1.5 Signal Strength Measurements

The specified operational bandwidth of the modems was between 16 and 30 kHz. However, during transmission the acoustic recorder detected an acoustic signal occupying a frequency range of approximately 14 to 22 kHz. This can be seen in Figure 4.1.7 which shows a power density spectrogram of a typical series of transmissions. This includes a long packet received from the interrogator, followed by the interrogation command. The associated responses of the receiver modem are also shown where saturation of the preamplifier input had occurred.

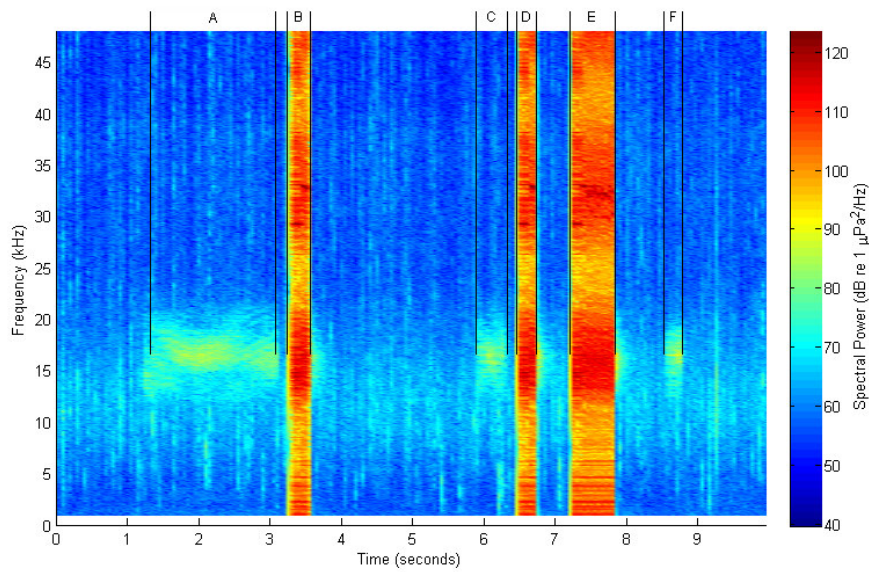


Figure 4.1.7. Spectrogram of various stages of modem communication. The observed clipping is due to the proximity of the receive hydrophone to the transducer. (A) Large test packet is received. (B) Acknowledgement is returned. (C) 'GETINFO' Command received. (D) Acknowledgement returned. (E) Receiver returns requested information. (F) Transmitter returns acknowledgement.

By analysing the high frequency recorder data the signal strength from the transmitter at various positions was determined. The Power Spectral Density (PSD) was calculated over 5 ms blocks of data for the entire set. The PSD produced three bins of interest with frequencies ranging between 15 - 24 kHz. By averaging each bin of interest the spectral power versus time was obtained over a bandwidth of 9 kHz. The average sensitivity of the hydrophone in this frequency range was determined to be -202.5 dB re 1 V/μPa and a system gain of 40.25 dB was applied.

A searching algorithm was developed to determine where a transmission had occurred during the acoustic recordings. Detection of received signals with the ambient noise recorder was primarily useful for calculating the average received signal strength. These measurements could then be related to the time of receipt and subsequently the transmitter-receiver distance.

The primary source of transmission loss in this deployment could be best approximated with a superposition of spherical and cylindrical spreading as given by Equation A.4 and Equation A.5 respectively. The modem separation distance for each detected signal was determined using the known GPS coordinates recorded by the vessel and the corrected position of the receiver. A compilation of signal strength observed by the recorder over the entire deployment was produced and the transmission loss experienced was compared to expectations. The source level of the modem was unknown so an offset matching the best fit to the data was used. Figure 4.1.8 demonstrates good agreement with spherical spreading at short range. As expected, at ranges far exceeding the depth of the water column, the spherical spreading estimate was no longer appropriate. The cylindrical spreading curve was shown to fit well from approximately 400 m and beyond.

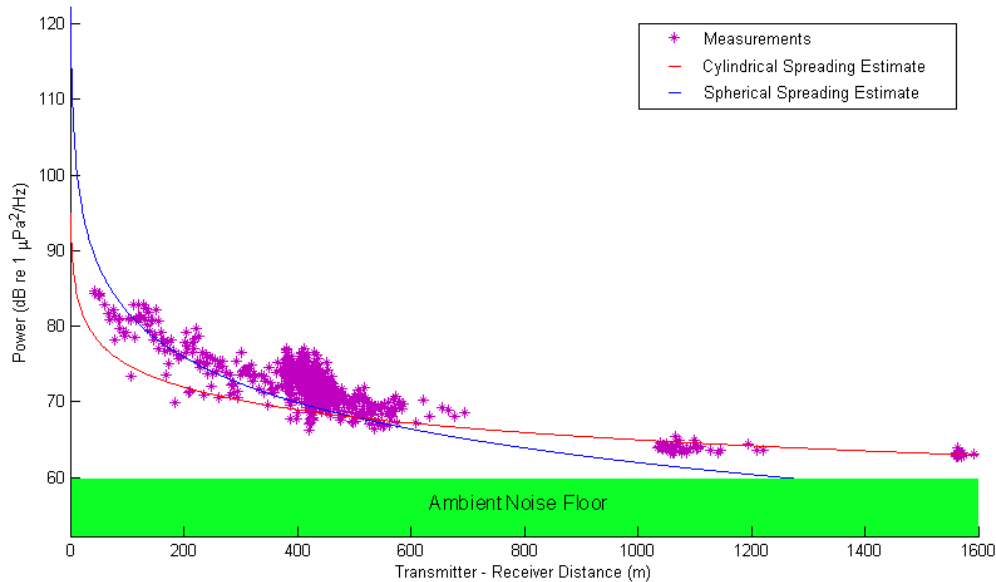


Figure 4.1.8. Signal strength as measured by the ambient noise recorder following use of the signal detection algorithm. The observed transmission loss was also compared to the estimate for spherical and cylindrical spreading.

4.1.6 Modem Reception

Processing of the logged modem transactions confirmed that their operating range was much shorter than expected. Analysis showed this limitation was most likely due to the lack of sensitivity of the receiving modem combined with a lack of power from the transmitter. Additionally, the noise levels in the transmitting bandwidth were too high for effective communication. It would be expected that in environments where snapping shrimp noise was less prominent the modems could have achieved longer range communication. These conclusions would attribute the lack of performance to the signal strength rather than a complex multipath environment. However, it is possible that ISI may have had an impact at longer ranges had the signals been detectable by the modem hardware.

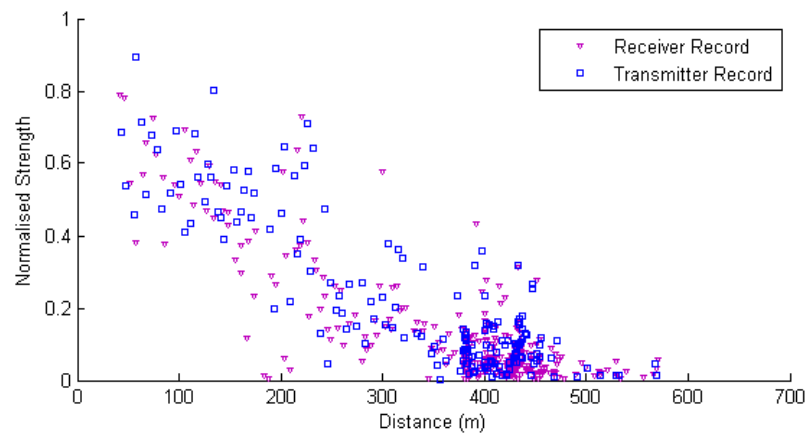


Figure 4.1.9. Signal strength as observed by each of the deployed modems, confirming lack of reception beyond approximately 500m. The strength scale presented here is unknown as the modem manufacturer could not provide any additional information.

Upon the successful detection of a modem signal, a debug string containing the nominal signal strength in hex format was recorded. By using the time stamps with the GPS data, the signal strength was calculated for the modem separation distances at each detection event. Figure 4.1.9 displays both the transmitter and receiver modem signal strength data, showing how the perceived signal strength was minimal towards ranges of 500 m or more. This result suggested the modem was operating well within its own sensitivity limitations. However, when compared to the signal detection algorithm operating successfully at up to 1400 m, the modem receiver was much less effective in signal detection than the ambient noise recorder.

A similar approach of compiling performance statistics relative to distance was used to determine the overall modem success rate with range. The modem success rate was quantified by calculating the number of acknowledged transmissions with respect to the number of attempted transmissions. These data were compared to GPS coordinates and binned in 40 m increments. The results are shown in Figure 4.1.10 which plots performance over the same range as shown in Figure 4.1.9. When the signal strength recorded by the modem was low at long ranges, the modem success rate dropped significantly. Figure 4.1.9 also shows the complete lack of connectivity beyond approximately 500 m.

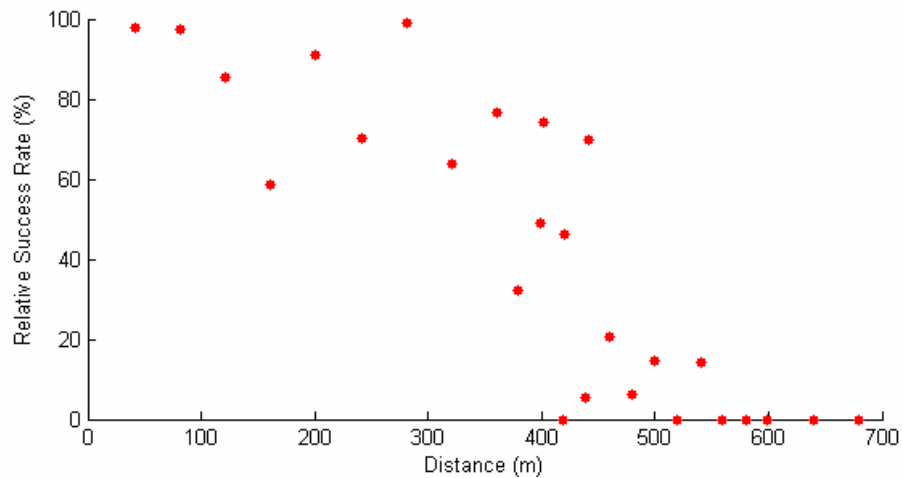


Figure 4.1.10. Relative success rate versus distance obtained by binning the success rate over 40 m blocks. The reception rate dramatically decreased beyond 500 m, correlating to the lack of signal strength shown in Figure 4.1.9

4.1.7 Summary

The first of several planned deployments, this trial provided insight into the shallow underwater performance of a commercial acoustic modem. It was determined that the reliability of communications in this specific study could not be accurately predicted for long range telemetry due to a low receiver SNR and some internal bugs.

However, communications were still effective within a range of approximately 500 m. Measurements from the high frequency noise recorder demonstrated the signal was detectable well beyond what the modem was capable of detecting. This

result suggested that with more developed signal processing techniques and improved gain, longer range may be achievable with the same output power.

The results of this trial affected the techniques planned for future deployments. Importantly, a technique to assess the performance of the modems in real-time during deployment was integrated into the equipment for the following field trial. This was intended to avoid the wasted effort of deploying in an area where the apparent signal strength is below the noise floor, such as TP1, TP2, TP8 and TP9 in this trial. Real-time view of the following trial's statistics was consequently accomplished by installing a Liquid Crystal Display (LCD) module into the plastic housing for the deployment described in Section 4.2. In addition, a co-operative relationship with the modem manufacturer of the newly acquired AQUAmodem for the following trials was anticipated to greatly assist in post-deployment data analysis which was a highlighted problem in this trial.

4.2 Perth Long Range Shallow Water Trial

4.2.1 Experimental Setup

On the 10th April 2009, a second short-term acoustic modem trial was conducted, this time using the AQUAmodem from Aquatec Group Ltd. The same custom external hardware used in previous experiments accompanied the modems during the deployment with an added noise recorder as part of the interrogating acoustic package. Whilst capable of recording at a 192 kHz sampling rate, the high frequency recorder operated in 20 minute blocks at 96 kHz. This was appropriate given that the AQUAmodem was configured to transmit using a frequency range of 7.5 - 12.0 kHz.

The deployment focussed on long range shallow water telemetry and was performed approximately 10 km off the coast of Perth, Western Australia. The main propagation path for the trial was located over a 30 m north-south depth contour as shown in Figure 4.2.1. For investigation of modem performance over rugged terrain, the modems were also positioned on either side of a collection of reef and rocks protruding from the sea surface. Using known bathymetry data for the area, two dimensional slices were extracted for each test position. Examples showing the propagation paths for TP9 and TP11 are shown in Figure 4.2.2. The seabed substrate for the majority of the deployment was sand covering limestone. The maximum range attempted was at TP9 with a modem separation distance of 11.2 km. Deployment cast times are given in Table 4.2.1.

Table 4.2.1. Deployment Times for each Test Point (TP) location. Times are given as the number of minutes from the first cast at 10:44:02 AM WST.

TP	Start Min	End Min	TP	Start Min	End Min	TP	Start Min	End Min
1	0	12.0	5	77.0	88.4	9	167.8	175.5
2	18.6	33.5	6	94.8	110.2	10	203.4	217.8
3	39.6	52.0	7	118.0	113.1	11	224.5	232.1
4	58.3	71.7	8	142.6	158.9	12	271.1	283.1

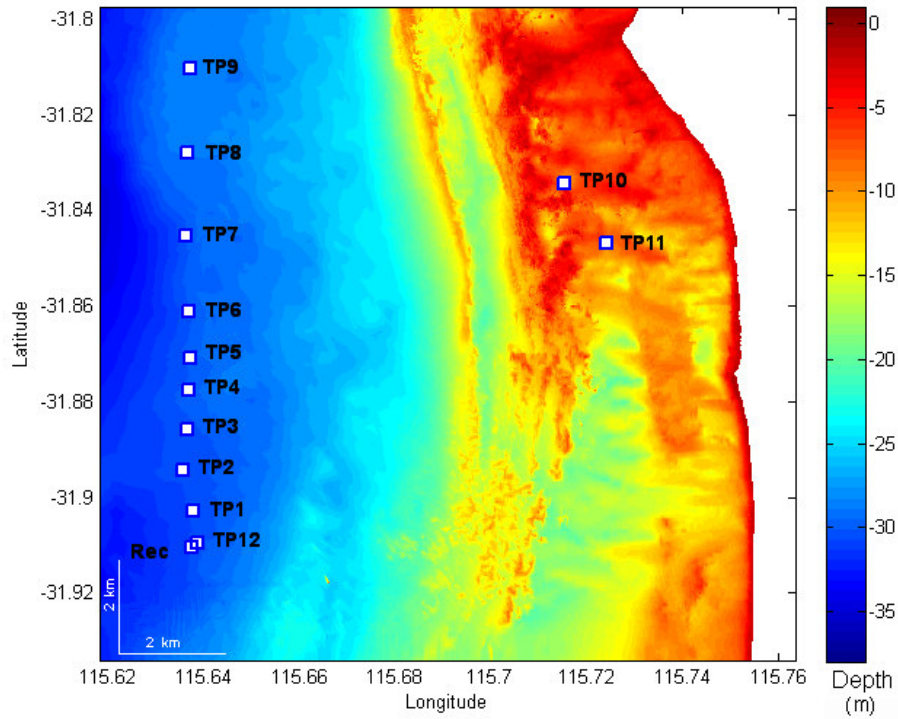


Figure 4.2.1. Bathymetry and locations of test positions used for the trial. The recorder (Rec) was located at the southern end of a northerly transect spanning approximately 11.2 km. Bathymetry data was obtained courtesy of the Department of Transport, Western Australia (www.transport.wa.gov.au), modified by Dirk Slawinski and Jason Waring.

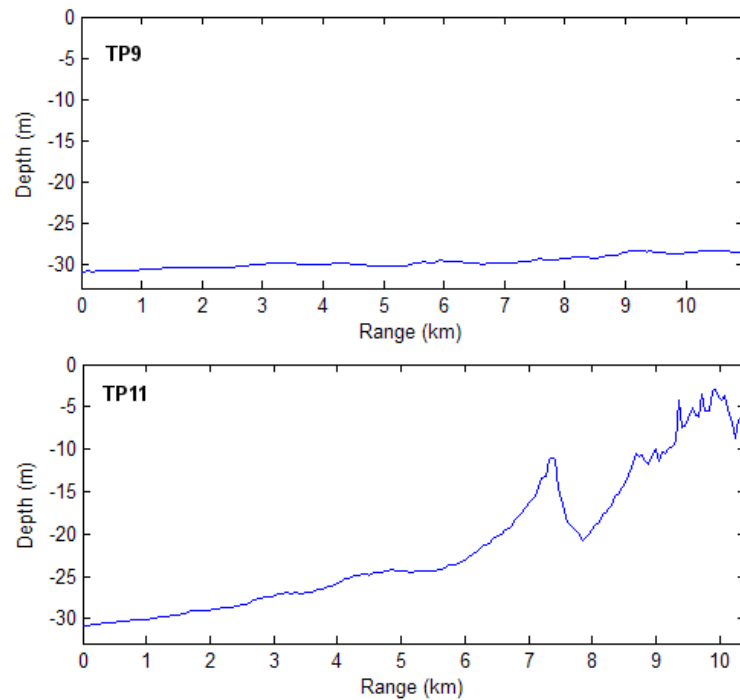


Figure 4.2.2. Two-dimensional bathymetry for two distinct propagation paths extracted from Figure 4.2.1.

The trial was performed using a receiving modem deployed to the seabed with the transducer facing directly upwards to reduce the impact of snapping shrimp on communication. An interrogating acoustic package was bundled with a CTD probe for deployment from the vessel. Both devices are shown in Figure 4.1.2. In contrast to the OEM board and transducer of the DSPComm modems, the AQUAModem was a fully housed package and the power and RS232 link was routed to the units via a subsea cable.

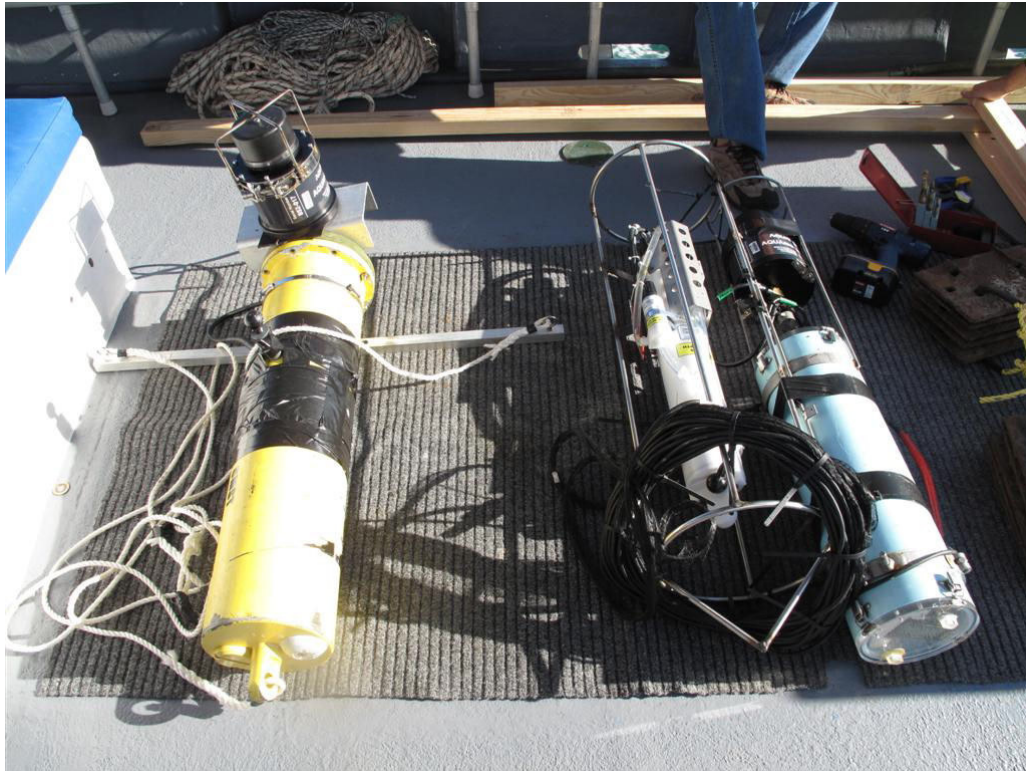


Figure 4.2.3. Photo of deployment gear. The seabed modem (left) was fixed to the deep water housing containing the ambient noise recorder and a T bar was used to stop any potential rolling. The transmitter bundle (right) included an ambient noise recorder, CTD and acoustic modem facing downwards for casting.

An additional hardware element was introduced to this trial to allow the real-time preview of the performance statistics to control experimental efficiency. An LCD module (Figure 4.2.4) was mounted to the clear Perspex end cap of the plastic housing and the relevant software was added to *ModCon*. Accompanied by a CTD profiler, the transmitting bundle was lowered to typically half the water depth for transmission. Interrogations lasted approximately 10 minutes during each cast.

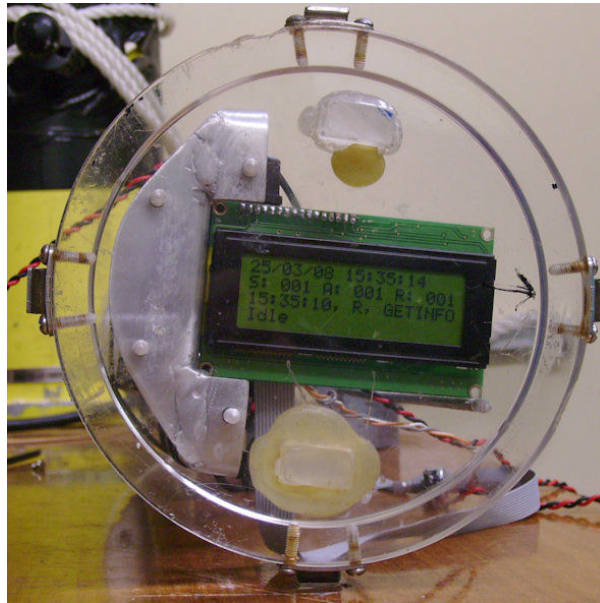


Figure 4.2.4. Photo of end cap of the plastic transmitter housing, showing the attachment of the LCD module. The feedback provided by the module via the MCS included date, time, performance statistics and the last received string.

Similar to previous deployments, the MCS software operated with no power management, running continuously. *PDALogger* was also implemented on the PDA for high level recording and modem control. The predominantly passive seabed receiver recorded ambient noise whilst awaiting an acoustic command from a transmitter. All modem events were also recorded to the PDA memory. When an interrogation string was received, the receiving modem responded with a similar short burst of acoustically encoded data. The primary transmitting modem was configured to send an acoustic request every 20 seconds. This packet also contained additional information regarding the remaining disk space on the internal recorder

The use of acknowledgement packets was a default inclusion with the AQUAmodems, however, they were disabled for this trial. The receiving modem responded to all transmissions with similar data regarding the recorder status and this was considered the acknowledgement. The response of the receiving modem, in addition to being logged by the transmitting software, was output to the LCD at each transmit and receive event. This feedback provided the user with updated information regarding both modem connectivity and the status of the recorder.

4.2.2 Modem Performance

During the trial, the interrogating modem did not report any successful communication with the receiving modem on the sea floor, despite close proximity and the signals being clearly audible to the crew on deck. Whilst data was effectively transmitted to the seabed receiver, it was discovered that the response could not be decoded by the interrogator.

After analysing the reception at the seabed, it was discovered that when the modem separation distance was small, the signal was mostly undecipherable by the receiving modem. The only exception was when the modems were near-vertically aligned with each other and perfect reception occurred. However, as the modem separation distance was increased, successful telemetry resumed. The success rate for data transmitted to the remote modem is shown in Figure 4.2.5. The data is shown as the ratio of transmissions successfully received to the known number of transmissions.

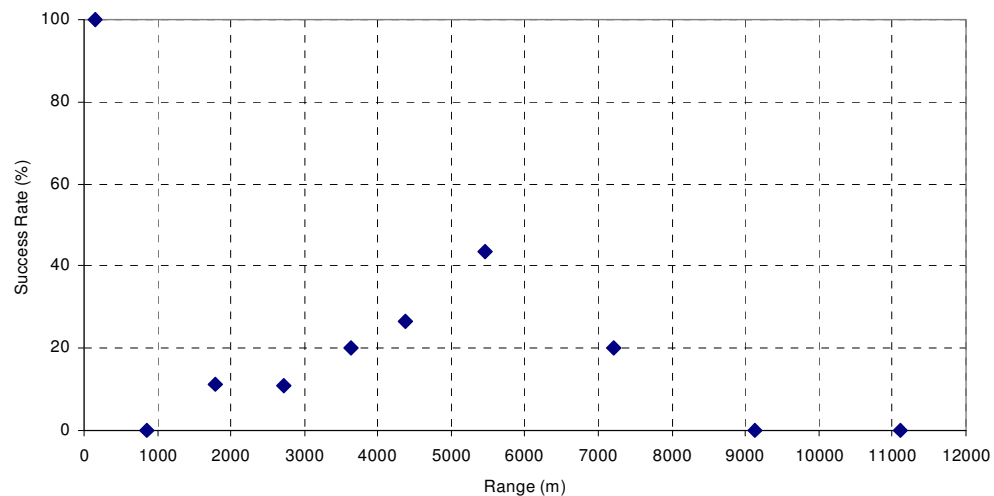


Figure 4.2.5. Success rate versus range for the transmission of data from the research vessel to the remote modem. Modem performance is shown to steadily increase with range until approximately 6 km where performance eventually drops.

Overall, the transmission success during the deployment was limited; however, it was quite capable over long range. Interestingly, two trends were found; the probability of success increased with range to approximately 6 km, followed by a distinct decline in the success rate. The drop in reception beyond approximately 6 km was followed by complete failure at further ranges. This lack of performance included the test points located behind the areas of reef.

4.2.3 Ambient Noise Analysis

Recordings from the seabed equipment were analysed to assess the acoustics of the environment over the deployment period. It was discovered that several noise sources were present during the deployment, dominated by significant amounts of vessel noise towards the end of the day. This was most likely due to deploying in close proximity to a local shipping channel, as well as an influx of recreational vessels in the area during the Easter long weekend. These fluctuations are highlighted by the power density spectrogram for the deployment which is shown in Figure 4.2.6.

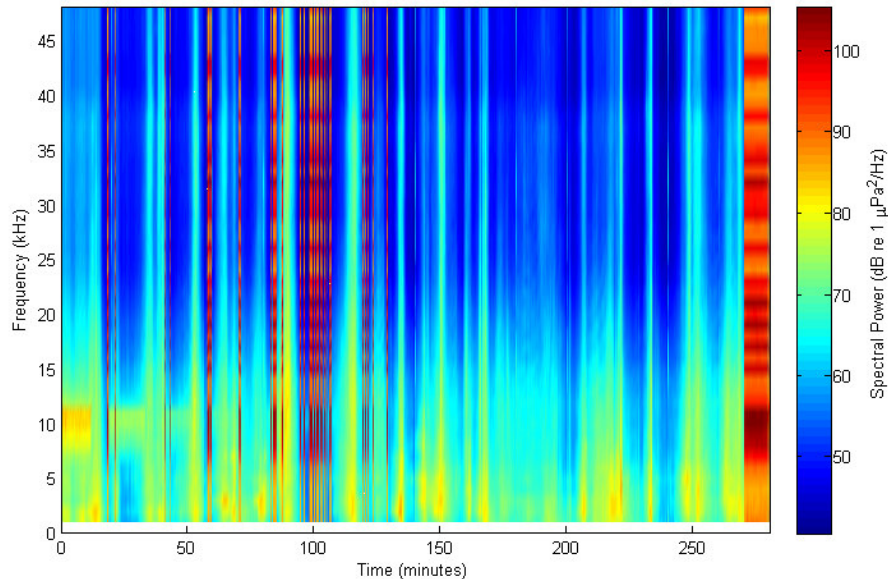


Figure 4.2.6. Power density spectrogram of the entire deployment, calculated using 20 s blocks of recordings. Several time periods of vessel noise are shown, as well as modem signals clearly visible in the first 30 minutes in the 7-11 kHz band. Vertical lines of saturation denote where the local modem was responding to an interrogation.

The ambient noise spectrum was also extracted using periods of low shipping noise and modem silence. By choosing two periods where vessel noise was minimal, the ambient noise spectrum was calculated and is shown in Figure 4.2.7.

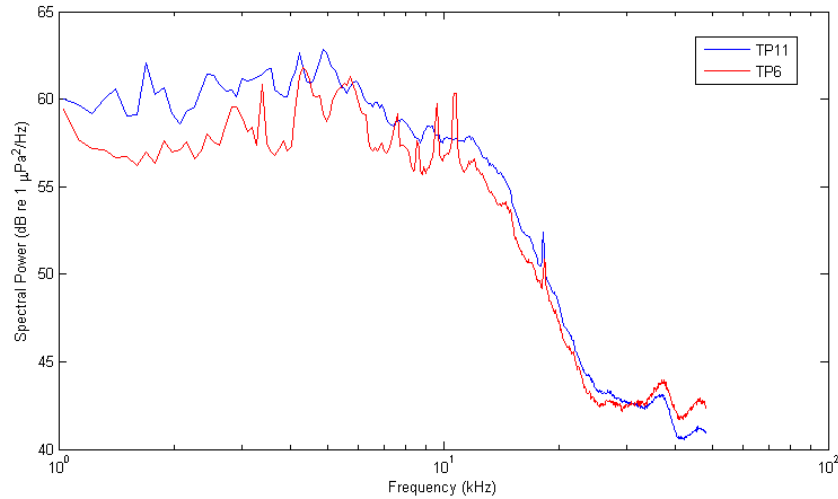


Figure 4.2.7. Noise power spectrum obtained using quiet periods of the deployment when vessel noise was minimised. The legend labels correspond to the position of the research vessel during the recording.

The ambient noise spectrum was dominated by shipping noise at lower frequencies. When compared to the PSD shown in Figure 4.1.5 the overall noise levels were found to be approximately 7 dB below the previous deployment suggesting snapping shrimp were not as prominent. This was confirmed following further analysis which discovered the ambient noise exhibited a near-Gaussian amplitude distribution (Figure 3.3.5). This discrepancy could be caused by differences in the environment such as the deeper deployment depth in this trial where snapping shrimp were less likely to be present.

4.2.4 Acoustic Signal Analysis

The ambient noise recordings from the seabed receiver were used to calculate the signal and noise levels throughout the deployment. GPS positions for each test point were used to determine relative distances of the modem pairs. An algorithm was designed and implemented to detect the occurrence of a signal and similarly to the previous trial, calculate the average signal and noise power for the separation

distance. Figure 4.2.8 demonstrates the average signal power compared to the ambient noise level recorded at each test point, highlighting the erratic noise levels during the deployment. A receiver bandwidth of 500 Hz centred at the higher carrier frequency was analysed. The standard deviation of calculated noise and signal power levels found by the algorithm over the duration of the deployment are also shown with error bars representing one standard deviation from the mean.

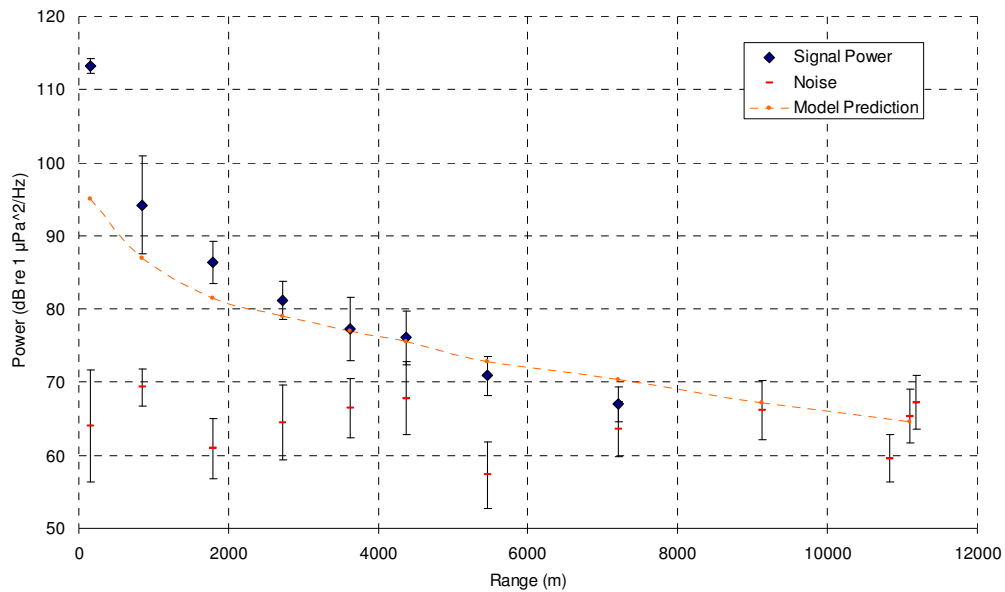


Figure 4.2.8. Summary of the received signal and noise powers as observed by the seabed underwater acoustic recorder. Error bars represent one standard deviation from the mean. The measured results are compared with the model prediction acquired using Bellhop with a best fit to the source level. The noise levels are also shown to fluctuate throughout the deployment.

During periods of the trial, the noise level varied significantly and in some cases, exceeded the signal power. In particular, data from TP7 (7 km) showed overlapping signal and noise power levels. The ambient noise level is seen in Figure 4.2.9 to exceed received signal strength during TP7, accounting for the drop in performance. This highlighted a possible confound to the performance statistics, however, TP7 was the only test point to have shown such a marginal SNR. Points beyond TP7 had no distinguishable signal in the ambient noise recordings and corresponded with no modem connectivity.

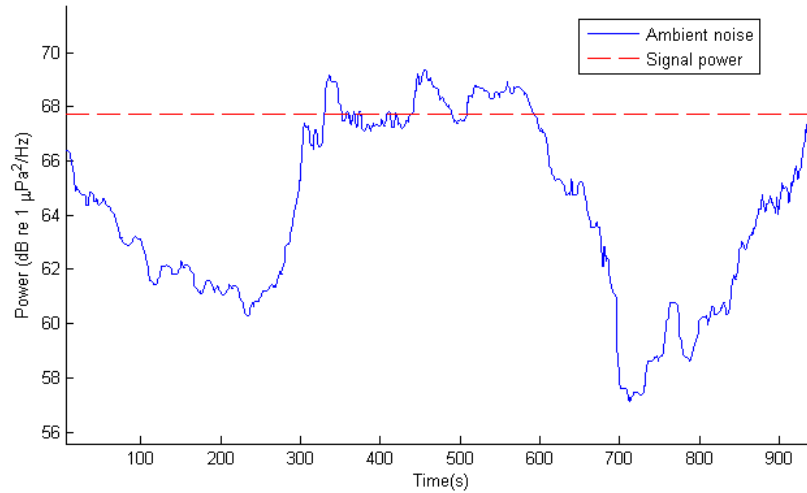


Figure 4.2.9. Comparing the ambient noise to the average signal power received for TP7. The fluctuations in ambient noise are shown to exceed signal strength and subsequently affect the validity of the results at this location.

Overall, an expected drop in signal strength was exhibited in Figure 4.2.8 as the range increased, following the Bellhop modelled prediction. These results demonstrated that SNR levels were sufficient for successful transmission at ranges up to 7km, consistent with the modem reception rate. This evaluation also confirms similarities between the detection sensitivity of the modem receiver and ambient noise recorder, in contrast to the discrepancy exhibited in the first trial with the AquaComm modems.

Overall, the FSK modem was shown to perform effectively in low SNR scenarios. Additionally, the performance decrease for close-range communication was not related to SNR, with multipath propagation and high amplitude ISI at close range likely to be the main cause.

4.2.5 Spatial Simulation of Shallow Water Perth Trial

Spatial simulations were performed for comparison with the long range shallow water Perth trial. With a water depth of approximately 30 m and trialled ranges up to 11 km, the impact of reflections was expected to be significant. Figure 4.2.10 demonstrates this with a sample simulator output for a transmitter located at a depth of 30 m, a receiver located at a depth of 15 m, and a modem separation of 4 km.

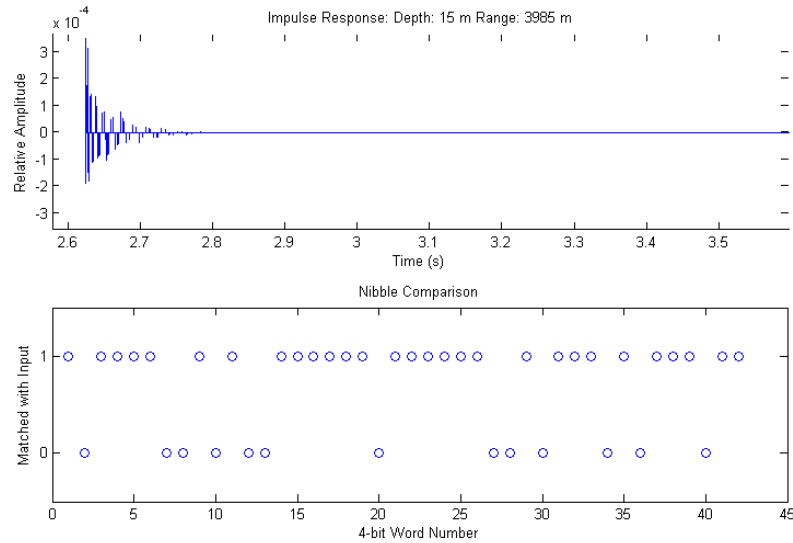


Figure 4.2.10. Simulator performance summary for a sample position ($D = 15$ m, $r = 4$ km) during the Perth long range trial. The transmitter was located at 30 m, approximately 80 cm from the seabed. Both the impulse response (top) and corresponding performance predictions (bottom) are shown.

The simulated impulse response resembled a decaying envelope of multiple arrivals. The subsequent increase in ISI was expected to be the primary cause of problems during the trial, especially where the envelope was high in amplitude for longer than the symbol duration. In the trial, one stationary modem was located on the seabed (30 m), with another mobile node at approximately half the depth of the water column (15 m). Preliminary investigations were performed using transmitters located at each of these depths, at the starting point of the trial ('Rec' in Figure 4.2.1). The bathymetry used for the simulation is shown in Figure 4.2.2 (top). Figure 4.2.11 shows the result of a two-dimensional spatial simulation for each transmitter depth, without the addition of ambient noise. Due to the high number of arrivals present in the shallow water environment, the resolution of the simulation was restricted to

optimise computational time. Additionally, only the strongest 100 arrivals were used for constructing the received signal. It was assumed that the sound speed profile was completely mixed (isothermal, slightly upwardly refracting) due to the shallow water depths. This assumption was also consistent with CTD data acquired in the area for the trial shown in Section 4.1.

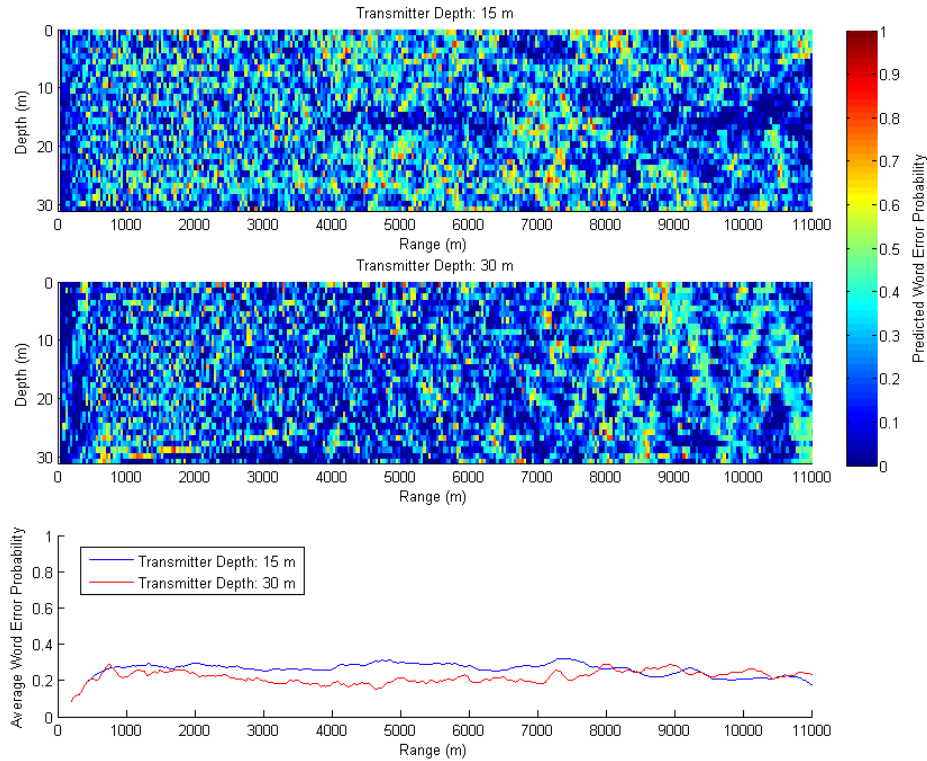


Figure 4.2.11. Two-dimensional predicted word error probability for the shallow water Perth trial for each modem depth at the recorder location, without the addition of ambient noise (top, middle). Results averaged over depth for both simulations (bottom).

The simulator predicted a “speckled” spatial distribution of modem performance which was relatively uniform with range. The only exception was at very close range ($D < 1000$ m) where lower error probabilities occurred. The large variation in word error probability over short distances demonstrated that communication performance was likely to be highly dependant on the small-scale location of the receiver. Fluctuations in the channel and modem movement would be expected to cause substantial fluctuations in communications performance during a deployment. The best estimate of error probability for comparison with trial performance was therefore considered to be the average over an area of interest.

Following an initial look at multipath effects alone, two-dimensional simulations were performed with the noise added to replicate the observed SNR, resulting in the range-dependant performance shown in Figure 4.2.12.

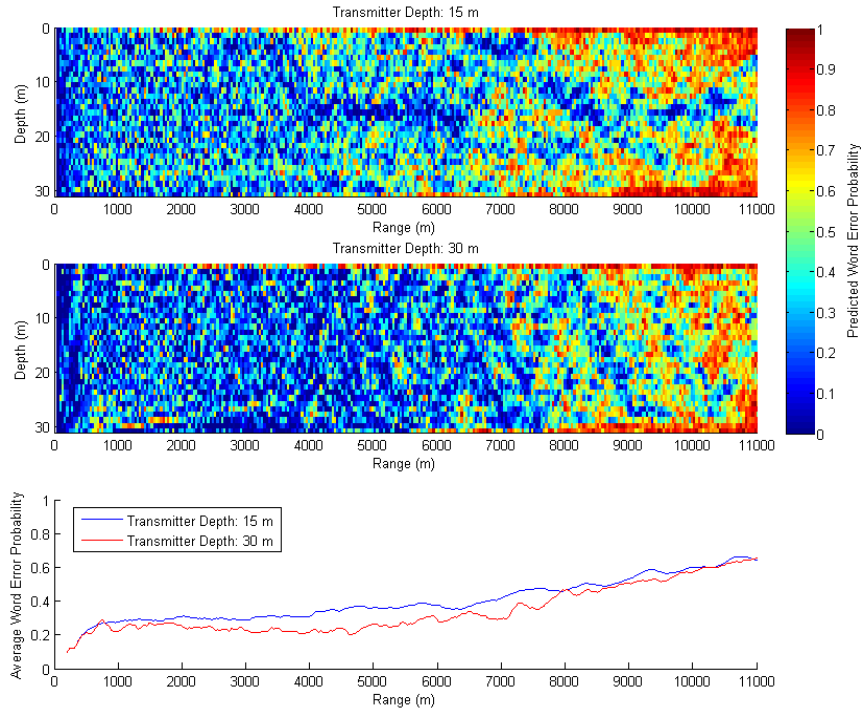


Figure 4.2.12. Two-dimensional predicted word error probability for shallow water Perth trial for two modem depths, with the inclusion of 75 dB re $1\mu\text{Pa}^2/\text{Hz}$ noise (top, middle). Also shown is the depth-averaged result for both simulations (bottom).

The seabed transmitter was found to produce marginally better overall performance for a wider range of receiver depths than the transmitter located at 15 m. Results from the full-scale simulations also showed that the most effective receiver depth for long-range communication was towards the middle of the water column, particularly for a transmitter also located at mid-depth. The long-range Perth trial involved vessel communication to a stationary seabed modem. Therefore, the most appropriate method to accurately incorporate the bathymetry into the simulations was to consider a stationary seabed transmitter with a mobile receiver centred at 15 m. The seabed modem for the simulations was located at a depth of 30 m which was approximately 80 cm from the sea floor, similar to the deployment.

A narrow, horizontal array (band) of receivers was distributed over the modelled environment at a depth of 15 m, 20 cm wide with 5 cm spacing. By averaging this region over depth, range-dependant word error probability was obtained.

Additionally, simulations of communication performance were repeated using an isovelocity SSP to determine any influences of the upwardly refracting environment. The results of these simulations are shown in Figure 4.2.13. The isovelocity SSP yielded a slight improvement in performance, both with and without the inclusion of noise in the simulations, particularly at longer ranges.

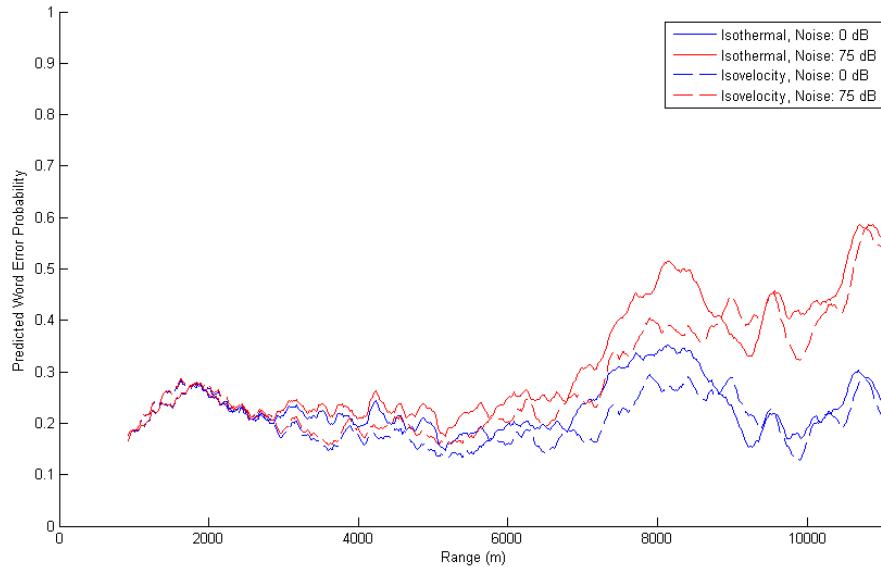


Figure 4.2.13. Smoothed depth-averaged word error probability for receivers centred at a depth of 15 m acquired from a high resolution focussed simulation.

The transmissions for this trial were of the same length and relatively uniform in content. Therefore, the simulated word error probability could be mapped to an approximate transmission failure probability by using knowledge of the modem receiver error processing methods. A nominal mapping function was established using a Binomial distribution. This method assumed that the modems were able to correct for 2 erroneous words in a transmission of 15 words for each block of data. The results from this treatment can only be considered indicative given that the distribution assumes that the successful reception of each word is independent which is not entirely accurate. A total transmission length of one block is also assumed, given that transmission lengths in the trial were also short. The resulting mapping function is shown in Figure 4.2.14.

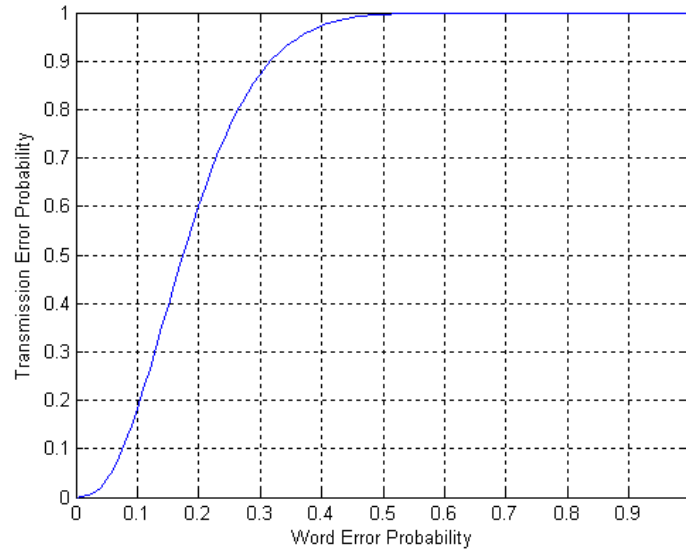


Figure 4.2.14. Nominal mapping function to obtain transmission error probability based on word error probability, using a Binomial distribution.

The mapping function was applied to the predicted word error probabilities for the isothermal sound speed profile with the results shown in Figure 4.2.15. These results allowed for a direct comparison with field data within the limits of the aforementioned assumptions.

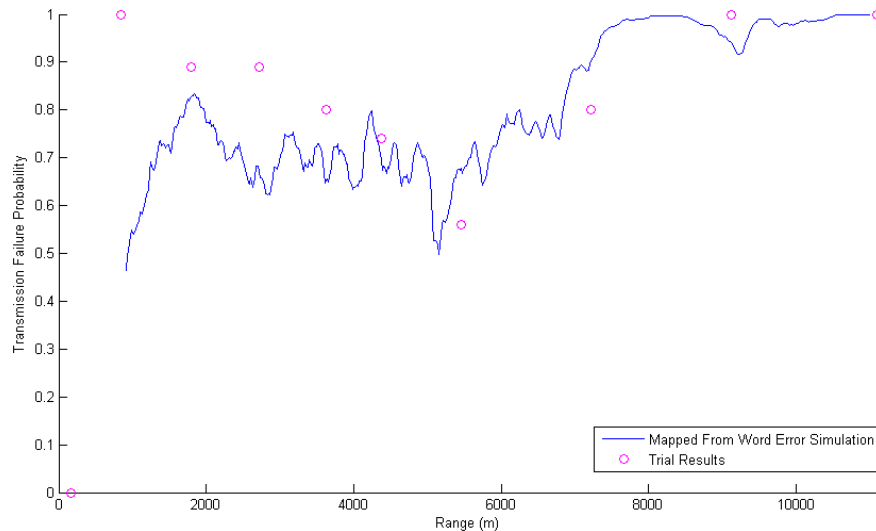


Figure 4.2.15. Smoothed depth-averaged transmission failure probability for receivers centred at a depth of 15 m acquired from a high resolution focussed word error prediction and mapped to transmission error using the curve shown in Figure 4.2.14. Also shown is the transmission success observed during the long range shallow water trial.

Simulated performance data exhibited a slightly downward trend in error probability towards the middle ranges (5 – 6 km). Additionally, lower error rates were predicted at ranges below 2 km with perfect reception expected for near-vertical alignment (best shown in Figure 4.2.12). Similar trends were observed in the trial data. Beyond approximately 7 km, errors due to multipath alone (noiseless simulation) were shown to increase slightly. Furthermore, the addition of ambient noise to the simulation increased error rates at longer ranges, explaining the cessation of communication beyond approximately 9 km. With the exception of one position (1 km) the simulated predictions were consistent with the trial observations. This includes where transmission success was the highest, at very close range (160 m), with mid-ranges also yielding intermittent communication.

Overall, the depth of the environment coupled with the seabed location of one of the modems was shown via simulations to be unsuited to the communication methods employed. The comparison simulations predicted that word error probability was marginally lowered at mid-range. Although seemingly insignificant, the difference in word error had a pronounced effect on the modems during the trial due to the error handling. The transmission failures recorded during the experimentation were consistent with the range dependent performance that was produced by the simulator.

4.2.6 Summary

The shallow deployment conditions in this trial were unfavourable for effective communication. Nearby vessel noise impacted modem performance throughout the trial. However, successful reception was possible at ranges up to 7.2 km. No signals were detected by the ambient noise recorder at testing positions beyond this range. It is expected that successful communication may have been achievable at longer ranges earlier in the day given the changes in vessel noise experienced. The modems were shown to operate in very low SNR environments.

Following customisation of the simulator to best suit the observed conditions, a reasonable agreement was found with the experimental data. The position for best signal strength and reduced multipath effects was generally found to be at mid-depths. The relatively high and fluctuating noise levels experienced during the trial were indicated by the simulations to have a detrimental affect on the telemetry at long range. Following the mapping of simulated word error to transmission failure probability, predicted modem performance was found to be consistent with what was observed during the trial.

Overall, the results obtained for the long-range Perth trial and related simulations provided a strong indication that for the shallow water environment, multipath propagation dominated the cause of problems, except at very long range where low SNR also affected performance. Additionally, the simulations provided a good overview of the advantages and disadvantages of different modem configurations which would be useful in the planning phase of other deployments.

4.3 French Long Range Deep Water Trial

On 19th February 2009, the manufacturer of the AQUAmodem, Aquatec Group Limited, conducted trials off the coast of Villefranche-sur-Mer, 6 km East of Nice, France (The candidate did not participate in data collection for this trial). This location provided access to large water depths relatively close to the shore, making it a convenient and effective area for deep water testing of the modems. The trial was conducted using two vessels, each fitted with an AQUAmodem which was deployed 25 m below the sea surface. This study involved analysis of data collected by a third party. The trial was initially intended only as a test of modem functionality, however, the information recorded to internal memory allowed for additional analysis of modem recordings. Additionally, this trial provided an opportunity to simulate modem performance in deeper waters using different sound speed profile characteristics to Western Australia.

4.3.1 Experimental Setup

Both modems were configured to record acoustic data in the event of successful transmission. These audio data were recorded onto internal memory, along with debug information used to assess modem performance. Telemetry during the trial involved the transmission of a short interrogation packet from the larger vessel located offshore which requested a block of data from the remote modem located in the bay. The requested packets varied in length to help assess the impact of packet length on communication reliability.

The smaller vessel was positioned in the vicinity of the bay (Figure 4.3.1) in approximately 350 m of water with the larger vessel being used to control the propagation path outside of the bay. The interrogation modem was towed to various positions outside the bay from an initial test position 150 m from the smaller vessel. Ranges increased up to 6 km in this trial, shown in Table 4.3.1. Due to the time constraints of the deployment, longer ranges were not explored.

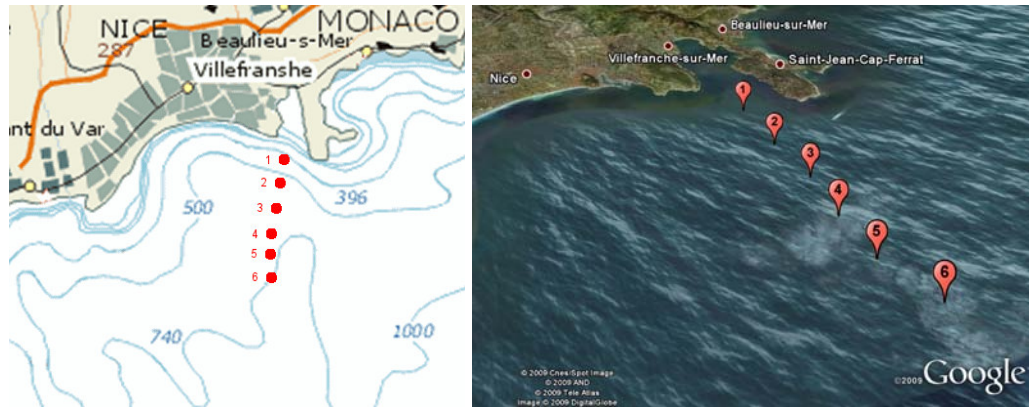


Figure 4.3.1. Vessel locations during trials off the coast of Nice, France. The stationary transmitter was located within 150 m of Test Position 1 for the duration of the trial.

Table 4.3.1. Deployment positions for the Nice trials. Approximate water depth at each modem position is also given.

Label	Modem Separation (m)	Depth (m)	Label	Modem Separation (m)	Depth (m)
TP1	150	370	TP4	3620	780
TP2	1340	500	TP5	4740	900
TP3	2485	650	TP6	5827	1000

4.3.2 Modem Performance

Overall, the acoustic modems performed reasonably well over the 6 km tested range; however, at TP5 with a range of approximately 5 km, the interrogation modem was unable to decode received transmissions. In an attempt to overcome this problem, both modems were increased to high power mode for the remaining range slice of the trial (TP6). This reconfiguration proved successful, with modems communicating effectively at the following test point at approximately 6 km. At first glance, this result suggested that the SNR was insufficient at the 5 km location. However, the possible consequences of multipath interference were not investigated at the time and may have provided a more accurate explanation. Consequently, an additional goal of this study was to determine the cause of this drop-out at TP5.

Aside from the problems exhibited at TP5, measured bit error rates were relatively small. It was found that prior to implementation of error correction, data packets exhibited a slight increase in bit error rate with range. This trend is shown in Figure 4.3.2. The data were obtained using single interrogation attempts, with no retries performed to rectify errors. The implementation of packet retries would have significantly reduced the BER, however, for the purposes of this deployment all error occurrences were included. The data point for the final range was also considered separate to the rest of the data as the transmission power was modified to ensure successful reception at long range. Further experiments utilising all three power levels would help to establish a relationship between signal strength and bit error rates but these were not performed during this trial.

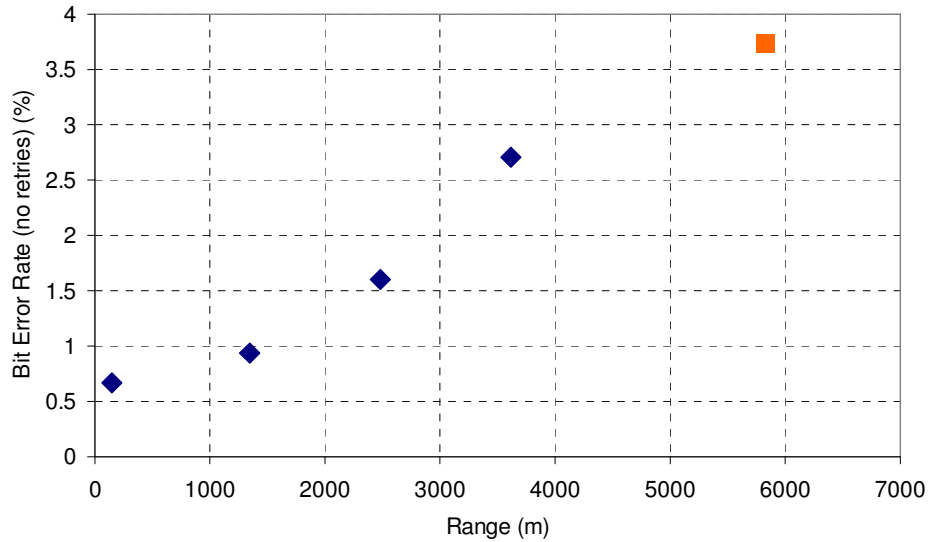


Figure 4.3.2. Summary of bit error rates versus range measured during the French trial. An expected increase in BER with range had occurred during the trial. The orange marker denotes where a higher than usual power level was used during the trial.

4.3.3 Signal to Noise Ratio

The observed SNR was suspected to be a likely factor in the reliability of acoustic communication in this trial and was consequently analysed for each transmission. Measurements of the average power spectral density (PSD) were performed over approximately 4 s of received signal. This averaging was performed to minimise the effect of fluctuations due to signal fading which was investigated later.

The communication protocol of the AQUAmodem utilised one of four possible frequencies at a time for a quarter of the total transmission length. The average spectral power for each transmission carrier frequency with a receiver bandwidth of 500 Hz was measured and the resulted SNRs are presented in Figure 4.3.3.

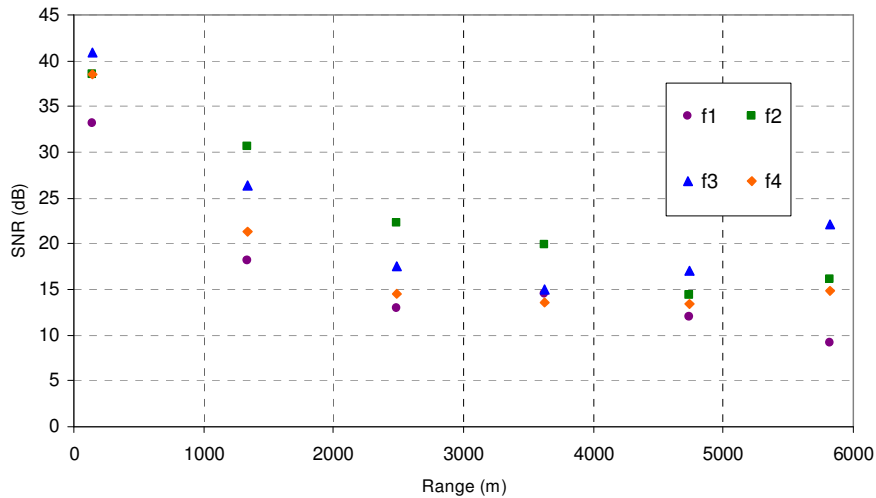


Figure 4.3.3. Calculated signal to noise ratio (SNR) based on modem recordings, showing the relative strength for each frequency component used in telemetry.

The measured SNR data demonstrated an expected downward trend with range. Additionally, an inconsistency was discovered between the SNR for separate frequency components. This finding was likely due to signal fading present in the underwater channel. The final data point in the figure was considered separate from the trend, as this utilised a high powered transmission mode. This amplified mode was designed to transmit approximately 9 dB louder than the regular low powered mode in this trial.

Estimates of transmission loss were obtained using Bellhop (described in Section 4.3.5). Figure 4.3.4 demonstrates the comparison between the Bellhop modelled Transmission Loss (TL) and the values calculated using measurements obtained during the trial. As there was no reference value for the modem power, the measured values were offset to best fit the TL curve.

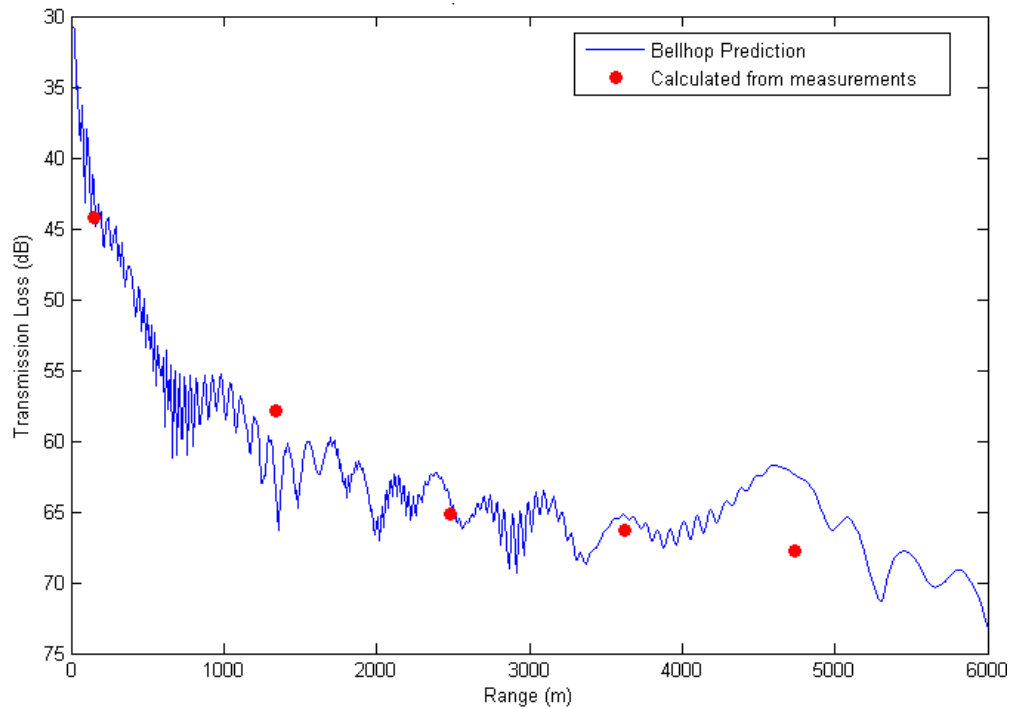


Figure 4.3.4. Averaged transmission loss versus range obtained from trials overlaid with predictions from the model. When the curves were aligned at the 150 m result, a good agreement in trend was found.

The results from the trial were found to be comparable to those obtained using Bellhop modelling. It is interesting to note that signal strength was not shown to drop dramatically at TP5 (5 km) where the interrogation modem was unable to decode data. In fact, a relative decrease in TL was predicted at this range which suggested that it was the location of a ray convergence zone.

When considering whether or not the SNR was a factor in the drop-out experienced at TP5, it was noted that the initial data request packet was received successfully by the stationary interrogated modem. The high predicted SNR and reception of the interrogation packet implied the signal power was not the main cause of the problems observed at TP5. Multipath effects such as ISI and selective fading were therefore likely to be the cause, creating decoding problems for the larger data packet. The repositioning of the modem might have been the reason telemetry resumed successfully at TP6 instead of the change to high power mode.

4.3.4 Signal Power Fluctuations

Effects of multipath were investigated by studying the variation of spectral power over the duration of a received signal. It was discovered that in some instances, periodic fading of the signal was significant and may have contributed to errors. Figure 4.3.5 shows the power levels measured for the relatively undisturbed signal observed at TP2 and for TP5 where only small interrogation packets were successfully received. The signal strength was found to vary more significantly for TP5. This effect may have increased the likelihood of reception errors should channel equalisation not have been able to adapt accordingly. It is conjectured that this effect was a possible cause of problems experienced at TP5. The problems associated with ISI do not simply increase with range which may explain why the modems operated effectively beyond TP5. The simple changing of reflection characteristics by relocation likely provided the solution rather than the increase in power.

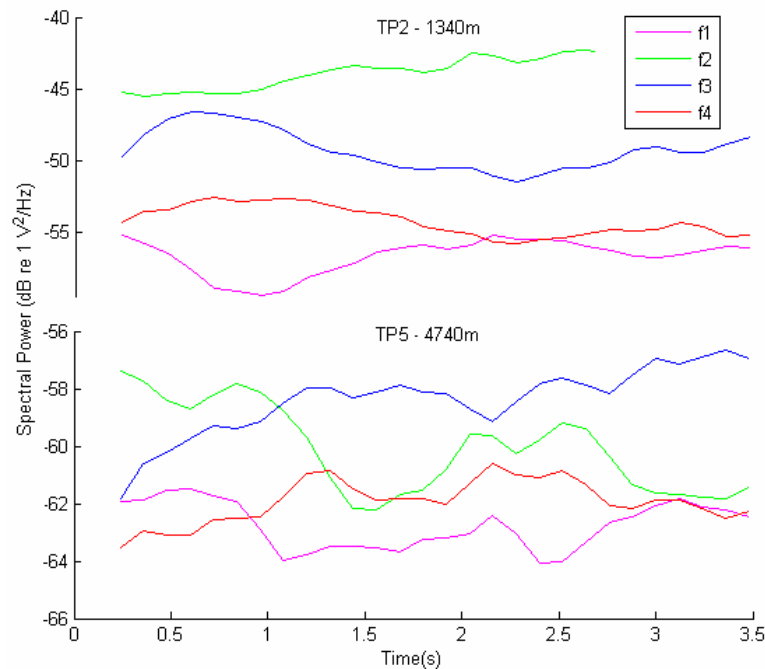


Figure 4.3.5. Smoothed signal power over the four adjacent frequency bands each with a bandwidth of 500 Hz. The multipath properties of the channel were shown to cause high amounts of signal fluctuation, with the more severe case occurring at long range.

4.3.5 Spatial Simulation of Deep Water French Trial

Simulations of the French trial were conducted similarly to those performed in Section 4.2.5, predicting performance for a modelled scenario using the measured environment data. The bathymetry was assumed from the depth charts to be an essentially linear decline from 350 m to 1000 m over the tested range of 6 km. CTD casts from inside the bay measured a uniform temperature profile which is typical given the time of the trial. Data from the World Ocean Atlas (nodc.noaa.gov) was used to confirm that an upward refracting SSP was likely to be present due solely to hydrostatic pressure. An estimated SSP was input into the models and a ray trace was first performed using Bellhop. The result of the ray trace is shown in Figure 4.3.6 which shows the estimated velocity profile and propagation paths. From analysis of the Bellhop model, the absence of a thermocline resulted in an upwardly refracting acoustic environment. This was beneficial when considering the shallow transmitter and receiver positions as surface duct propagation would have likely occurred. As a result of these propagation characteristics, a direct acoustic path between the transmitter and receiver was likely present at all ranges tested in the experiment.

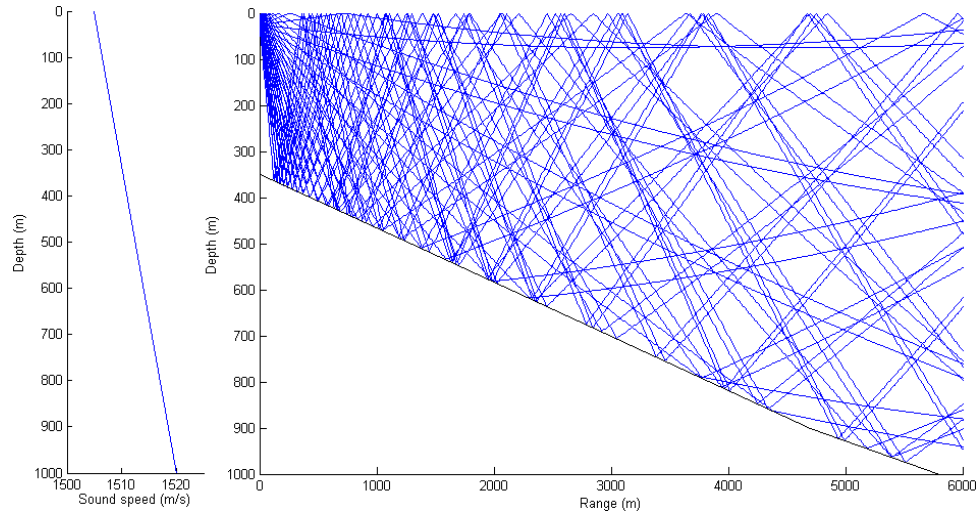


Figure 4.3.6. Sound speed profile and ray path diagram for declining bathymetry modelled to simulate trial data from the Villefranche-sur-Mer coast.

For the simulations, a receiver array spanning the entire water column was utilised with a transmitter located 25 m below the surface, similar to the field trial. Receivers were located at 10 m intervals horizontally and 5 m vertically. A preliminary

simulation (Figure 4.3.7) was performed without the addition of ambient noise to assess the overall performance of the acoustic modems based purely on ray propagation and the resulting channel impulse response.

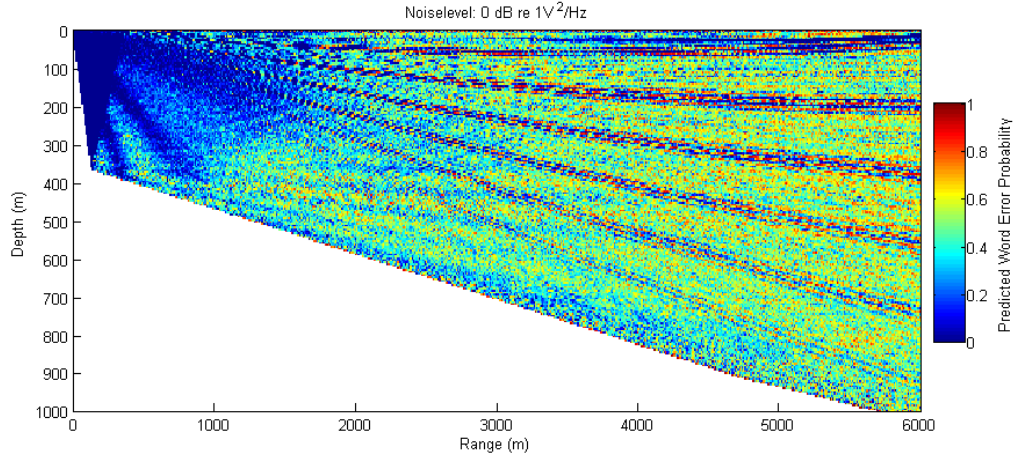


Figure 4.3.7. Word error probability over a depth-range grid predicted from simulations of the French trial using an upwardly refracting SSP and without adding noise.

Initial predictions indicated that the upwardly refracting SSP yielded effective long-range communication at shallow depths, with other advantageous zones located near the seabed. Receivers located close to the transmitter were found to perform well due to a direct path of higher amplitude than later arrivals reflected from the boundaries. Overall performance was demonstrated to decrease with range due only to multipath propagation as no noise was introduced into the simulation at this stage. Artefacts of the Bellhop model were present which were not indicative of any performance characteristic. For example, distinguishable lines throughout the middle of the water column were likely caused by aliasing of the small-scale interference patterns created by the superposition of arrivals from different directions. It was expected that modem movement and slight channel fluctuations would similarly limit the validity of these predictions.

Noise was introduced into the simulation following the initial look at the effect of multipath propagation. The transmitter was set to a nominal source level of 180 dB re 1 μ Pa @ 1 m as the exact levels during the trial were unknown. The appropriate level of ambient noise was calculated using the SNR values shown in Figure 4.3.3. Assuming an average SNR of 40 dB at a range of 150 m and using a

spherical spreading estimate for transmission loss, the appropriate noise level was calculated to be approximately 70 dB re $1 \mu\text{Pa}^2/\text{Hz}$ at a minimum. Figure 4.3.8 shows the French simulation results when including a 70 and 80 dB re $1 \mu\text{Pa}^2/\text{Hz}$ Gaussian noise component. The effect of noise is clearly shown with a decline in performance with range superimposed onto multipath effects.

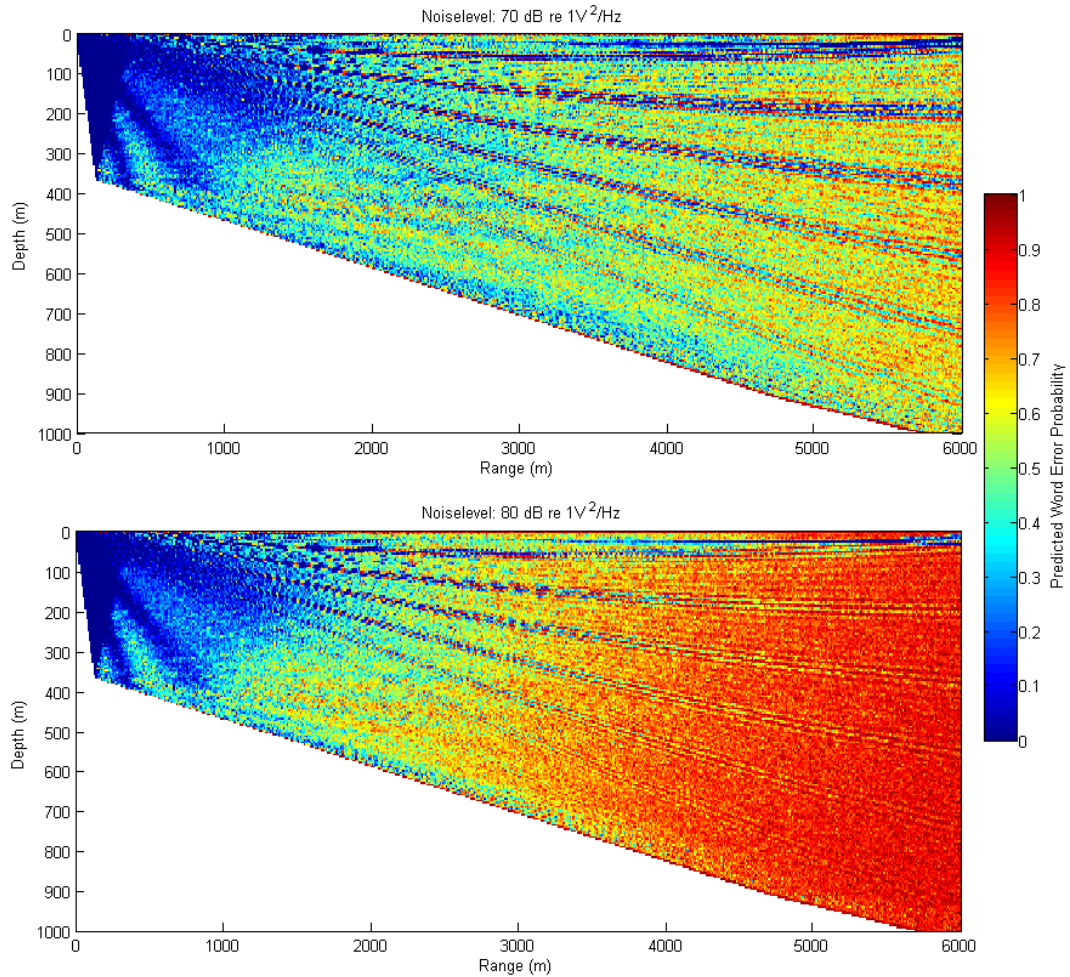


Figure 4.3.8. Simulation result for the French modem trial using an upwardly refracting SSP, including noise. Two different values of noise were used to show the likely performance effect of 70 dB re $1 \mu\text{Pa}^2/\text{Hz}$ (approximate value expected given measurements of SNR) (top) and 80 dB re $1 \mu\text{Pa}^2/\text{Hz}$ (bottom) to highlight the effect of increased noise.

Following the calculation of two-dimensional spatial simulation data, simulator results were refined to produce a prediction for comparison with trial data.

Simulations using a higher spatial resolution were conducted by decreasing the total area covered, allowing for the consideration of any interference patterns whilst still

obtaining a practical simulation run time. A 2 m strip in depth, covering the entire range, centred at a depth of 25 m was evaluated with the simulator. A finer depth resolution of 5 cm was used with a range resolution of 100 m. Figure 4.3.9 shows the resulting predictions for a receiver located between 24 m and 26 m below the water surface at 10 m increments for simulations using 0, 70 and 80 dB re $1 \mu\text{Pa}^2/\text{Hz}$ noise. Finally, the depth-averaged prediction for each SNR was calculated and is also shown alongside observed performance.

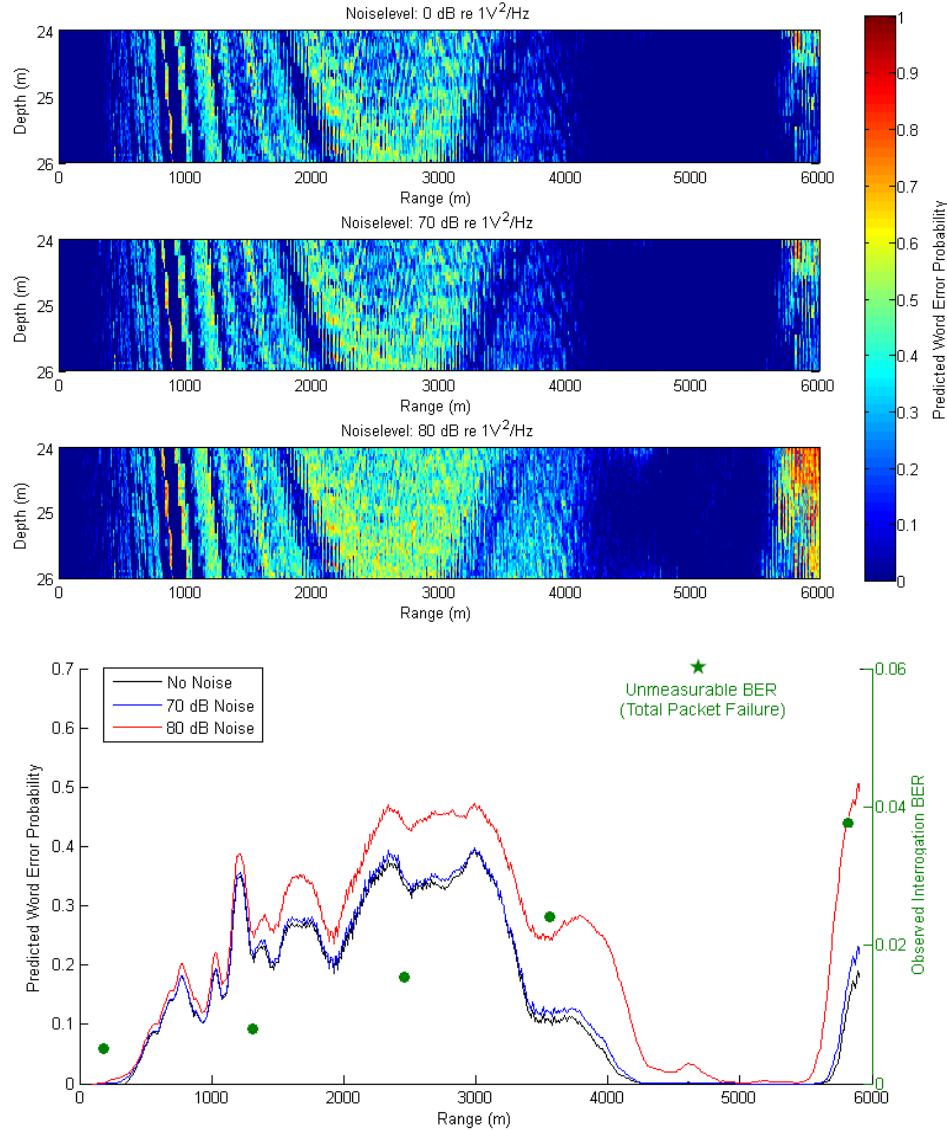


Figure 4.3.9. Results from high resolution range simulation of the French trials with a centre depth of 25 m (top). By averaging with depth, the overall simulated performance for a receiver located at approximately 25 m is also plotted with the trial results (bottom).

Comparison with the trial results found that the simulator predicted near-perfect performance at a range of 4700 m where no telemetry was observed. The position of poor observed performance could, however, be reflective of a similar decline in performance predicted at approximately 3600 m in the presented simulation, where multipath interference was shown to be high. The discrepancy in position may be explained by the lack of precise environmental measurements of the area.

Specifically, the bathymetry was obtained by interpolating the results from a relatively imprecise chart and the lower portion of the SSP of the water column was calculated using averaged historical data records. This possible explanation is supported by measurements of transmission loss (Figure 4.3.4) which showed a similar discrepancy in TL at TP5. Both TL and performance comparisons show similarities in the overall shape of the trends which suggest the locations of existing features were misplaced by the simulator. Consequently, it is conceivable that if environmental parameters were more accurately known, the simulation may have provided a more accurate prediction. However, this is somewhat speculative given the lack of trial and environmental data.

Overall, the simulation model lacked the accuracy to sufficiently predict the observed modem performance. However, the simulation result indicated that noise was not an impacting factor on the performance of the acoustic modems. This is supported by both the high SNR observed during the trial as well as the existence of interference zones, which could account for the transmission drop-out exhibited within the trialled range.

The SSP for the trialled environment yielded only upwardly refracting energy due to the winter conditions. However, data from Salon *et al.*, 2003, Zheng *et al.*, 1996 and the World Ocean Atlas (nodc.noaa.gov) showed a distinctly different SSP in summer, when a thermocline existed down to depths of approximately 50 - 100 m. The dependence of deep water acoustic propagation on the SSP indicated a possible variability in trial performance based on a particular season. As an additional investigation, the summer case was analysed. The summer SSP is shown in Figure 4.3.10, along with a ray propagation diagram which demonstrates downward refracting energy from a transmitter located 25 m below the sea surface.

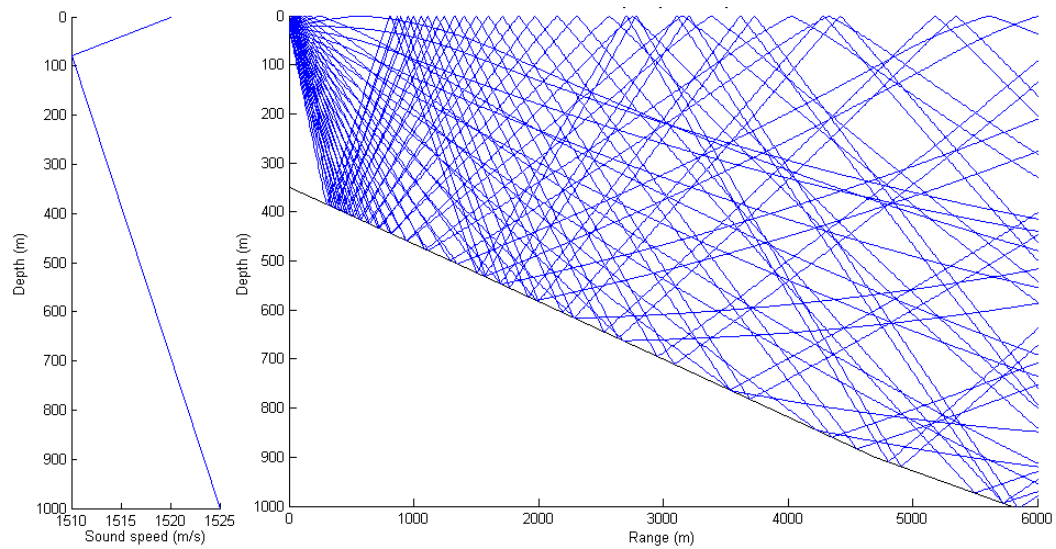


Figure 4.3.10. Summer SSP for the French modem trial showing a thermocline giving both downward and upward bending rays.

Due to the shallow transmitter location, a direct path to a receiver located near the surface was shown to be impossible at long range. This indicated that a receiver located at the surface would likely exhibit poorer performance when compared to the trial performed in winter. This also suggested that a receiver position below the thermocline would be most optimal for obtaining effective acoustic communication using a transmitter located above the thermocline. Similarly to the winter study, a spatial simulation was conducted for different noise levels with the results shown in Figure 4.3.11.

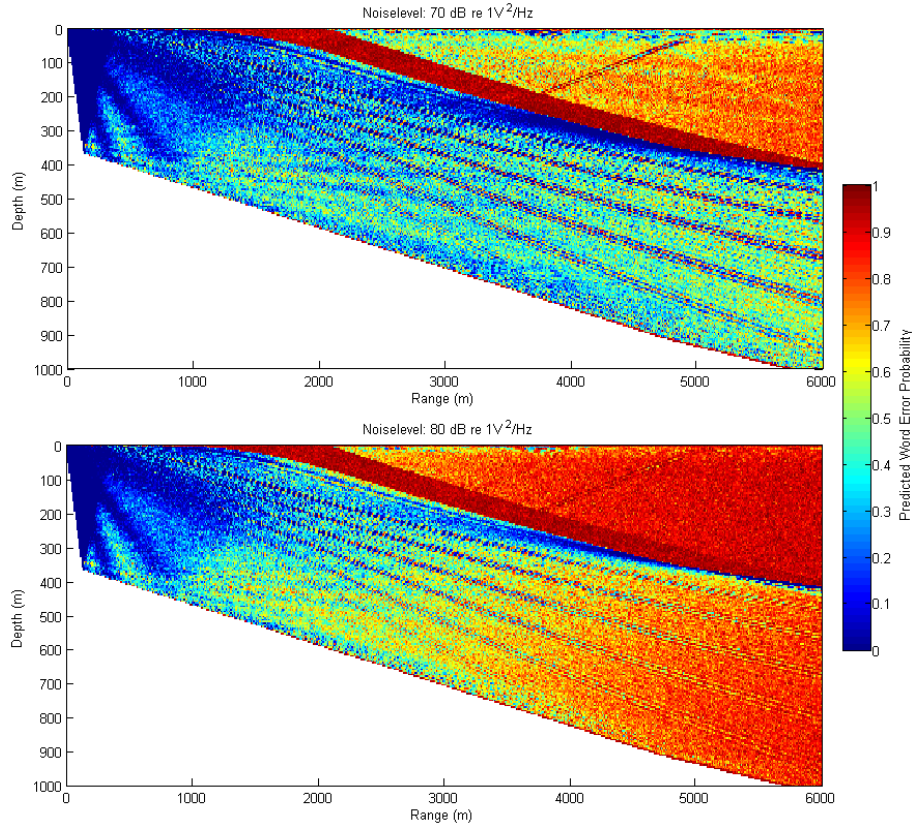


Figure 4.3.11. Simulation result obtained for the French trial using a summer SSP with noise. Two different values of noise were used to show the effect of 70 dB re 1 $\mu\text{Pa}^2/\text{Hz}$ (top) and 80 dB re 1 $\mu\text{Pa}^2/\text{Hz}$ (bottom).

A “red band” of extremely poor performance sloping downward into the middle of the column was observed in the simulation results. According to the modelled ray pattern shown in Figure 4.3.10, this band was located at the edge of the area occupied by direct rays from a transmitter placed below the sea surface. It was found by investigating the impulse response that the cause of poor performance was due to a first arrival of low intensity which affected the receiving algorithm. Only the edge of the beam energy profile for the direct path was present and signals reflected from the sea surface and seabed were much higher in amplitude. The simulator used this first arrival to synchronise the receiving algorithm and was therefore unable to correctly decode the data. As a modification to the synchronisation using the first arrival (‘first’ method), the simulator was temporarily reconfigured to utilise the maximum amplitude arrival (‘max’ method) which reflected the performance of an ideal receiver. The simulation was rerun for comparison with the result shown in Figure 4.3.11 (top) with the differences between the results of the two different

algorithms shown in Figure 4.3.12. With most of the original simulation unaltered, the red band was removed upon utilising the ‘max’ method. This result highlights the importance of efficient synchronisation algorithms as low amplitude first arrivals can occur in the field.

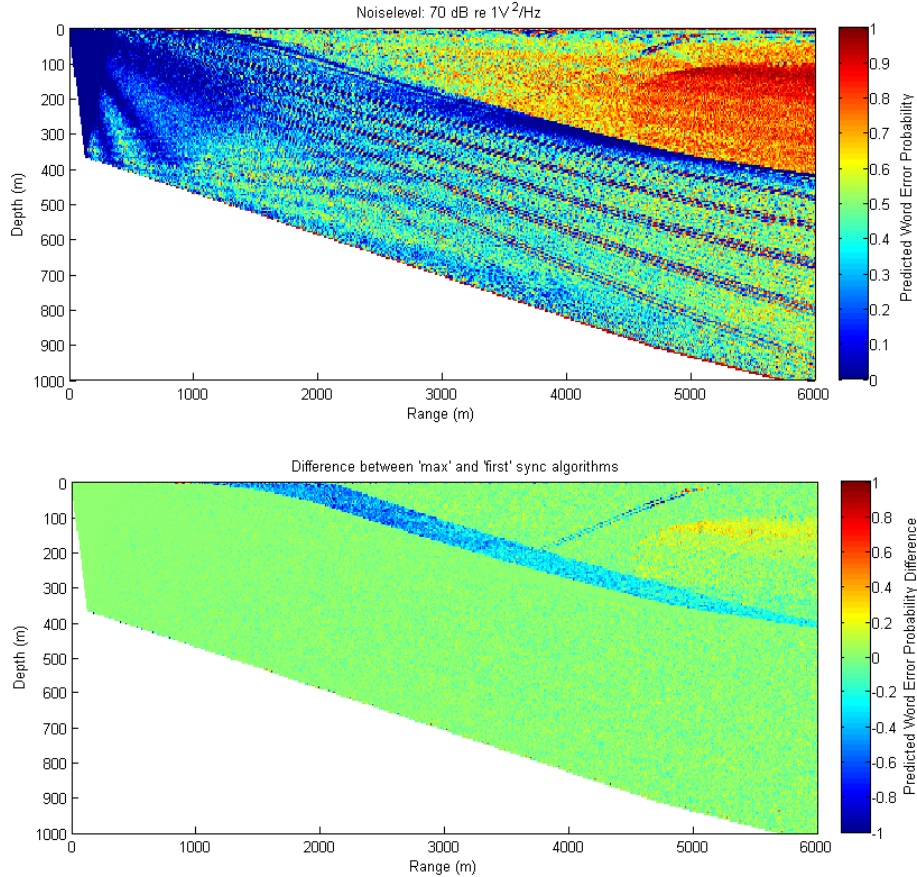


Figure 4.3.12. Simulation of the French trials during summer using the ‘max’ algorithm which synchronises the receiver to the maximum amplitude arrival (top). Also shown is the difference between the two synchronisation methods, highlighting areas where low amplitude first arrivals were problematic (bottom).

Overall, the predicted modem performance with a summer SSP demonstrated vastly different results to those obtained in both the winter trial and simulation. In contrast to mostly surface duct propagation in winter, the summer simulation shows most of the energy being projected downward. This is evident in the higher noise scenario, where the lack of a direct path at the surface resulted in an unsuitable SNR and poor performance. Figure 4.3.13 shows comparisons between summer and winter simulations using the same modem positions and noise settings to demonstrate the expected effect of a summer thermocline on the transmission characteristics.

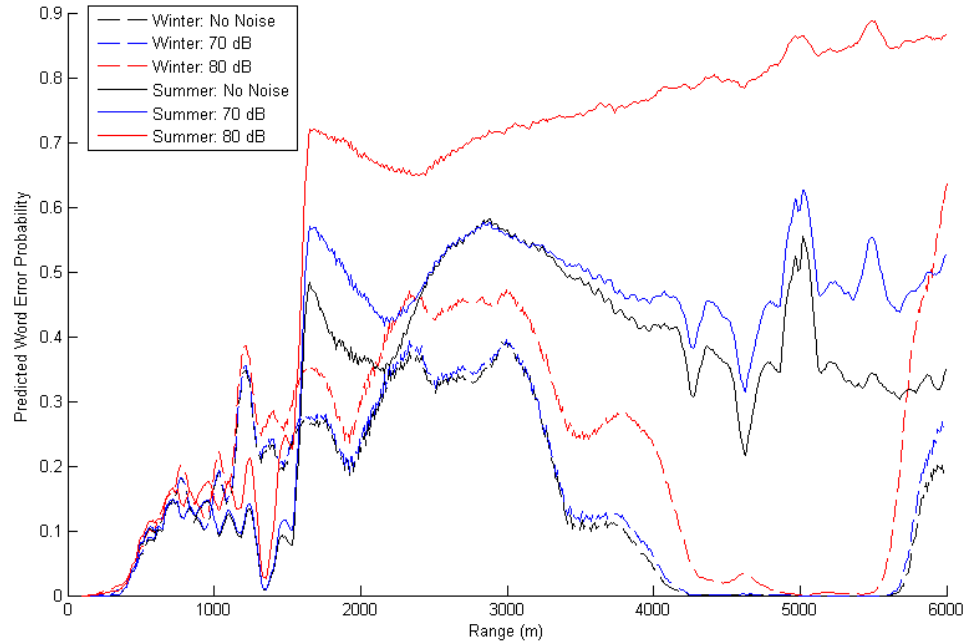


Figure 4.3.13. Summary from high resolution range simulations of the French trials, showing the differences between obtained results using a summer and winter SSP. By averaging with depth, the overall simulated performance for a receiver located 25 m below the surface is plotted. The ‘max’ synchronisation method was utilised to remove the ‘red band’ where low amplitude first arrivals occurred.

4.3.6 Summary

Trials conducted by Aquatec Group Limited demonstrated effective modem performance over a downward sloping seabed with an upwardly refracting sound speed profile. A Bellhop model of acoustic propagation in the area was used to provide predictions of both transmission loss and multipath effects. The shallow positioning of the modems was predicted to result in favourable channel conditions given the presence of a surface duct. A drop-out experienced at one of the intermediate ranges was determined to have not been caused by insufficient SNR suggesting it was a possible consequence of multipath interference. The average SNR exhibited at the receiver was measured to be approximately 10 dB in the worst cases. The raw BER was shown to increase with range; up to 4 % at approximately 6 km.

Simulations were performed which predicted an overall performance decrease with range, however, the drop-out experienced at approximately 5 km was not accurately predicted. This may have been a result of the relatively inaccurate knowledge of the environment and it was hypothesised that an area of high ISI predicted by the simulator was not positioned accurately, explaining the discrepancy. Further simulation of the same environment using a typical summer SSP found contrasting propagation characteristics with the majority of acoustic energy propagated downwards.

Overall, the simulation results confirmed that the shallow position of the modem was advantageous for this particular trial given the winter SSP. However, for a long-term deployment, the characteristics of the underwater channel would change seasonally. As a result, the performance of an underwater acoustic communication system could vary significantly, dependant on the location of the nodes.

5 Long-term Investigation of Environmental Parameters Affecting Communication

A primary component of this study was to investigate the performance of underwater acoustic communication in a long-term deployment. This chapter outlines the methodology and results from a long-term trial off the coast of Perth, Western Australia. The results of performance predictions made using the underwater acoustic communication simulator are also presented and compared to the experimental data.

A long-term shallow water study was performed prior to the following experiment, using the same recording hardware with acoustic identification tags. The results of the analysis demonstrated a correlation between the acoustic tag detection rates and ambient noise levels, which were likely caused by a combination of wind and wave fluctuations as well as snapping shrimp which were prevalent in the area. A detailed report on this study can be found in Appendix C with further discussion of the results in Chapter 6.

5.1 Experimental Setup

In order to understand the long-term environmental effects on a stationary underwater telemetry system, a trial similar to KauaiEx (Section 2.5) was performed using a single pair of AQUAmodems. The initial deployment of the equipment was conducted on 26th February 2010 with recovery performed on 16th March 2010. Two sets of instruments were placed on the seabed with a separation of approximately 5 km in a water depth of approximately 100 m.

The location of deployment was approximately 20 km North West from the coast of Rottnest Island, Western Australia as shown in Figure 5.1.1. This location is near the edge of the west coast continental shelf which is influenced by the Leeuwin Current

which flows southward along the shelf edge, generating mesoscale eddies in the surrounding ocean (Waite et al., 2007). It was anticipated that the Leeuwin Current and its associated eddies would generate a dynamic range of environmental conditions at the deployment location that would affect the performance of underwater acoustic communication.

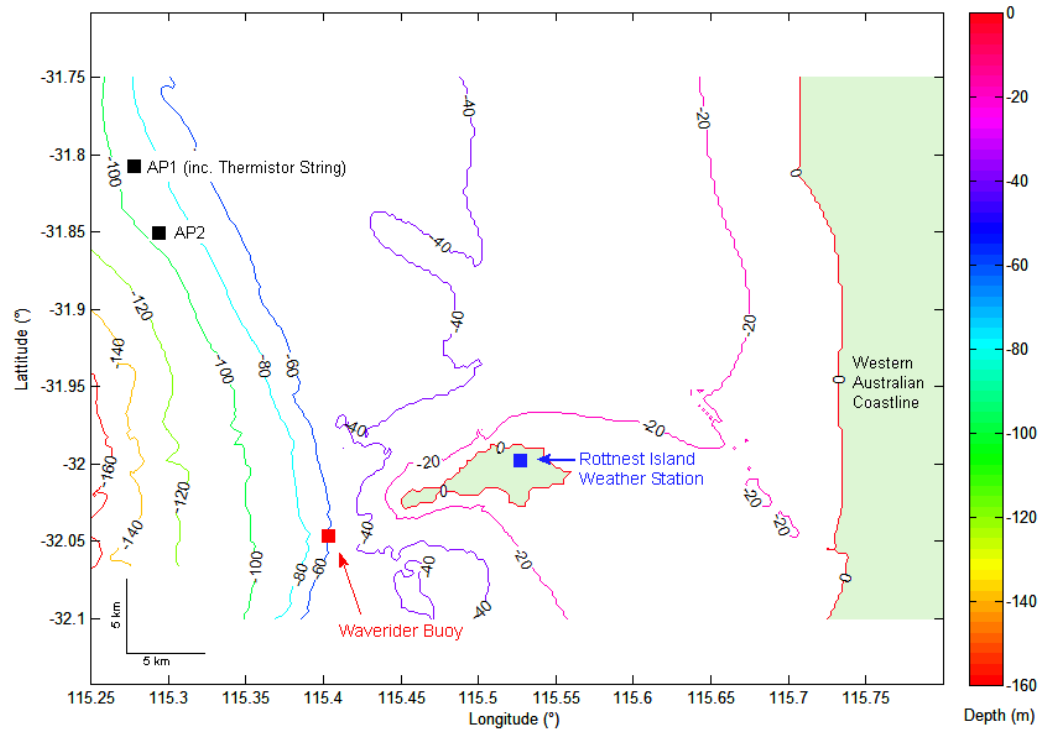


Figure 5.1.1. Locations of the two acoustic packages (AP1 and AP2) and other sensors used for the long-term deployment off the coast of Western Australia. The two acoustic packages were deployed in a depth of approximately 100 m with a separation distance of approximately 5 km. Bathymetry data courtesy of Geosciences Australia (Whiteway, 2009).

As with previous deployments using the AQUAmodem, two high frequency ambient noise recorders were integrated into a subsea logger system using the MCS and placed in deep water housings. The recorder housings were positioned on the seabed with the modems suspended approximately 4 m above using a rope taped to a subsea electrical cable connecting each modem to the equipment base. The hydrophone for the recorder was located along the support rope, approximately 1 m above the seabed. Figure 5.1.2 shows the deployment layout, with photos of the equipment prior to their deployment given in Figure 5.1.3.

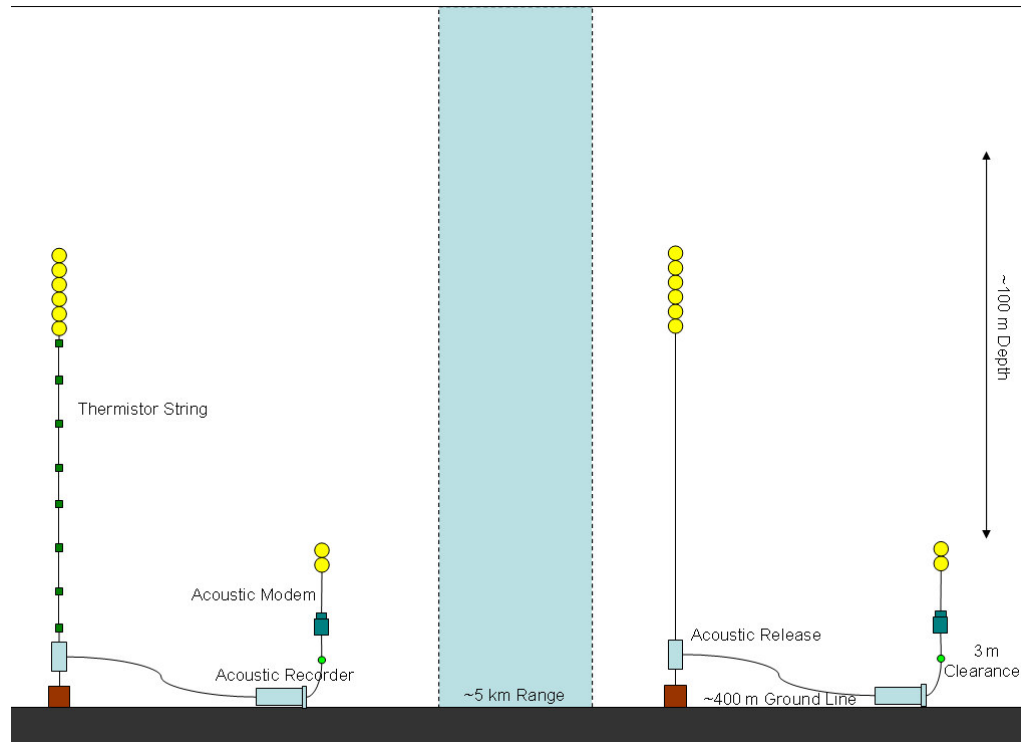


Figure 5.1.2. Experimental setup for the long-term trial showing all equipment used in the deployment. Two sets of equipment were deployed which periodically communicated with one another while recording information including ambient noise levels and a temperature profile for the bottom 50 m of the water column.

Data pertaining to the surrounding conditions were simultaneously collected during the deployment using additional sensors. Additional data included water temperature profiles which were obtained using an 8-element thermistor string attached to one of the ambient noise recorders and spanning the bottom 50 m of the water column. Additionally, two pressure sensors were positioned 22 m and 49 m above the seabed on the same line to provide mooring pull-down information. Table 5.1.1 shows the positions and assignments of each array element.



Figure 5.1.3. Configuration of some of the equipment unique to the Perth long-term modem deployment. Each underwater acoustic modem was suspended using two floats approximately 4 m above a deep water housing anchored to the seabed. A subsea cable was used to route power and communications from the main seabed housing. The inset shows one of eight elements used to form the thermistor string. After being secured to the riser via a rope splice, each unit was taped to the line to restrict movement.

Table 5.1.1. Summary of temperature and pressure sensor positions along the riser for Acoustic Package (AP) 1. Depths provided are based on a 100 m deep water column and the separation distance of the sensor from the seabed.

Element Number / Pressure (P) Temperature (T)	Estimated Average Depth (m)	Element Number / Pressure (P) Temperature (T)	Estimated Average Depth (m)
PT1	51	PT5	78
T2	58	T6	84
T3	65	T7	91
T4	71	T8	97

Given the relationship between seawater temperature and sound speed shown with Equation A.11, the thermistor string data provided information directly related to the sound speed profile of the water column. This information allowed for the characterisation of acoustic signal propagation through the channel. Additional information about the local sea surface conditions, including wind data (Rottneest Island Weather Station, Figure 5.1.1) as well as waves and tides data (Rottneest Waverider Buoy, Figure 5.1.1) was obtained courtesy of the local Department of Transport and the Bureau of Meteorology.

In contrast to the short-term trials presented in earlier sections, this experiment involved long-term operation of the deployed equipment. This placed importance on effective power management implemented by the software on board the MCS and acoustic recorder. The MCS software, *ModCon* operated in Deployment Mode B which based the power management on a duty cycle, shown in Figure 5.1.4. For this deployment, the power cycle lasted 7 minutes of every half hour. This was accomplished using *PDALogger Skinny*, operating on the recording hardware, providing storage of acoustic recordings as well as recording the modem transmission statistics.

Device operation over the 7 minute cycle included both interrogations and one-way transmissions between the modems as shown in Figure 5.1.4. Occupying a half of the full cycle, each modem transmitted a data request to the remote modem of three increasing sizes, 8, 30 and 63 bytes. These were initiated directly by low level control from *ModCon*. Additionally, the interrogations were interleaved with short transmissions of remaining disk space to the remote modem with no acknowledgment request. These one-way transmissions were initiated by *PDALogger Skinny* and were therefore dependant on the successful operation of the recorder as well as the MCS.

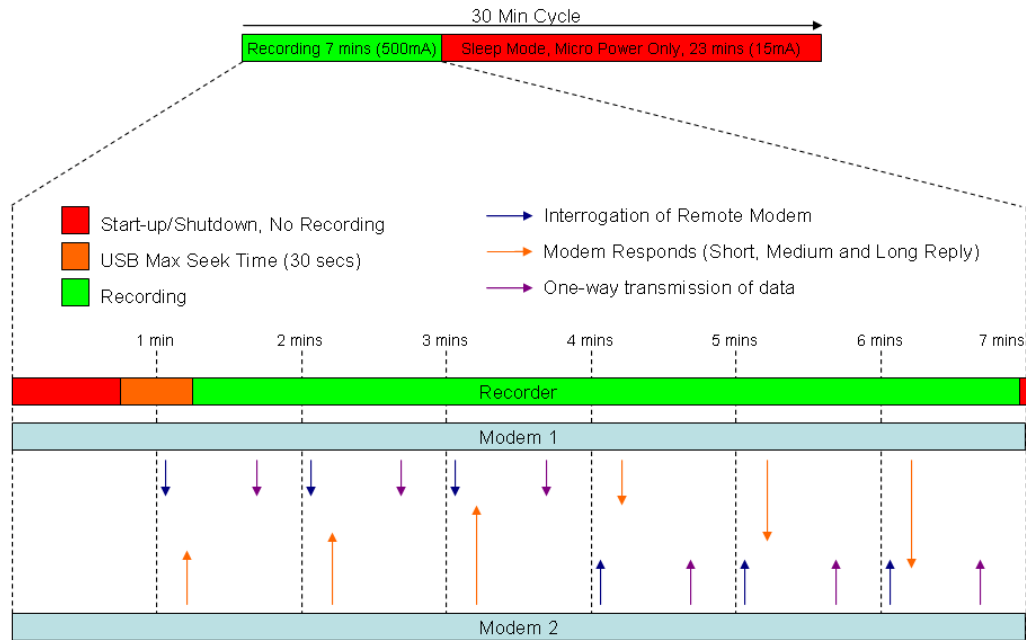


Figure 5.1.4. Software cycle for the long-term trial, showing the various phases of recording and communication. Operating one cycle every 30 minutes, the devices were expected to record for up to approximately 6.5 minutes depending on the disk space available. During this time, modem communication involved memory requests, memory returns and one-way transmissions. Memory requests included different sized packets to investigate any effects on the decoding stability.

Shorter modem transmissions were each uniquely identified by a timestamp and serial number (disk space remaining in MB) allowing for the easy identification of successful transmissions in post-deployment analysis. Requested memory blocks were also known and provided additional data regarding the transmission of various sized packets. In total, a successful duty cycle resulted in 18 modem transmissions, 12 when excluding the unrecorded packet requests. Excluding a three-pulse wakeup sequence, the acoustic duration of each packet varied between 1.2 seconds for the short serial number packet to 7.8 seconds for a 63 byte memory packet.

5.2 Recovery and Initial Analysis

The equipment was retrieved three weeks after the deployment date in order to maximise use of the 32 GB capacity of the recorders operating at 48 kS/s on the prescribed duty cycle. Upon recovery, it was discovered that the acoustic modem transducers and surrounding cables on both sets of equipment had been lacerated as shown in Figure 5.2.1. The damage was found only on the transmitting components of the gear and was thought to have been caused by marine life, probably fish. Analysis showed the damage to have occurred approximately 3 days prior to recovery, which is when the devices began to fail, as shown later.



Figure 5.2.1. Photos of the underwater acoustic modems following recovery after three weeks of operation. The images show lacerations in the subsea cable in close proximity to the modem (top), as well as a gouge in the modem transducer itself (bottom).

Following preliminary analysis of the data and given the deployment times, the starting point of the trial was set at 12:30pm on the 26th February 2010. The end was 07:00 on the 17th March 2010. References to elapsed time throughout this chapter are relative to the starting point with a total deployment duration of approximately 21 days.

The damage to the exterior of the modems and surrounding cabling was suspected to have caused failure in at least one of the modems. For this reason, the data relating to the responses from the modems required additional analysis. The communication lines between the modem and MCS shared the same cable as the power source. To best determine when the cable shielding was compromised the RS232 communication link was investigated to establish if and when the connection between the two devices was unstable or non-existent.

Investigation of AP1 yielded no point in time where serial communication was interrupted, reflecting only the minor damage to modem cabling with the majority of marks on the modem transducer. However, AP2, which was found to be not operating upon recovery, had lost reliable communication by approximately 23:00, 14th March 2010. The low powered MCS was found to be operating at recovery, suggesting the battery supply was not depleted by the end of the trial. Additionally, intermittent and corrupt communication present for 24 hours following the disruption point suggested a problem with the RS232 lines. However, faults occurring when the modem was expected to draw more current indicated a fault in the power supply. It was therefore surmised that the removal of the protective casing of the internal wires led to an eventual submersion of both serial and power lines around this point in time, resulting in the failure. The end time of the acoustic communication performance measurements was therefore set at 23:00, 14th March 2010 providing approximately 16.5 days of statistics.

5.3 *Experimental Data*

5.3.1 Temperature Measurements and Sound Speed Profile

The thermistor string was found to operate effectively over the entire trial period. The data obtained from the string provided a detailed overview of the evolution of the sound speed profile of the bottom 50 m of the water column during the trial. Figure 5.3.1 shows the temperature profile over the period of deployment as recorded by the sensors.

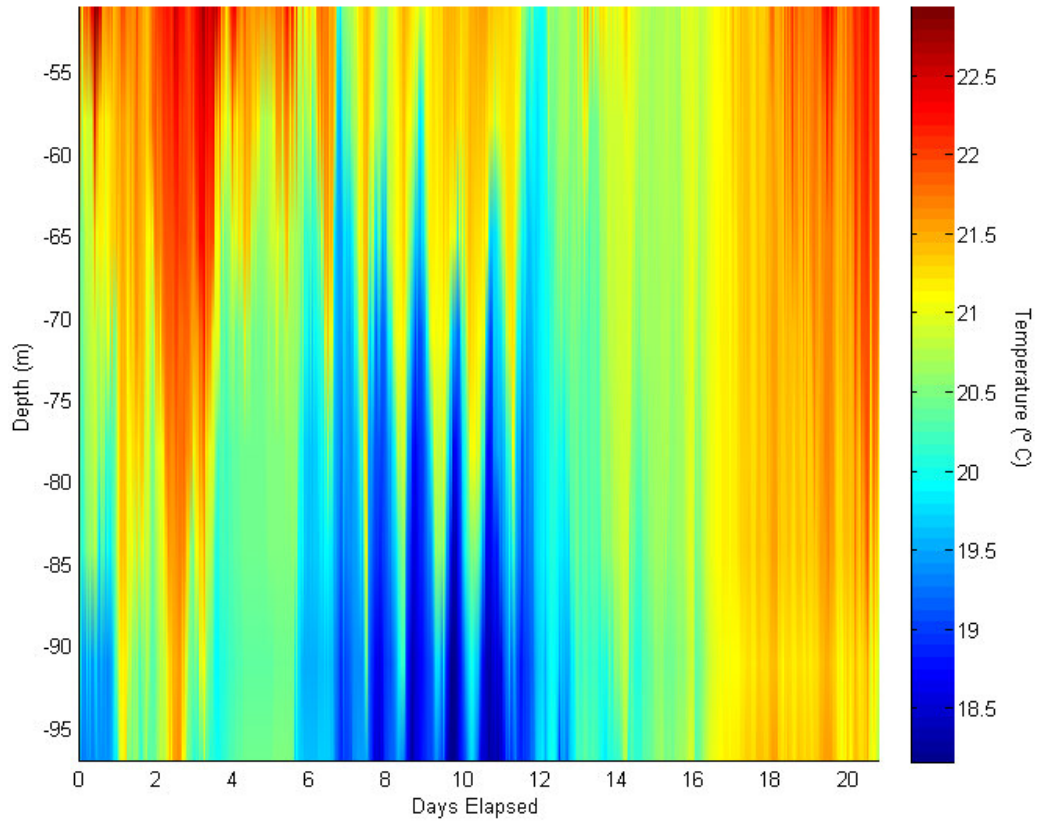


Figure 5.3.1. Temperature profile as recorded by the eight-element thermistor string deployed with Acoustic Package (AP) 1. Only the bottom half of the water column was captured.

The temperature variations present over the deployment period showed several distinct areas. A tidal pattern was observed, dropping to temperatures below 18.5 °C during the mid-term of the trial. Additionally, the bottom 50 m of the water column became virtually isothermal towards the end of the deployment. Some abrupt changes of the SSP at all depths were also consistent with the advection of eddies from the Leeuwin Current, discussed earlier.

Underwater currents were likely to cause distortion to the shape of the thermistor string during the trial. Using the pressure sensors located on two of the elements, the changes in sensor depth were calculated. Additionally, tidal movements observed at Fremantle Harbour were used for depth correction. It was interesting to note that the presence of spring tides at the beginning and middle of the deployment period (Figure 5.3.2) correspond to the large temperature changes observed by the thermistor string.

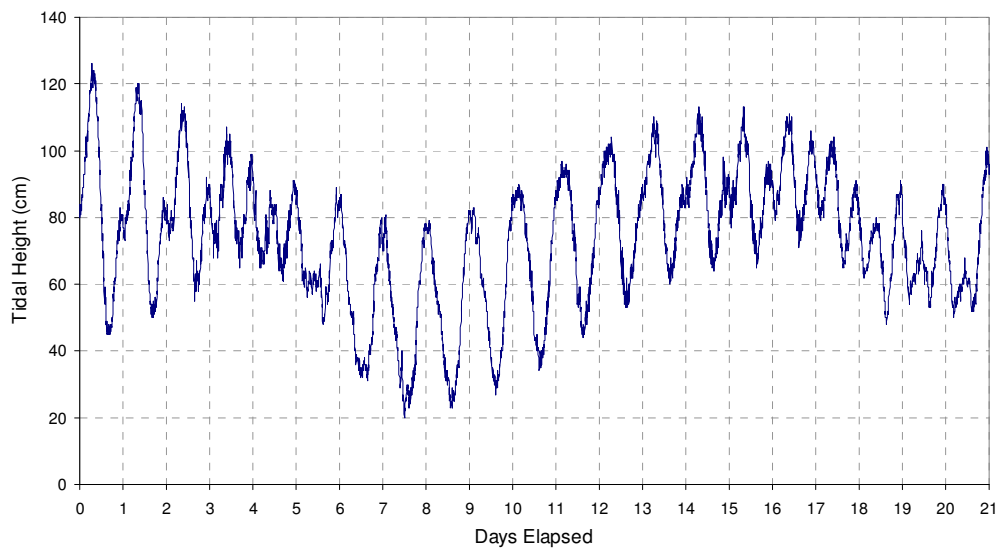


Figure 5.3.2. Measured tide at Fremantle Harbour (Perth) during the deployment period. Data courtesy of the Department of Transport, Western Australia

Figure 5.3.3 shows the calculated depth readings from the pressure sensors located at approximately 25 m and 50 m above the seabed. Using this data, the time dependant depths of the temperature sensors along the line were determined and are also shown, corrected to compensate for tidal movements.

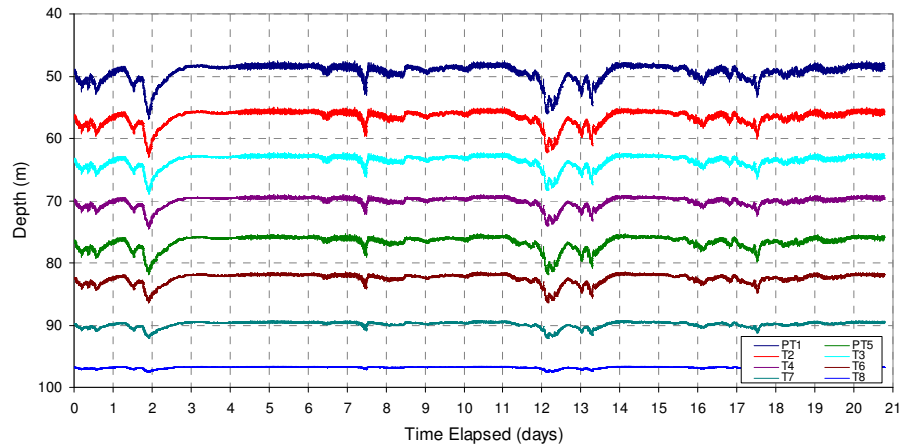


Figure 5.3.3. Calculated depths for PT1 and PT4 (See Table 5.1.1) along the thermistor string using the measurements from the pressure sensors. Fluctuations are shown with a maximum overall change in depth of approximately 7 m experienced at the top of the string.

Following the inclusion of the depth fluctuation data from the pressure sensors and correcting for tide height, the sound speed profile over the deployment duration was calculated and is shown in Figure 5.3.4. The calculation using Equation A.11 assumed a fixed salinity of 35.7 psu which was the value measured at a depth of 50 m upon recovery of the equipment.

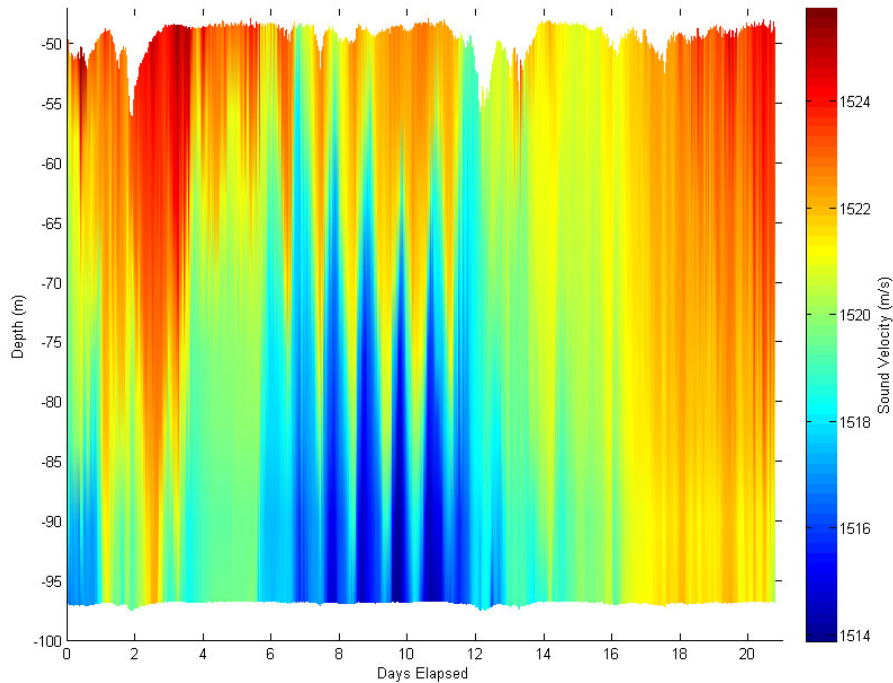


Figure 5.3.4. Sound speed profile as calculated using data from the eight-element thermistor string deployed with acoustic package (AP) 1 and corrected for changes in sensor depth.

Useful for comparison with other data sets such as modem performance and ambient noise, the changes in the gradient of the thermocline were represented by calculating the least squares linear fit of the temperature profile measured by the thermistors, shown in Figure 5.3.5. Although only spanning the bottom half of the water column, the SSP gradient provided a useful indication of the amount of refraction for horizontal near-seabed acoustic propagation.

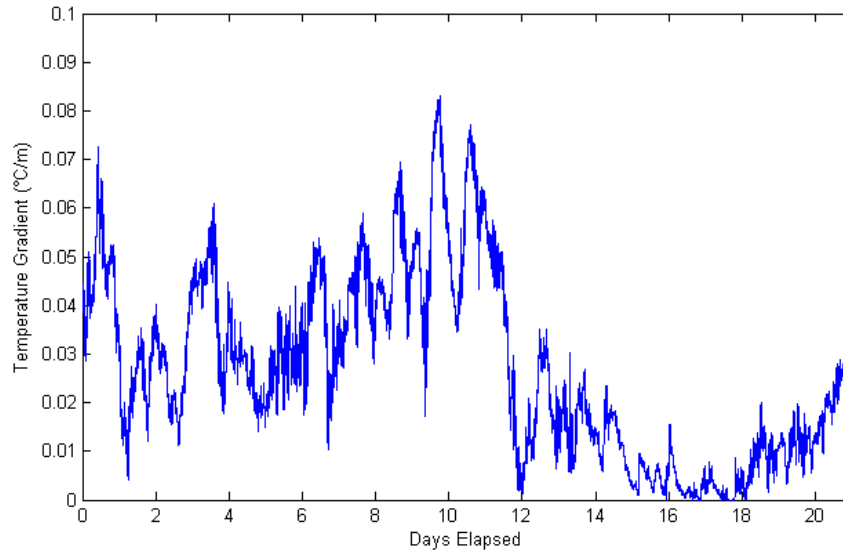


Figure 5.3.5. Plot of temperature gradient vs. time using the least squares linear fit over eight elements in the bottom 50 m of the water column. The gradient of this thermocline dictates the refraction characteristics of the bottom half of the water column.

To obtain sound speed profile data spanning all depths of the water column, sea surface temperature (SST) was obtained from NASA (www.nasa.gov) and used to interpolate a temperature estimate of the upper 50 m. Daily SST data measured by satellite were extracted for the deployment location over the trial period. It was possible to assess the quality of the measured data as each SST segment was in Hierarchical Data Format (HDF). Cloud cover, sun glint, high camera angles and other uncontrollable factors all contributed to reduced quality of the SST data. The SST data points were each categorised using the quality flags within the HDF format (Figure 5.3.6). SST was determined not to have fluctuated beyond approximately 2 °C with a downward trend from 24.5 °C to 22.5 °C. An estimation of SST over time was interpolated for the trial duration and is also shown in Figure 5.3.6.

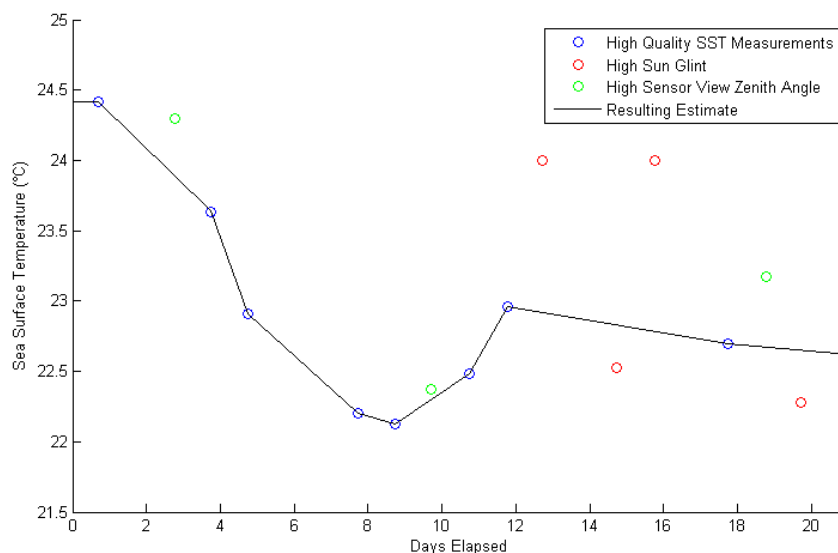


Figure 5.3.6. Sea surface temperature measured at the deployment location via satellite. Data was separated to represent the quality control flags within the data set with an interpolated estimate of temperature trends during the trial. SST data courtesy of NASA (www.nasa.gov)

Following estimation of the SST, a subsequent estimate of the full temperature profile over time was used to calculate the sound speed profile during the deployment and is shown in Figure 5.3.7.

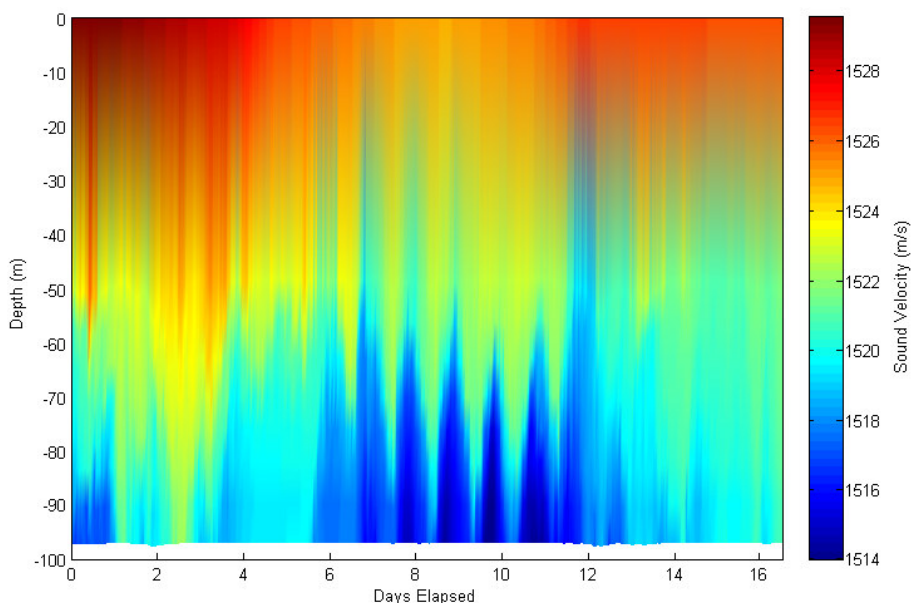


Figure 5.3.7. Sound speed profile for Perth long-term deployment following the inclusion of SST measurements.

5.3.2 Wind and Waves

Wind speed and wave height information was obtained for comparison with other data collected during the trial. Figure 5.3.8 shows the wind speed measured at Rottnest Island during the deployment. Wind speed was shown to exhibit both high frequency (approximately diurnal) fluctuations and long-term changes. Additionally, some days experienced two peaks with the middle of the day often relatively calm.

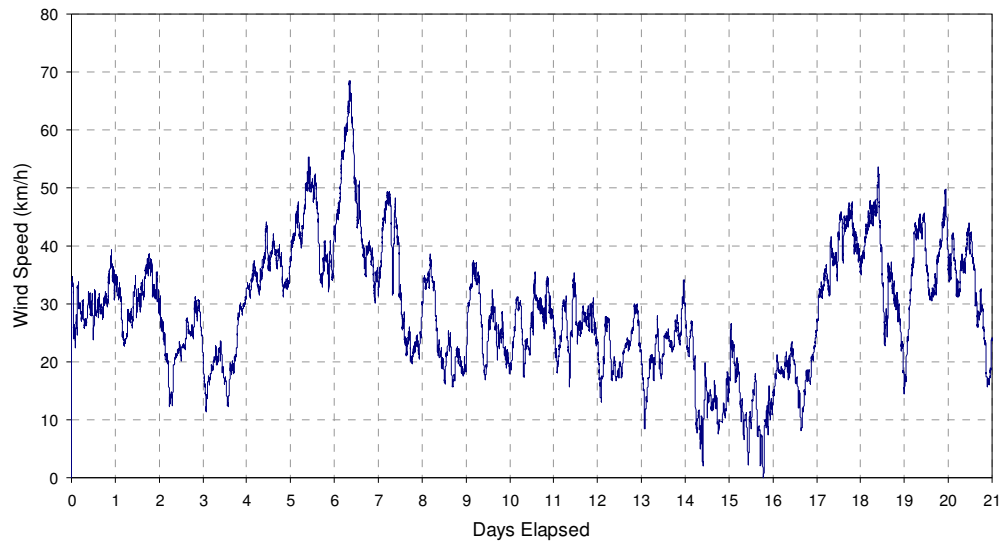


Figure 5.3.8. Wind speed as observed during the deployment period by a weather station at Rottnest Island. Data courtesy of Bureau of Meteorology, Australia.

Data from a nearby Waverider buoy (Figure 5.1.1) were used to evaluate the wave height over the trial period. Total wave height data contained periods of high and low amplitudes and included both sea and swell contributions, as shown in Figure 5.3.9. As the swell typically involves much longer wavelengths, wave height contributions from the shorter term sea (wind) waves were also extracted for use in the data analysis. A relationship between wind speed and wave height was investigated and is shown later.

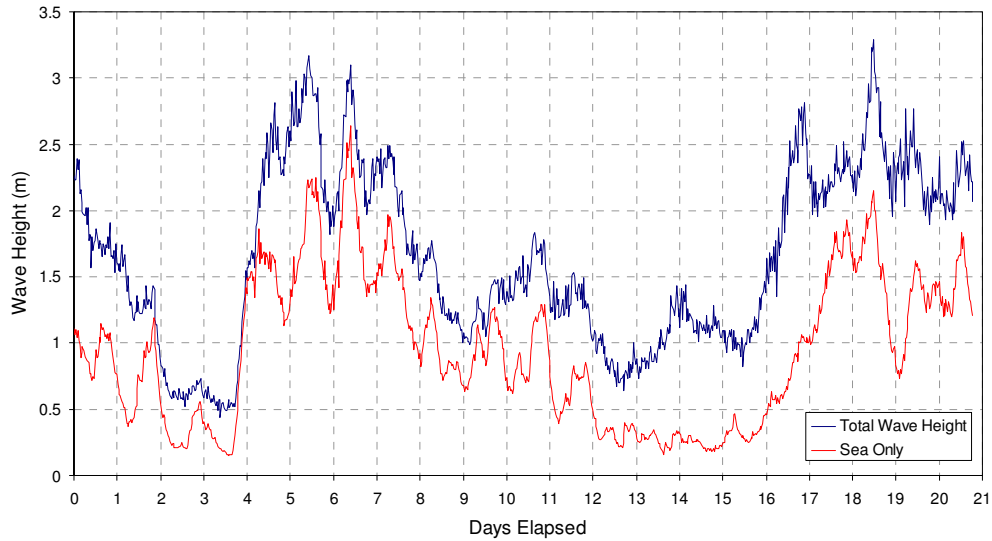


Figure 5.3.9. Total wave height and sea contribution as observed during the deployment period by the Rottnest Waverider buoy. Data courtesy of the Department of Transport, Western Australia

5.3.3 Modem Performance: Standard Communication

Error correction statistics were only available from the modems for the first 2-3 days of communication due to the limitations of internal memory on each device. It was determined that an average of 95% of detected packets contained no errors and did not require the use of error correction techniques. Additionally, 4% of packets were successfully restored using error correction codes implemented on the modems. Given that the average detection failure rate during this period was about 15 – 20 %, the results suggested that whilst error correction techniques were effective, they made little impact on the overall transmission statistics acquired for this study.

Modem performance analysis was divided into two main sections. First, the individual transmissions initiated by PDALogger, each containing a unique serial number (disk space and timestamp), were evaluated. The serial numbers recorded at each transmitter was compared with those successfully received by the remote modem. The compilation of these results provided a success report based on 6 transmissions for each 30 minute operation cycle, shown in Figure 5.3.10.

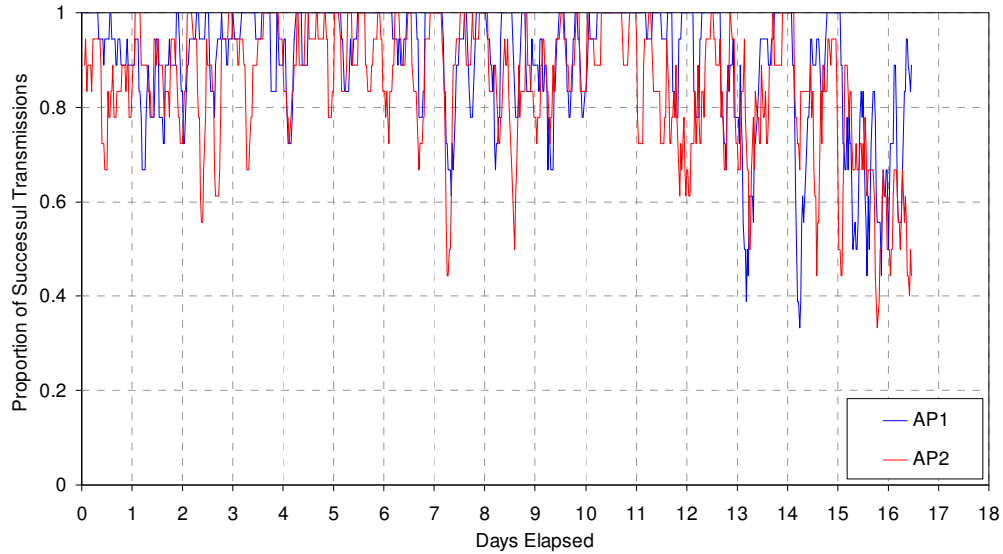


Figure 5.3.10. Proportion of successful transmissions for both modems based on one way individual short transmissions. Each transmission from the modems contained a unique serial number which was compared to the received data at the remote end to produce the statistics. The results were smoothed with a 3 hour averaging window.

When analysing the data obtained using single transmissions a disparity between the performances of the two modems was discovered. Observed over the entire deployment, the overall transmission success probability based on one-way telemetry for AP1 and AP2 was 89.5% and 84.5% respectively. The total one-way transmission count for both modems was 2355 from 785 successful program cycles where systems acted synchronously. Logged data from any period where one acoustic package failed to properly initialise was not used in the study as both systems needed to be fully operational for the collection of these statistics.

Several distinct periods of high and low communication performance were present. Prominent periods of high communication probability were experienced, particularly during days 10-11. Periods of poor performance were also observed, particularly towards the end of the trial on days 13 and 16. Smoothing of the performance statistics highlighted periodic fluctuations in the overall performance of telemetry as shown in Figure 5.3.11. The smoothed data set from one-way transmissions showed both high frequency fluctuations in modem performance and trends that were experienced over more than two days.

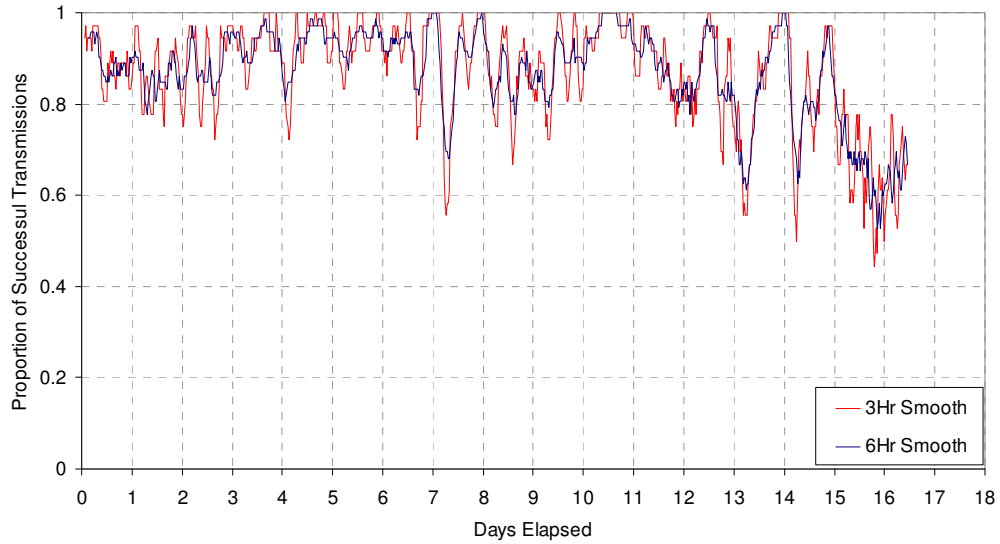


Figure 5.3.11. Proportion of successful transmissions averaged for both modems based on one way individual short transmissions. Each transmission from the modems contained a unique serial number which was compared to the received data at the remote end to produce the statistics. The results were smoothed with a 3 and 6 hour averaging window.

5.3.4 Modem Performance: Interrogations

In addition to one-way transmissions from each acoustic package as initiated by the on-board PDA, the modems were configured to request a block of internal memory data from the remote node during each cycle. These requests were performed three times, each with a different memory block length. Table 5.3.1 summarises the overall performance of the memory requests, calculated using the number of unreturned data blocks. Analysis of both successful and unsuccessful packet requests showed a total interrogation count for AP1 and AP2 of 2362 and 2389 attempts respectively. The subsequent number of requests for each of the three packet sizes was therefore 787 and 786 respectively. The slight difference in requests is due to the previously discussed intermittent PDA outages where interrogation results were not recorded.

Table 5.3.1. Table summarising the results of memory interrogations conducted throughout the deployments.

Modem	Packet Size	Unreturned Packets	Failure Probability (%)	Overall Success Probability (%)
AP1	8 Bytes	123	15.6	78.8
	30 Bytes	177	22.5	
	63 Bytes	201	25.6	
AP2	8 Bytes	183	23.3	73.3
	30 Bytes	207	26.3	
	63 Bytes	246	31.3	

An initial look at the memory request performance showed that interrogations from AP1 to AP2 were less successful. From the statistical data alone, it was difficult to attribute this effect to a particular modem as the reception of a packet request command was not recorded by either the modem or the on-board logger. The error in a single request may have occurred either in the forward transmission or the returned packet; however, by analysing the acoustic recordings, it was possible to determine the reception of the request packet by observing the acoustic response. This acoustic analysis is discussed later in Section 5.3.6, with the results summarised as an average packet success probability of 94.0% and 90.4% for request packets originating from AP1 and AP2 respectively. Closer analysis of the overall interrogation performance yielded significant variation over time. This variation is depicted in Figure 5.3.12 which shows the interrogation performance for AP1 and AP2 as a function of time.

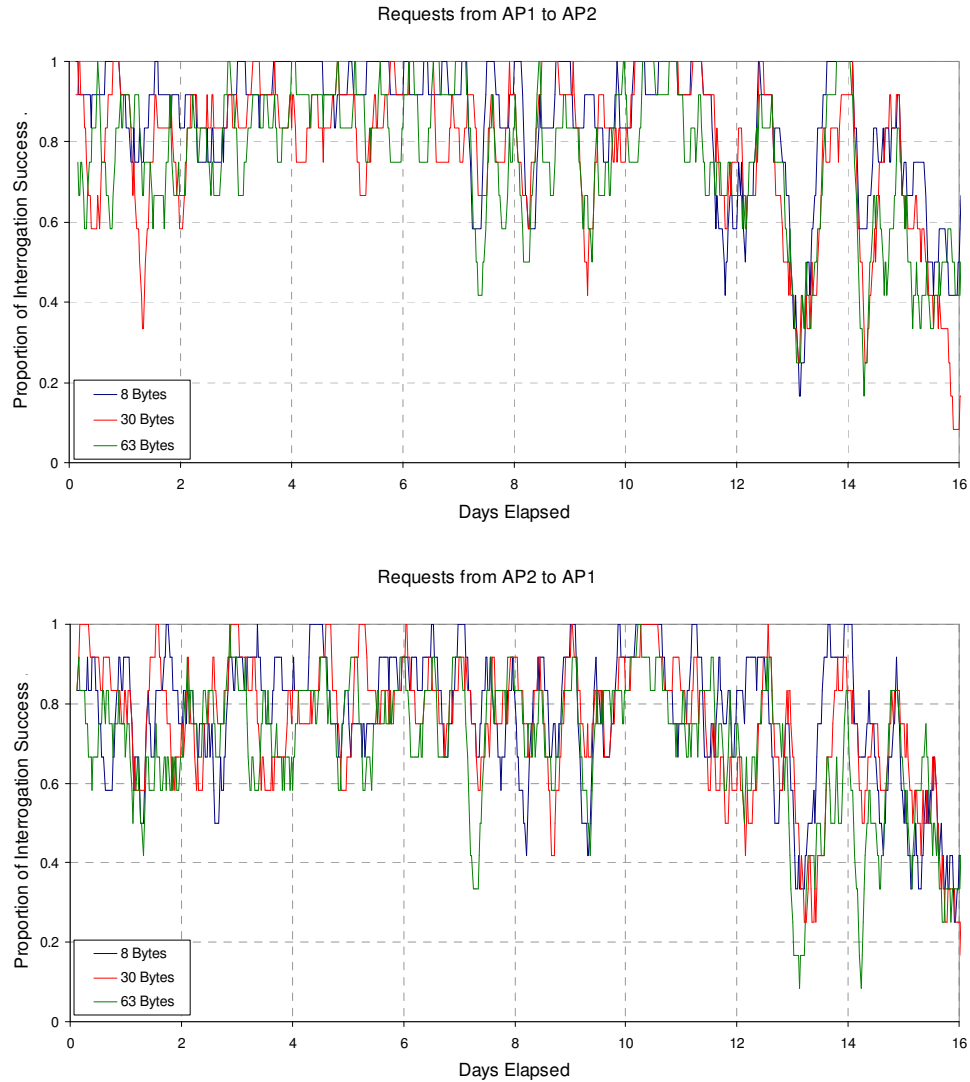


Figure 5.3.12. Success rate for modem interrogations originating from AP1 (top) and AP2 (bottom). The total number of returned packets was compared to the number of interrogation requests to compile the statistics. As packet request transmissions needed to be correctly decoded by the remote modem, one successful result relied on two successful transmissions.

An initial look at the interrogation performance showed the distinct points of high transmission success found in the previous data set such as days 10-11. These periods of high modem performance were observed regardless of packet length, signifying overall good conditions for modem communication. Statistics acquired for day 13 and late day 14 demonstrated poor performances for all packet sizes, where communication was inhibited and success rates dropped below 20%. To highlight differences found with differing transmission lengths, the mean success rate for both transmission directions was calculated. The results are shown in Figure 5.3.13.

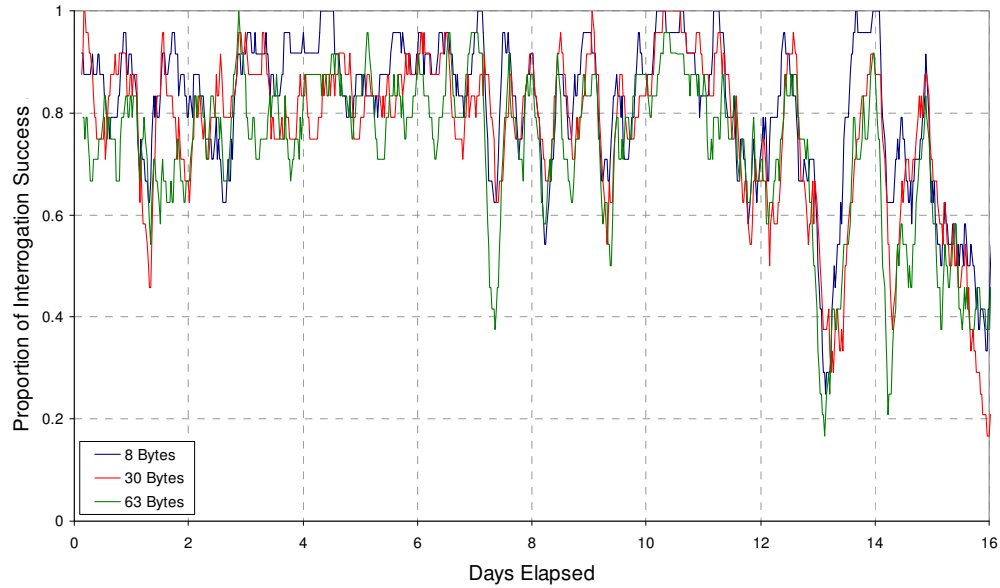


Figure 5.3.13. Mean proportion of interrogation success for both modems versus time, for each requested packet size. Three different packet sizes were utilised for the study involving different lengths of transmission.

As expected, the success probability was found to be increased for the smaller packets, likely a result of the significantly smaller transmission time. Figure 5.3.13 shows a close relationship between the 30 byte and 63 byte transmissions, particularly towards the end of the trial. This indicated the temporal variations in the channel had a stronger impact on transmissions longer than a certain length, rather than being a linear function of the size difference. A possible explanation for this behaviour would be that the smaller packet was successfully received before multipath interference significantly inhibited the performance. As a result, any packet large enough to be affected by multipath interference underwent the same decoding challenges, regardless of size. Such a hypothesis is largely dependant on the delay spread experienced within the acoustic channel which, itself, was expected to be time dependant.

To highlight differences between the interrogating modems without factoring in the packet length, the interrogation statistics were averaged over packet size to produce Figure 5.3.14. The result showed a close correlation between modems for some periods of the deployment and also further highlighted the poorer performance of

AP2. However, periods particularly in the first half of the deployment indicated a discrepancy of receiving capabilities between the two sites. These differences appeared only as communication drop-outs by transmissions from AP2. As this effect was more pronounced in the interrogation data than for one-way transmissions (shown in Figure 5.3.10), it was inferred that the larger packet sizes were more severely affected by the environmental conditions during these periods.

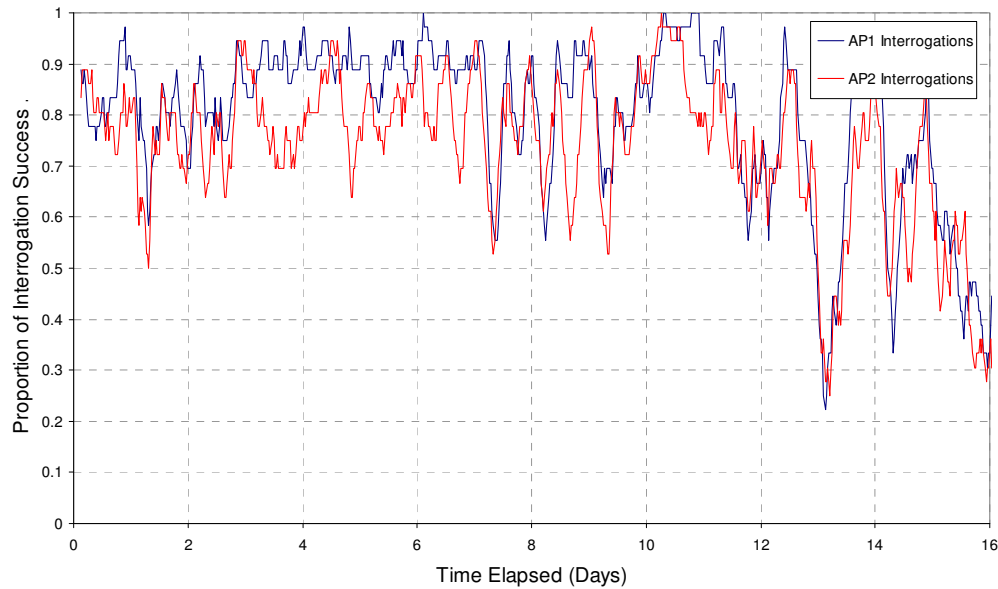


Figure 5.3.14. Memory interrogation success probability, averaged over all transmission lengths. A performance discrepancy, particularly apparent in the first half of the deployment showed situations where modem performance in a particular direction was favoured.

To provide an overall view of telemetry performance between the two modems over the entire deployment, statistics from one-way communication were combined with the modem-specific memory request data. The overall trends for each individual modem are shown in Figure 5.3.15, along with their average. In this analysis, the one-way transmission success for a particular modem was averaged with the interrogation performance initiated from the same location. As each interrogation result required the successful reception of two transmissions, the statistics were weighted accordingly by producing the square root before averaging. Finally, the average between the two modems was calculated, characterising the overall performance of the data link over the deployment period.

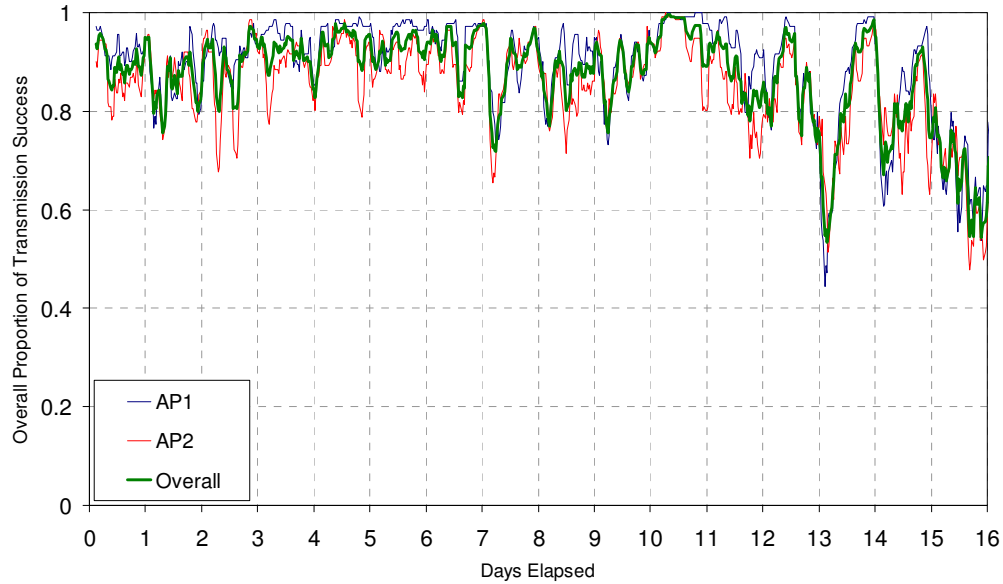


Figure 5.3.15. Overall modem performance versus time utilising both the one way transmissions and memory interrogations. As memory interrogations required two successful transmissions, the averages were weighted accordingly.

Analysis of the overall communication link showed several periods of interest including prolonged success peaks observed during day 10 which was indicative of excellent environmental conditions. The end of the deployment exhibited deteriorating communication from day 11, with several extended periods of poor performance such as day 13.

5.3.5 Acoustic Noise Analysis

Both of the underwater acoustic recorders operated until the 32 GB memory capacity was filled. AP1 recorded high quality data with little interference. A possible preamplifier malfunction combined with a faulty hydrophone cable resulted in acoustic recordings from AP2 yielding mostly electronic noise. For the purposes of this study, only the acoustic recordings from AP1 were analysed in detail. Recording ceased due to lack of disk space at 15:00 on 18th March, approximately 20 days from deployment. AP2 stopped recording earlier due to the lacerations of the cable.

For the analysis, the calibrated gain of 40.25 dB was used for the recordings at AP1. From Figure 3.1.3 the sensitivity of the hydrophone was determined to be 201.5 dB re 1 V / μPa for the frequency range considered (7500 Hz – 10500 Hz). However, the presented spectral data was calibrated using the broadband hydrophone sensitivity. Figure 5.3.16 shows a spectrogram of a typical recording of one sample calculated using a 480 point power spectrum over 0.25 s time slices.

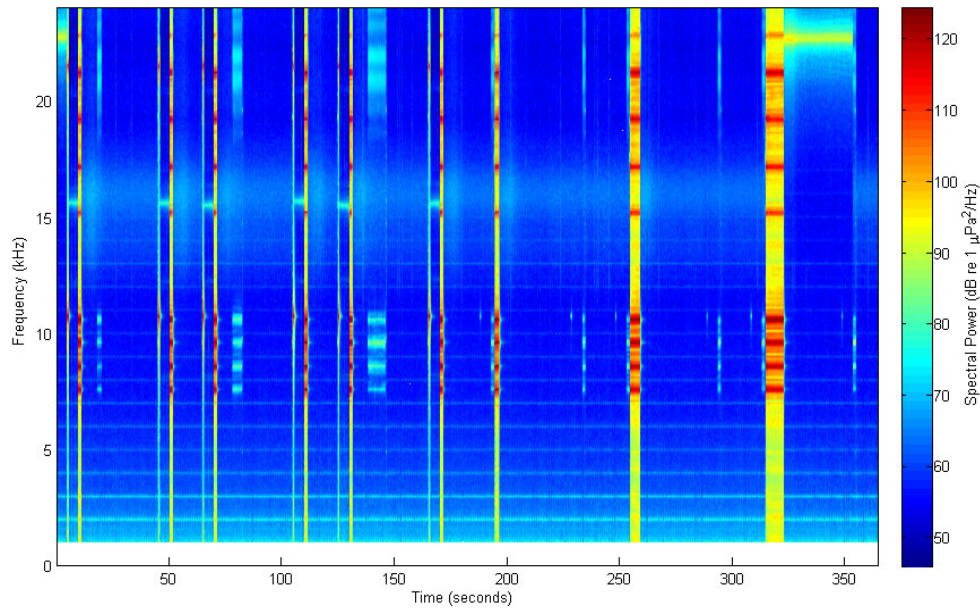


Figure 5.3.16. Spectrogram of one sample recording showing perfect modem performance in both directions.

The power spectrogram showed the three phases of communication for each modem, starting with transmissions from the local modem. In the second half of the recording, the transmission roles were switched and the local modem responded to remote requests. When the local modem transmitted, the recordings became clipped and the energy spectrum was saturated. Electronic interference at a fundamental frequency of 1 kHz was present as was seen in previous trials and thought to be caused by the writing of data to disk.

The close proximity of the recording hydrophone to the modem cable was thought to have created two distinct anomalies in the noise spectrum, highlighted in Figure 5.3.17. Firstly, the electronic noise from disk writing was amplified as the entire system operated on the same power supply. Secondly, the expected roll off beyond

10 kHz was replaced by a broadband ‘hump’. As the presence of this hump was shown in the spectrogram to be dependant on the modem operation it was assumed to be electronic interference from subsea cable originating from the modem. Both of these characteristics were present in both recorders. However, a discrepancy existed in the gain at AP2, further confirming a fault in the recorder which prevented acoustic analysis.

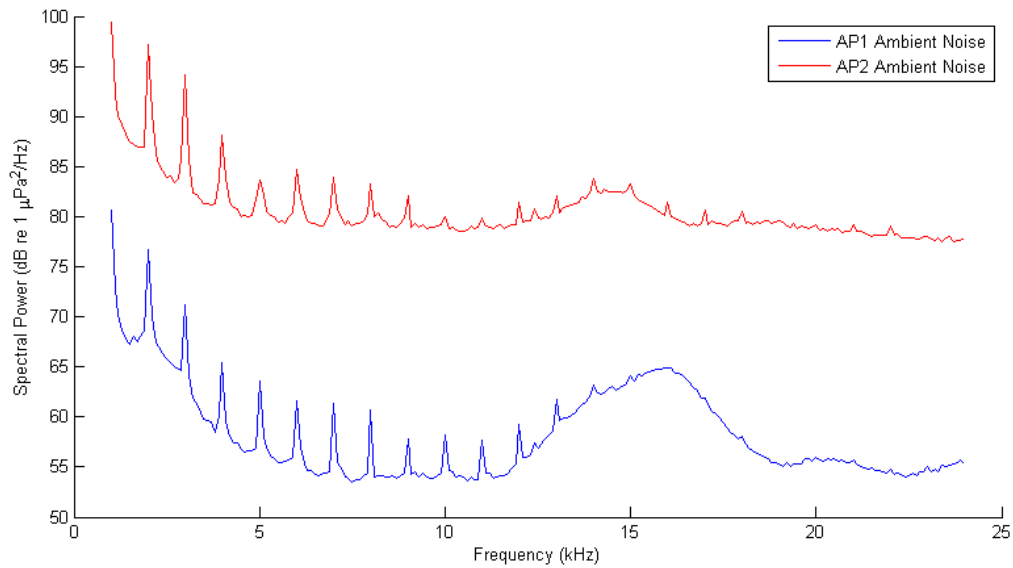


Figure 5.3.17. Sample ambient noise spectrum as measured by AP1 and AP2, using 10 s of noise from the point denoted by N3 in Figure 5.3.20.

The ambient noise calculations were performed on the areas of each recording where modem communication was not taking place. Specifically, 10 s of modem silence (denoted by N1 in Figure 5.3.20) was extracted from the recording and the PSD was calculated for all frequencies with 100 Hz spacing. The ambient noise spectrogram over the entire deployment was then obtained by collating the PSD over time. The overall ambient noise spectrogram as recorded by AP1 is shown in Figure 5.3.18.

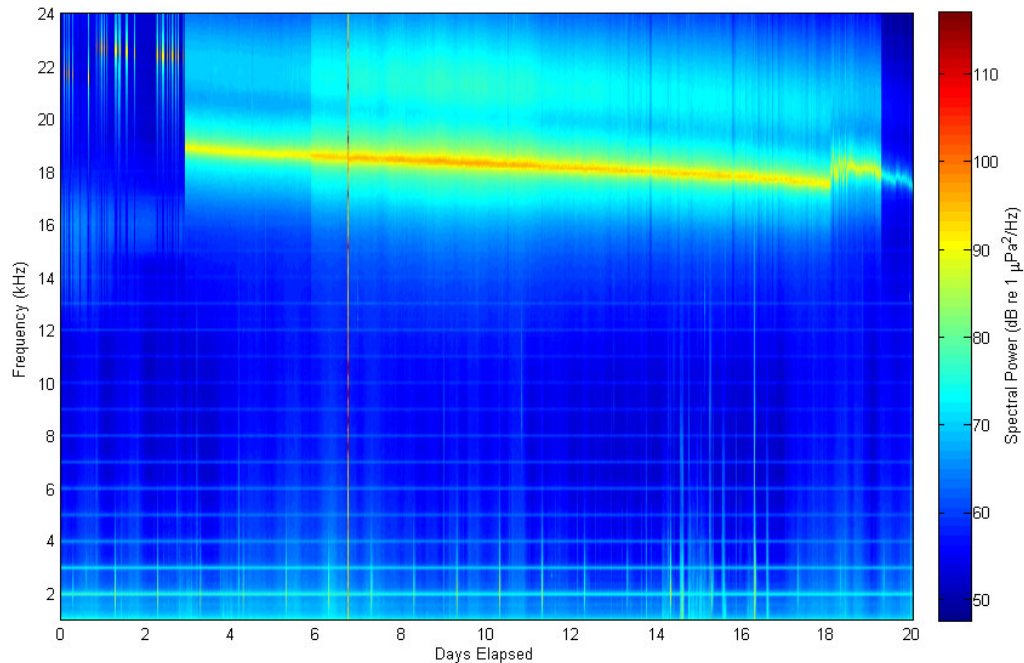


Figure 5.3.18. Overall spectral power versus time for the deployment duration as recorded by AP1. The large amount of noise at higher frequencies corresponds to modem electronic noise picked up by the hydrophone coupled to the interface cable. Noise fluctuations in the lower end of the spectrum are wind and wave noise with periods of shipping throughout, particularly through days 14 to 16.

The most defined spectral component was found to be electronic noise emitted by the modem at higher frequencies. The noise originated as an irregular occurrence but became defined after approximately 3 days. This interference was found to correlate with the point at which the modem internal memory was full and data was no longer logged. The reason for the presence of the interference and cause of the slowly decreasing frequency is still unknown. Although AP2 was found to exhibit only electronic noise, the data was useful in confirming whether or not points of interest in AP1 recordings were due to acoustic or electronic sources, given both acoustic packages were identical. The electronic noise spectrogram for the recorder at AP2 is given in Figure 5.3.19

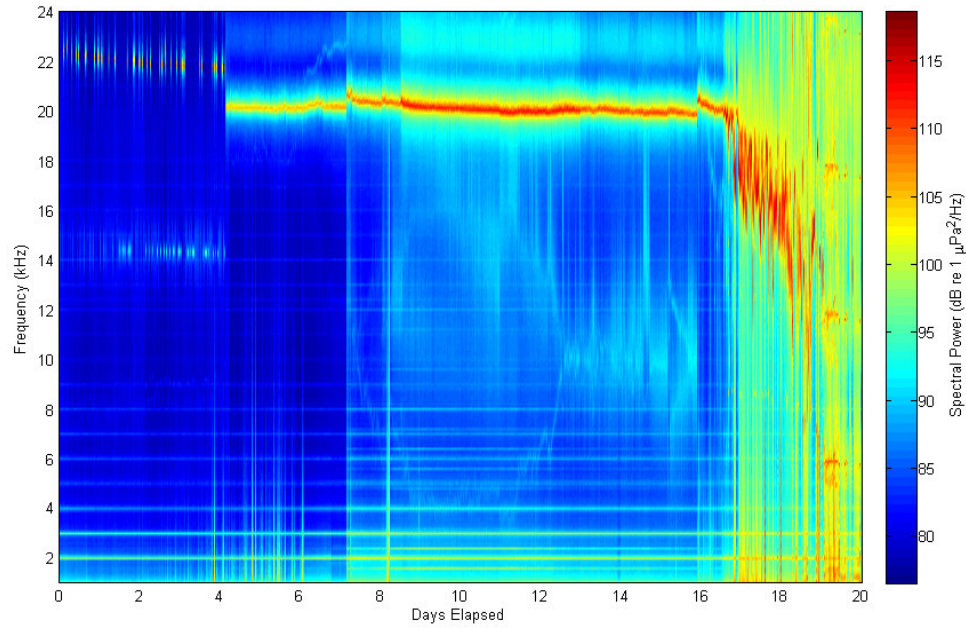


Figure 5.3.19. Overall spectral power versus time for the deployment duration as recorded by AP2. Electronic interference was much more prominent in this recorder as with other deployments, characterised by increased interference. Whilst the acoustic data contained in the recordings was of little use, the electronic activity provided detail regarding the damage to the subsea modem interface cable as well as helping to define the source of noise in AP1.

The sudden onset of high frequency noise shortly after 4 days coincided with the AP2 modem debug data becoming full, further confirming the modem as the cause. Broadband noise between days 4 and 6 was found to be caused by periodic static, likely the beginning of cable damage by marine life. Day 7 yielded further amplification of electronic noise with more periods of erratic static observed up until day 17 when the preamplifier began to malfunction. This malfunction was likely due to seawater surrounding exposed wires shorting a combination of the power, communication and hydrophone inputs, and correlated with the complete cessation of modem connectivity discussed in Section 5.3.3.

The ambient acoustic noise levels in the area were found to be much lower than those measured in previous deployments due to the deeper environment and colder water limiting the occurrence of snapping shrimp. Shipping noise was minimal and had little effect on the frequency bands used for communication for most of the deployment, despite vessel activity observed during days 14 – 16.

5.3.6 Acoustic Signal Analysis

Following a preliminary look at the data, a more thorough investigation of the frequencies relevant to transmission was undertaken. The recordings from AP1 were each synchronised using an algorithm seeking the point marked by S in Figure 5.3.20.

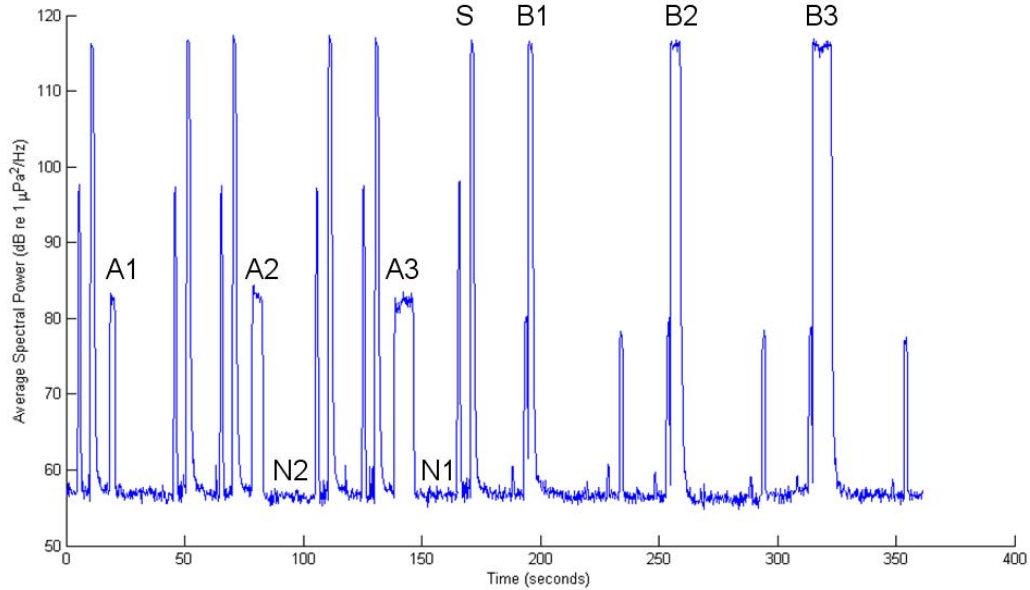


Figure 5.3.20. Extracted spectral power present in the 9600 Hz carrier frequency band. The points of interest for the acoustic analysis are highlighted: A - Interrogation response from AP2 for each memory length (1,2,3); B - Interrogation response from AP1 for each memory length (1,2,3) and; N - Areas where ambient noise was calculated. A2 and A3 were also utilised for determining the average signal power during each recording.

The points of interest for analysis were located relative to the synchronisation point, S. For ambient noise measurements, periods of silence marked by N1 and N2 were utilised. For signal strength analysis, the two larger remote modem signals (denoted by A2 and A3) were analysed. In the case that the algorithm detected no transmission taking place during periods A2 or A3 (i.e. power levels close to the noise floor), the data was not included in the signal strength analysis. This measure was taken to ensure that missed transmissions (due to a failed interrogation packet) would not bias the results.

To determine the effectiveness of using two measurement points for each recording, the power levels were compared for both signal and noise analysis. The difference values in Table 5.3.2 demonstrate the consistency between the two measurement points of each recording. The slight variations in the remote signal strength between S1 and S2 implied the presence of short-term fluctuations of the channel propagation characteristics.

Table 5.3.2. Summary of analysis of the acoustic recordings showing measured signal and noise levels during the deployment

Freq (Hz)	Noise Power (A&B)			Signal Power (C&D)		
	Power calculated using N1 & N2 (dB)	Difference between points N1 and N2 (dB)		Power calculated using A2 and A3 (dB)	Difference between points A2 and A3 (dB)	
	Mean	Mean	Std. Dev.	Mean	Mean	Std. Dev.
7600	57.01	-0.05	0.45	80.08	0.19	0.45
8600	56.78	-0.03	0.40	80.11	-0.12	0.40
9600	56.73	-0.04	0.43	83.26	0.00	1.31
10600	56.73	-0.05	0.40	79.69	-0.06	1.14

As the differences between the values at the two measurement points were minimal, the mean of A2 and A3 was assumed to be representative of the observed power levels. Noise values did not vary significantly from one another and were averaged for the remainder of the acoustic analysis. The relationship between the mean power calculations for each carrier frequency highlighted a disparity in the overall power received. This result was consistent with previous experiments where the 9600 kHz frequency band exhibited noticeably higher output power at all times. It was expected that the power disparity was most likely due to the frequency response of the transducers.

Using the signal and noise detection algorithm, the signal power versus time for each frequency band was calculated. The average noise was also calculated and is shown in Figure 5.3.21, providing an overall picture of the acoustic conditions.

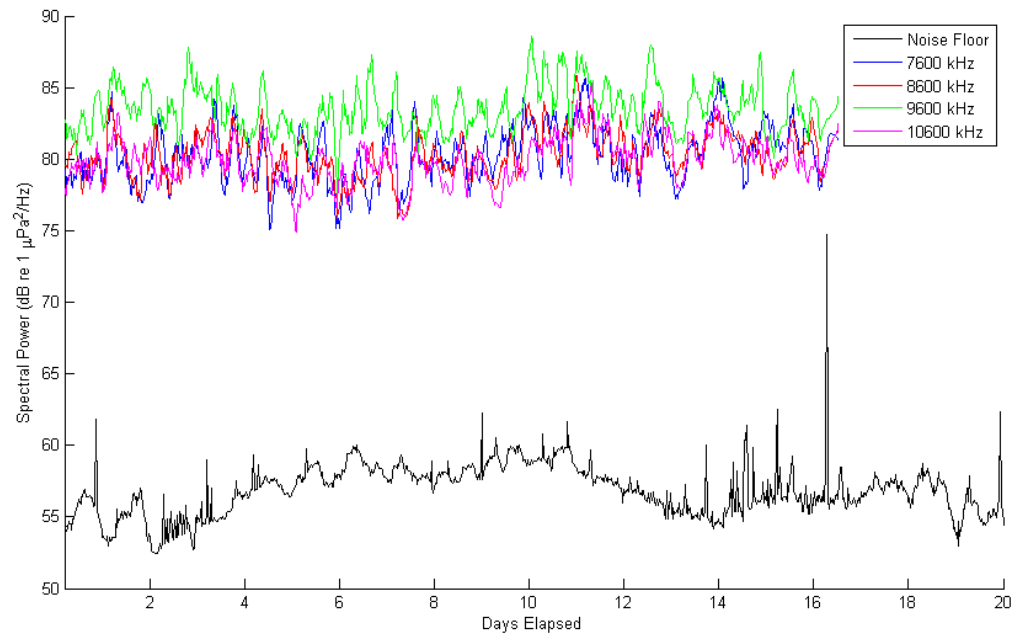


Figure 5.3.21. Spectral power versus time for each frequency component utilised by the modems. The average ambient noise levels over the communication band is also provided.

Both the noise and signal power levels fluctuated over the deployment. The movements of the individual frequency components correlated closely with one another. As the noise level trends were not smoothed, the singular peak of high noise on day 16 was prominent due to shipping at very close proximity. Averaging the power levels over the frequencies of interest, a single curve for signal power and a 3 hour smoothed noise power curve are presented in Figure 5.3.22.

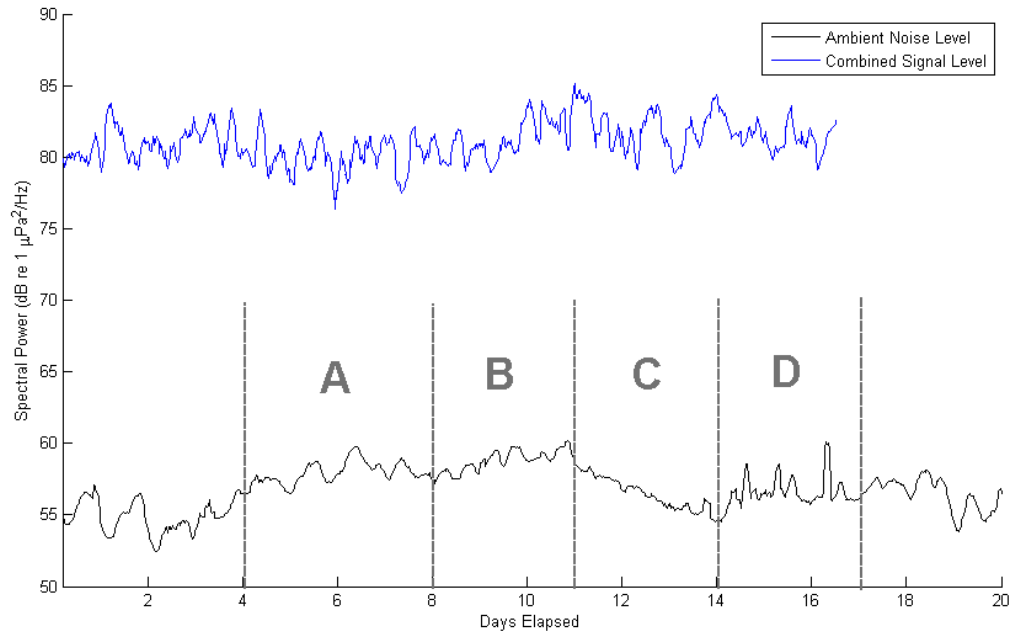


Figure 5.3.22. Averaged spectral power for both the signal and noise components from the acoustic analysis. The curves have been smoothed to highlight cyclic patterns and four periods of interest are highlighted: A) increase of ambient noise begins B) a second period with different periodicity, C) noise levels begin to return to normal with no cyclic influence and D) high levels of shipping noise.

The overall noise in the frequency bands of interest exhibited fluctuations throughout the duration of the deployment. A sustained period of higher than average noise occurred starting on day 4 (A), continuing with a higher frequency of fluctuation (B), followed by a decrease observed over days 11 – 14 (C). A two day period of erratic noise from days 14 – 16 (D) was due to heavy shipping. Signal power fluctuations showed time dependence within a range of up to 5 dB throughout the deployment. Both of these curves are used for cross-comparison with environmental conditions in Section 5.5.

5.3.7 Statistical Analysis using Acoustic Data

The acoustic analysis was helpful in confirming the statistics acquired using the modem feedback from AP1 and AP2 that were described in Section 5.3.4. Specifically, the successful reception of interrogation requests could only be ascertained by determining whether or not the response transmission took place. The modems provided no feedback if an acoustic command was received, only if the acoustic packet contained data to be transferred onto the PDA. An algorithm was consequently developed to seek out the response transmissions, denoted by the A and B peaks in Figure 5.3.20. If a transmission took place, it was assumed that the modem had successfully interpreted the request command. Using this analysis, the successful reception of the requests was determined over the deployment duration and is given in Figure 5.3.23.

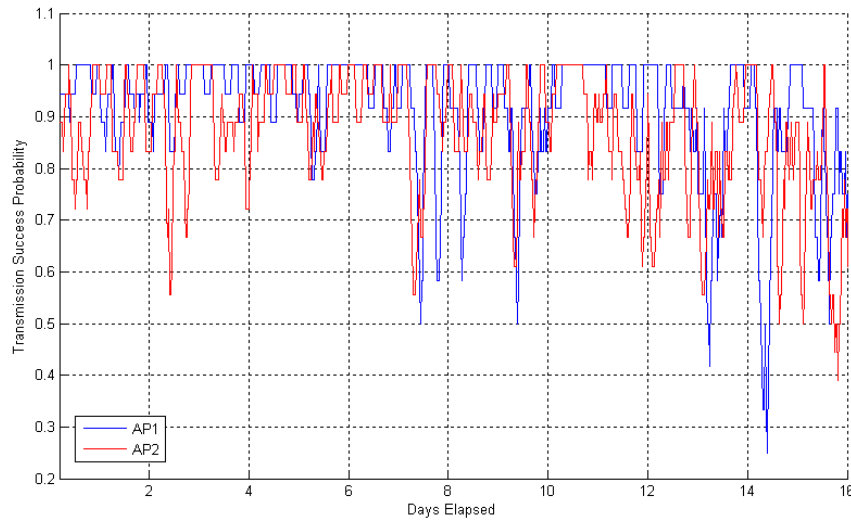


Figure 5.3.23. Probability of transmitted memory requests being successfully interpreted by the remote modem. These statistics were calculated by determining whether or not a memory return packet was transmitted at the expected time.

The trends shown by acoustical analysis provided statistics similar to those obtained through analysis of serial numbered transmissions that were shown in Figure 5.3.10. The close correlation is reflective of both packet types being 16 bytes or less in length. By summarising the successful reception of the interrogation packets, the contribution of the overall interrogation error for each transmission direction was established and is shown in Table 5.3.3

Table 5.3.3. Table summarising the results of memory interrogations conducted throughout the deployments with additional information obtained from acoustic analysis showing failures in reception of the initial data request packet.

Interrogating Modem	Packet Size	Total Failure Statistics (%)	Error Contribution of Request Packet (%)	Calculated Error Contribution of Reply (%)
AP1	8 Bytes	15.6	N/A	N/A
	30 Bytes	22.5	9.4	13.1
	63 Bytes	25.6	9.8	15.8
AP2	8 Bytes	23.3	13.7	9.6
	30 Bytes	26.3	13.5	12.8
	63 Bytes	31.3	14.7	16.6

Due to the increasing disk seek time over the deployment length and consequent increase in delay before each recording, data including the 8 byte interrogation from AP1 were limited to only approximately 4 days and could not be included in the summary. The contribution of errors originating from the returned packet transmission was shown to increase with packet size. The error rate of approximately 9.6% and 14.0% for requests from AP1 and AP2 respectively showed good correlation with one way transmission statistics where relative error rates of 10.5% and 15.5% were observed. These results reinforced and confirmed that transmissions from AP2 were approximately 5% more likely to incur a failure at the receiver.

5.4 Temporal Simulation of Long-term Perth Trial

The long-term deployment off the coast of Perth represented a unique opportunity to capture telemetry performance with changes in environmental conditions over a 2 – 3 week period. By knowing the environmental conditions to a higher degree of accuracy than in other deployments, it was anticipated that a more accurate simulator prediction of telemetry performance could be established. Rather than previous simulations which implemented static parameters with a wide range of receiver locations for a spatial investigation, this study focused on a single location using a compact receive array. Environmental parameters (RMS noise, wave height and SSP) were then updated with time to represent fluctuations measured during the trial. The resulting simulation was developed to predict the long-term performance of acoustic telemetry as experienced during the trial.

In order to optimise the computational time for the long-term simulations, a compact array of receivers was distributed within a small area of interest which represented the location of the receiving modem. Shown in Figure 5.4.1, performance patterns typically occurred over much smaller depth intervals than range intervals. To account for uncertainty in the modem position, an area of interest of 2 m in depth was investigated with only 20 cm required in range. The range interval of 20 cm was found to account for the short-range performance fluctuations with little difference in the average result when longer ranges were used. Similarly, the depth interval of 2 m was selected as the most optimum, to reduce the impact of interference effects and minimise computational time. Averaging was performed over the area to help account for changes in the modem position and environment which would likely have given a similar final result. The optimum receiver spacing was determined to be 5 cm horizontally and 10 cm vertically, which gave a consistent result without excessive computational time.

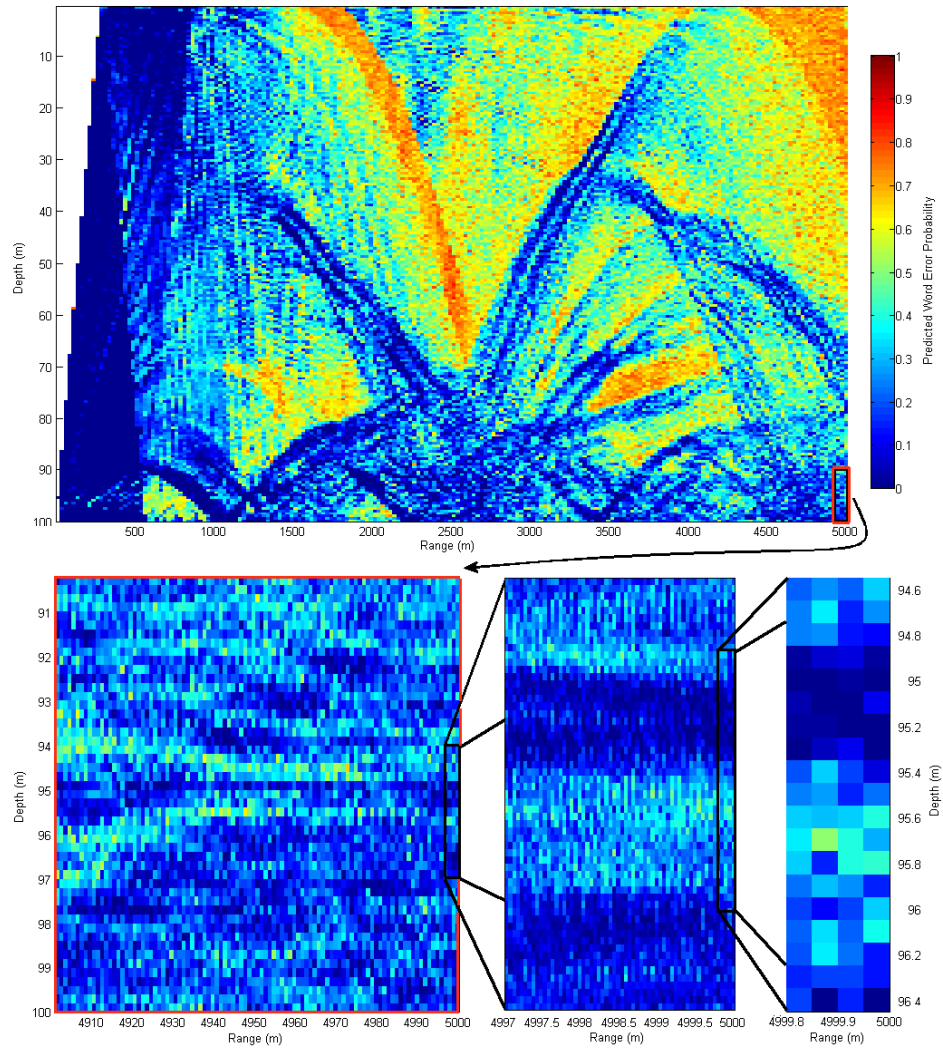


Figure 5.4.1. Sample spatial simulation ($t = 13$ hours) showing typical predicted performance. The area of interest is zoomed, showing both the size and resolution of the data block (lower right) which was averaged to obtain word error probability for a particular time.

Modem performance simulations involved running the Bellhop propagation model at one-hour time intervals and applying the estimated SSP at each time step. After obtaining amplitude and delay information from the model at each interval, performance analysis was carried out using the simulator. Calculations were performed for each receiver position, producing a spatial simulation within the area of interest. The average word error probability was then calculated to produce a performance estimate at one hour intervals. For the long-term simulation analysis, word error probability calculated by the simulator was inverted to word success probability for trend comparison with transmission success as calculated in the long-term Perth trial.

The result of the initial temporal simulations, without consideration of ambient noise, is shown in Figure 5.4.2. Also shown are the results of an investigation into the consistency of the results with varying Bellhop parameters; numbers of rays and ray launch angles.

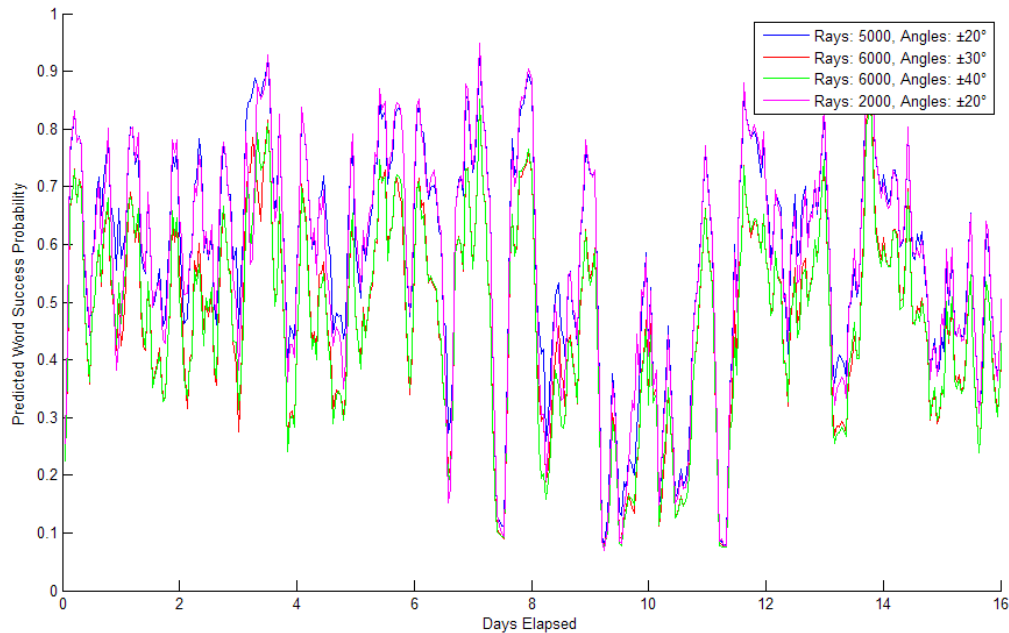


Figure 5.4.2. Simulated time dependant performance for Perth trial, calculated using various Bellhop model parameters to assess the impact of ray count and launch angle.

The simulator predicted large fluctuations in performance. Importantly, it was determined that neither the number of rays, nor the ray launch angle had a significant effect on the prediction. However, the success rate reduced during periods of high performance when larger ray launch angles were implemented. This result was consistent with an increased ray fan introducing further spread of the signal due to multipath. Overall, however, the predicted performance trends remained relatively consistent with one another, despite increased complexity in the simulation. As a result, the optimal Bellhop configuration for the long-term Perth simulation was determined to be 2000 rays with a ray fan of $\pm 20^\circ$. Such a simulation required approximately 10 hours of computational time on a standard PC running Matlab.

It was determined that the areas of poor performance were a result of inadequate synchronisation by the simulator, consistent with low amplitude first arrivals. As a result, the synchronisation algorithm was improved to remove the anomalies. Similarly to the simulation for the French summer scenario presented in Section 4.3.5, the synchronisation method was updated use the maximum amplitude arrival ('max' method) as opposed to the first arrival ('first' method). This better represented the synchronisation performance of the modems, providing improved performance statistics as shown in Figure 5.4.3. In addition to removing the areas of poor performance, the new synchronisation method also predicted better performance overall when compared to the initial results.

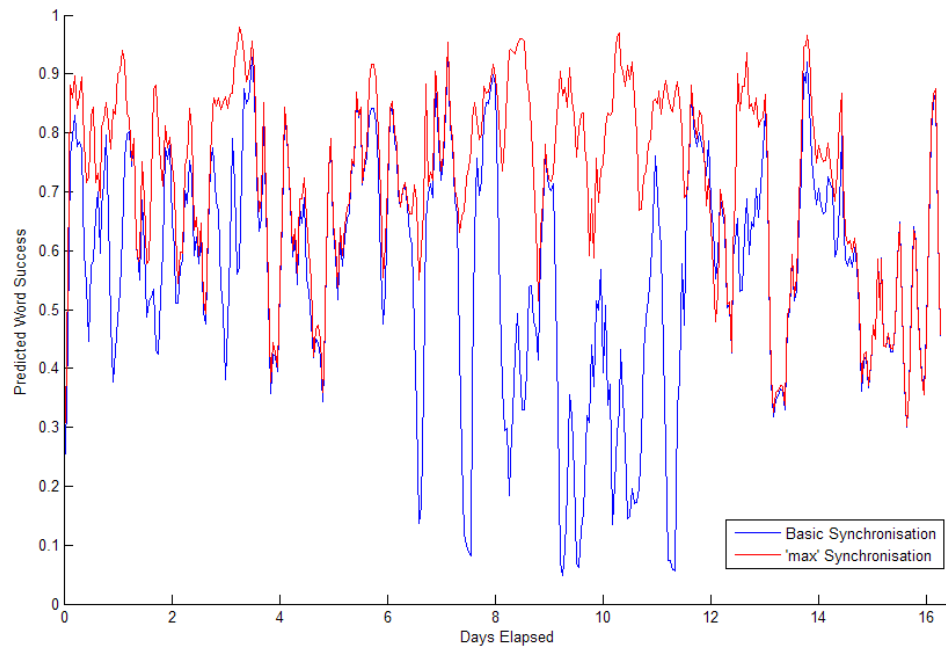


Figure 5.4.3. Overlaid simulated performance using the basic 'first' and the later added 'max' method, showing the overall increase in performance and removal of synchronisation errors.

Noise was added to the simulations which used updated synchronisation method. Time variation in ambient noise was calculated during the trial using an underwater ambient noise recorder with the resulting curve shown in Figure 5.3.22. In addition to utilising a sound speed profile measured for each hour, the simulator noise component was set to a level corresponding to the trial measurements at that time. Figure 5.4.4 demonstrates the effect of the inclusion of noise in the long-term simulation.

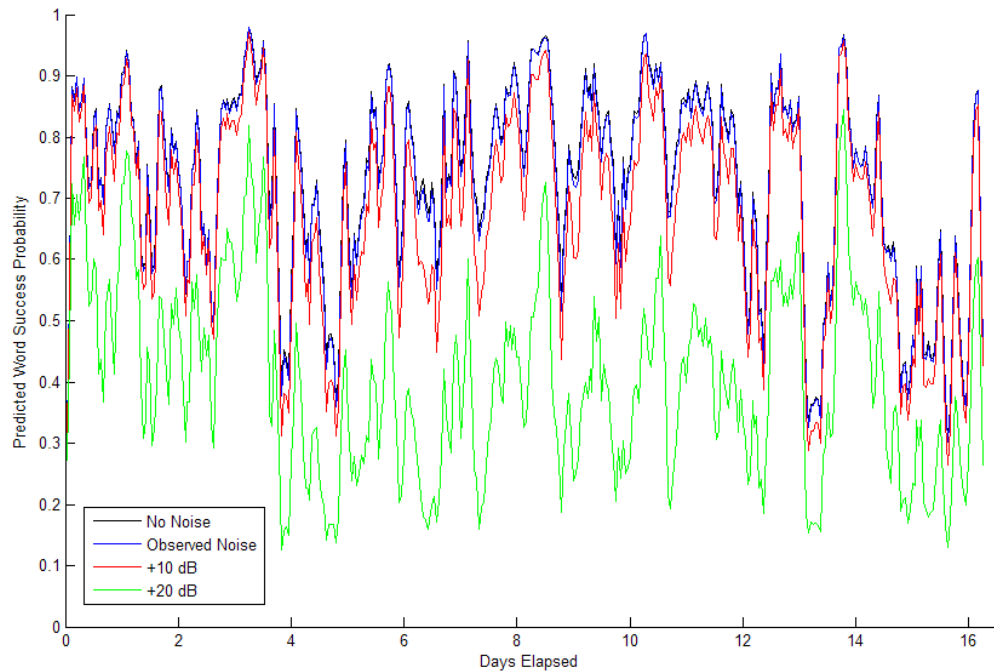


Figure 5.4.4. Simulated time dependant performance for Perth trial using ‘max’ synchronisation method, calculated using various levels of ambient noise to illustrate the effects. Note: The noiseless result is almost indistinguishable from the result using noise levels observed during the trial due to the high SNR.

As a further investigation, the ambient noise was increased by additional amounts; 10 dB and 20 dB above the measured levels. After inputting the noise levels observed during the trial, a strong correlation with the noiseless simulations indicated very little effect of noise on the predicted performance. This result suggested that fluctuations in SNR had little to no effect on the performance of the acoustic modems during the trial. This was expected given the high overall SNR observed at the receiver. The scatter plot shown in Figure 5.4.5 confirmed that had the SNR been reduced, the performance would have been impacted.

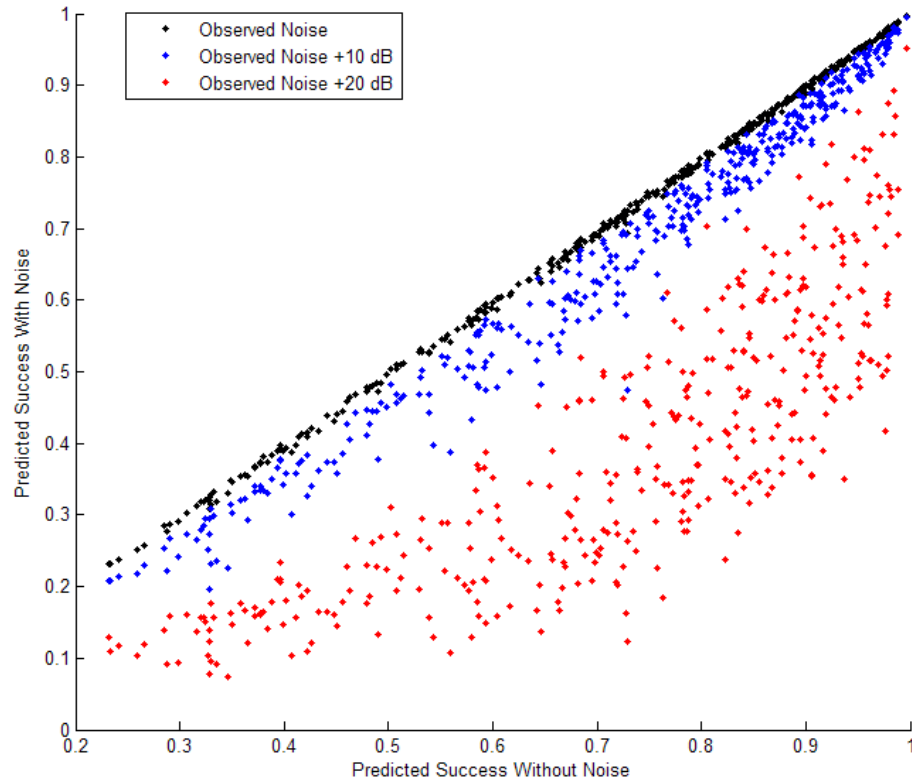


Figure 5.4.5. Scatter plot of predicted word success rates with various amounts of noise compared to the noise-less simulation. This plot demonstrates the effect of lowering the SNR showing the rate at which noise levels affect the simulated modem performance.

Finally, the reduction in the sea surface reflection coefficient due to scattering by surface waves measured during the long-term Perth trial was introduced into the simulator. This was done for each ray by multiplying the amplitude by \check{R}^N , where \check{R} was obtained from Equation A.9 and N was the number of ray surface reflections. Each amplitude adjustment took into consideration the significant wave height and the grazing angle at the surface. Using Snell's Law, this angle could be calculated using the sound speed at the surface and at the seabed, where the modem was located, and the grazing angle at the source. Figure 5.4.6 shows the adjustment to ray amplitude with respect to launch angle for a sample receiver position using various values for significant wave height. As expected, rays with a direct path or small grazing angles (represented by a small launch angle) were unaffected by wave height, while those incident on the sea surface were attenuated. The symmetry shown is representative of rays with negative launch angles reflecting from the seabed immediately after launch, exhibiting essentially the same directional characteristics as those launched upwards.

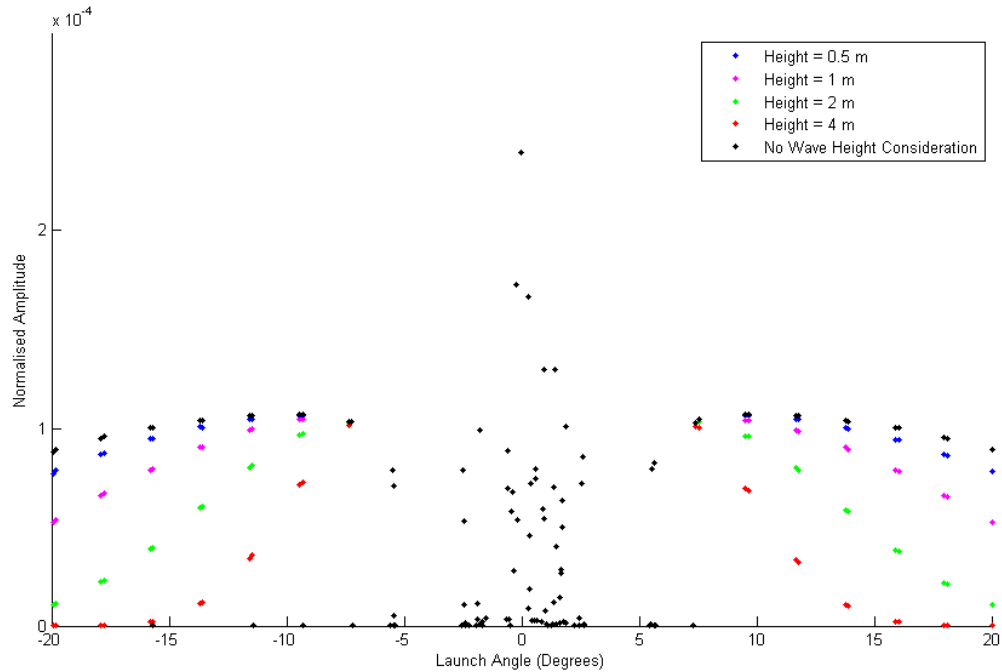


Figure 5.4.6. Ray amplitude distribution with respect to launch angle, showing the effect of introducing significant wave height into the simulator to adjust the amplitudes used in constructing the temporal impulse response in the simulator. Overlapping of points at launch angles below $\pm 8^\circ$ signifies no effect on ray amplitude.

The simulation involving the ‘max’ synchronisation method with the trial-observed noise levels was repeated with the inclusion of wave height obtained from the trial. The resulting prediction was a performance simulation incorporating the time dependant SSP, ambient noise and surface roughness as observed in the long-term Perth trial. This prediction is shown in Figure 5.4.7. An increase in performance was discovered when incorporating wave height, consistent with an expected decrease in multipath interference. Figure 5.4.8 highlights the positive effect of wave height on performance by plotting the performance increases with significant wave height.

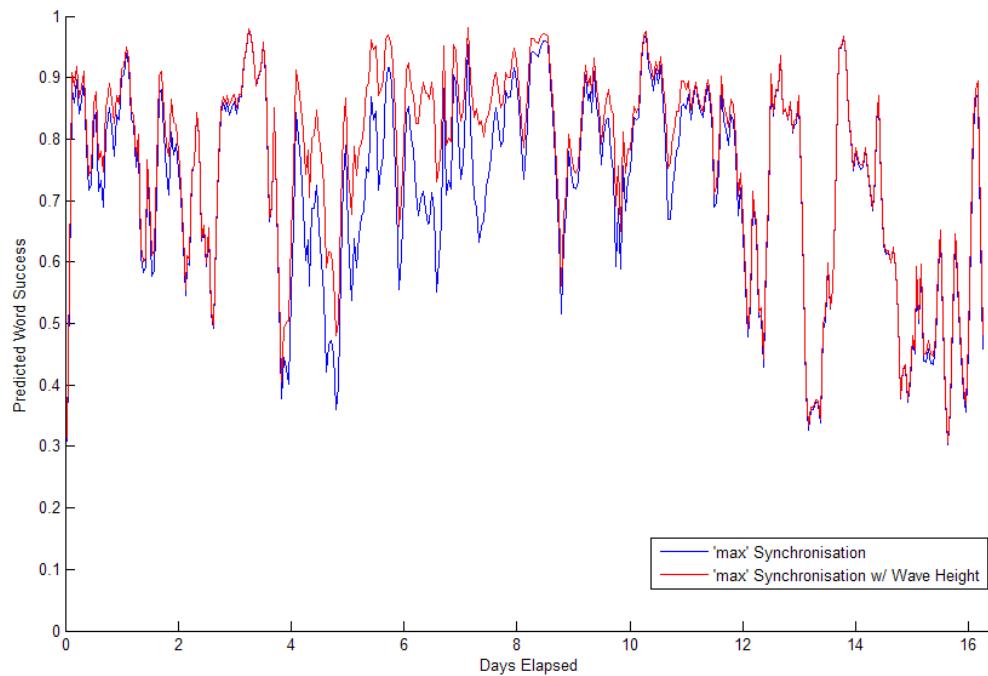


Figure 5.4.7. Simulated performance using the 'max' synchronisation method during the long-term Perth trial, with and without considerations of surface roughness.

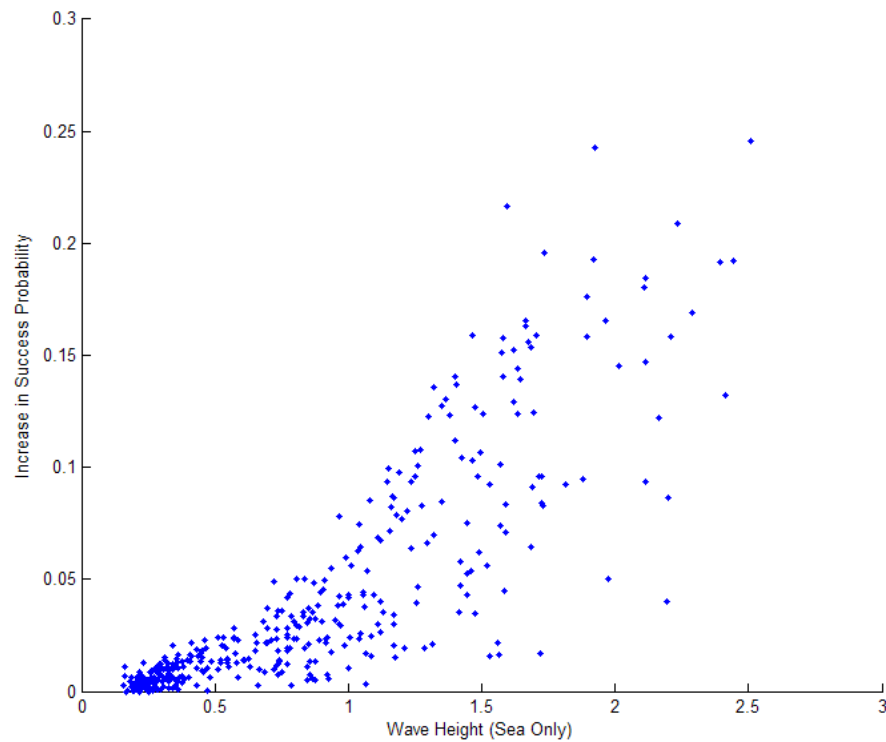


Figure 5.4.8. Scatter plot of performance increase with wave height, demonstrating a positive effect of surface roughness.

The simulator calculated the average 4-bit word error probability over 100 receiver simulations within the area shown previously in Figure 5.4.1. An investigation into the standard deviation of these individual results was performed, with the result shown in Figure 5.4.9.

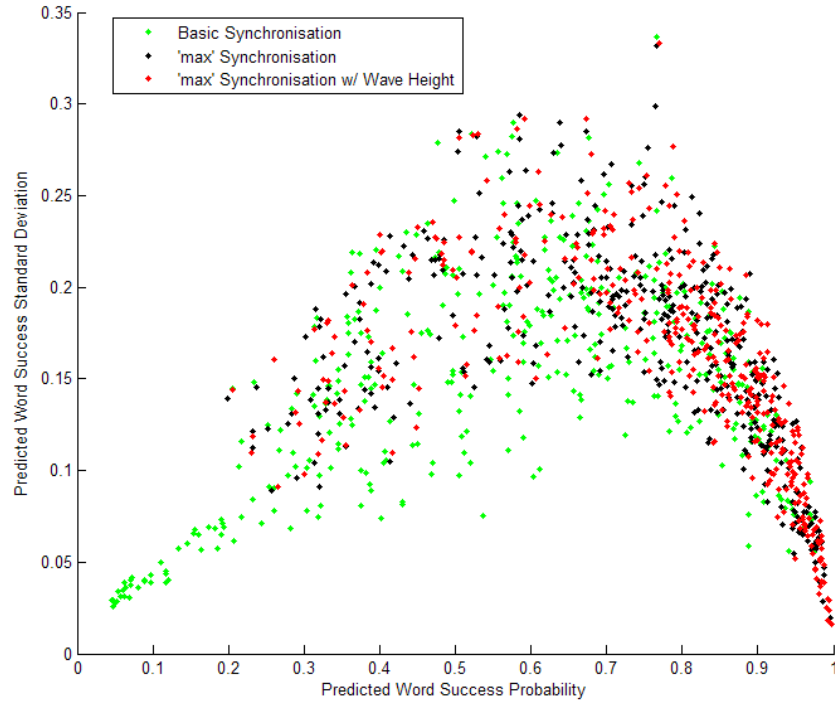


Figure 5.4.9. Standard deviation of simulated performance within each area of interest as a function of the average calculated performance.

Figure 5.4.9 demonstrates the impact of low amplitude first arrivals on the initial simulations with a higher spread of points and a collection of low performance “certainty” in the bottom left corner. Even following the addition of more parameters, a simple relationship between the average word error within an area of interest and the standard deviation could not be determined. However, the final curve utilising advanced synchronisation and wave height consideration was found to have the highest correlation with measured data, suggesting higher simulator reliability. The results from the final simulation which included the observed noise level and wave height data were used for comparison with the trial data which is shown in the following section. The standard deviation was also included with this performance data to take into account the uncertainty of the simulated results.

5.5 Assessment of the Predictability of Long-term Communication Performance

A major objective of this thesis is to establish a relationship between the performance of acoustic communication and the surrounding environmental parameters. The long-term Perth trial was best suited for such a study as environmental data was collected simultaneously with modem operation. In this section, the impacts of independent environmental parameters are first investigated using multiple linear regression. The results from the simulator are then assessed by comparing the predictions with the field data.

5.5.1 Environmental Contributions to Ambient Noise

As shown in the experimental data, the SNR for the long-term Perth trial was high when compared to other trials such as the acoustic tag investigation given in Appendix C. As a result of high SNR, it was expected that the measured environmental influences on performance in the Perth trial would be independent of SNR. However, the influences of environmental parameters on ambient noise were still investigated to determine which parameters related to acoustic propagation were also related to ambient noise.

Wave height was expected to be influenced by wind fluctuations so these two data sets could not, therefore, be considered as independent environmental parameters. To confirm this correlation, an initial investigation was performed with wind and sea wave data obtained during the trial (Figure 5.5.1). The data sets were divided into low and high frequency components to separate diurnal and semi-diurnal fluctuations from longer term changes. Specifically, movements with a period of greater than 2 days were considered low frequency components. Fluctuations with a period lasting between 3 hours and 2 days were also separated out and considered high frequency components.

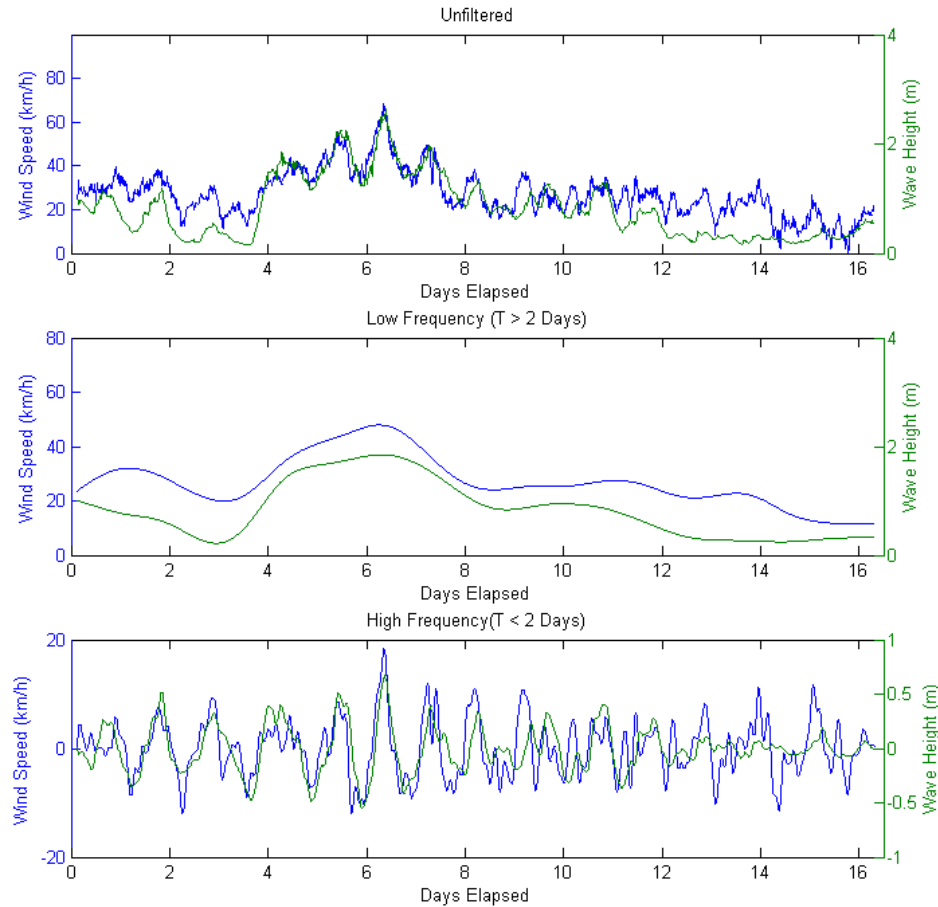


Figure 5.5.1. Trend comparisons for the wind and wave data collected during the long-term Perth trial. The measured data (top) was filtered to highlight comparisons between only low (middle) and high (bottom) frequency trends.

A correlation between wind speed and wave height measured at the deployment location was found in both high and low frequency components. It was determined using cross correlation of the high frequency components that a wave height lag of approximately 1.5 hours existed. This result is consistent with wind causing the build-up of wave height. When the trends were aligned, a correlation between wind speed and wave height was determined with the correlation coefficients shown in Figure 5.5.2. Results from the analysis showed an expected causal relationship between wind speed and wave height.

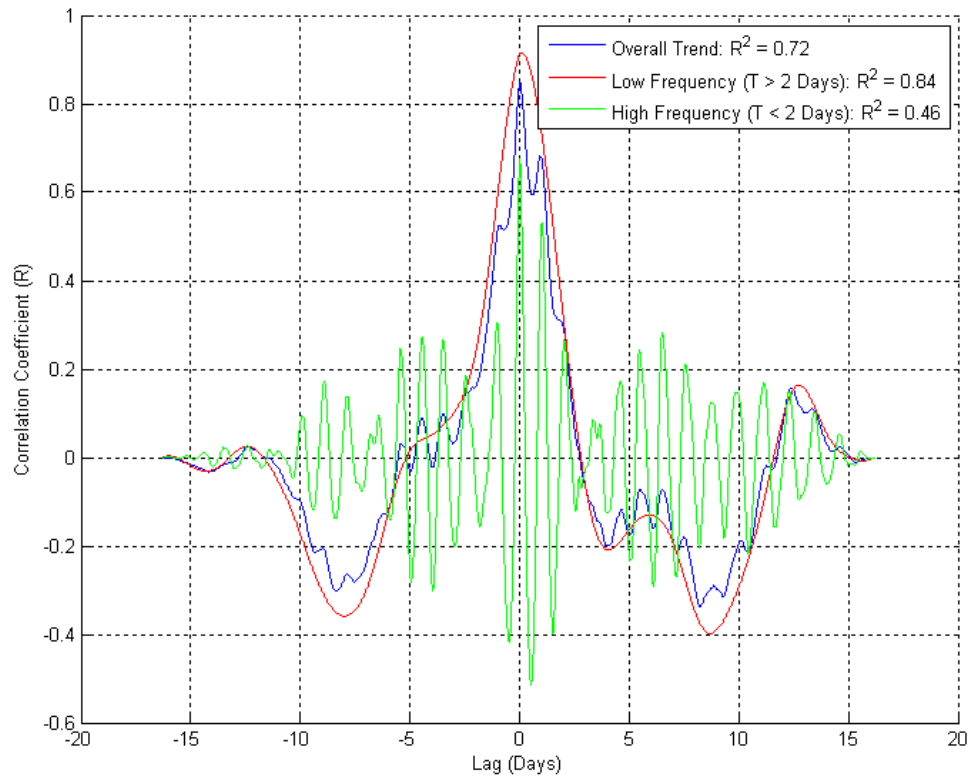


Figure 5.5.2. Cross correlation between wind speed and wave height showing the correlation between measurements from the Perth long-term trial. The original data set was also separated into high and low frequency components with the results also compared.

Ambient noise levels in the ocean have been related to wind speed (Appendix A.2.4). Although the wave motion influenced by wind is typically the mechanism for the contributions to ambient noise, wind speed generally provides a suitable correlation (Urick, 1983). As a result, wind speed can be considered a surrogate that is also easier to measure in the field. Linear regression was performed to determine the contribution of both wind speed and wave height to ambient noise levels measured in the Perth trial. Additionally, the inclusion of water temperature was found to significantly improve the predictions using the linear model. The best correlation was obtained using the mean water column temperature and the temperature difference between the seabed and sea surface. The results for each study are summarised in Table 5.5.1 with the cross correlations of predicted and real ambient noise levels also shown in Figure 5.5.3.

Table 5.5.1. Best prediction curves for ambient noise, obtained using multiple linear regression with wind and wave data, the mean of the sea surface and seabed temperature and the difference between them. The components were also normalised to their standard deviation to determine their relative contribution to the prediction.

Parameter	Wind Investigation Linear Coefficients (Normalised Contribution)	Wave Investigation Linear Coefficients (Normalised Contribution)
β_1 (Wind Speed)	0.044 (22%)	N/A
β_2 (Wave Height)	N/A	1.082 (30%)
β_3 (Mean Water Temperature)	-2.128 (64%)	-1.886 (58%)
β_4 (Temperature Difference)	0.418 (14%)	0.362 (12%)
(R^2)	0.61	0.65

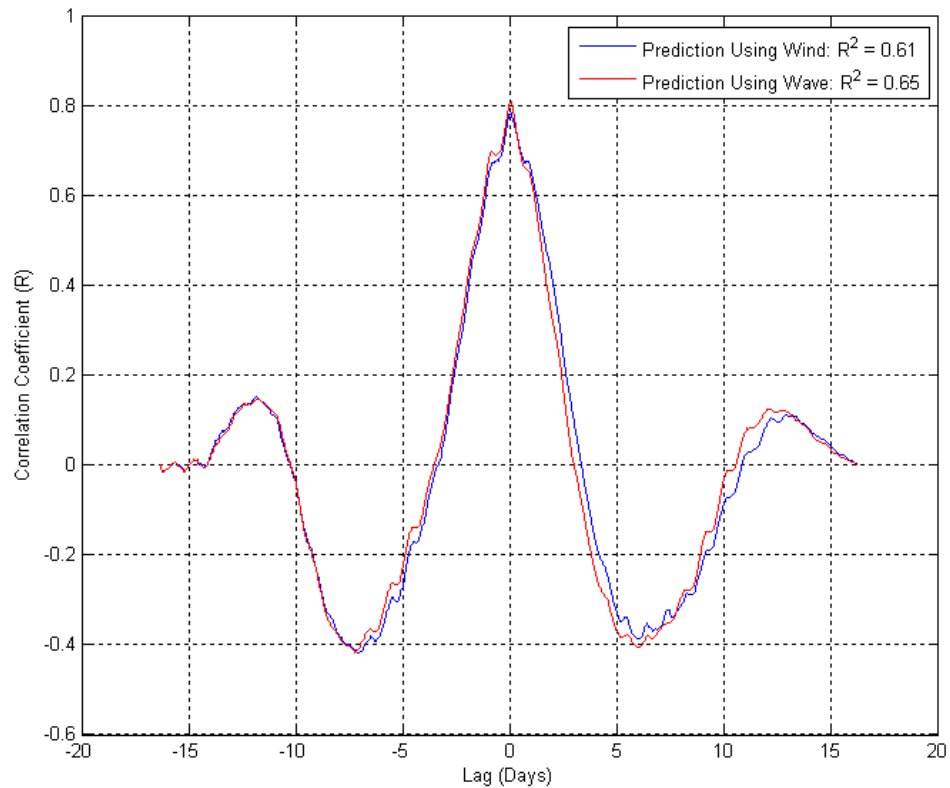


Figure 5.5.3. Cross correlation of measured ambient noise levels with those using the linear combination of sea wave height, sea surface temperature and seabed temperature (Table 5.5.1). The result using wind speed instead of wave height is also shown.

A marginally stronger correlation was found when using the wave data rather than the wind speed. Interestingly, the mean temperature was found to contribute greatly to the correlation, whereas it was expected that the temperature gradient would play a

larger role. The observed dependence on the temperature difference could be related to an increasing SSP gradient which would have refracted more surface noise downwards to the seabed, where the hydrophone was located. The high dependence on the mean water temperature may have been related to additional parameters that could have correlated with temperature such as biological entities or water currents. However, these possibilities can only be considered speculative as no obvious correlations between the mean temperature and other measured data in this trial was apparent.

As expected, the analysis showed that the ambient noise levels were not independent of the sea surface state and temperature profile. Importantly, these two parameters could also be related to the propagation characteristics of the underwater channel. Therefore, a low SNR experienced during this trial would have resulted in difficulty in determining if the environmental influences on performance were due to SNR or changes in the channel propagation characteristics. As the modems in this trial always exhibited high SNR, the observed changes in performance could be attributed more to the environmental impacts on channel propagation rather than their influences on ambient noise.

5.5.2 Factors Affecting Acoustic Modem Performance in the Perth Trial

A multiple linear regression was performed to assess the correlation between each environmental variable and the measured modem performance. In reality, such a straightforward solution to predict the performance based on the environment is unlikely to exist. However, multiple linear regression allowed for the determination of which parameters had significant influences on the measured performance. As established earlier, wave height and wind speed were strongly correlated and consequently were not used together for the analysis. A more accurate prediction of performance was found when utilising the wind speed ($R^2 = 0.44$) instead of wave height ($R^2 = 0.38$) and as a result, wind speed was used for the analysis that follows.

The degree of downward refraction in the water column was represented by the slope of a linear least squares regression fit of the SSP measured by the thermistor string (Figure 5.3.5). Only the bottom half of the water column was utilised which excluded the interpolated upper 50 m determined using SST measurements. This was justified given the higher importance of refraction characteristics in the lower portion of the water column as well as the higher resolution and more accurate measurements made in this region during the trial.

The ambient noise levels were subtracted from the measured signal levels in dB to help determine if SNR fluctuations had any effect on communication during the trial. Additionally, it was determined that removal of the tide height from the estimate provided no reduction in prediction quality for both filtered and unfiltered trends. As a result, SNR, Wind Speed and SSP Gradient were used in the regression analysis. The results are summarised in Table 5.5.2 showing the linear contributions calculated using filtered and unfiltered data. Additionally, the plot of the cross correlation between the prediction curves and measured performance is shown in Figure 5.5.4.

Table 5.5.2. Contributions of each environmental parameter following the use of multiple linear regression to obtain the best prediction curve for the communication success rate during the long-term Perth trial. Each component was normalised to its standard deviation and computed as a percentage of the sum of influences. Negative numbers denote where the component has a negative impact. Results using filtered data (above and below two days duration) are also shown.

Parameter	AP1 Modem (%)			AP2 Modem (%)			Overall (%)		
	Original Data	T > 2 d	T < 2 d	Original Data	T > 2 d	T < 2 d	Original Data	T > 2 d	T < 2 d
β_1 SNR	21	22	64	23	20	58	22	21	61
β_2 Wind Speed	37	40	-4	37	39	27	37	40	16
β_3 SSP Gradient	42	38	32	40	41	15	41	39	23
R^2	0.43	0.82	0.13	0.44	0.82	0.18	0.44	0.82	0.17

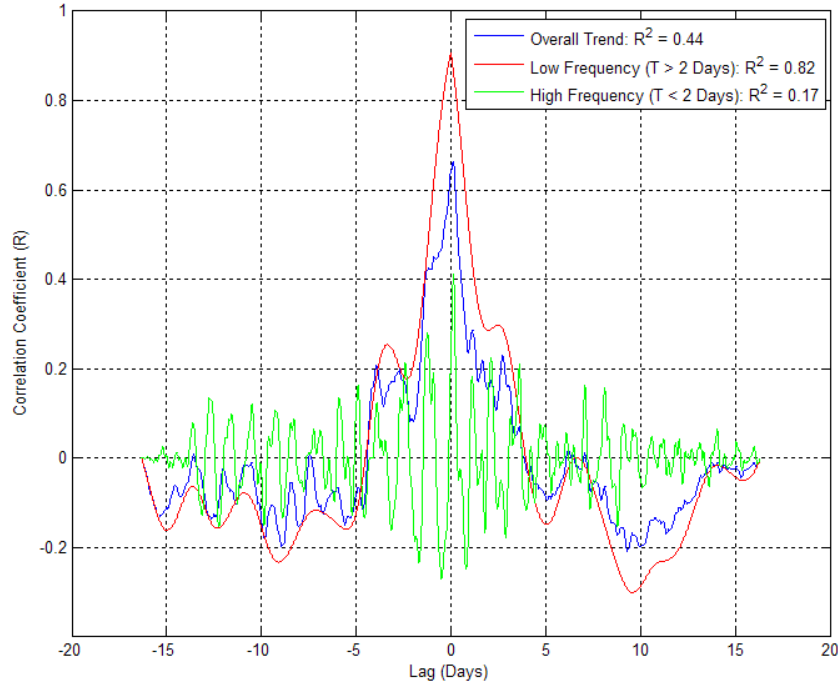


Figure 5.5.4. Plot of cross correlation between the linear regression prediction for acoustic modem performance and the statistics obtained from the long-term Perth trial. The overall performance is also shown with the low-pass and high-pass filtered data.

A low correlation between predicted and measured high frequency fluctuations highlighted the limitations of applying linear methods and also suggested that other short-term factors may have impacted acoustic communication performance. For low frequency changes, however, the multiple linear regression method provided an effective way to calculate the contributions from each environmental parameter. Expectedly, SNR was shown to have a positive impact on communication, although less correlated with the data in this trial due to the consistently high levels.

Regression analysis showed that the wind speed and SSP gradient were the highest contributing factors to acoustic communication performance in the high SNR scenario. As both signal and noise were previously shown to be related to wind speed and SSP gradient, a multiple linear regression was performed with only these two components to determine the accuracy of a simpler prediction. It was determined that a model utilising just wind speed and SSP gradient could be obtained with the coefficients shown in Table 5.5.3. Figure 5.5.5 shows the unfiltered observed trends alongside those predicted using the simplified models.

Table 5.5.3. Coefficients from a simplified multiple linear regression analysis, utilising only wind speed and SSP gradient for both unfiltered and low frequency modem performance trends.

Parameter	Unfiltered Data (% Contribution)	Low Frequency (> 2 days) (% Contribution)
β_1 Wind Speed (km/hour)	0.03 (30%)	0.03 (29%)
β_2 SSP Gradient ($^{\circ}\text{C}/\text{m}$)	2.51 (70%)	2.97 (71%)
R^2	0.30	0.62

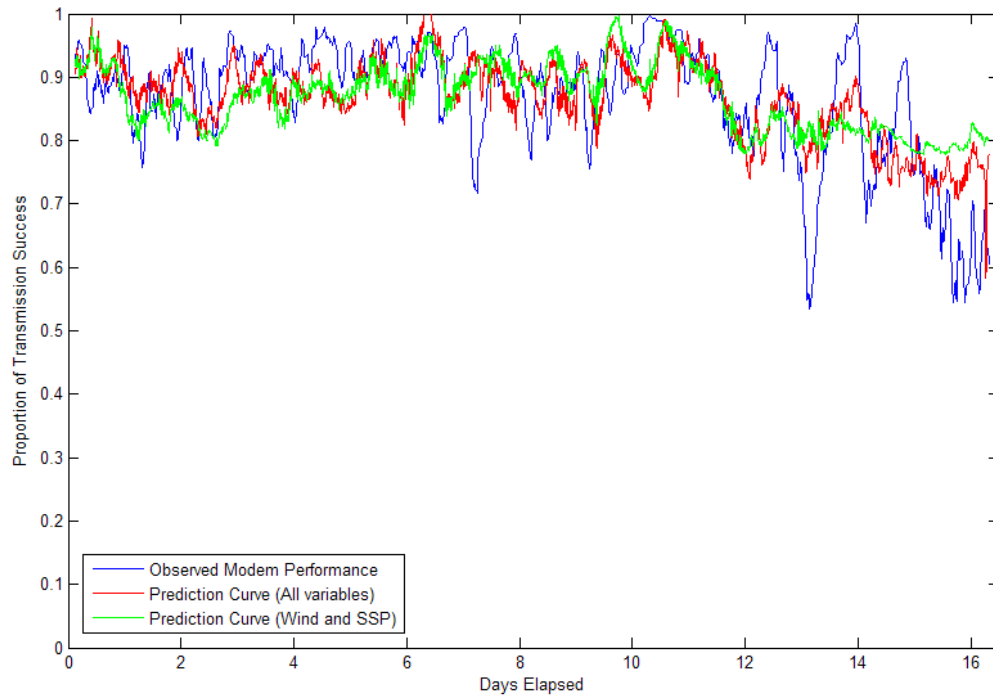


Figure 5.5.5. Direct comparison of measured performance trends with predictions using linear models. One prediction curve utilised all environmental parameters whilst the other included only wind speed and SSP gradient.

A high dependence of modem performance on the SSP gradient was found by the regression techniques which is indicative of a downward refracting physical channel being optimal for acoustic communication to a seabed receiver. Interestingly, the results suggested a positive impact of wind speed on the performance of acoustic communication. Comparing the wave height directly with the received acoustic signal strength found a negative correlation between the two variables with $R^2 = 0.18$ and $R_{\text{low}}^2 = 0.40$. This result further suggested that increases in surface scattering

from waves may have resulted in less impact of multipath arrivals at a receiver. Despite the improvement of performance with increasing wind speed found in this trial, these results may have been reversed had the SNR not been as high and ambient noise fluctuations played a larger role.

5.5.3 Comparison with Long-term Simulation Results

Predictions from the underwater acoustic communication simulator described in Section 5.4 were compared with the statistics acquired from the long-term Perth trial. The simulations were designed to operate with similar spatial parameters to the experiment, incorporating the evolving sound speed profile, ambient noise levels and wave height into each time step. Comparison between the measured performance and the final simulation is shown in Figure 5.5.6 and Figure 5.5.7.

In Section 4.2.5, a mapping function was used to estimate the predicted transmission failure rate based on the simulated word error which produced a more accurate fit to the trial data. A similar approach to predicting the transmission success for this trial was not performed. Instead of attempting to predict the absolute performance parameters of communication at discrete points, this particular trial sought use continuous data collection to identify and compare the trends in reliability and to determine the impacting environmental factors. Furthermore, unlike the short-term experiments, this trial involved transmissions of varying lengths and complexities which would require a more complicated approach to mapping the transmission success and likely yield higher uncertainty in the final result.

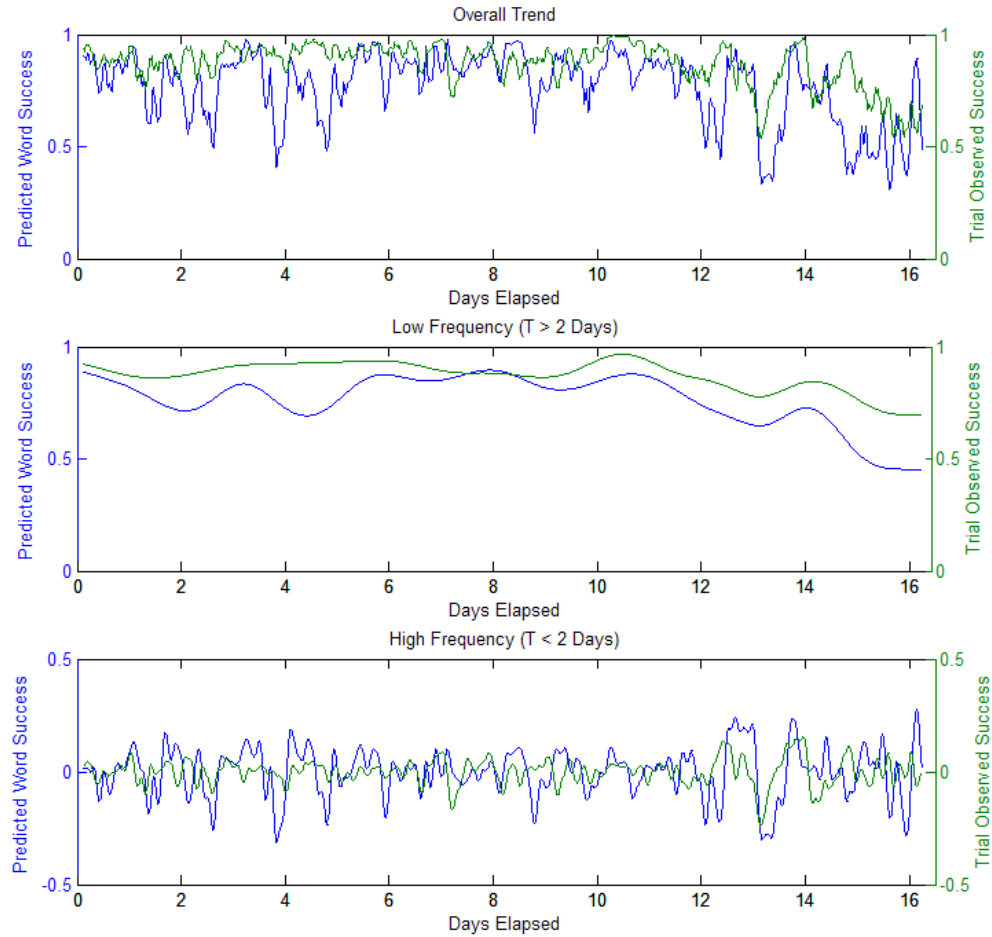


Figure 5.5.6. Comparison of performance trends from simulations and measured data from the long-term Perth trial. The data were also separated into high and low frequency components to highlight similarities

Comparison between simulated and measured performance trends indicated some periods of good agreement, with discrepancies evident when comparing the positions of troughs. The correlation increased with the addition of environmental parameters in the model. Progressing from the ‘min’ synchronisation method to the ‘max’ method and finally to the addition of wave height yielded coefficients of determination (R^2) of 0.01, 0.19 and 0.27 respectively. Inclusion of the standard deviation from the simulated output was not found to have any significant effect on the predictability of the performance. Similarly to previous investigations, a lower correlation was obtained when using only the short-term trends and the best result was found when considering only long-term variations (Figure 5.5.7).

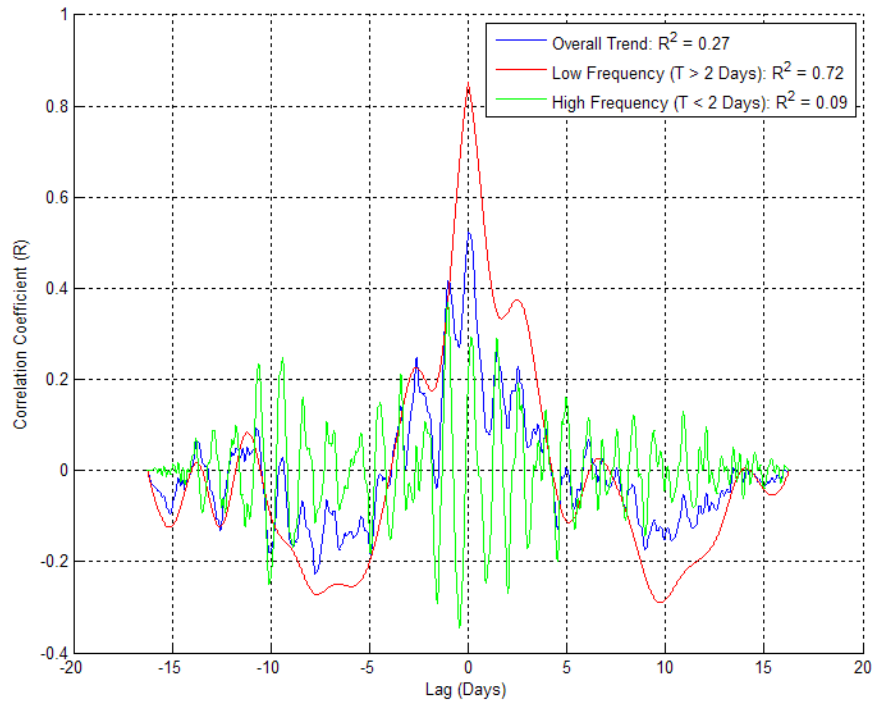


Figure 5.5.7. Cross correlation of performance trends from simulations and data obtained from the long-term Perth trial. The trends were also separated into high and low frequency components and correlated.

5.5.4 Interpretation and Discussion

The fitting curve that was obtained using multiple linear regression correlated more with the field data ($R^2 = 0.44$) when compared to the results from the underwater acoustic communication simulator ($R^2 = 0.27$). However, multiple linear regression was dependant on the trial results and could not be used for forward prediction of performance in different scenarios. The simulator results were produced independently of the measured performance which demonstrates a broader and more useful prediction method that can be reapplied to other scenarios.

The SSP gradient was shown to correlate well with the measured performance. This was consistent with a downwardly refracting sound speed profile directing more energy towards the seabed. It was also determined that the wind speed and wave height correlated with ambient noise which negatively impacted communication performance. However, wind speed and wave height positively correlated with

communication performance. This is consistent with the high SNR remaining relatively unaffected by marginal fluctuations in ambient noise levels. Therefore, the sea surface state mostly affected only the propagation characteristics of the channel. It was conjectured that an increase in wind speed produced a higher level of sea surface roughness which likely caused more scattering of multipath. Consequently, the surface reflections which contributed to the multipath effects would have been attenuated, reducing the impact of ISI and ultimately improving performance.

It was discovered that with the addition of more environmental parameters to the underwater acoustic communication simulator, the predicted performance correlated better with the measured statistics. This showed promise for the simulator, indicating that further customisation would yield more accurate results. Possible enhancements could include the introduction of additional features to help incorporate range-dependant variations of the physical channel. An example of where such a feature would be useful was highlighted with the periodic time-offset of performance troughs observed when comparing simulated and measured data (Figure 5.5.6). This effect may have been brought about by fluctuating parameters which were not taken into account, such as internal waves. Furthermore, the advection of mesoscale eddies associated with the Leeuwin Current (briefly discussed in Section 5.1) may have created anomalies in the propagation characteristics of the channel, effectively introducing a range dependence to the refraction characteristics.

In addition to short-term channel variability, environmental influences which are difficult to measure such as internal currents and waves may always limit the accuracy of communication performance predictions. However, the major environmental parameters that affected acoustic modem performance in the long-term Perth trial were effectively determined using multiple linear regression. Additionally, the simulator demonstrated an additional step towards more accurate predictions of underwater acoustic communication, and possesses the flexibility to be refined in the future.

5.6 Summary of Findings

The long-term Perth deployment was designed to utilise the collection of several different data sets in order to better understand the various effects of oceanographic parameters on acoustic propagation. Data obtained from the deployed equipment included modem performance statistics for over 16 days, ambient noise recordings for up to 20 days and the temperature profile of the bottom half of the water column for 21 days. Environmental data including wind speed, wave height and tidal movements were obtained from nearby monitoring stations to further aid analysis.

Communication statistics were divided into one way transmissions and interrogations. Results from analysis of the recorded modem data were further backed up using acoustical analysis which was used to determine the point of failure for interrogations. Transmissions originating from the modem located at AP2 were found to have an approximate 5% higher chance of reception failure compared to transmissions originating from AP1. Additionally, analysis of interrogation data demonstrated that an increased size of data packet increased the error probability in reception.

Investigation of the ambient noise recordings from AP1 found both short-term and long-term changes. A multiple linear regression method determined that fluctuations measured at the sea surface including wind speed and wave height were likely contributors to the ambient noise levels. Additionally, the downward refracting SSP was found to have a positive effect on noise, suggesting surface activity was a dominant contributor, given the proximity of the hydrophones to the seabed. Sporadic shipping noise was present, particularly towards the end of the trial, but did not affect communication. Overall, the measured SNR was relatively high at approximately 25 - 30 dB which suggested ambient noise had little to no impact on communication.

By using multiple linear regression, the SNR contributions to the observed communication performance fluctuations were found to be small. Furthermore, surface roughness combined with the SSP gradient in the lower half of the water column were found to be major positive contributors, particularly when investigating long-term trends. Interestingly, this result suggested that in the presence of a high SNR, surface roughness was a positive influence on communication as it reduced the impact of multipath effects.

Predictions of trial performance over time were obtained using the underwater acoustic communication simulator tailored for the same FSK-based communication method utilised by the modems. The simulator was progressively updated with a more effective synchronisation algorithm and the inclusion of more environmental parameters including noise levels and surface roughness. Comparison with the measured statistics showed a reasonable, but erratic agreement as performance troughs were offset by varying amounts in time. The possible range-dependence of the refraction characteristics caused by internal waves and influences from the Leeuwin Current was proposed as possible a reason for this discrepancy. The simulated performance did not correlate as well with measured data when considering only the short-term fluctuations. Nevertheless, the simulator demonstrated an effective method for obtaining predictions of modem performance with flexibility which would allow for the implementation of additional features.

This study successfully simultaneously acquired and compared the long-term variations in several environmental parameters with the performance of underwater acoustic communication. Additionally, simulations were effectively used to predict communication performance. The results from this investigation provided valuable insight into the contributing factors for performance when considering FSK based modems and further enhanced the knowledge of environmental influences on underwater communication signals.

6 Discussion

The results from the investigations in the preceding chapters highlight many of the issues related to the use of underwater acoustic communication as a real-time method of sensor data retrieval. Conducting short-term trials with varied modem positions provided insight into the spatial parameters that affect modem performance, as well as the influences of signal and noise fluctuations. The long-term experiments provided information regarding the impact of time-varying environmental conditions on communication for over 16 days. Finally, an underwater acoustic communication simulator was able to predict the performance measured during experimentation and help determine the primary factors impacting underwater acoustic communication.

6.1 Evaluation of Methods

Specialised equipment was custom built for the simultaneous acquisition of ambient noise data and acoustic modem performance statistics. Overall, the hardware operated effectively during the program. The most significant problem encountered was large amounts of electronic interference entering the recordings on the secondary recorder. This problem was later determined to be caused by a faulty preamplifier or hydrophone cable and reduced the effectiveness of the analysis. Thankfully, the primary acoustic recorder did not exhibit problems during the deployments so its acoustic data set was of high quality. Additionally, recordings of the electronic interference in the long-term Perth trial (Figure 5.3.19) proved useful in identifying which data measured by the primary recorder was real acoustic data. A less critical problem was discovered during the short-term short range trial (Section 4.1), where a lack of instant modem feedback resulted in much time being spent testing communication with unsuitable separation distances over 500 m (Figure 4.1.3). Improvements made to the equipment over time proved useful, such as the addition of instant modem feedback using an LCD module attached to a transparent end-cap of the transmitter system (Figure 4.2.4). This feature allowed for preliminary analysis to be performed on the vessel without the need to open the equipment housing.

It is possible that the signal and noise levels received by the modem transducers with hemispherical beam patterns were different to those recorded by the omni-directional hydrophones in the presented trials. For example, in the shallow water trial presented in Section 4.1, noise recorded from close-proximity snapping shrimp was likely less intense at the modem receiver than that received by the hydrophone. Performance fluctuations may also have been a consequence of unforeseen changes in beam angle arising from drifting nodes. Consideration of these factors was difficult given the limited modem memory for acoustic recordings. However, work on better predicting the implications of different transducer types would be useful for the future.

The modulation techniques used in the trials involved only non-coherent protocols. These included a spread spectrum technique for a preliminary investigation, a pulse modulation method for acoustic tagging, and most of all, a FSK-based method utilised in the AQUAmodems. With the inclusion of underwater acoustic recorders in the trials, algorithms were used to independently detect and in some cases decode the received signal from a hydrophone. The independent ambient noise recorder proved useful where an algorithm was able to detect signals at a longer range (Figure 4.1.8) than the DSPComm modems (Figure 4.1.9) presented in the preliminary trial (Section 4.1). This result attributed the shorter range detection performance of the modems to a lacklustre performance in a low SNR environment which could be improved by modifying the sensitivity of the receiver. Isolation of similar characteristics discovered during the trials may not have been possible if a more complex modulation scheme was implemented, due to limitations of the recording hardware and possible commercial restrictions on information sharing.

Comparisons with models and simulations were aided by the straightforward implementation of communication methods. Had a simulation been conducted with more complex modulation techniques, the results would be helpful only for modems with similar features, which was not the intention of this study. As the studies in this thesis were performed using relatively simple signal processing algorithms, the raw impact of environmental parameters was established. Following the determination of the major source of modem errors, the benefits from the addition of protocol enhancements such as equalisation and error correction techniques could be assessed.

Overall, the methods described in this thesis were sufficient to characterise the performance of acoustic communication in the scenarios studied. Additionally, the capabilities of the MCS (Section 3.1.2) in particular demonstrated the possibility for the future integration of a subsea monitoring system into the existing equipment. Using two onboard UARTs (one reserved for the modem) and other various interfaces on the C8051F120 microcontroller, data from an ambient noise recorder was acoustically transmitted to the remote recorder using the MCS. This method was used for most of the presented experiments, effectively trialling a simple monitoring system. A demonstration of this system can be seen in Figure 6.1.1 which shows the remaining disk space of the recorder located at AP1 which was acoustically transmitted to AP2 throughout the duration of the long-term trial (Chapter 5).

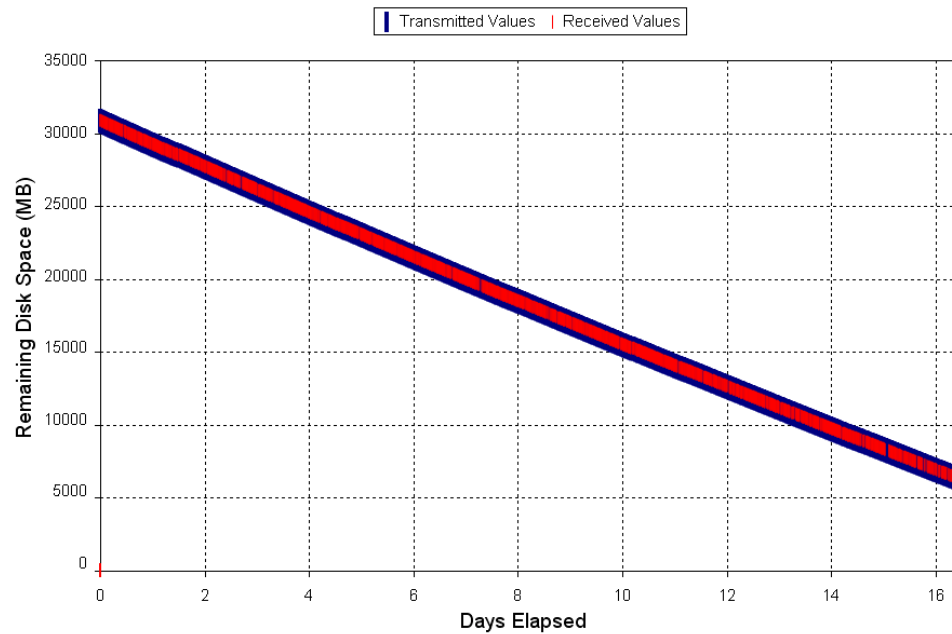


Figure 6.1.1. Remaining disk space as a function of time as received acoustically by one of the remote modems in the long-term Perth trial. Very little discontinuity in the received values demonstrates a relatively reliable link over the deployment period.

Despite the error rates measured during the trial, AP2 was capable of monitoring the overall status of the recordings at AP1, and vice versa using underwater acoustic communication. Very little evidence of an unstable link over the deployment period was observed. This current system could be reconfigured for the monitoring of other parameters including temperature, pressure and data input from external devices.

6.2 Considerations for the use of Underwater Acoustic Communication

Various environments were trialled in the experimental program: three shallow water ($D < 30$ m) studies (Section 4.1, 4.2 and Appendix C), 2 deep water ($D \leq 1000$ m) studies (Section 4.3 and Appendix B) and a final long-term trial using a moderate water depth of 100 m (Chapter 5). It was determined that the critical factors affecting communication performance in an undersea channel changed dramatically with the deployment conditions.

6.2.1 Modem Positioning

When deploying in shallow water, multipath propagation was found to be the dominant source of problems encountered for an underwater acoustic communication system. The only exception to this finding was in the Cockburn Sound trial which utilised pulse modulation techniques for acoustic tag emissions. As the pulses were separated by a significantly large time, ISI was not found to be an issue for communication (Appendix C.4). This allowed for the investigation to focus on other environmental parameters such as received SNR.

The spatial simulations of the second shallow water trial off the coast of Perth (Section 4.2.5) showed that the position of the modem played a vital role in communication performance. Furthermore, the modem performance could not be precisely predicted using the simulator as results yielded irregular performance patterns over a range-depth grid (Figure 4.2.11). The four carrier frequencies of the modems would have had wavelengths of approximately 14, 16, 18 and 20 cm. Not only does this result also imply that performance fluctuations would occur over a small spatial scale, but the effects would have been different for each carrier frequency used. This dependency is also shown with the multipath effects experienced in the French trial (Section 4.3) at TP5 (Figure 4.3.5) which was thought to have prevented communication in the high SNR situation.

Changes in the physical channel would complicate predictions as the location of nodes and antinodes due to constructive and destructive interference would vary over the transmission duration. The middle depths of the water column were found to be the optimum location for a transmitter and receiver pair in the shallow water environment in the Cockburn Sound trials (Appendix C). This result stems from a marked decrease found in acoustic tag detections when the transmitter and receiver were both lowered by 1 m mid-way during the trial. Importantly, as the pingers in the Cockburn Sound trial were not affected by multipath propagation, an increase in performance at mid-depth could be attributed to something other than ISI. A likely explanation for the performance increase at mid-depths could be higher signal strength and less distortion due to a higher number of near-horizontal acoustic paths. This explanation is also supported by the findings of the shallow water simulations where the middle of the environment produced more favourable results after the inclusion of noise into the model (Figure 4.2.12).

The optimal positioning of underwater acoustic modems for horizontal communication in deeper waters is highly dependant on the sound speed profile. Obtaining a strong direct acoustic path is optimum for efficient communication over deep-water channels. The trials presented in this thesis have involved upwardly (Section 4.3 and Appendix B) and downwardly (Chapter 5) refracting subsea channels. In each case, the modems were located within tens of metres from the boundary towards which rays were refracted, and communication was possible at the ranges tested. Furthermore, simulations of the deep water French trial (Figure 4.3.8) as well as the long-term Perth trial (Figure 5.4.1) showed modem positions close to these boundaries to be ideal. However, it was noticed during the simulations that modem positions very close (within metres) of the boundary would not be as suitable for effective communication. This result was most likely due to reflected arrivals with similar amplitudes interfering with the original paths at the receiver.

The impact of interference close to the boundary was not as pronounced for acoustic propagation along the seabed, shown in Figure 5.4.1. This was possibly due to the substrate type (sand in Chapter 5) giving a lower reflectivity compared to the sea surface. This result signifies an advantage for communication via seabed bounce

paths when compared to sea surface reflected paths. Additionally, when considering the sea surface boundary, wind, waves and bubble plumes which all generate noise at the surface also need to be considered. In the long-term trial, the SSP profile and wind speed was shown to correlate with ambient noise at the receiver (Section 5.5.1) which was consistent with wind noise being refracted downwards. This result indicated that the seabed location of the modems was favourable for reducing the impact of noise originating at the surface.

In the trials and simulations presented in this thesis, a deep sound (SOFAR) channel was not investigated. In such a case, the optimum modem position is expected to be within the SOFAR convergence zone, or as mentioned in previous studies (Essebbar *et al.*, 1994), a marginal distance from the sound speed minimum to reduce the impact of interference.

An important effect discovered during deep water simulations was a dramatic variation in performance with changes to the SSP. For example, in the French trial simulations (Section 4.3.5), both winter and summer SSPs were input into the model, yielding vastly different propagation characteristics. The major difference between the two environments was the existence of a thermocline, brought about by a warmer mixed layer at the surface. Consequently, the performance of a modem pair positioned in the same location was shown to be dramatically different for the two differing temperature profiles (Figure 4.3.13). This was also evident with variations in performance found in original simulations of the long-term Perth trial which incorporated only SSP fluctuations. (Figure 5.4.2).

Overall, the best location of modems used for an underwater acoustic communication system was found to be highly dependant on the SSP with emphasis given on establishing a strong direct acoustic path between two nodes. Additionally, positioning the modems several wavelengths away from the areas of ray convergence was predicted to be effective in reducing the impact of multipath interference.

6.2.2 Effects of Received Signal Strength

In scenarios where the effects of multipath propagation were minimised, the impact of the SNR on communication performance varied, with two distinct behaviours observed. When the SNR was already high (approximately 20 dB and higher), variations in the signal or noise levels did not drastically affect the overall error rates observed. In situations with reduced SNR, however, the performance could be positively correlated with the measured SNR levels during the trial. This larger dependence on other parameters is illustrated in Figure 5.4.5 where the increased noise level decreases the overall performance as well as producing higher variability.

In the French trial (Section 4.3), the FSK-based modems were utilised in deeper waters with a receiver depth of approximately 25 m. The SNR was above 10 dB over the 6 km range trialled (Section 4.3.3). Similarly, when investigating the simulator results for the French trials, no SNR limit was observed over the region following the input of the measured noise levels (Figure 4.3.8). The long-term trial (Chapter 5) also yielded a high SNR for a constant modem separation of 5 km in varying oceanographic conditions. A high average SNR of 20 dB was observed, helped by the downward refracting environment which increased the received signal power (Section 5.3.6). Additionally, the seabed location of the receiver minimised the impact of ambient noise originating at the sea surface. It was found using simulations (Figure 5.4.4) and regression analysis with measured data (Section 5.5) that the SNR levels experienced during the trial had minimal impact on telemetry performance.

In the short-term trials presented in Chapter 4, the increasing ranges demonstrated that decreasing signal strength negatively impacted modem performance. For the first of these trials which used a DSSS-based modem (Section 4.1), the effect of decreased signal strength was pronounced at short distances with packet detections failing beyond 500 m where the SNR was relatively high (approximately 10 dB). An algorithm applied to the independent recordings was able to detect the signal up to 1.4 km away (Section 4.1.5), highlighting a lack of modem receiver sensitivity and not a limitation of the modulation scheme itself.

In the second short-term trial (Section 4.2), FSK-based modems were utilised and the signal was detected by both the remote modem and acoustic recorder at up to 7 km from the transmitter. The signals not detected by the modem at longer ranges correlated with those undetected by the underwater acoustic recorder (Section 4.2.4). Additionally, simulations incorporating the observed noise predicted a similar effect of SNR at ranges beyond 7km (Figure 4.2.13). This result also suggested little discrepancy in the detection sensitivity between the ambient noise recorder and modem receivers.

It was originally proposed in Section 4.2 that the cause for poor performance in a shallow water environment at close range was high amplitude ISI which may have saturated the receiver. The possibility of saturation occurring raises issues regarding the gain levels of an acoustic modem. For stationary monitoring systems, saturation is unlikely to occur given adequate knowledge of the distance between communication nodes. However, in the case of utilising mobile nodes for navigation or data muling, it would be important to ensure that saturation at the receiver was minimised to prevent reflected arrivals being observed as just as significant in amplitude as the direct path. Such a consideration would be important for shallow water scenarios where the path distance between direct and reflected rays is reduced.

6.2.3 Noise Sources

Ambient noise was found to be a limiting factor for effective communication as it decreased the SNR at the receiver. With the exception of snapping shrimp, most of the environmental ambient noise characterised in the studies was generated at the sea surface. For example, wind speed and subsequent wave height in the long-term Perth trial (Chapter 5) showed a high correlation with the ambient noise detected at the seabed. Additionally, the large amounts of vessel traffic measured in the short-term Perth trial (Section 4.2) was shown to give periodic and high fluctuations in ambient noise levels, which in some cases, exceeded the signal strength. This result indicated possible complications if a monitoring system was located in an area of high shipping traffic, particularly close to shore and in shallow waters.

Marine life noise encountered in these trials was mostly from snapping shrimp which was apparent in the Perth short range trial (Section 4.1) and the Cockburn Sound trial (Appendix C). Shrimp noise was clearly audible in the recordings and also showed similarities when compared to noise prediction spectra. This existence was confirmed by investigating the amplitude distribution of the measured ambient noise which was shown to be non-Gaussian (Figure 3.3.5), consistent with snapping shrimp, previously investigated by Legg (2009). The ambient noise levels in Cockburn Sound were found to have a strong impact on acoustic communication performance, yielding a strong correlation with tag detections (Figure C.17). This result demonstrated that even with high carrier frequencies (69 kHz), snapping shrimp have the potential to affect an underwater acoustic communication system.

As evident in the Arctic trials (Appendix B), interference from a vessel can have a dramatic impact on the receiving quality of underwater acoustic modems. When investigating the ambient noise at each of the modems mounted from their respective vessels, varied levels were measured. The highest noise levels originated from a modem interfaced electronically with the wet-lab of the main vessel (Figure B.8). For an unattended monitoring system, this type of electronic interference is not a concern. However, the ambient noise recorders used for the majority of the experiments both exhibited levels of interference from their internal electronics. For one of the ambient noise recorders deployed during the Cockburn Sound experiment, electronic interference was present with a fundamental frequency of 1.0 kHz. Consequently, measurements of SNR and overall detection sensitivity for this particular recorder were mostly unusable as the carrier frequency (69.0 kHz) was directly over the interference band (Figure C.9). This problem highlights the importance of effective electronic shielding of the recording components which could potentially provide dramatic increases to SNR. A lower ambient noise floor would be particularly useful for deep water deployments where acoustic noise is significantly reduced, greatly enhancing receive sensitivity.

6.3 Predictability of Modem Performance

Predicting the performance of underwater acoustic communication is difficult given the changing environmental parameters and their effects on a received signal. Despite this, the presented simulator has shown potential to provide a communication performance prediction based on a number of environmental parameters. Several aspects of the presented simulator left room for performance improvements, some of which were deliberate to ensure the addition of features was not counter-productive. For example, error correction was not implemented to better show the effects of channel propagation alone. Furthermore, the effect of error correction was found to be negligible in the long-term study (Section 5.3.3), so the exclusion of error correction in the simulation was expected to have little impact on the comparisons. Additionally, by predicting the raw errors, modem developers would be able to determine what error correction techniques would be best suited to the application.

In the simulations presented in Sections 4.3.5 and 5.4, the optimal depth of a receiver for a given transmitter location was observed to be in or around areas where the modems were deployed in the experiments. However, a discrepancy in the locations of performance peaks and troughs was found when comparing the simulated and experimental results for the French trial (Figure 4.3.9). It was inferred that lack of accurate environmental data caused the displacement of the predicted trends, reiterating the importance of including as precise detail as possible about the environmental data in a simulator model. The positive effect of adding experimental measurements is highlighted in Section 5.4 where the time-dependant simulation was updated to include noise, wave height and a more accurate synchronisation method. The coefficient of determination (R^2) between the simulated data and the experimental results rose from an original 0.01 to 0.19 with the addition of a new synchronisation method and finally to 0.27 with all data included in the model.

An important consideration when evaluating the presented underwater acoustic communication simulator was the assumption of a physical channel that was

stationary in time. Described in Appendix A.2.7, the time-variability of an underwater acoustic channel is a characteristic that can be divided into low and high frequency components. The time dependant simulations presented in Section 5.4 were able to account for slower moving elements of the underwater channel, including the evolving sound speed profile and average sea surface roughness. Although the results demonstrated these inclusions to be effective, particularly over long durations, it was evident that faster moving trends were not as accurately predicted. When considering the even faster fluctuations resulting from rapid changes in the environment and transmitter and receiver motion, the simulator did not include any appropriate statistical models when deriving the channel transfer function.

Described in Appendix A.2.7 and Section 2.3, there is still some degree of disagreement amongst researchers regarding the best statistical model for estimating the fading characteristics of some underwater acoustic channels. An initial application of implementing Rayleigh or Rice statistics into the existing impulse response determined by the ray traces described in this thesis may provide an improvement of prediction accuracy. However, unless an integrated statistical model was to also vary with space and/or time, it would be reasonable to expect that it may have a limited impact on the observed overall trend. With this in mind, implementation of a statistical model would require greater knowledge of the fading statistics (from the use of probe signals or other means) to effectively predict the communication performance in the presented trials. Furthermore, an interesting result was found in the simulations of the shallow water scenario given in Section 4.2.5, which showed a highly variable spatial distribution of predicted performance (Figure 4.2.11). The observed spatial fluctuations can, to some degree, be considered as an alternative to incorporating models of high frequency temporal variations. In this study these fluctuations were averaged to produce the final estimate of channel performance during the evaluation. This averaging proved to be effective in predicting the overall performance at longer ranges in the short-term shallow water Perth trial and also in the long-term trial.

The three simulated data sets presented in this thesis were each used for unique methods of comparison. In Section 4.2.5, it was possible to estimate the packet transmission failure given the predicted word error from the simulator using a non-linear mapping function. This method assumed each 4-bit word was independent and that the transmissions were of the same content. This method was suitable for the short-term trials given the small packet sizes used and their similarities in content. Direct comparison found very good agreement with the data which showed good performance at very close range (160 m) and intermittent communication at mid-range (4 km – 6 km) (Figure 4.2.15). The performance statistics collected during the French trial presented in Section 4.3 were obtained as the bit error rate, calculated from the 4-bit word error observed by the modem hardware. This allowed the comparison of individual errors within packets rather than the errors in receiving entire transmissions. In the long-term trial (Chapter 5), comparison between observed and predicted performance involved investigating the overall trends in two continuous sets of data. One interesting feature from this comparison was that the predicted success rate for individual 4-bit words was (in most cases) lower than the overall observed transmission success (Figure 5.5.6), the opposite of what was observed in the short-term Perth trial. This demonstrated that the simulator was not as effective in predicting the absolute performance of the modems in the temporal study. However, a reasonable comparison was discovered between the overall trends which verified the effectiveness of the simulator for predicting changes in reliability.

The simulations presented in this thesis provided adequate performance predictions for comparison with the trial data. Furthermore, modem manufacturers and developers of communication techniques would benefit from such a simulator given its flexibility to be modified to suit their design, potentially reducing the amount of costly field experimentation. The most prominent limiting factor of the acoustic communication simulator was determined to be the assumption of a physical channel that is stationary in time. Further work in characterising the changing propagation characteristics of a subsea channel would aid in allowing a simulation to factor in the short-term fluctuations in the transfer function. This work may involve the inclusion statistical models (as presented in previous studies) into the existing methods to help predict the effects of a fluctuating ocean. Despite this, the methods employed to

simulate modem performance based on measured environmental data in this study proved effective within their limitations.

In addition to performing simulations to determine the predictability of the long-term deployment presented in Chapter 5, a multiple linear regression approach was used to determine a first order estimate of the parameters that affected communication performance during the trial. Despite the simulator taking into account the full SSP, the regression analysis provided a better prediction of the experimental results when using only a linear least squares fit of the bottom 50 m of the SSP. However, the prediction method acquired using multiple linear regression is not suitable for applications in other experiments, whereas the simulator can be applied to other scenarios with the appropriate reconfiguration.

As a final illustration of the complexities in acoustic communication performance prediction, consider the regression analysis of the long-term Perth trial (Chapter 5). The most dominant factors all positively affecting communication were determined to be the SSP gradient (41%) and sea surface roughness (37%), with some contribution from the SNR (22%). In this particular trial, the SNR remained very high (approximately 20 dB) due to high received signal power. This minimised the effect of ambient noise fluctuations, which were found to be positively correlated with the SSP gradient and sea surface roughness (Section 5.5.1). It is therefore possible to assert that a primary reason for good performance in this particular trial was the high signal power which minimised the effects of ambient noise on communication. With this consideration, in a low SNR environment the SSP gradient and sea surface height could have a completely different impact on communication success, both possibly having a negative impact.

6.4 Underwater Acoustic Communication for Real-time Monitoring and Control Systems

The final long-term experiment discussed in Chapter 5 demonstrated a basic two-way acoustic monitoring system operating over a 5 km subsea channel. Ambient noise recorders used in the experiment constantly communicated with one another using acoustic modems, sharing information regarding the amount of internal disk space remaining, shown in Figure 6.1.1. The effective operation of the devices for over 16 days demonstrates that it is feasible to use acoustic communication for the continuous monitoring of subsea parameters. However, the information held in current literature in addition to the results from the experiments presented in this thesis highlight several important considerations for the deployment of a full-scale system. A practical implementation would require longer-term monitoring with a faster, longer range, more reliable link between more than two nodes.

For a communication system used for long-term deployment in real-time monitoring systems, a series of advanced communication techniques would be required to ensure both speed and stability. Shown in the results of this thesis, the environmental changes can have a significant impact on the performance of underwater acoustic communication. For this reason, channel characterisation would be paramount for any subsea telemetry system to ensure adaption to the properties of the acoustic channel. By characterising the subsea channel, a suitable time-reversal method such as passive phase conjugation could be utilised in conjunction with decision feedback equalisation to counteract short-term channel fluctuations (Section 2.2). Ideally, channel characterisation via a training sequence would occur before every transmission with this channel estimate updated with each symbol, previously demonstrated by Rouseff *et al.* (2004).

Wider bandwidth would be useful for adding redundancy for additional reliability, faster data rates and the integration of several networked nodes. For a simple monitoring system, the moderate speeds quoted in the literature and the 100 bps used during the presented trials would be sufficient to relay basic messages in an undersea

network of very few nodes, provided the link was reliable. However, for advanced monitoring such as live camera feeds or control of elements such as a Remotely Operated Vehicle (ROV), a subsea link would require both higher speeds and increased reliability.

Although much faster speeds have been established as discussed in the literature review (Chapter 2), the technology still requires further advances to make it applicable to a broader range of physical channels. These channels include a range of challenging scenarios such as high multipath and low SNR situations which are typically avoided when experimenting with complex algorithms and high data rates. Additionally, transplanting the spatial, computational and power capabilities expressed in advanced telemetry studies to a portable device may prove difficult in the near future. It is therefore expected that most compact underwater acoustic modems would need emphasis on effective signal processing techniques and power efficient design. Importantly, acoustic modems utilising compact receive arrays instead of single transducers would benefit from taking advantage of spatial diversity which was shown to produce much better results (Section 2.2).

The favoured type of network topology for a subsea monitoring system has been shown previously as a distributed network of nodes with the use of a gateway buoy for RF access to a land-based control station. The Seaweb program (Section 2.4) is a suitable case-study for the use of underwater modems for subsea sensor measurement retrieval, having gone through several iterations and providing an advanced underwater network prototype. However, this thesis investigated horizontal communication as a means to assess the performance of a multi-hop network better suited to relay digital data to shore without the use of sea-surface infrastructure.

Given the variability of the environment seen both daily as well as seasonally, the structure of any network would require redundancy to ensure the stability of an undersea link in all circumstances. For a multi-hop network, an obvious method of redundancy would include placing nodes closer together and facilitating ad-hoc connections, should an adjacent modem be disabled. Reconfiguration of the network

is important for establishing a reliable and sustainable connection for long-term deployments and has previously been deployed with projects including the Seaweb program. The modems in this thesis have demonstrated the effectiveness of modifying data rates where the baud rate was quadrupled via an acoustic command (Section B.4). As a monitoring system places importance on reliability, the ability to modify communication parameters such as data rates, frequency band and even modulation technique would prove extremely useful.

As with all underwater equipment, marine growth is a concern that would typically need to be addressed for subsea modem technology, particularly for long-term deployments. In the long-term study presented in Chapter 5, marine life damaged the transmitting components and their surrounds. In addition to reducing the impact of marine growth on communication, additional physical protection would be necessary in an acoustic communication system as the device activity would likely attract marine life. Overall, the communicating systems would need to be closely monitored and tested to ensure that they remained operational. This consideration is particularly important for back-up systems where a breakage of the infrastructure would not be immediately apparent.

The use of underwater acoustic communication in a subsea network has the potential to create both a viable and economical solution for either a primary or backup data link. Additionally, the use of acoustic communication could be further utilised to provide access to other applications of underwater acoustics such as active or passive localisation which was demonstrated when analysing data from the initial Perth trial (Section 4.1.3). Additionally, AUV technology could be integrated into a network using acoustic modem transmitters as navigation beacons similar to the study performed by Dunbabin *et al.* (2006). As each network node would consist of an acoustic transmitter and receiver, some oceanographic characteristics may be easily measureable, dependant on the modem properties. Even if the modem technology was only used as a backup form of communication, the acoustical components of the devices may be useful for other tasks.

Despite recent dramatic advancements in the technology, the performance of underwater acoustic communication still requires extensive research before it can be considered a viable alternative to cabled systems for all subsea telemetry, particularly over long ranges. Characterisation of the environment is vital for ensuring a stable connection for any acoustic communication system. This must be followed up with compensation for the time varying channel fluctuations at a receiver. With the use of simulations, the time and expense in conducting field trials would be considerably decreased, allowing for faster development of signal processing techniques tailored to digital underwater acoustic communication. With the appropriate research, coupled with advances in low cost and low powered technology, acoustic modems will continue to substitute traditional forms of underwater communication. However, it is expected that given the relative unreliability in their current state, their use in critical systems would be limited to applications as back-up communication methods in the near future.

7 Conclusions and Opportunities for Future Research

7.1 *Conclusions*

The horizontal performance of underwater acoustic communication has been characterised in various scenarios using data obtained from both field trials and performance simulations. A series of custom hardware and software developments were made to experimentally evaluate the performance of commercial underwater acoustic modems whilst simultaneously measuring environmental conditions. The equipment was deployed to measure communication performance over deep and shallow subsea channels in different configurations, including long-range, arctic and long-term deployments. The data from these experiments was examined to assess the performance impacts of environmental parameters. Additionally, an underwater acoustic communication simulator was developed in Matlab to estimate the modem performance statistics in any given two-dimensional environment. The simulator was applied to three of the presented experiments and the results were compared to evaluate the predictability of acoustic modem performance. Finally, a foundation for use of underwater acoustic communication in long-range subsea monitoring and control applications was established, combining the findings from the investigations.

It was revealed in the literature review that the speeds and reliability of an underwater acoustic data link were relatively low compared to cabled and RF counterparts because of the challenging time-varying properties of the physical channel. This was consistent with the experimental results which demonstrated several complications for underwater acoustic communication. For shallow water communication ($D < 30$ m), ISI was found to become problematic for signal decoding at a receiver despite a high received SNR. The optimal modem positioning was determined to be at mid-depths to reduce the impact of reflected arrivals on

communication performance. Over a deep water channel ($D \leq 1000$ m), the effects of ISI were reduced. However, the refraction of acoustic paths placed high importance on understanding the sound speed profile in order to achieve adequate SNR and reduce multipath effects. Each of these findings was supported by results from the underwater acoustic communication simulator which provided two-dimensional range-depth grid estimates of telemetry performance. Performance predictions for the shallow water trial produced very similar statistics to those found during the experiment. Simulations of the French trial produced a similar overall trend but with a spatial discrepancy, possibly caused by inaccurate knowledge of the environment.

A long-term experiment was conducted which simultaneously collected performance data from an underwater acoustic modem as well as environmental parameters including the water temperature profile and ambient noise. Additional data including wind speed, wave height and tidal movements were obtained from nearby monitoring stations. As the received signal strength was high during this trial, the problems encountered by the modems could be attributed to propagation characteristics alone, rather than SNR. Using multiple linear regression, an estimate of the contributions from each environmental parameter was produced. It was discovered that the sound speed profile gradient and wind speed were best correlated with the performance observed over the 16 day deployment period. Interestingly, the wind speed correlated positively with performance which indicated the advantage of an increased sea surface roughness for reducing the effects of multipath. However, these findings were most likely dependant on the high SNR which reduced the impact of noise fluctuations on the observed performance.

Finally, the underwater acoustic communication simulator was configured to input the measured environmental parameters including sound speed profile, ambient noise level and wave height for a prediction of modem performance over time. By progressively adding more parameters, it was discovered that the accuracy of the simulations increased. Additionally, the modification of the synchronisation algorithm to better replicate the behaviour of the modem receiver was found to increase simulation accuracy.

When combining the knowledge obtained from the literature review and experimental work detailed in this thesis, it was determined that underwater acoustic communication is effective in many scenarios and could be applied to some subsea monitoring and control systems. Unfortunately, the speeds and reliability of an acoustic link are still not at a level that would allow it to become a viable alternative to all applications that utilise cabled telemetry. In particular, crucial monitoring and control systems which operate over long-range and complex underwater acoustic channels would currently benefit from the use of acoustic communication only as a back-up method. However, with future research and progress in channel prediction and equalisation methods, acoustic communication will likely become a much faster and more reliable technology for use in more complex environments.

Overall, the methodology and results detailed in this thesis provide an extensive investigation into the factors that affect underwater acoustic communication in several scenarios, offering a solid foundation for the use of the technology in subsea monitoring systems. Additionally, the developed simulator provided an effective tool for predicting the performance of an acoustic communication system which could be easily modified to best suit the technology and environment of deployment. The results and tools discussed in this thesis provide an effective contribution to the knowledge for the development of subsea telemetry for applications in real-time sensor data retrieval over horizontal channels.

7.2 Opportunities for Future Research

Following from the research outlined in this thesis, further investigation into the predictability of modem performance would be paramount for reducing the cost of conducting field trials. This would involve further work with simulations and conducting more comparisons with the experimental results already obtained. In this study, both spatial and temporal simulations took at least 8 hours to produce a complete result. Consequently, a first consideration for future work would involve optimising the simulator code. The majority of computational time for the simulator was allocated to generating the simulated signal from the impulse response. It is

likely that this code could be optimised with little effect on the simulator accuracy. Following optimisation of the simulator routines for repeated use, the simulator could also be updated to suit the modulation schemes and signal processing used in a variety of underwater acoustic modems. These include the addition of error correction coding and other synchronisation algorithms, as well as the use of advanced signal processing techniques such as passive time reversal methods.

A natural experimental progression from the performance investigations outlined in this thesis would include the use of channel characterisation using a probe signal. This would involve the deployment of a transducer matched with a hydrophone at prospective modem sites. A series of signals including simple sharp pulses or sweeps would be transmitted to the hydrophone via a physical channel with the response recorded by ambient noise recorders similar to those described in this thesis. By utilising channel probing, the fundamental transfer function of the subsea environment would be recorded to give an overview of the changes with time. This transfer function could be directly compared with the result obtained using modelling, removing the need to measure modem performance in the field. From here, the quality of simulations provided using models such as Bellhop could be further assessed. The accuracy of the simulator would ultimately be improved with the inclusion of more data which would then allow for further customisation. Eventually, the number of field trials to determine the effectiveness of protocols would be reduced through the use of accurate simulations.

Building onto the communication simulator, a further iteration would involve the development of a network simulator which would allow for the dedicated trialling of different network protocols. Finding a suitable network protocol would require specific knowledge of the number of nodes, type of data throughput and intended speed of the network before development. It was found in the literature review that network simulations were typically performed using a mixture of methods, some designed for latency-free networks. By forming a dedicated network development tool for underwater acoustics, solving issues regarding the delays inherent in underwater communication is expected to be more efficient.

The eventual deployment of multi-hopping network prototypes would be essential for the investigation of their usefulness in subsea networks. The deployment of a prototype would follow on from the development of a flexible, reliable subsea communication system using a combination of simulations and field trials. Initially, the trial would involve relatively simple transfer of sensor data from an offshore source towards an inland base station such as a harbour station or nearby buoy. Eventually, however, an ideal study would involve the application of underwater acoustic communication along existing infrastructure. This could include a subsea pipeline using a linear array of multi-hop nodes, integrated into a monitoring system.

By building onto existing communication infrastructure, modems would act as a secondary communication method, taking advantage of power fed via umbilicals. By allowing a prototype to operate for months at a time, a much more detailed overview could be established regarding the environmental fluctuations and their impact on the performance of an underwater communication system. The natural progression, should such a prototype be successful, would be the indefinite employment of a refined system, capable of acting independently of existing infrastructure if required. In the case of an emergency such as a break in wire-line communication, an acoustic link would operate as a backup link, useful for monitoring of the situation as well as providing a form of control to prevent or limit the impact of any hazards.

It is anticipated that with further advancements in the technology, underwater acoustic modems could be utilised as a primary method of subsea communication. However, in addition to developing communication protocols and coping with the underwater environment, issues regarding the portability of modems will need to be addressed. Although most commercial acoustic modems utilise a single transducer, compact receive arrays may provide a large increase in performance. Additionally, effective power management would allow a node to run without the need for constant power supply replacements. Given that a modem is an active acoustical device, the power consumption is very much dependant on the transmission characteristics. This leaves room for research in both the transmission power efficiency of acoustic modems as well as developing the most efficient communication protocols for a desired application.

8 References

- Akyildiz I F 2004 Challenges for efficient communication in underwater acoustic sensor networks *ACM SIGBED Review* **1** 3
- Akyildiz I F, Pompili D and Melodia T 2005 Underwater Acoustic Sensor Networks: Research Challenges *Ad Hoc Networks (Elsevier)* **3** 257-79
- Antaki G A 2003 *Piping and Pipeline Engineering - Design, Construction, Maintenance, Integrity, and Repair*: CRC Press)
- Bai Y 2001 *Pipelines and Risers* (Oxford: Elsevier Science Ltd)
- Bannon R T 1998 ROVs and Undersea Cable Maintenance *Underwater Technology, 1998. Proceedings of the 1998 International Symposium on* 69-74
- Barr R, Jones D L and Rodger C J 2000 ELF and VLF radio waves *Journal of Atmospheric and Solar-Terrestrial Physics* **62** 1689-718
- Brekhovskikh L and Lysanov Y 1982 *Fundamentals of Ocean Acoustics* (New York, USA: Springer-Verlag)
- Catipovic J, Deffenbaugh M, Freitag L and Frye D 1989 An Acoustic Telemetry System for Deep Ocean Mooring Data Acquisition and Control. In: *OCEANS '89. Proceedings*, pp 887-92
- Cato D H 2009 Measurements of Anthropogenic and Natural Ambient Noise in the Context of Effects on Marine Animals. In: *Underwater Acoustic Measurements: Technologies and Results*, (Nafplion, Greece
- Cato D H and McCauley R D 2002 Australian Research In Ambient Sea Noise *Acoustics Australia* **30** 13-20
- Chen C-T and Millero F J 1977 Speed of sound in seawater at high pressures *The Journal of the Acoustical Society of America* **62** 1129-35
- Cheng D K 1989 *Field and Wave Electromagnetics* (Reading, Massachusetts, USA: Addison-Wesley Publishing Company, Inc)
- Chengbing H, Jianguo H and Zhi D 2009 A Variable-Rate Spread-Spectrum System for Underwater Acoustic Communications *Oceanic Engineering, IEEE Journal of* **34** 624-33

- Chitre M, Ong S H and Potter J 2005 Performance of coded OFDM in very shallow water channels and snapping shrimp noise. In: *OCEANS, 2005. Proceedings of MTS/IEEE*, pp 996-1001 Vol. 2
- Chitre M, Shahabudeen S and Stojanovic M 2008 Underwater acoustic communications and networking: Recent advances and future challenges *Marine Technology Society Journal* **42** 103-116
- Choi J Y, Lim H and Yi B-J 2006 Semi-Automatic Pipeline Inspection Robot Systems. In: *SICE-ICASE*, (Seoul, Korea: IEEE)
- Coates R, Stoner R and Wang L S 1994 The BASS 600 underwater acoustic communication link. In: *Electronic Engineering in Oceanography, 1994., Sixth International Conference on*, pp 111-6
- Coates R F W, Ming Z and Liansheng W 1996 "BASS 300 PARACOM": a 'model' underwater parametric communication system *IEEE Journal of, Oceanic Engineering* **21** 225-32
- Codiga D L, Rice J A and Baxley P A 2004 Networked Acoustic Modems for Real-Time Data Delivery from Distributed Subsurface Instruments in the Coastal Ocean: Initial System Development and Performance *Journal of Atmospheric and Oceanic Technology* **21** 331-46
- Committee on the Safety of Marine Pipelines M B, National Research Council 1994 *Improving the Safety of Marine Pipelines* (Washington DC)
- Coppens A B 1981 Simple equations for the speed of sound in Neptunian waters *The Journal of the Acoustical Society of America* **69** 862-3
- Courmontagne P, Fages G and Beaujean P P 2008 A chirp FSK improvement for communications in shallow water using bandwidth overlapping. In: *OCEANS 2008*, pp 1-7
- Creber R K, Rice J A, Baxley P A and Fletcher C L 2001 Performance of undersea acoustic networking using RTS/CTS handshaking and ARQ retransmission. In: *OCEANS, 2001. MTS/IEEE Conference and Exhibition*, pp 2083-6 vol.4
- Cui J H 2006 The challenges of building scalable mobile underwater wireless sensor networks for aquatic applications *IEEE network* **20** 12
- Del Grosso V A 1974 New equation for the speed of sound in natural waters (with comparisons to other equations) *The Journal of the Acoustical Society of America* **56** 1084-91

- Dunbabin M, Corke P, Vasilescu I and Rus D 2006 Data muling over underwater wireless sensor networks using an autonomous underwater vehicle. In: *Robotics and Automation, 2006. ICRA 2006. Proceedings 2006 IEEE International Conference on*, pp 2091-8
- Dushaw B D, Worcester P F and D.Cornuelle B 1993 On equations for the speed of sound in sea water *The Journal of the Acoustical Society of America* **93** 225-75
- Dutra F d S, Galvez-Durand F and Alves V C 2002 System on a Chip for Petroleum Inspection. In: *Symposium on Integrated Circuits and Systems Design*, (Univ. Fed. do Rio de Janeiro, Brazil: IEEE) pp 331-6
- Edelmann G F, Akal T, Hodgkiss W S, Seongil K, Kuperman W A and Hee Chun S 2002 An initial demonstration of underwater acoustic communication using time reversal *Oceanic Engineering, IEEE Journal of* **27** 602-9
- Essebbar A, Loubet G and Vial F 1994 Underwater acoustic channel simulations for communication. In: *OCEANS '94. 'Oceans Engineering for Today's Technology and Tomorrow's Preservation.'* *Proceedings*, pp III/495-III/500 vol.3
- Etter P C 2003 *Underwater Acoustic Modeling and Simulation* (London: Spon Press)
- Fisher F H and Simmons V P 1977 Sound absorption in sea water *The Journal of the Acoustical Society of America* **62** 558-64
- Fletcher C L, Rice J A and Creber R K 2003 Operator access to Acoustically Networked Undersea Systems through the Seaweb server. In: *OCEANS 2003. Proceedings*, pp 1-5 Vol.1
- Freitag L, Stojanovic M, Kilfoyle D and J.Preisig 2004 High-Rate Phase-Coherent Acoustic Communication: A Review of a Decade of Research and a Perspective on Future Challenges. In: *Seventh European Conference on Underwater Acoustics, ECUA 2004*, (Delft, The Netherlands
- Freitag L, Stojanovic M, Singh S and Johnson M 2001 Analysis of channel effects on direct-sequence and frequency-hopped spread-spectrum acoustic communication *Oceanic Engineering, IEEE Journal of* **26** 586-93
- Garrood D and Miller N 1982 Acoustic telemetry for underwater control. In: *OCEANS 1984*, pp 111-4
- Gold R, Casselman B and Chazan G 2010 Leaking Oil Well Lacked Safeguard Device. In: *The Wall Street Journal*, 28/03/2010

- Green D and Rice J 2004 Synthetic Undersea Acoustic Transmission Channels. In: *Ocean Acoustics Conferences 2004*, (La Jolla, California)
- Green M, Rice J A and Merriam S 1998 Underwater acoustic modem configured for use in a local area network (LAN). In: *OCEANS '98 Conference Proceedings*, pp 634-8 vol.2
- Guo B, Song S, Chacko J and Ghalambor A 2005 *Offshore Pipelines* (Burlington, MA, USA: Elsevier, Inc)
- Guosong Z 2009 A Simple Time Synchronization Method for Underwater Communication Receivers. ed M H Jens, *et al.* pp 289-93
- Haartsen J C 2000 The Bluetooth radio system *Personal Communications, IEEE* **7** 28-36
- Harris A F and Zorzi M 2007 Modeling the underwater acoustic channel in ns2. In: *Proceedings of the 2nd international conference on Performance evaluation methodologies and tools*, (Nantes, France: ICST (Institute for Computer Sciences, Social-Informatics and Telecommunications Engineering))
- Hayward T J and Yang T C 2004 Underwater Acoustic Communication Channel Capacity: A Simulation Study *AIP Conference Proceedings* **728** 114-21
- Heidemann J, Ye W, Wills J, Syed A and Li Y 2006 Research Challenges and Applications for Underwater Sensor Networking. In: *IEEE Wireless Communications and Networking Conference*, (Las Vegas, Nevada: IEEE)
- Hursky P, Porter M B, McDonald V K and Rice J A 2001 Passive phase-conjugate signaling using pulse-position modulation *The Journal of the Acoustical Society of America* **109** 2477
- Iltis R A, Hua L, Kastner R, Doonan D, Fu T, Moore R and Chin M 2005 An underwater acoustic telemetry modem for eco-sensing. In: *OCEANS, 2005. Proceedings of MTS/IEEE*, pp 1844-50 Vol. 2
- Jakeman E and Pusey P 1976 A model for non-Rayleigh sea echo. In *IEEE Transactions on Antennas and Propagation* pp 806-814 Vol. 24
- Jensen F B, Kuperman W A, Porter M B and Schmidt H 2000 *Computational Ocean Acoustics* (New York, USA: Springer-Verlag)
- Jones E 2007 The Application of Software Radio Techniques to Underwater Acoustic Communications. In: *OCEANS 2007 - Europe*, pp 1-6

- Kebkal K G 2004 A frequency-modulated-carrier digital communication technique for multipath underwater acoustic channels *Acoustical physics* **50** 177
- Kebkal K G and Bannasch R 2002 Sweep-spread carrier for underwater communication over acoustic channels with strong multipath propagation *The Journal of the Acoustical Society of America* **112** 2043-52
- Kebkal K G, Bannasch R and Kebkal A G 2004 Estimation of phase error limits for PSK-modulated sweep-spread carrier signal. In: *OCEANS '04. MTS/IEEE TECHNO-OCEAN '04*, pp 748-56 Vol.2
- Kebkal K G, Bannasch R and Kebkal A G 2005 Theory and experiment for evaluation of the methodical error for a matched filtered phase-encoded sweep-spread carrier signal. In: *Underwater Acoustics Measurements*, (Heraklion, Crete, Greece)
- Kennedy J L 1984 *Oil and Gas Pipeline Fundamentals* (Tulsa, Oklahoma, USA: PennWell Publishing Company)
- Kerman B R 1988 *Sea Surface Sound: Natural Mechanisms of Surface Generated Noise in the Ocean* (Dordrecht, The Netherlands: Kluwer)
- Kilfoyle D B and Baggeroer A B 2000 The state of the art in underwater acoustic telemetry *Oceanic Engineering, IEEE Journal of* **25** 4-27
- King P, Venkatesan R and Li C 2009 Modeling a shallow water acoustic communication channel using environmental data for seafloor sensor networks *Wireless Communications and Mobile Computing*
- Kopp L, Cano D, Dubois E, Wang L, Smith B and Coates R F W 2000 Potential performance of parametric communications *Oceanic Engineering, IEEE Journal of* **25** 282-95
- Kraus D and Kalangi P P 2004 Modelling and Simulation of an Underwater Acoustic Communication Channel. In: *51st Open Seminar on Acoustics*, (Gdansk, Poland)
- Kuchpil C, Xavier A L F, da Silva J A P and Jimenez M R B P L 1997 Autonomous control system for offshore oil exploitation using digital acoustic communication. In: *OCEANS '97. MTS/IEEE Conference Proceedings*, pp 849-53 vol.2
- Kuperman W A, Hodgkiss W S, Song H C, Akal T, Ferla C and Jackson D R 1998 Phase conjugation in the ocean: Experimental demonstration of an acoustic time-reversal mirror *The Journal of the Acoustical Society of America* **103** 25-40

- Laferriere A B 2011 K-distribution fading models for Bayesian estimation of an underwater acoustic channel, Thesis, (MSc) Massachusetts Institute of Technology
- LeBlanc L R, Beaujean P P, Singer M, Boubli C and Strutt G T 1999 Chirp FSK modem for high reliability communication in shallow water. In: *OCEANS '99 MTS/IEEE. Riding the Crest into the 21st Century*, pp 222-7 vol.1
- LeBlanc L R, Singer M, Beaujean P P, Boubli C and Alleyne J R 2000 Improved chirp FSK modem for high reliability communications in shallow water. In: *OCEANS 2000 MTS/IEEE Conference and Exhibition*, pp 601-3 vol.1
- Lee E A 1994 *Digital Communication* (Norwell, MA: Kluwer Academic Publishers)
- Legg M W 2009 Non-Gaussian and non-homogeneous Poisson models of snapping shrimp noise. In: *Faculty of Science and Engineering. Department of Imaging and Applied Physics*. Thesis, (PhD). (Perth, Western Australia: Curtin University of Technology)
- Leus G and van Walree P 2008 Multiband OFDM for Covert Acoustic Communications *Selected Areas in Communications, IEEE Journal on* **26** 1662-73
- Loubet G, Vial F, Essebbbar A, Kopp L and Cano D 1996 Parametric transmission of wide-band signals. In: *OCEANS '96. MTS/IEEE. 'Prospects for the 21st Century'. Conference Proceedings*, pp 839-44 vol.2
- Lurton X 2010 *An Introduction to Underwater Acoustics: Principles and Applications, 2nd Edition* (Springer-Verlag)
- Mackenzie K V 1981 Nine-term equation for sound speed in the oceans *The Journal of the Acoustical Society of America* **70** 807-12
- Mar C H and Seah W K G 2006 DS/CDMA throughput of multi-hop sensor network in a Rayleigh fading underwater acoustic channel. In: *Advanced Information Networking and Applications, 2006. AINA 2006. 20th International Conference on*, p 5 pp.
- Matthew S G 2005 *802.11 Wireless Networks: The Definitive Guide, Second Edition* (O'Reilly Media, Inc.)
- Medwin H 1975 Speed of sound in water: a simple equation for realistic parameters *Acoustical Society of America* **58** 1318-9
- Medwin H and Clay C S 1998 *Fundamentals of Acoustical Oceanography* (San Diego, CA: Academic Press)

- Millero F J and Li X 1994 Comments on ``On equations for the speed of sound in seawater" [J. Acoust. Soc. Am. [bold 93], 255--275 (1993)] *The Journal of the Acoustical Society of America* **95** 2757-9
- Mohitpour M, Szabo J and Hardeveld T V 2005 *Pipeline Operation & Maintenance* (New York, NY: ASME)
- Muir T G 1974 Nonlinear Parametric Transduction in Underwater Acoustics. In: *1974 Ultrasonics Symposium*, pp 603-12
- Munoz Gutierrez M A, Prospero Sanchez P L and do Vale Neto J V 2005 An eigenpath underwater acoustic communication channel simulation. In: *OCEANS, 2005. Proceedings of MTS/IEEE*, pp 355-62 Vol. 1
- Okunev Y 1997 *Phase and phase-difference modulation in digital communications* (Norwood, MA: Artech House, Inc)
- Otnes R, Jensrud T, Voldhaug J E and Solberg C 2009 A roadmap to ubiquitous underwater acoustic communications and networking. In: *Underwater Acoustic Measurements: Technologies & Results*, (Nafplion, Greece)
- Passerieux J-M Socheleau F-X and Laot C 2010 Shallow Water Acoustic Communications: How far are we from the Channel Capacity? *European Conference on Underwater Acoustics (ECUA) '10*
- Porter M B and Bucker H P 1987 Gaussian beam tracing for computing ocean acoustic fields *The Journal of the Acoustical Society of America* **82** 1349-59
- Porter M B, Hursky P, Siderius M, Badiey M, Caruthers J, Hodgkiss W S, Raghukumar K, Rouseff D, Fox W, de Moustier C, Calder B, Kraft B J, McDonald K, Stein P, Lewis J K and Rajan S 2004 The Kauai Experiment. In: *High Frequency Ocean Acoustics: High Frequency Ocean Acoustics Conference*, (La Jolla, California (USA): AIP) pp 307-21
- Porter T R, Knickmeyer E H and Wade R L 1990 Pipeline Geometry Pigging: Application of Strapdown INS. In: *IEEE PLANS*, (Las Vegas, NV, USA: IEEE)
- Preisig J 2007 Acoustic propagation considerations for underwater acoustic communications network development *SIGMOBILE Mob. Comput. Commun. Rev.* **11** 2-10
- Proakis J G and Salehi M 2008 *Digital Communications 5th Edition* (McGraw-Hill Companies, Inc.)
- Proakis J G, Rice J A, Sozer E M and Stojanovic M 2001 Shallow Water Acoustic Networks. In: *IEEE Communications Magazine*,

- Reimers U 1997 DVB-T: the COFDM-based system for terrestrial television
Electronics & Communications Engineering Journal **9** 28-32
- Rice J, Creber B, Fletcher C, Baxley P, Rogers K, McDonald K, Rees D, Wolf M, Merriam S, Mehio R, Proakis J, Scussel K, Porta D, Baker J, Hardiman J and Green D 2000 Evolution of Seaweb underwater acoustic networking. In: *OCEANS 2000 MTS/IEEE Conference and Exhibition*, pp 2007-17 vol.3
- Rouseff D 2005 Intersymbol interference in underwater acoustic communications using time-reversal signal processing *The Journal of the Acoustical Society of America* **117** 780-8
- Rouseff D, Flynn J A, Ritcey J A and Fox W L J 2004 Acoustic Communication Using Time-Reversal Signal Processing: Spatial and Frequency Diversity. In: *High Frequency Ocean Acoustics: High Frequency Ocean Acoustics Conference*, (La Jolla, California (USA): AIP) pp 83-9
- Salon S, Crise A, P. Picco, Marinis E d and Gasparani O 2003 Sound speed in the Mediterranean Sea: an analysis from a climatological data set *Annales Geophysicae* **21** 833-46
- Scussel K F, Rice J A and Merriam S 1997 A new MFSK acoustic modem for operation in adverse underwater channels. In: *OCEANS '97. MTS/IEEE Conference Proceedings*, pp 247-54 vol.1
- Siderius M, Porter M B, and the KauaiEx Group 2004 Impact of Thermocline Variability on Underwater Acoustic Communications: Results from KauaiEx In: *High Frequency Ocean Acoustics: High Frequency Ocean Acoustics Conference*, (La Jolla, California (USA): AIP) pp 360-65
- Siderius M, Porter M B, Hursky P, McDonald V and the KauaiEx Group 2007 Effects of ocean thermocline variability on noncoherent underwater acoustic communications *The Journal of the Acoustical Society of America* **121** 1895
- Skaropoulos N C, Yagridou H D and Chrissoulidis D P 2003 Interactive resonant scattering by a cluster of air bubbles in water *The Journal of the Acoustical Society of America* **113** 3001-11
- Smith K B, Abrantes A A M and Larraza A 2003 Examination of time-reversal acoustics in shallow water and applications to noncoherent underwater communications *The Journal of the Acoustical Society of America* **113** 3095-110
- Socheleau F-X Laot C and Passerieux J-M 2010 A Maximum Entropy Framework for Statistical Modeling of Underwater Acoustic Communication Channels *IEEE OCEANS '10*

- Socheleau F-X Passerieux J-M and Laot C 2009 Characterisation of time-varying underwater acoustic communication channel with application to channel capacity *Underwater Acoustic Measurements'09*
- Song A, Badiy M, Song H C, Hodgkiss W S, Porter M B and the KauaiEx Group 2008 Impact of ocean variability on coherent underwater acoustic communications during the Kauai experiment (KauaiEx) *The Journal of the Acoustical Society of America* **123** 856-65
- Sozer E M 2000 Underwater acoustic networks *IEEE journal of oceanic engineering* **25** 72
- Sozer E M, Proakis J G, Stojanovic R, Rice J A, Benson A and Hatch M 1999 Direct sequence spread spectrum based modem for under water acoustic communication and channel measurements. In: *OCEANS '99 MTS/IEEE. Riding the Crest into the 21st Century*, pp 228-33 vol.1
- Stoianov I, Nachman L and Madden S 2007 PIPENET: A Wireless Sensor Network for Pipeline Monitoring. In: *Information Processing in Sensor Networks*, (Cambridge, Massachusetts, USA: ACM)
- Stojanovic M 1998 *Wiley Encyclopedia of Electrical and Electronics Engineering*, pp 688-98
- Stojanovic M 2005 Retrofocusing techniques for high rate acoustic communications *The Journal of the Acoustical Society of America* **117** 1173-85
- Stojanovic M 2006 On the relationship between capacity and distance in an underwater acoustic communication channel *Proceedings of the 1st ACM international workshop on Underwater networks* (WUWNet '06)
- Stojanovic M, Catipovic J A and Proakis J G 1993 Adaptive multichannel combining and equalization for underwater acoustic communications *The Journal of the Acoustical Society of America* **94** 1621-31
- Stojanovic M, Catipovic J A and Proakis J G 1994 Phase-coherent digital communications for underwater acoustic channels. In: *Oceanic Engineering, IEEE Journal of*, pp 100-11
- Stojanovic M, Catipovic J A and Proakis J G 1995 Reduced-complexity spatial and temporal processing of underwater acoustic communication signals *The Journal of the Acoustical Society of America* **98** 961-72
- Stojanovic M and Freitag L 2006 Multichannel Detection for Wideband Underwater Acoustic CDMA Communications *IEEE Journal of Oceanic Engineering* **31** 685-95

- Stojanovic M and Preisig J 2009 Underwater Acoustic Communication Channels: Propagation Models and Statistical Characterisation *IEEE Communications Magazine*
- Stojmenovic I 2005 *Handbook of sensor networks: algorithms and architectures* (Hoboken, New Jersey, USA: John Wiley & Sons, Inc)
- Syed A A and Heidemann J 2006 Time Synchronization for High Latency Acoustic Networks.
- Thorp W H 1967 Analytic Description of the Low-Frequency Attenuation Coefficient *The Journal of the Acoustical Society of America* **42** 270
- Tiratsoo J N H 1999 *Pipeline Pigging Technology 2nd Edition* (Houston, TX, USA: Butterworth-Heinemann)
- Urick R J 1983 *Principles of underwater sound* (Los Altos, California: Peninsula Publishing)
- van Gijzen M B and van Walree P A 2000 Shallow-water acoustic communication with high bit rate BPSK signals. In: *OCEANS 2000 MTS/IEEE Conference and Exhibition*, pp 1621-4 vol.3
- van Nee R and Prasad, R. 2000 *OFDM for wireless multimedia communications* Artech House universal personal communications series. (Boston: Artech House)
- van Walree P A and Leus G 2009 Robust Underwater Telemetry With Adaptive Turbo Multiband Equalization *Oceanic Engineering, IEEE Journal of* **34** 645-55
- Vasilescu I, Kotay K, Rus D, Dunbabin M and Corke P 2005 Data Collection, Storage, and Retrieval with an Underwater Sensor Network. In: *SenSys '05*, (San Diego, California: ACM)
- Versluis M, Schmitz B, Heydt A v d and Lohse D 2000 How snapping shrimp snap: through cavitating bubbles *Science* **289** 2114-7
- Viala C, Noel C and Lapierre G 2002 Simulation of acoustic signal in time-varying multipath underwater channel *Underwater Acoustics for Deep Sea Applications*. More info regarding RAYSON: <http://semantic-ts.fr/>
- Voudouri-Maniati E 2002 Multiuser robust CDMA detection for underwater acoustic communication channels. In: *OCEANS '02 MTS/IEEE*, pp 612-8 vol.1

- Waite A M, Thompson P A, Pesant S, Feng M, Beckley L E, Domingues C M, Gaughan D, Hanson C E, Holl C M, Koslow T, Meuleners M, Montoya J P, Moore T, Muhling B A, Paterson H, Rennie S, Strzelecki J and Twomey L The Leeuwin Current and its eddies: An introductory overview *Deep Sea Research Part II: Topical Studies in Oceanography* **54** 789-96
- Wenz G M 1962 Acoustic Ambient Noise in the Ocean: Spectra and Sources *The Journal of the Acoustical Society of America* **34** 1936-56
- Whiteway, T.G., 2009. Australian Bathymetry and Topography Grid, June 2009. Geoscience Australia Record 2009/21. 46pp.
- Wills J, Ye W and Heidemann J 2006 Low-Power Acoustic Modem for Dense Underwater Sensor Networks. In: *WUWNet '06*, (Los Angeles, California, USA: ACM)
- Wong G S K and Zhu S-m 1995 Speed of sound in seawater as a function of salinity, temperature, and pressure *The Journal of the Acoustical Society of America* **97** 1732-6
- Wright P J 2000 Optical fiber's gigabit bandwidth, 200km range attractive for subsea work. In: *Offshore Magazine*,
- Yang T C and Yang W-B 2008 Performance analysis of direct-sequence spread-spectrum underwater acoustic communications with low signal-to-noise-ratio input signals *The Journal of the Acoustical Society of America* **123** 842-55
- Yang W-B and Yang T C 2006 M-ary frequency shift keying communications over an underwater acoustic channel: Performance comparison of data with models *The Journal of the Acoustical Society of America* **120** 2694-701
- Yoon S W, Crum L A, Prosperetti A and Lu N Q 1991 An investigation of the collective oscillations of a bubble cloud *The Journal of the Acoustical Society of America* **89** 700-6
- Yu X 2000 Wireline Quality Underwater Wireless Communication Using High Speed Acoustic Modems. In: *Oceans, 2000*, (Providence, RI, USA: IEEE)
- Zheng M, Coates R F W, Wang L and Stoner R 1996 Underwater acoustic communication utilising parametric transduction with M-ary DPSK modulation. In: *OCEANS '96. MTS/IEEE. 'Prospects for the 21st Century'. Conference Proceedings*, p 7 suppl.
- Zheng M, Wang L, Stoner R and Coates R F W 1999 Underwater digital communication utilising parametric sonar with M-ary DPSK modulation *Radar, Sonar and Navigation, IEE Proceedings -* **146** 213-8

- Zhou G and Shim T 2008 Simulation Analysis of High Speed Underwater Acoustic Communication Based on a Statistical Channel Model. In: *Image and Signal Processing, 2008. CISP '08. Congress on*, pp 512-7
- Zhou G and Shim T 2009 Estimation of high data rate underwater acoustic communication channel capacity *Underwater Technology: The International Journal of the Society for Underwater* **28** 67
- Ziemer R E 2007 *Fundamentals of Spread Spectrum Modulation* (San Rafael, California: Morgan & Claypool Publishers)
- Zimmermann H 1980 OSI Reference Model--The ISO Model of Architecture for Open Systems Interconnection *Communications, IEEE Transactions on* **28** 425-32

Every reasonable effort has been made to acknowledge the owners of copyright material. I would be pleased to hear from any copyright owner who has been omitted or incorrectly acknowledged.

Appendix A

Background Information and Theory

A.1 *Subsea Pipelines*

A.1.1 **Distribution and Hazards**

With the first sub-sea pipelines constructed as early as 1897, offshore oil reserves are being continuously explored to meet the high demand for fuel sources (Guo *et al.*, 2005). Pipelines have since become the norm in efficiently transporting resources from offshore wells to shore-based processing plants. The materials transported through these pipelines include but are not limited to various forms of oil, natural gas and water.

In the planning phase for the establishment of subsea pipelines several considerations need to be addressed before the project is realised. Design of a system to withstand the expected internal pressures is dependant on the commodity being transported and is relatively straightforward. However, exposure to the elements and external stresses pose the most risk to the structural integrity of a pipeline. This is apparent when considering underwater pipelines which undergo additional stress during lowering, given the spatial restrictions of the vessels used for their deployment. The susceptibility to buckling of a pipeline due to external forces is dependant on several variables. These include the diameter, thickness and materials used to support the structure such as the concrete coating which adds to on-bottom stability (Antaki, 2003).

When considering the long-term reliability of a subsea pipeline there are several oceanographic processes that can affect its structural integrity. A primary concern pertains to the ocean currents created by dynamic weather conditions. The stability of a pipeline during moments of extreme weather conditions is paramount to safe operation. For example, ocean currents have the capability to disturb the seabed surrounding an underwater pipeline, creating free-spans and other higher-risk

situations (Figure A.1). These risks can also occur when the pipeline itself is disturbed by strong ocean currents. Much work has been documented on the impact of various external forces on a pipeline and its surroundings. Additionally, methods to maximise the on-bottom stability have been well established (Bai, 2001).

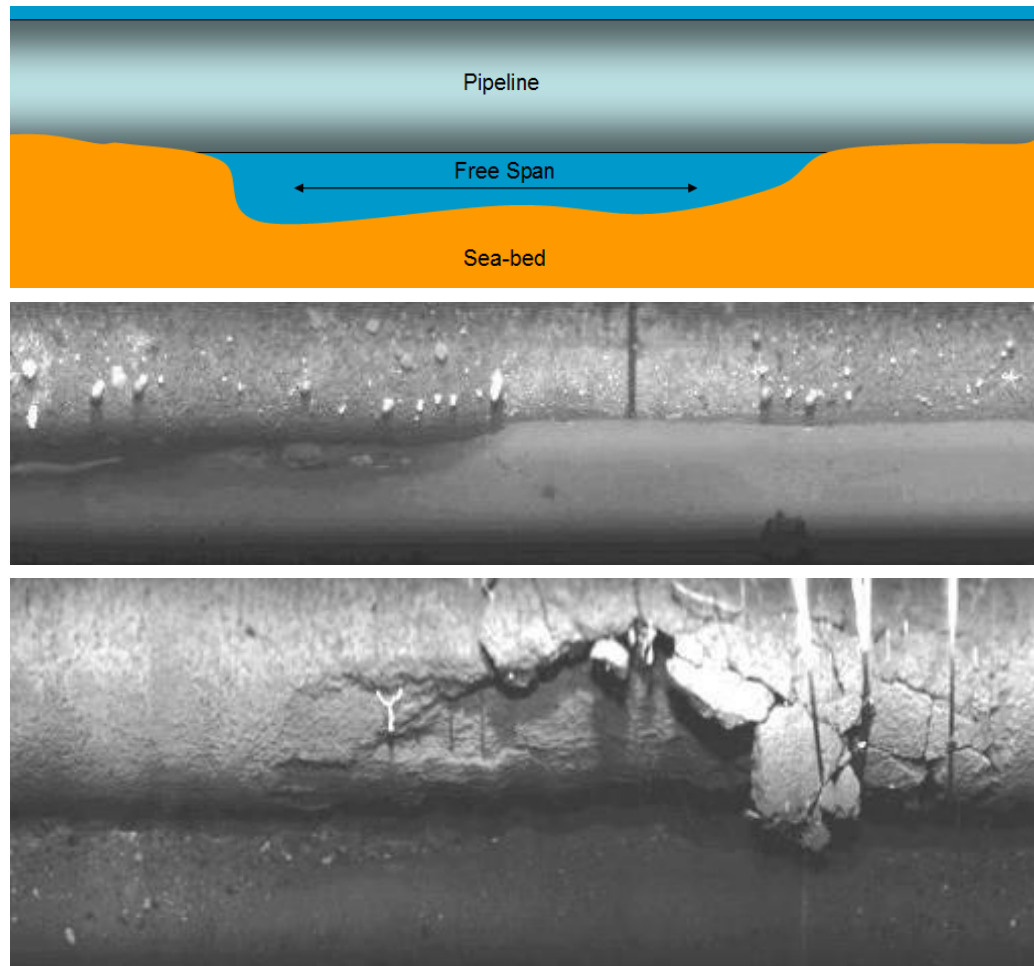


Figure A.1. Illustration of a typical free-span (top). Image of a free-span, captured by a ROV mounted inspection system (middle). An image depicting a cracked concrete coating (bottom). (Images were acquired by the Xplisit pipeline inspection system. Courtesy Norsk Elektro Optikk AS, Norway)

Unfortunately, pipelines pose a huge environmental and financial risk should they ever fail during their lifetime. Failures are generally due to either ongoing deterioration of the pipeline and its surrounds, or more direct failures stemming from events such as shipping collisions and biological interaction. Both types of incidents create considerable damage to the environment regardless of the pipeline material, depth or operational status. Additionally, one large study highlighted that whilst 49%

of failures were due to corrosion, they only caused 2% of the overall pollution. In contrast, shipping mishaps constituted 14% of failures but 90% of the overall pollution (Antaki, 2003). Further information from this study can be found in a report by the Committee on the Safety of Marine Pipelines (1994). These statistics place high importance on the maintenance of pipelines to reduce the financial costs of failures due to corrosion. Additionally, it demonstrates the importance of applying the necessary controls to ensure collisions with maritime vessels are avoided.

A.1.2 Monitoring of Pipelines and Repair Techniques

A common inline method of pipeline inspection is the deployment of a device known as a Pipeline Inspection Gauge (pig), an example of which is shown in Figure A.2. The pig was originally used for cleaning the build up of products such as wax within pipelines (Tiratsoo, 1999) and is propelled through pipes using the internal fluid pressure. Technology development for pigs has allowed the cleaning tool to be expanded into an intricate data acquisition system. In one such design, a pigging system is deployed with a measurement unit allowing the device to run autonomously for a week or longer. When in operation, advanced pigs can also collect continuous information regarding position, orientation and curvature of the pipeline (Porter *et al.*, 1990).



Figure A.2. Demonstration piece of the Trans Alaskan Oil Pipeline showing the integration of a pipeline inspection gauge (pig). (Photo courtesy of Harvey Barrison, 2007)

Sensors within a pigging unit allow for the detection of dents and leaks to aid in the forecast of possible failures. One such example of an electronic unit for use in petroleum pipelines is demonstrated by Dutra *et al.* (2002). Integrated systems are capable of locating potential leaks and in some cases making minor repairs. An example of this is a system developed to ensure the delivery of clean drinking water by Choi *et al.* (2006). This work demonstrates a semi-automatic pipeline inspection robot capable of operating within household water pipes with a diameter of 13mm.

Whilst the pig provides an effective method for internal pipeline maintenance and fault detection, the limitations of the instrument include the inability to effectively deliver data to the user in real-time. Whilst some systems employ interface cables to allow immediate response from the inspection device, the pipeline generally needs to be shut down and/or put in restricted operation for the inspection to take place. Additionally, internal examination of a pipeline inspects only a portion of the overall structure so an external examination of a pipeline is generally needed. External examination provides more detailed information on the structural integrity of the pipeline, particularly for those of large diameter. For submerged pipelines the difficulty in accessing the exterior of the structure poses limitations in external inspection. Furthermore, repairs become much more complicated than those for on-shore pipelines (see Mohitpour *et al.* (2005) for land-based methods) and pipeline retrieval may be necessary. This places importance on the consistent and reliable monitoring of the pipeline to minimise any risks.

For underwater pipelines the dynamic ocean environment yields a necessity in monitoring environmental conditions such as seismic activity, wind and water currents. This allows for the swift detection and subsequent reaction to hazards such as free spans due to seabed scouring. In addition to pigging, a complimentary approach to subsea pipeline monitoring and control is the utilisation of in-line and external gauges and sensors to continuously monitor conditions (Kennedy, 1984). The challenge lies in the method to transport these data to monitoring stations in real-time for submerged pipelines. External wireless pipeline sensor networks are often used for land-based monitoring and control systems with the development of networks such as PipeNet (Stoianov *et al.*, 2007). These networks are designed to

detect and locate leaks within large diameter water pipelines. In PipeNet, a sensor network is integrated using a mobile phone (GPRS) modem link with a number of sensor nodes delivering information to a base station in real-time.

An application of radio frequency (RF) communication techniques directly to a subsea environment is inappropriate due to the partial conductivity of seawater significantly attenuating radio waves. The amount of energy required to transmit any more than a few centimetres underwater renders RF data transfer unrealistic for underwater links (Cheng, 1989). Examples of underwater RF transfer include one-way Extremely Low Frequency (ELF) links with submarines, requiring large amounts of power and infrastructure to operate (Barr *et al.* 2000).

For the same reasons relating to attenuation of electromagnetic waves in general, communication using optical wavelengths such as infra-red transfer in the ocean is also severely limited in transmission range. This can also be dependant on the environment with the varying amounts of optical scatterers including suspended sediment in the water column having a significant effect. Optical transmission has been shown to be useful for short-range communication. Vasilescu *et al.* (2005) present an effective optical link for recovery of sensor data using an acoustically guided Autonomous Underwater Vehicle (AUV). This allows high-speed optical and acoustic communication to be integrated with an underwater sensor network. The results demonstrate a co-operative approach to data muling using mobile nodes.

Consequently, most underwater communication over substantial distances is generally restricted to two main categories: umbilical cables carrying electrical conductors or fibre optics, or acoustic transmission. Umbilicals are widely used as a reliable and fast method of data communication. In particular, fibre optic technology has increased in popularity for offshore platforms (Wright, 2000). As with all underwater equipment, however, the costs associated with laying, maintaining and repairing submarine cables can become excessive, particularly for deeper deployments. Utilisation of Remotely Operated Vehicle (ROV) technology has become a common method of locating and repairing problems for deep underwater cabling (Bannon, 1998).

Underwater acoustic communication is becoming more widely used for some off-shore applications with the deployment of small-packaged acoustic modems being used in place of umbilicals. In certain cases it has been shown to produce results comparable to wired systems, particularly for vertical communication (Yu, 2000). As the deployment of a network of acoustic modems could provide a simpler method of data retrieval for pipeline systems, the investigation into their use on a pipeline is necessary.

The current limitations of acoustic technology include both data rate restrictions and reliability problems. It is therefore unlikely that an acoustic data transmission system would be used as the primary method of telemetry in crucial underwater systems, at least for now. However, an acoustic backup link in case of an umbilical failure is paramount for ensuring safe and reliable communication infrastructure in the unforgiving subsea environment. Furthermore, methods to maintain and repair cables including AUV and ROV technology can be applied to facilitate any maintenance or repair of underwater devices in a similar manner. The progression of these acoustic telemetry methods is an important factor in ensuring adequate evolution of subsea pipeline maintenance techniques.

A.2 *Underwater Acoustic Propagation*

Underwater acoustic communication can be considered one of the most technically and computationally challenging methods of telemetry. The major difficulty in developing efficient and reliable acoustic telemetry techniques is the inability to satisfactorily predict the underwater channel characteristics. The nature of underwater acoustic propagation is extremely complex with several parameters dictating the performance of an acoustic channel. Preisig (2007) provides an overview of the applicable limitations for underwater acoustic communication. This section provides an overview of the underwater acoustic propagation characteristics that pertain to acoustic communication. The dictating parameters for these characteristics can generally be placed into two categories: static and time-varying.

Static parameters include variables such as range, depth, bathymetry, seabed type and bottom roughness. These considerations are related to the boundaries of the water column as a waveguide and can vary markedly from one location to another. In addition, some of the environmental variables (seabed type, roughness, etc) can be unique to a particular location. For this reason, the performance of underwater communication varies significantly from one location to the next for reasons beyond a simple change in range and/or depth.

Such parameters as water temperature, salinity, sea surface characteristics and atmospheric conditions are time-varying. For underwater acoustic propagation the unpredictability of these parameters adds complexity and modifies the channel characteristics. Consequently, underwater acoustic communication methods need to be able to adapt to these changes as they occur. Whilst some can be seasonal variations, many changes can happen much more frequently and need real-time correction.

A.2.1 Signal Power and Signal to Noise Ratio

The output signal power level of a transmitter is fundamentally limited by the cavitation process. The cavitation limit represents the signal power level where pressure fluctuations are high enough to cause vaporisation at the face of the transducer, inhibiting its function (Lurton, 2010). Typically, however, power output levels are limited by other factors, such as power availability and potential damage to equipment or the environment. A primary requirement of effective and reliable data communication is obtaining a suitable signal to noise ratio (SNR) for reception at a distance from the transmitter. Being a direct ratio of the received signal level and noise level, the SNR can be described in the logarithmic scale by the following sonar equation, valid for an omnidirectional receiver:

$$SNR(dB) = RL - NL \quad \text{Equation A.1}$$

where RL is the received signal level in decibels (dB re 1 μ Pa) and NL is the noise level present in the receiver bandwidth in dB re 1 μ Pa.

Given the propagation parameters the transmission of a signal also exhibits an amount of attenuation. This is characterised by the transmission loss of an underwater channel:

$$TL(dB) = RL - SL \quad \text{Equation A.2}$$

where TL is the transmission loss, RL is the received signal level and SL is the source level of the transmitter, measured at 1 m from the emitter, in dB re 1 μ Pa.

Substituting Equation A.2 into Equation A.1 yields the sonar equation describing the SNR in terms of the transmission loss exhibited over the acoustic channel and the noise levels at the receiver.

$$SNR(dB) = SL - TL - NL$$

Equation A.3

It is therefore important to understand the transmission loss (attenuation) and noise characteristics of an underwater environment to better predict the received power and subsequent SNR.

A.2.2 Spreading Loss

Signal energy spreading is a key component of attenuation that is exhibited in most wireless communication systems. When considering an output of an omnidirectional emitter, the intensity levels are shown to exhibit spherical spreading. This is consistent with the radiation of other forms of energy including light. The transmission loss due to spherical spreading is described by Jensen *et al.* (2000):

$$TL(dB) = 20 \log r$$

Equation A.4

where r is the range from the emitter in metres

For long range horizontal communication the water column is treated as a waveguide bounded in the vertical direction. Here it is more appropriate to approximate the energy spreading with a cylindrical spreading law as sound waves reflected from the seabed and sea surface also propagate within the waveguide:

$$TL(dB) = 10 \log r$$

Equation A.5

where r is the range in metres, assuming the water depth $D \ll r$

The precise rate of attenuation due to signal spreading becomes quite complicated for underwater acoustic communication with the reflectivity of the boundaries poorly predictable and for sea surface reflections, time varying. The predictability of

transmission loss due to spreading is therefore limited by the occurrence and type of boundaries and is described in Section A.2.5.

A.2.3 Absorption Loss

An important characteristic of underwater acoustics is the frequency dependence of absorption. There are several equations relating sound absorption in sea water to variations in temperature, pressure, salinity, pH and frequency. A fundamental look at absorption and several examples can be found in literature by Medwin and Clay (1998) and Etter (2003). This literature highlights the basic theory where the absorption due to the transfer of kinetic energy is related to the relaxation frequency of the fluid constituents. Further analysis of absorption and comparison with experimental results is performed by Fisher and Simmons (1977) from which Figure A.3 is taken. This includes a comparison with the Thorp equation (Thorp, 1967), a simplified equation to suit most applications which is extended for a wider frequency range in seawater.

$$\alpha\left(\frac{dB}{km}\right) = \frac{0.11f^2}{1+f^2} + \frac{44f^2}{4100+f^2} + 2.75 \times 10^{-4} f^2 + 0.003 \quad \text{Equation A.6}$$

where α is the absorption in dB per km and f is the frequency of the acoustic wave in kHz.

The last two terms in Equation A.6 were added later to deal with very high and very low frequencies. The equation is most valid for a temperature of 4 °C and depth of approximately 1000 m (Urick, 1983). When considering carrier frequencies for underwater acoustic communication protocols, frequency dependant absorption restricts the power efficiency of higher frequency signals. Unfortunately, modulation schemes favour higher frequencies to provide higher bandwidths.

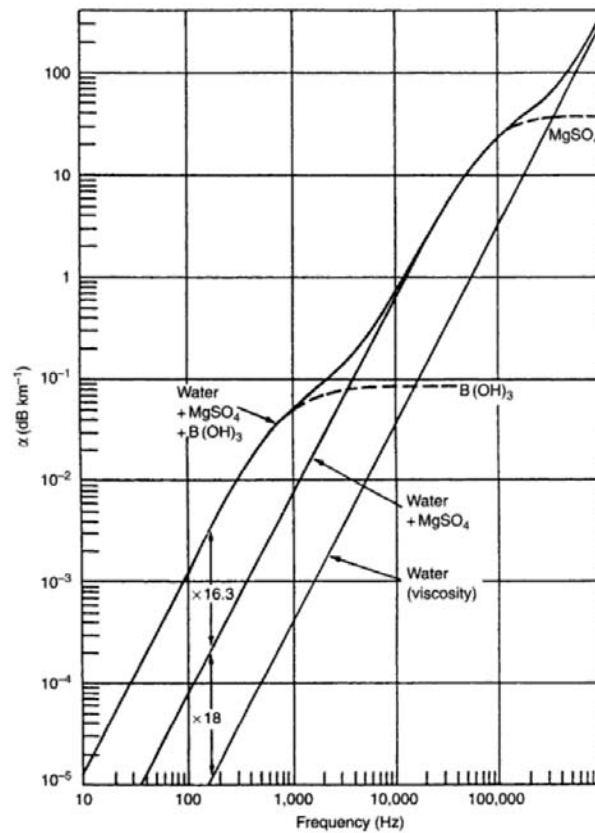


Figure A.3. Absorption coefficient of seawater as calculated in laboratory measurements. The contribution of different constituents (boric acid, magnesium sulphate and water) is shown. (Fisher and Simmons, 1977, adapted by Etter, 2003)

By combining Equation A.4 and Equation A.6, the contributions of spreading and absorption to the total transmission loss produce an attenuation estimate. Figure A.4 provides a prediction of the transmission loss due to spherical spreading and absorption for different frequencies. This demonstrates the effect of carrier frequency choice on long range communication. As an example, consider a simple modem system with a source level of 180 dB re 1 μ Pa @ 1 m and an environmental noise level of 80 dB re 1 μ Pa within the receiver bandwidth (see later in this section for reasoning). Using Equation A.3, a total attenuation level above 100 dB results in negative SNR (not including any processing gain). In this case, efficient telemetry over ranges above 5 km is shown to be limited to frequencies below approximately 10 kHz. However, for short range communication, the contribution of absorption is similar to that of spreading for higher frequencies. The negligible contribution to attenuation by absorption at high frequencies over short ranges provides for higher bandwidth signals with little loss in power efficiency.

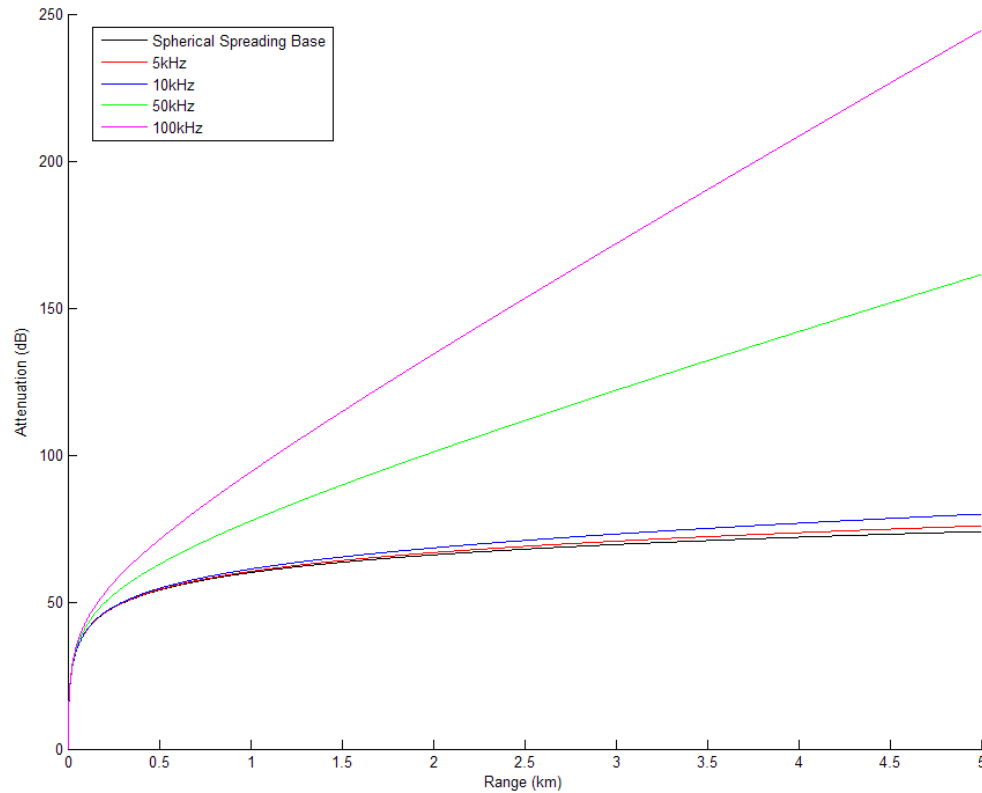


Figure A.4. Attenuation loss due to the combination of spherical spreading and absorption for different frequencies, calculated by combining Equation A.4 and Equation A.6

Whilst there is an option to counteract inefficient transmission of higher frequencies with a higher transmit power (source level), it would undoubtedly become unethical in terms of the overall impact on marine life and the environment. Additionally, limitations on the available power and transducer efficiency prevent the use of high power levels. A compromise between data rate and transmission range is typically adopted. For this reason, long-range acoustic communications generally utilise frequency bands of around 6-12 kHz. Systems using a higher bandwidth and data rate typically operate over a much shorter range and even so, tend to stay within frequencies below 100 kHz. Section A.3.2 provides a detailed overview of the frequency bands currently being utilised for acoustic communication.

A.2.4 Acoustic Noise

Acoustic receiving devices including modems will exhibit an amount of unwanted noise which degrades the usefulness of a received signal. Assuming the recording electronics are suitably designed and the partial conductivity of seawater provides enough electromagnetic protection from outside electromagnetic sources, acoustic noise is the primary concern.

To maximise the efficiency of an underwater communication system, knowledge of the sources of ambient noise within its operating environment is crucial. Ocean noise varies depending on factors including depth, weather conditions and biological occupancy. Furthermore, shipping noise in an environment also needs to be studied to assess its impact in terms of noise generation. Much work has gone into characterising underwater noise all over the world, however, this thesis considers primarily the noise characterisation of Australian waters as outlined by Cato and McCauley (2002).

Ocean ambient noise can be divided into several different components. In a publication by Wenz (1962), ocean noise is presented as a composite of several contributors over a diverse frequency range. In this particular study three components are presented, each having a separate but overlapping spectral contribution over the entire frequency range. These are turbulent-pressure fluctuations present in the lower frequency bands, then to ocean traffic and surface noise from bubbles in the higher frequency spectrum. The Wenz curves are widely used for noise prediction models and Australian composites have been developed. A notable composite developed by Cato (2009) shows the latest in noise prediction curves from measurements off the Australian coast (see Figure A.5).

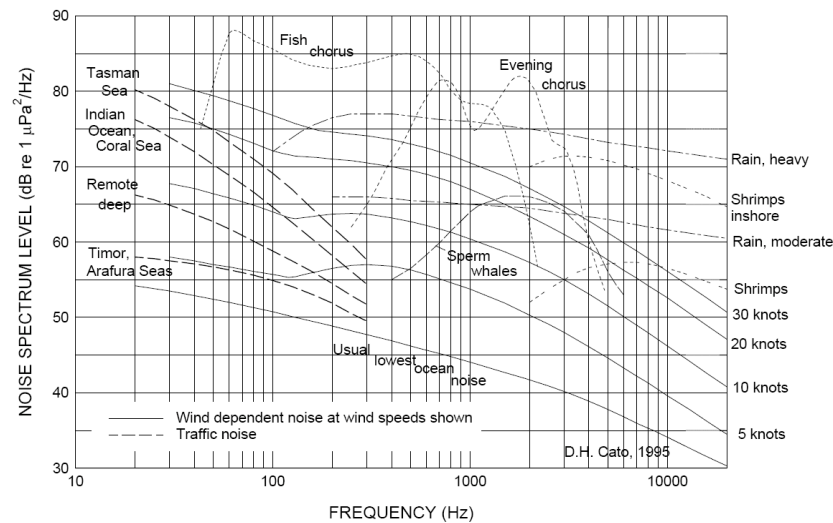


Figure A.5. Latest ambient noise prediction curves in the Australian region showing wind dependant noise sources as well as typical marine and traffic contributions. (Cato, 2009)

For acoustic communication it is reasonable to assume the carrier frequency lies between 1 kHz and 100 kHz. In this frequency range the majority of noise is generated by surface fluctuations due to wind and waves as well as biological sources such as snapping shrimps. Further information on these and other contributions can be found in Kerman (1988). Wind over the surface of an ocean creates other sources of ambient noise in the ocean as well as generating noise itself. These include breaking waves which result in sub-surface bubbles which oscillate to produce noise. Bubbles present several additional complications for acoustics as the noise characteristics vary with their size and density distributions in the surface layer. Their occurrence is also somewhat unpredictable temporally. These implications of bubbles have been shown by simple laboratory experimentations such as those by Yoon *et al.* (1991). In addition to noise contributions, Section A.2.5 discusses how bubbles affect the propagation of acoustic energy by scattering.

Many biological noise sources in the ocean emit sound at frequencies below those used for acoustic communication. While most are relatively low power and benign to acoustic communication, highly impulsive noises have the potential to greatly affect telemetry in some situations. In warm, shallow waters in particular noise produced by snapping shrimp can inhibit performance of telemetry with frequent sharp “snaps” (Versluis *et al.*, 2000). These highly impulsive sounds have a broadband spectrum

which can interfere over a wide frequency range. In addition, the amplitude characteristics of noise from snapping shrimp have been found by Legg (2009) to exhibit non-Gaussian statistics. This adds difficulty in predicting the impact of snapping shrimp on telemetry using simulations as discussed in Chapter 3.3.

A.2.5 Scattering and Boundary Reflections

The boundaries of an underwater waveguide affect the transmission of the signal in two significant ways: transmission loss at each reflection and distortion of the signal due to the effects of multipath propagation. The first involves the interaction of the signal at each boundary interface along the propagation path. The scattering characteristics of the boundary play a significant role when considering the transmission loss of a channel. This includes sea surface reflections which result in a phase inversion in the reflected wave. Additionally, the difference in sound speed and density between two fluid media (such as air or certain seabed substrates) yields an acoustic impedance mismatch with the impedance, Z , given by Jensen *et al.* (2000):

$$Z = \frac{\rho \cdot c}{\sin \theta} \quad \text{Equation A.7}$$

where ρ and c are the respective density and compressional wave speed of the medium and θ is the grazing angle at which the wave is incident.

When an acoustic wave is incident on an interface between media with different acoustic impedances, sound energy is both reflected from and transmitted through the boundary. The relative amounts of energy are dependant on the impedance mismatch between the primary and interface medium, denoted below with subscripts 1 and 2 respectively:

$$R = \frac{Z_2 - Z_1}{Z_2 + Z_1} = \frac{\rho_2 c_2 \sin \theta_2 - \rho_1 c_1 \sin \theta_1}{\rho_2 c_2 \sin \theta_2 + \rho_1 c_1 \sin \theta_1} \quad \text{Equation A.8}$$

The sea surface interface can be considered perfectly reflecting with little acoustic energy transmitted into the air as both the density and speed of sound are markedly different. Particularly for ocean waters it would, however, be unrealistic to consider the sea surface as a perfectly flat reflector due to sea surface waves. To consider reflections from a rough surface, Brekhovskikh and Lysanov (1982) has shown the coherent (mean) reflectivity of the sea surface and seabed \check{R} to be determined as a function of the root mean square (RMS) of the wave height (Jensen *et al.*, 2000):

$$\check{R}(\theta) = R(\theta)e^{-0.5\Gamma^2} \quad \text{Equation A.9}$$

where \check{R} is the coherent reflection coefficient depending on the reflection coefficient R from a flat surface. Γ is known as the Rayleigh roughness parameter, given by:

$$\Gamma = 2k\sigma \sin \theta \quad \text{Equation A.10}$$

where k is the wave number, σ is the RMS roughness height and θ is the grazing angle at which the wave is incident.

The validity of Equation A.9 is limited to cases where $\Gamma < 2$ and depends on long correlation lengths and assumes normally distributed roughness heights. In the case of sea surface reflections, the coherent reflection coefficient $R(\theta)$ for a flat surface is presumed to be -1, simplifying the equation further.

The predictions of sea surface reflections can be further hindered by occurrences of objects generally found close to the boundary such as air bubbles. As well as producing noise themselves (see Section A.2.4), bubbles scatter and absorb sound. This is related to the individual resonant frequency of each bubble which is dependant on its size and depth. Furthermore, it has been shown that large plumes of bubbles can react with one other, changing this resonance characteristic (Skaropoulos *et al.*, 2003). Additionally, the presence of air bubbles also changes the compressibility of the water, resulting in a change in sound speed. When considering propagation in environments where air bubbles are widespread, it would be expected

an acoustic transmission would undergo distortion in both the spatial and frequency domain. As well as modifying the scattering characteristics of the interacting region, acoustic energy would undergo frequency dependant absorption, reflective of the size and distribution of the bubble mass.

The consideration of reflections from the seabed is more complicated than sea surface scattering. Some materials such as sand and silt can be considered fluid given the negligible transmission of shear waves. Other types such as basalt or limestone are considered solids but are generally covered by various layers of fluid-like unconsolidated sediment. For flat fluid-fluid interfaces the treatment of reflections is handled with Equation A.8. However, acoustic waves incident on a layered seabed result in a significant proportion of transmitted energy penetrating into the next layer which is then incident on another. The overall reflection eventually becomes the sum of several reflections from the inner layers as well as the initial reflection from the water-seabed interface.

When considering the fluid-solid interface the mechanisms involved in shear wave propagation dramatically change the reflectivity. This is particularly evident at shallow grazing angles. For fluid-fluid boundaries, total internal reflection occurs below a critical angle where there is significant reflection of the incident energy. When including the shear wave propagation characteristics of a solid medium, energy incident below the critical angle is instead typically propagated into the seabed as a shear wave, lowering the reflection coefficient.

The number of boundary reflections is a primary concern when developing telemetry techniques due to complications resulting from multipath propagation. This occurs when a source transmission emitted from a non-directional transducer propagates along several separate acoustic paths. Waves propagated along each of these paths interact with boundaries separately and reach the receiver at different times or sometimes not at all. The severity of multipath effects depends largely on the environment in which a particular system is deployed. For example, for deep water vertical propagation echoes due to seabed and sea surface reflections are the only

dominant source of reverberation in an underwater channel. As discussed in Section A.2.6, the sound velocity varies significantly more over depth than over the same horizontal distance. This results in near horizontal rays undergoing much more bending due to refraction than near vertical rays, making vertical propagation more predictable and intuitive.

In the shallow water environment the travel time difference along separate paths decreases significantly and it becomes difficult to distinguish them from the direct path. The reception of two or more signals of different arrival times, each containing the same bit stream, gives rise to intersymbol interference (ISI). The impact of intersymbol interference varies significantly with location. This phenomenon is a major contributor to the problems experienced in developing reliable protocols for subsea acoustic communication. These effects are further complicated when transmitting over a large horizontal distance where arrival times are much less predictable due to the variations of bathymetry and other environmental parameters. Here, advanced signal processing should be used and signal overlap must be accounted for to achieve efficient operation.

When considering a much shorter time scale, two or more signals arriving at a receiver with little difference in travel time exhibit constructive and destructive interference. A consequence of destructive interference is frequency dependant cancelling of the signal known as selective fading. Due to the often slight temporal variations in the path lengths and signal travel times involved the signal power observed at a receiver becomes time-dependant. These fluctuations give rise to many difficulties for an acoustic communication system and protocol measures such as frequency diversity need to be implemented. In most cases underwater acoustic modems use a form of channel equalisation to compensate for selective fading.

Whilst the problems of multipath propagation are well understood a trivial solution does not exist, particularly with subsea telemetry. Section 2.2 discusses several approaches to channel equalisation to combat the effects of intersymbol interference.

A.2.6 Refraction of Acoustic Paths

A major contributor to the complexity in acoustic communications is the varying speed of sound within the medium. The speed of sound has been demonstrated to vary with temperature, salinity and pressure with several empirical measurements being made over the last several decades. Two notable equations for seawater sound velocity have been developed using laboratory experimentation and are discussed rigorously in literature. These are the Del Grosso Equation (Del Grosso, 1974) and Chen and Millero Equation (Chen and Millero, 1977). The Chen and Millero equation is widely adopted as a more accurate formula. However, some studies have shown the Del Grosso equation to provide a better correlation with experimental results (Dushaw *et al.*, 1993). Subsequent variations of both equations have also been established to provide a more accurate calculation in some areas (Millero and Li, 1994). Additionally, both equations have been adjusted with the introduction of the international temperature scale in 1990 (Wong and Zhu, 1995).

Whilst these rigorously studied sound speed equations are widely accepted in calculating the speed of sound in seawater, they can become extensively detailed. Simpler equations do exist and are regularly adopted. These include the Mackenzie equation (Mackenzie, 1981), Coppens equation (Coppens, 1981) and an even simpler formula developed by Herman Medwin (Medwin, 1975). Each of these equations calculates the speed of sound in water based on the temperature, salinity and depth. Medwin's equation is:

$$c = 1449.2 + 4.6T - 0.055T^2 + (1.34 - 0.010T)(S - 35) + 0.016D \quad \text{Equation A.11}$$

Here, c is the speed of sound in metres per second, T is the temperature in degrees Celsius, S is the salinity in Practical Salinity Units (psu) and D is the depth in metres.

The more computationally efficient equations have obvious limitations but are valid for typical environments. Equation A.11 depicts the strong dependence of the speed of sound on the temperature of the medium as well as on the depth. This is an

important consideration for acoustic propagation as the temperature of oceanic water varies significantly spatially, particularly with depth. With the depth expected to be well known when predicting the propagation of sound within a water column, temperature and salinity variations are the environmental factors typically measured before making estimates of the sound speed profile (SSP). A consolidation of work discussing the SSP (also referred to as the velocity profile) of the ocean can be found by Urlick (1983).

As temperature, and consequentially sound speed, varies much more rapidly with depth than with range, knowledge of the vertical SSP is generally paramount to determining the nature of signal propagation. This is particularly important for horizontal propagation. The wavelengths considered for acoustic communication are generally much less than the depth of the water column and sound waves can alternatively be considered as a group of rays which interact with layers of differing sound speeds and channel boundaries. The refraction of acoustic rays can also be related to optics which dictates the refraction of a propagation path towards the area of least velocity. More on ray theory is found in Section A.2.8.

The SSP can be measured using probes cast to the seabed recording temperature (and other parameters such as salinity if possible) over time and/or depth. A common example is the conductivity, temperature and depth (CTD) probe which is used in the experiments presented here. Another example used by large vessels is the expendable bathythermograph (XBT) which involves a disposable temperature probe that transmits data back to the mother ship during the cast before disconnecting itself.

The SSP of a water column yields a horizontal acoustic channel which can be classified from the resulting refraction characteristics. The profile can be characterised by several distinct areas of depth in the column. This includes the mixed layer located near the surface. This surface layer is the most susceptible to fluctuations of surface air temperature and wind. The amount of mixture depends on the atmospheric conditions. However, in warm, calm environments the mixed layer is thin and the temperature of the water below it tends to decrease with depth. This

area is known as the thermocline and is generally prevalent in Australian waters where the ambient air temperatures do not reach Arctic lows for prolonged periods. The upper part of the thermocline can vary due to fluctuations at the surface but typically only shows seasonal variations. In deep waters the pressure or depth component dominates the result of Equation A.11 in a deep isothermal layer. This is characterised by an increase in sound speed with depth and typically begins at depths of approximately 1000 m but can vary with location. A general example of a deep-sea sound speed profile with the layers of interest labelled is shown in Figure A.6.

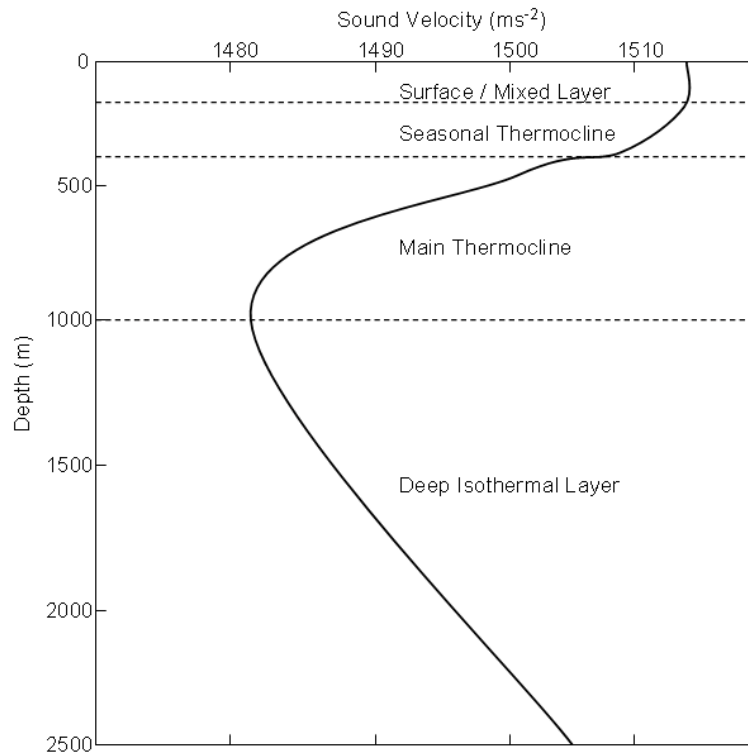


Figure A.6. A typical sound speed profile highlighting the various depth-dependent regions that can occur in the ocean. Adapted from Urlick (1983).

In deep waters the minimum sound velocity is typically located at the transition between the thermocline and deep isothermal layer. This area is important in characterising the propagation of acoustic energy over long range. The adjacent water layers act as a lens, bending propagation paths back toward the depth of lowest sound velocity. This particular depth is known as the axis of the deep sound channel or Sound Fixing and Ranging (SOFAR) channel. Figure A.7 depicts the SOFAR channel with the sound speed minimum occurring at 1000 m.

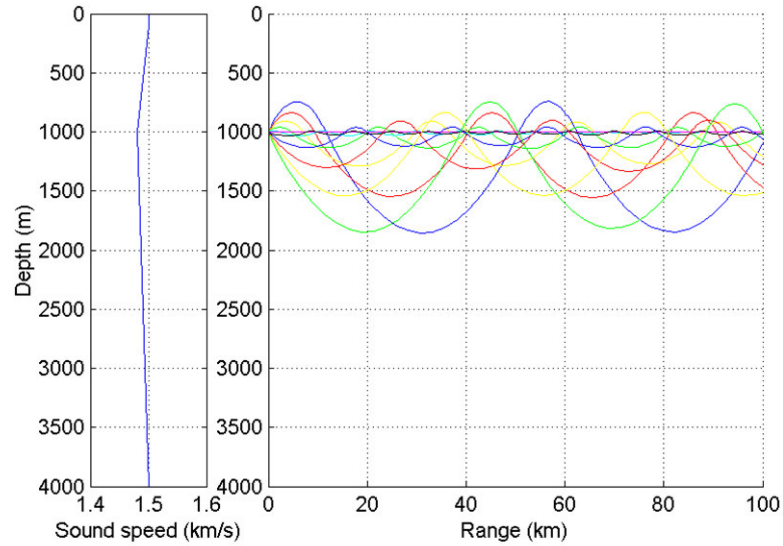


Figure A.7. Illustrative ray trace of acoustic energy propagating through the SOFAR deep underwater sound channel. (Duncan, 2006)

A mixed layer that results in any increase of sound speed with depth promotes propagation towards the surface. Here, rays are refracted upwards and undergo a series of surface reflections. This is known as surface duct propagation and can co-exist in the same water column with the deep sound channel. A moderately deep water scenario shown in Figure A.8 highlights surface duct propagation, where the transmitted energy is bound by the upwardly refracting portion ($D < 100$ m) of the SSP.

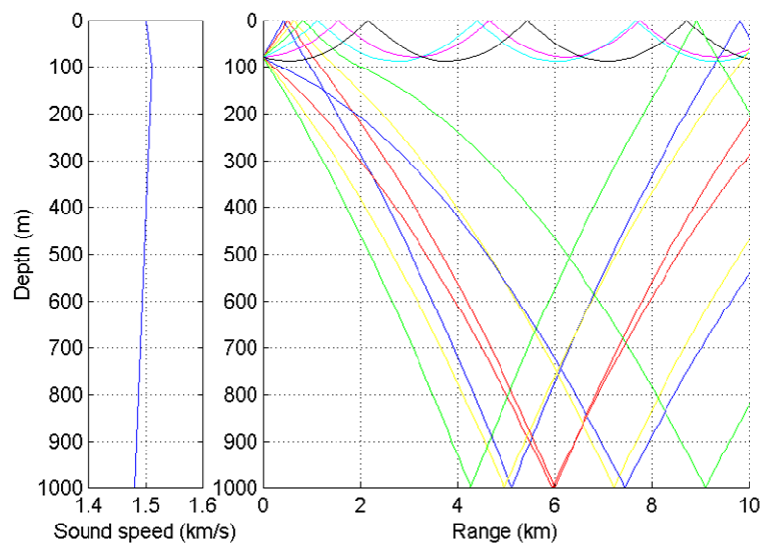


Figure A.8. Ray trace for a notional environment where transmissions originating near the surface propagate through the surface duct. (Duncan, 2006)

The effects of refraction within a water column need to be well understood to predict the propagation paths of acoustic energy. This knowledge is important when choosing the deployment location of any modem pair. Deep sound channel propagation is the most efficient transfer due to the decreased impact of boundary reflections and minimal path length, however, this can be difficult to establish. To make effective use of the deep sound channel both the transmitter and receiver need to be located at the correct depths. For example, a receiver located in the mixed layer of a water column will receive little from a transmitter located at the sound speed minimum over a long propagation distance. This is due to the concentration of rays around a separate horizontal axis and decreased propagation into the mixed layer.

Areas where adjacent rays intersect or focus onto one another create what is known as a convergence zone, yielding higher received acoustic power levels. Conversely, areas where no rays are present are known as shadow zones, resulting in high transmission loss. Areas such as convergence and shadow zones need to be characterised in an underwater environment when attempting to establish a strong communication link. In shallower waters, the depths required to adequately bend rays are not available. Whilst shadow zones still exist in such a situation, the differences in TL are comparatively smaller. In warm climates with waters of less than about 1000m, a downward refracting SSP may be present. This is due to the improbability of a sound speed minimum occurring above the seabed. Such a SSP would result in propagation being concentrated either in the surface duct, if the mixed layer promotes it, or near the seabed, depending on the transmitter location.

When developing an acoustic telemetry system, the vertical positions of the transmitter and receiver are best determined by modelling the sound propagation parameters. For example, it is possible to deduce that for an omnidirectional transmitter located at the surface of a water column the favourable receiver location for long range propagation depends primarily on the mixed layer and thermocline. If sound speed is shown to dramatically decrease with depth, surface duct propagation is impossible and a deeper receiver position is preferred. Conversely, a receiver is likely to be least effective if placed at the surface with a transmitter below the thermocline. There are, however, exceptions to these general principles, such as

Arctic waters where it is common to find an upwardly refracting SSP (Urlick, 1983). Propagation in Arctic waters is also complicated by ice cover presenting a solid scattering boundary at the surface.

A.2.7 Time-variability of an Underwater Acoustic Channel

Fluctuations in the amplitude, phase and frequency of an underwater signal are due to variations in the aforementioned propagation conditions over time. Expressed by Urlick (1983), fluctuations of transmitted sound can be said to be caused by moving inhomogeneities in the sea, including both the environment and the observer. Some of these movements can be predicted and accounted for, particularly where movement is slow and regular, such as seasonal variations in temperature profiles. However, movements exhibiting shorter time periods such as sea surface waves cause rapid fluctuations in the geometric acoustic path. These changes typically affect the amplitude and phase of a signal. However, for a mobile platform such as a vessel, short term movements also induce changes in frequency (Doppler Effect) due to changes in the relative velocities of a transmitter/receiver pair.

Characterisation of signal fluctuations is a topic of significant interest, particularly for underwater acoustics. Short-term fluctuations are best approximated by use of statistical methods. Examples include Gaussian, Rayleigh and Rice distributions, where the most effective method is highly dependant on the application or scenario (Lurton, 2010). The Gaussian distribution is a basic starting point for statistical distributions, given by the probability density function for a variable a :

$$f(a) = \frac{1}{\sigma\sqrt{2\pi}} \exp\left(-\frac{(a-a_0)^2}{2\sigma^2}\right) \quad \text{Equation A.12}$$

where a_0 is the mean and σ^2 is the variance.

In most cases, the Rayleigh distribution is a more widely used approximation to the physical properties of the underwater acoustic channel, given by:

$$f(a) = \frac{a}{\sigma^2} \exp\left(-\frac{a^2}{2\sigma^2}\right) \quad \text{Equation A.13}$$

The Rayleigh distribution can be considered a summation of several arrivals of random phase. The Rice distribution also represents the same superposition of arrivals of random phase with the addition of a dominant coherent component:

$$f(a) = \frac{a}{\sigma^2} \exp\left(-\frac{a^2 + a_0^2}{2\sigma^2}\right) I_0\left(\frac{a a_0}{\sigma^2}\right) \quad \text{Equation A.14}$$

where I_0 is the Bessel function of the first kind and order 0.

The Rice distribution can be likened to a coherent signal path accompanied by micropaths. This particular effect may be experienced when transmitting over a propagation path where a dominant signal is received amongst several arrivals of lower amplitude. When the power of this dominant component tends towards zero, the Rice distribution becomes the Rayleigh distribution.

Recently, the K-distribution has received attention as suitable method of predicting fading statistics of an underwater acoustic communications channel. It was first introduced for radar and sonar applications and was originally developed by Jakeman and Pusey (1976). The probability density function of a K-distribution can be given by (Laferriere, 2011):

$$f(a) = \frac{2}{\alpha \Gamma(v+1)} \left(\frac{a}{2\alpha}\right)^{v+1} K_v\left(\frac{a}{\alpha}\right) \quad \text{Equation A.15}$$

where v is the shape parameter and α is the scale parameter. Γ represents the gamma function and K is the Basset function (a modified Bessel function) of order v .

Utilisation of statistical distributions can be useful for predicting the fluctuations inherent in received underwater acoustic signals, particularly communication signals.

For example, the impulse response of an underwater channel may be described from each ray path arrival derived from ray theory being modelled using one of the above distributions. Outlined by Chitre *et al.* (2008), a primary limitation of shallow water channel simulations (where multipath is prominent) is establishing an accurate channel model. As a result, there is currently no standard application of statistical models for simulation of the underwater acoustic communication channel, especially for shallow water scenarios.

More information regarding these distributions and their applicability in underwater acoustics is given by Lurton (2010). Section 2.3 also describes their use in underwater acoustic communication simulations.

A.2.8 Ray Modelling Methods

The prediction of propagation paths is important for characterising the distortion an underwater acoustic communication signal will undergo. Following the determination of the boundary conditions and sound speed profile as discussed in the earlier sections, it is possible to model the individual paths of an acoustic signal using ray theory. As communications tend to utilise the higher frequencies for increased bandwidth, it is generally acceptable to use ray theory to model propagation as a finite number of rays emitted from a transmitter. This involves mapping the individual trajectories of each ray from the source with detailed information about this found in Jensen *et al.*, (2000).

Ray theory based acoustic propagation modelling is much simpler to implement than the methods required for low-frequency transmission. It also allows a more intuitive way of interpreting the complex reflections from the sea surface, seabed and other marine objects which can be treated similarly to light propagation models. Another notable resource on ray theory and other aspects of underwater acoustic propagation has been produced by Brekhovskikh and Lysanov (1982).

A further application of ray theory is the determination of transmission loss over the propagation distance of each ray path, based on spreading, absorption and the boundary interactions the rays undergo. One method of doing this involves the expansion from rays into beams of finite width with a Gaussian intensity profile. For further information about Gaussian beam tracing see Porter and Bucker (1987). This method removes problems associated with caustics (perfect convergence) and shadow zones and addresses issues with interacting paths seen with conventional ray theory.

The propagation model used for the analysis in this project is Bellhop, a Gaussian beam model written by Mike Porter at HLS Research. This method allows the propagation models to include environment data such as bathymetry, seabed type and bottom and surface roughness as well as the sound speed profile. The information provided by the model includes the expected transmission paths of acoustic communication signals and the effects of their interaction with boundaries and each other. This helps with predicting the performance of acoustic transmissions in a given environment before deployment and allows for more accurate planning.

A.3 *Communication and Signal Processing*

A.3.1 Introduction

The following sections detail the basic principles of digital communication relevant to underwater transmission. A more detailed overview of current progress on protocols developed specifically for subsea telemetry can be found in Section 2.1.

The theory of digital communication has been developed quite significantly over the past decade, providing faster and more reliable data transmission over channels exhibiting various complexities. Wireless data communication is generally associated with the transmission of data using electromagnetic waves. Common examples include Bluetooth (Haartsen, 2000), used for low powered wireless connections, WiFi 802.11 (Matthew, 2005), for wireless networking and DVB-T (Reimers, 1997), employed in Australia for broadcasting digital television. Each protocol is designed to achieve the specifications set out by the developer including range and bit rate expectations. The same customising needs to be done for acoustic communication; however, the variety of applications for subsea telemetry and limitations of the underwater channel has limited the adoption of a simple solution.

By adopting the techniques used by conventional digital wireless technology with radio waves, much of the communication theory is already available for implementation with subsea data links. However, several added constraints exist when adapting the methods to underwater acoustic communication. The most significant difference between the channels is the delay in arrival time of the signals. This delay is due to a five orders of magnitude reduction in propagation speed for acoustic waves when compared to radio waves. Other differences include stronger multipath propagation and restrictions on carrier frequencies. An example of an adaptation method for ISI is to ensure the transmission of each symbol is separated by a length of time appropriate to ensuring the reverberation is complete. This time period is generally referred to as a guard time. However, practical data rates cannot be achieved using this method alone, particularly for long range transmissions and

shallow depths. A discussion of several considerations for underwater acoustic modems for subsea networks is presented in literature by Heidemann *et al.* (2006).

A communication protocol is composed of up to seven layers in the current Open System Interconnection (OSI) model (Figure A.9). An introduction to this model can be found in Zimmermann (1980). For underwater acoustic communication, only the bottom four layers need to be adapted. These are the physical, data link, networking and transport layers. The upper layers of the OSI model provide the means to optimise the connectivity of an individual application and are less affected by differences in the physical layer.

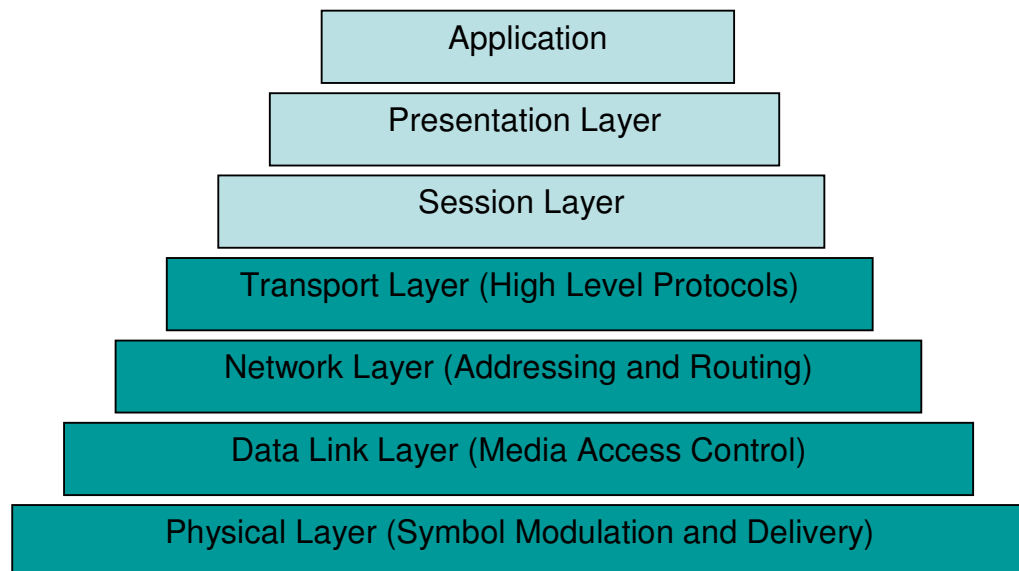


Figure A.9. Open System Interconnection (OSI) layer model for networking systems. Only the lower four (green) elements need channel specific considerations for underwater telemetry.

A.3.2 Signal Modulation Techniques

The basic operating platform for an underwater communication system is to adopt the techniques of the conventional modem (MODulator/DEMODulator) to provide the physical link. Here the transmission of data over a channel is achieved by modulating one or more parameters of a harmonic carrier signal, S , over time, t :

$$S(t) = a \sin(\omega t + \varphi) \quad \text{Equation A.16}$$

where a is the amplitude, ω represents the angular frequency and φ denotes the phase of any given sinusoidal signal. (Okunev, 1997)

Within the limitations of the channel the modulated component ideally needs to be relatively undistorted by the environment for optimum reception. Each data bit is modulated into a specific symbol denoting a digital representation (generally 0 or 1 in simple cases). The duration of each symbol is inversely proportional to the bit rate achieved in the overall system. However, shorter bit duration is more difficult for a receiver to resolve, particularly in multipath environments which create fluctuations in the temporal response of the channel. To determine the data rate of an underwater telemetry system a compromise needs to be made between the data rate and the reliability to best suit the environmental conditions.

Modulation techniques applied in underwater acoustics can generally be described by a variant of one or a combination of a number of the digital modulation methods described in Table A.1. These techniques can also be categorised by whether or not a method employs phase synchronisation in the receiver, as being either a coherent or non-coherent communication scheme. Phase coherence can become difficult and computationally expensive to acquire in digital communication compared to non-coherent methods. However, the substantially higher data rates and noise resistance of phase coherent methods, along with dramatic advancements in digital signal processor (DSP) technology, has led to a recent increase in their use, discussed in Section 2.1.

Table A.1. Examples of methods used to transmit digital communication. A variant of one or more these methods is generally utilised for underwater acoustic telemetry.

Method	Sub-forms	General Description
Frequency Shift Keying (FSK)	Binary-FSK (BFSK)	A bit stream (0, 1) is encoded with the carrier frequency alternating between two possibilities.
	Multiple-FSK (MFSK)	Similar to BFSK, with more than two frequencies utilised at once to increase throughput
Phase Shift Keying (PSK)	Binary PSK (BPSK)	A bit stream (0, 1) is encoded with the phase of the carrier either in phase (0°) or out of phase (180°)
	Quadrature / Multiple PSK (QPSK / MPSK)	Phases are encoded into 4 or more equally spaced possibilities (e.g. 0°, 90°, 180°, 270°) to increase throughput.
	Differential PSK (DPSK)	Same as PSK methods, however, the difference in phase between adjacent symbols is encoded instead of the absolute value.
Spread Spectrum	Frequency Hopping Spread Spectrum (FHSS)	Carrier frequency of a transmission is hopped between several variants over a wide band of frequencies at regular intervals. This sequence needs to be known at the receiver.
	Direct Sequence Spread Spectrum (DSSS)	Data stream is multiplied by a pseudorandom sequence over a wide band of frequencies. This sequence needs to be known by the receiver and otherwise appears as noise, making it useful for covert telemetry.
	Chirp Modulation	Can also be considered a variant of FSK. Data is encoded into the upward-sweep or downward-sweep of the carrier frequency.

A robust and relatively simple modulation scheme for underwater data telemetry involves the use of frequency shift keying (FSK) based techniques. A basic example of FSK includes early voice modems operating at 300 bps utilising binary FSK (Lee, 1994). FSK has since advanced significantly with the inclusion of other coding schemes such as 1-of-4 modulation (Scussel *et al.*, 1997). The primary disadvantage of FSK is the limited bandwidth available underwater, further inhibited by frequency selective fading from multipath interference. Phase shift keying (PSK) has gained recent popularity due to its noise resistance increasing the reliability of transmission, particularly in wireless environments. Additionally, implementation of PSK is relatively simple and cost effective with today's technology. Many current PSK designs utilise binary or quadrature phase shift keying (BPSK or QPSK) which involves the discrete variation of the phase of a carrier frequency f_0 into a number of orthogonal components.

Another widely used technique for underwater acoustic communications is Spread Spectrum based technology. This involves two main variants, Direct Sequence Spread Spectrum (DSSS) and Frequency Hopping Spread Spectrum (FHSS). An introduction to spread spectrum communication is provided by Ziemer (2007). Both methods often involve utilisation of a larger transmission bandwidth and subsequently higher transmission frequencies. This higher frequency diversity provides more resistance to multipath fading and noise. By spreading the energy over a wider bandwidth using coding methods, spread spectrum is also preferred when considering the security of data transmissions. Additionally, several nodes of a network can access the same medium by utilising a separate coding scheme. These can be particularly useful for underwater networking, utilising various codes to enable efficient use of the channel by more than one device.

A.3.3 Channel Capacity

A signal propagated over a physical channel undergoes a certain amount of distortion before arriving at a receiver. Signal distortions can include noise, attenuation, fading and interference. By being able to model these effects, a theoretical channel capacity can be determined, providing the upper boundary of the achievable data rate. As an example, consider the commonly implemented Additive White Gaussian Noise (AWGN) channel model, which incorporates only the addition of Gaussian noise to a received signal. The capacity (Shannon Capacity) C in bits per second of an AWGN channel can be given by:

$$C = W \log \left(1 + \frac{P}{N_0 W} \right) \quad \text{Equation A.17}$$

where W is the bandwidth, P is the signal power and N_0 is the noise variance. Alternatively, $P/N_0 W$ is considered the signal to noise ratio (SNR). (Proakis, 2008)

For an underwater acoustic communication channel exhibiting multipath it is ideal to consider a finite state channel: a channel model for a time-varying environment

(Proakis, 2008). The dynamic underwater environment yields high multipath, resulting in levels of both low and high frequency signal fading. It is therefore appropriate to consider the ergodic capacity of a fading channel which incorporates the fading statistics into the channel model. Rayleigh and Rice fading statistics (Appendix A.2.7) are typically used for estimating the ergodic channel capacity in underwater acoustic communication. In addition to the fading statistics themselves, the ergodic channel capacity is dependant on knowledge of the channel state information at the transmitter and receiver. Socheleau *et al.* (2009) provides a recent investigation into the capacity of fading channels and compares the results of implementing various modelled scenarios to an equivalent AWGN channel.

More detailed information regarding the derivation of the capacity of digital communication channels can be found in Proakis (2008). However, an underwater acoustic channel is a complex environment which requires the consideration of many scenario-dependent elements which, in most cases, are time varying. As a result, the derivation of an accurate theoretical channel capacity for subsea telemetry is given focus in many simulations as shown in Section 2.3.

A.3.4 Error Correction Algorithms

Most communication methods are strengthened by employing advanced coding systems and error correction codes. This involves transmitting additional codes that may subsequently reduce the transmission speed of the payload data. Forward Error Correction (FEC) codes allow the receiver to correct any minor detected errors, whilst unrecoverable problems can be corrected by a requested retransmission. Despite the performance increases associated with FEC codes, many modems still tend to implement acknowledgement transmissions from a receiving modem. This involves a confirmation of receipt transmitted back to the initial source. In a particularly dynamic acoustic environment, however, the return of an acknowledgement packet may not be correctly interpreted by the transmitter. For data hopping or networking, the compulsory use of acknowledgement packets can lead to an unnecessarily slow network with little gain in data integrity. The type of

error correction and quality control used in an underwater communication system is therefore based on a compromise between speed and reliability.

A.3.5 Multiple Node Access to the Underwater Channel

An important consideration for underwater networks is the data communication protocol being implemented, specifically the medium access control (MAC). This need arises as all nodes are sharing the same physical medium and becomes even more complicated when considering the signal delay. The goal of the MAC is to ensure that all nodes are provided with a fair amount of transmission time, whilst minimising the latency of the network. An overview of this and other considerations have been established by Stojmenovic (2005).

Common MAC methods include frequency, time and more recently code division multiple access (FDMA, TDMA, CDMA respectively). Whilst FDMA and TDMA distinguish nodes using frequency and time separation respectively, CDMA is a more complex procedure, utilising frequency hopping or sequencing with spread spectrum methods. Another method known as Carrier Sense Multiple Access (CSMA) determines if a transmission is taking place before attempting to communicate.

An appreciation for the underwater acoustic environment indicates the difficulty in implementing FDMA in a low bandwidth environment. The difficulty in time synchronisation and inability to accurately determine signal delay renders TDMA and CSMA based protocols inefficient. CDMA with the appropriate filter implementation arises as one of the more favourable MAC options and is expected to be a promising approach to underwater networks (Akyildiz *et al.*, 2005).

Appendix B

Modem Performance Measurements in the Arctic

In October 2009, the author represented Aquatec Group Limited during an at-sea Arctic cruise aboard the Norwegian coastguard icebreaker, KV Svalbard (KVS). The vessel departed Longyearbyen, Svalbard, on 18th October 2009 and returned to the Fjord on 27th October 2009. The primary aim of the cruise was the deployment and recovery of various scientific moorings in the Fram Strait as part of the DAMOCLES and ACOBAR projects. Between tasks it was also possible to periodically conduct additional tests of the acoustic modem technology used in these projects. Several trials were conducted to assess the Arctic performance of the AQUAmodem. Specifically the vertical and horizontal telemetry performance of the modems was to be investigated, as well as the ability for the modems to operate in sub-zero temperatures. The trials were also used to investigate the performance of a recently added high speed (400 bps) mode in the modem software. The locations of the three particular tests presented in this section are shown in Figure B.1.

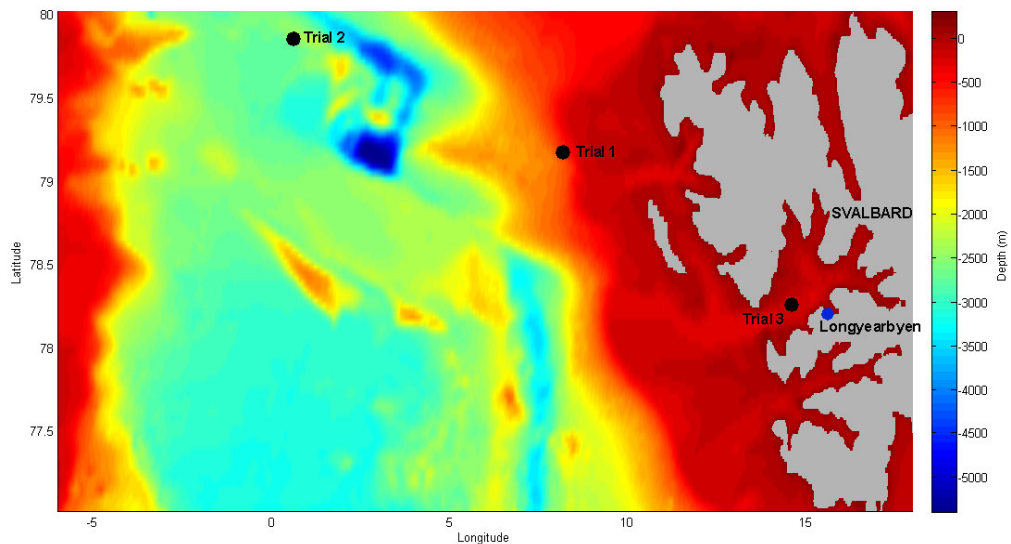


Figure B.1. Location of the Fram Strait where the majority of the Arctic Cruise took place aboard the KV Svalbard. The location of the three modem trials discussed here are shown, West of Svalbard. The vessel departed Longyearbyen, located at the southern end of the Fjord where Trial 3 took place.

B.1 Experimental Setup

Unlike previous deployments the modem trials performed during this cruise utilised standalone modems, without the addition of an attached recorder or control device. Furthermore, three modems were utilised for the majority of tests instead of two. A diagram depicting the trial configuration is shown in Figure B.2. Two modems were typically lowered from KVS, one of which was connected to a laptop computer in the wet-lab (KVS deck) for control. Another modem, a standalone receiving modem, was powered by internal batteries and no interface cable was required. This allowed the deployment of the modem to depths of up to 1000 m from the aft-deck of KVS using a crane (KVS deep).

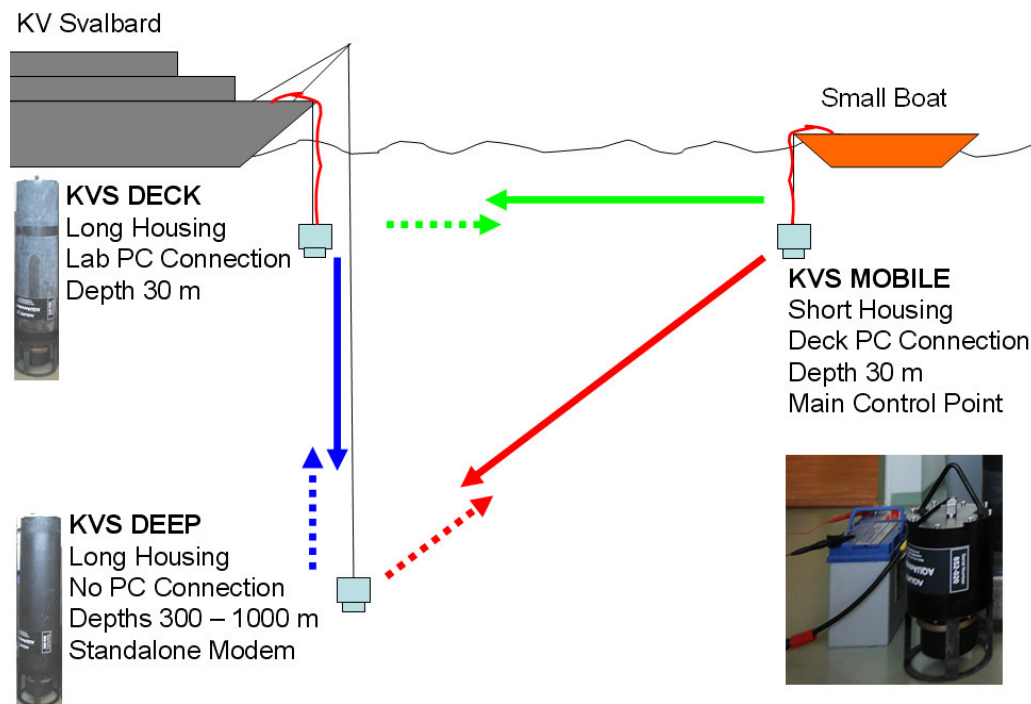


Figure B.2. Deployment plan showing the orientation of equipment to be tested. Both vertical and horizontal modes were investigated. Control was typically performed via a deck computer either on KVS or a small vessel which was deployed at range with KVS mobile. A laboratory computer was also connected to KVS deck for debugging data and some control if necessary.

The final mobile modem (KVS mobile) was placed in a subsea housing similar to the trials conducted off the coast of Australia. The small size of the modem allowed for lowering from one of the two smaller vessels deployable from KVS. The mobile modem was the primary interrogator; however, during many deployments the deck modem was configured to periodically transmit to the standalone modem to ensure both were still in operation. Photographs depicting some aspects of the trial are shown in Figure B.3 and Figure B.4.



Figure B.3. Photographs taken during the deployment showing deployment in ice (left) and small boat operations with KVS mobile in the Fjord (right)



Figure B.4. Preparation in the wet lab on KV Svalbard. Two interface PCs (top right) and the assortment of modems stacked on a pallet for storage (middle). The cables and lead-acid battery used for small boat deployment is also shown (bottom left).

The Arctic modem trials were conducted for six consecutive days in the second half of the cruise with an added day of deck testing, following problems experienced in the first trial. Approximately half of these trials involved deployment of the small boat to obtain range data. During one of the trials an external recorder was deployed from the smaller vessel to record the deck modem waveforms at various ranges. The data analysed in this section involves approximately half of the total cruise data collected, as the majority of the trial concerned only the internal development of the modems and not the communication statistics.

The following levels of testing were generally attempted for each modem deployment. However, the exact procedure differed slightly for each trial depending on the success of each level. These tasks were carried out using a RS232 connection from the PC using software written specifically for the AQUAmodem, originally based on *PDALogger*. This software can be found on the attached media.

- 1) First, a simple communications check was performed. This involved sending a ping request to the remote modem(s). If no response was detected by the interrogator, personnel would listen for an audible response if possible.
- 2) The transmission of packets of varying length was initiated. Different block sizes were transmitted, ranging from 8 - 250 bytes in length. These transmissions did not request an acknowledgement.
- 3) Memory blocks were requested from the remote modem(s), similar to the French trials presented in Section 4.2.5. If no response was detected an audible check was performed.
- 4) The remote modem was placed into a high bit rate mode by transmitting an acoustic command. If an acknowledgement was not detected the command was repeated three more times before continuing.
- 5) Finally, procedures 1 - 3 were performed with high speed mode activated on the local modem. It was expected at this point that the remote modem(s) were also in high speed mode.

B.2 Trial 1: Initial Communication and Acoustic Recordings

An initial test of communications was performed using all three acoustic modems. This involved deploying KVS deep and deck modems while interrogating both from the small boat at a distance away from KVS. The method used to determine depth and SSP of the area was the launching of an XBT. However, in a previous research activity the XBT launcher aboard KVS malfunctioned and became inoperable. Using the bathymetry map also shown in Figure B.1 it was predicted that the depth in the area was approximately 1000 m.

The small vessel was launched before the two KVS modems were lowered from the deck. Once approximately 1 km from the mother ship the mobile node started interrogations of both the KVS deck and deep modems. The deep water modem was determined to have malfunctioned before the mobile node started interrogation. However, communication with the KVS deck modem located close to the surface was successful. All interrogations were successful with the largest returned block size being 63 bytes long. This initial position yielded excellent communication statistics with no failures recorded.

After moving on to the next test point the mobile node was found to be malfunctioning. It was determined following this trial that the low temperatures of the Arctic waters were affecting a critical hardware component of the modems, preventing the power management from operating as required. This problem was later fixed by replacing the faulty components. For the remainder of the trials the modems were able to operate without incident, provided the sleep function was not initiated. This issue highlighted possible unforeseen effects of an environment on the hardware components of underwater devices and not just the impact on acoustic signal propagation.

The data obtained by the modems was analysed briefly, where the signal strength measured at each modem was compared using debug memory aboard both the KVS deck and mobile modems. A receiver bandwidth of 400 Hz was assumed and the average received power for the lowest MFSK frequency component (7600 Hz) was calculated for each position. These power levels were measured as -15 dB re 1 V² and -17 dB re 1 V² for KVS Deck and KVS Mobile respectively. This finding highlighted the expectation of the transmission loss being identical given the same transmission path, regardless of direction. Additionally, the 2 dB discrepancy was thought to have been contributed to by vessel noise from KVS.

Following the modem connectivity measurements, an underwater acoustic recorder was used to record the transmission of the KVS deck modem from various distances. The acoustic recorder involved a handheld recorder sampling at 44.1 kHz with 24 bit precision. The receiving hydrophones consisted of a 4 element array of total length of approximately 1 m, suspended in a cylindrical tube of oil. This hydrophone was lowered manually with essentially all of the 150 m of cable submerged. Recordings lasted 5 minutes while the KVS deck modem repeatedly transmitted a short packet via control from the lab PC. Due to the visibility and safety policy aboard KVS, the maximum separation distance trialled was 7.5 km. Table B.1 demonstrates the test positions used for the recordings.

Table B.1. Separation distances for ambient noise recordings during the Arctic trials, as radioed by control aboard the mother ship.

Test Point	Separation (km)
1	1.4 km
2	3.7 km
3	5.6 km
4	7.4 km

Multipath interference was found to have much less of an impact on communication and the nature of ISI was vastly different to previous deployments. This finding can be visualised in Figure B.6 which compares the 1024-point PSD over time for two

signals. These identical signals were recorded at the minimum separation distance of approximately 1.4 km and the farthest at 7.4 km. In both recordings, the dominant signal arrival terminates at approximately 6.2 seconds.

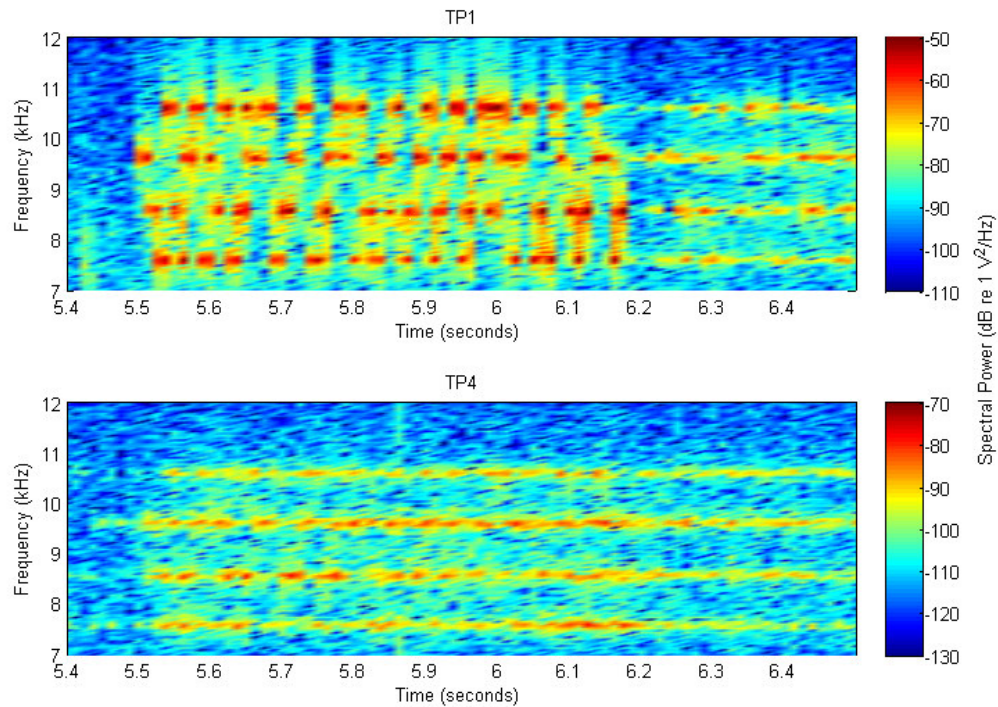


Figure B.5. Spectrogram of two recordings depicting identical transmissions originating from the KVS deck modem. Two ranges, TP1 (1.4 km) and TP2 (7.4 km) are shown. The transmitter was located 30 m from the sea surface at the distances depicted in Table B.1, with the hydrophone 150 m below the sea surface at the small vessel.

In Figure B.5, the spectrogram shows clean and distinct symbol patterns in deep water over a path length of 1.4 km. In fact, it is possible to distinguish the active symbols over time by visual inspection and one could manually decode the data. This result reflected the perfect modem connectivity discovered at similar ranges earlier in the trial. At long range, however, more ISI is observed as signal spread increased.

Further to multipath investigation, a study on the arrival spread for each range was conducted using the same recordings. To measure this spread the wake-up sequence used by the modems was analysed. As this sequence involved three 25 ms bursts 500 ms before the main data, the multiple arrivals could be distinguished visually as shown in Figure B.6. The spectrogram for the received wakeup sequence at the four test points is shown, with clearly distinguishable differences in multipath arrivals.

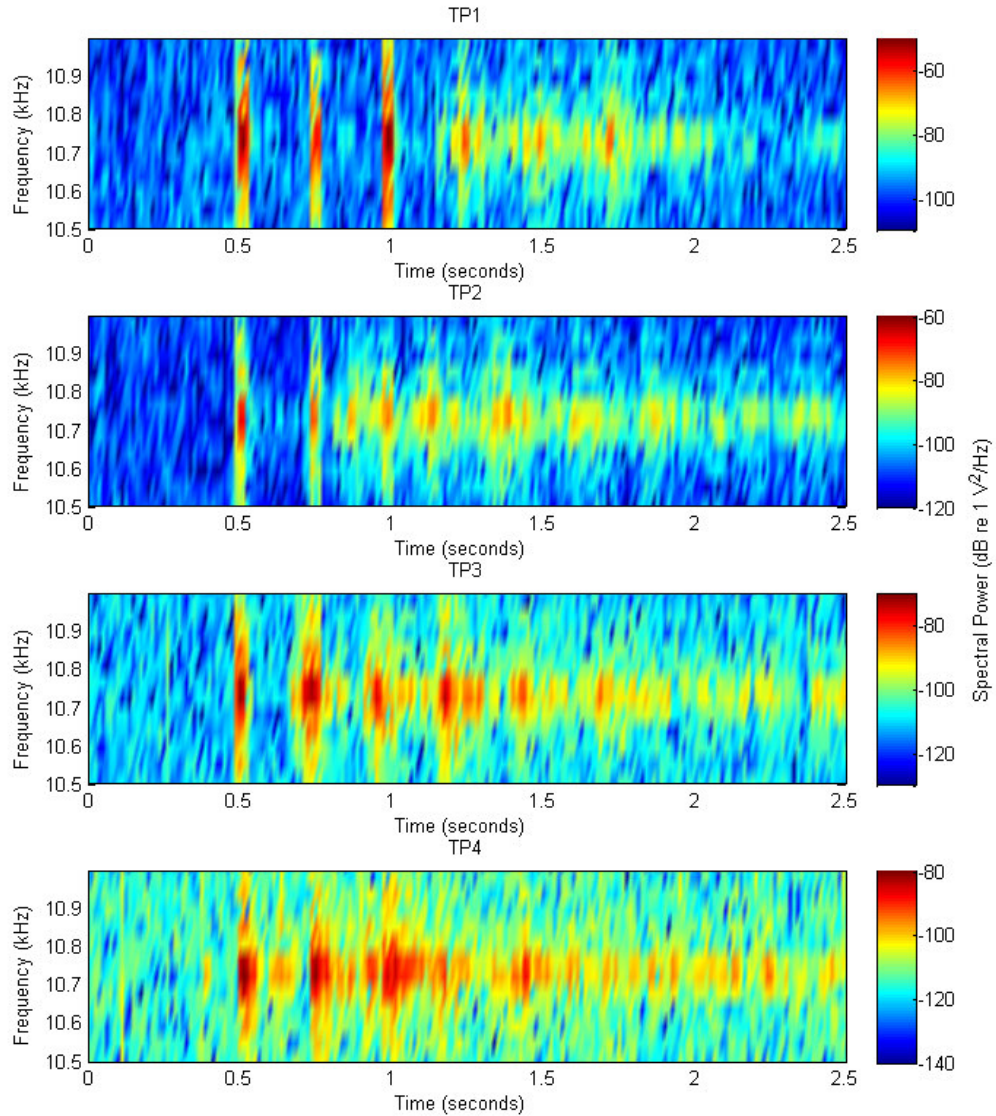


Figure B.6. Spectrograms of recordings of the wake-up sequence transmitted by the modems. The timing of multipath arrivals is shown to differ significantly at each test point. Particularly evident, the arrival delay between the primary and secondary eigenray is shown to decrease with distance.

Further analysis showed the time between the first and second arrivals at 1.4 km to be approximately 0.7 s corresponding to a path difference of 1 km, when assuming an average Arctic water sound speed of 1450 ms⁻¹. This is consistent with the total path length of 2.4 km for the first reflection from the seabed, shown in Figure B.7.

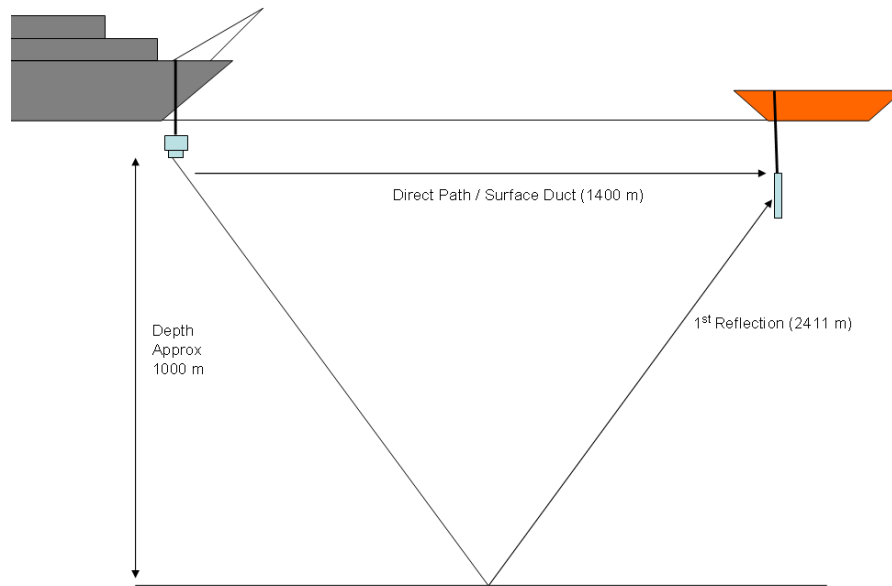


Figure B.7. Simple ray trace geometry depicting the predicted path length for the first two eigenrays received at the hydrophone. The path length difference of approximately 1 km corresponded to the observed 0.7 s delay at TP1.

At the longer ranges in the trial, the path difference between each arrival is shown to decrease. Furthermore, at TP4 the dominant arrival was no longer observed as the first arrival. This consequence of long range propagation was expected to be a challenge for the modem software to overcome in detecting and decoding the signal. Higher amplitude secondary arrivals would interfere with those first acquired by the modem unless such a channel characteristic could be accounted for.

Although the modems were not functional for much of this trial, the recordings of modem transmissions at various ranges provided insight into the effects of multipath propagation. Specifically, the predicted effects of the boundaries using ray traces were validated with data clearly demonstrating effects including ISI. It was reaffirmed in this trial that shorter ranges and larger depths provided excellent clarity for underwater acoustic communications. This effect is particularly true provided the transmission time is shorter than the time taken for subsequent reflections to arrive.

B.3 *Trial 2: Vertical Communication Test*

Trials involving the small boat were not able to be undertaken safely during some periods of the voyage due to rough ocean conditions. During one of these periods the crane was used to lower KVS Deep to various depths while keeping KVS Surface approximately 30 m below the sea surface. This trial was short with a deployment time of approximately one hour. To ensure the modems did not enter a sleep state, the deep modem was periodically raised towards the surface until there were signs that it was still operational. Such signs included either an audible acknowledgement heard aboard KVS or the interrogating modem reporting a response. The goal of this experiment was to determine the vertical capabilities of interrogation amongst high amounts of noise such as that emitted by KVS.

The trial consisted mostly of pings initiated from the deck modem. When these pings were successfully returned, memory requests were made. However, essentially all ping and memory requests failed to be recognised when the transmitting modem was lowered beyond 100 m. Feedback from the deck modem suggested the ship noise (described later) contributed to false detections of transmissions. This problem was also reflected in the sub-par success rate of transmissions which is shown in Table B.2.

Table B.2. Statistics acquired during a vertical transmission test aboard KV Svalbard. The depth of the deck modem remained at approximately 30 m. The deep modem ranged between 30 – 200 m to ensure connectivity was audible on deck.

Link	Payload Size (Bytes)	Packets Transmitted	Packets Received	Percent Success	Total Success (%)
Deck - Deep	< 10	54	36	67	56
	10 - 100	19	6	32	
	> 100	5	2	40	
Deep - Deck	< 10	26	14	54	40
	10 - 100	6	2	33	

The smaller packets were found to perform better generally throughout the vertical test; however, there was no dramatic decrease in telemetry for larger blocks. This suggested that the acquisition of the signal was the primary obstacle for the modem receivers. Additionally, the upward link was shown to perform more poorly than the downward link, highlighting the consequences of deploying in close proximity to a noisy vessel.

The average noise at each modem over the carrier frequencies was measured using portions of the modem recordings where no transmission was taking place. The ships propellers were shut off during the operation, however, some critical systems were still running including the steering mechanism and power generators. The typical noise power spectrum measured by the modems is presented in Figure B.8, demonstrating the presence of noise harmonics due primarily to vessel proximity. Furthermore, it was likely that additional noise measured by the KVS deck modem was due to electromagnetic interference picked up via the subsea cable originating from the wet lab.

The results of Trial 2 highlighted the problems associated with deploying modems from the aft deck of a vessel such as KVS, which especially utilised electronic systems throughout, including propulsion. For the FSK based modems used in this trial the fluctuations in noise yielded the false detection of incoming signals. Whilst false detections did not corrupt incoming data, it most likely interfered with the overall success probability of a transmitted packet. The results from this experiment suggested that the successful interrogation of remote modems was best suited to a modem being deployed away from large noise sources to ensure reliability in acquiring and decoding a transmission.

B.4 Trial 3: Fjord Testing and High Speed Communication

Before KVS returned to Longyearbyen following the cruise an acoustic modem trial was conducted in the nearby Fjord in a depth of approximately 200 m. The trial involved use of all three modems. KVS deep was deployed first at approximately 100 m depth. The deck modem deployment followed, positioned approximately 15 m below the water surface. Interrogations were carried out vertically before the small boat was deployed to assess horizontal performance. The small vessel was positioned approximately 2.5 km from KVS with the engines shut off during the trial.

Trial procedures were identical to previous experiments with regular pings and memory requests made by the mobile modem. However, the deck modem was configured to transmit a ping request from the deep modem every 40 s to ensure it did not power down. This added transmission opened the possibility for two modems to transmit at once to investigate the consequences of modem interference. At the conclusion of the trial the higher speed mode was tested thoroughly by transmitting high speed data without acknowledgement requests.

The remote signal power as observed by the modems over a 400 Hz bandwidth was calculated for signals of approximately 1 s duration. Measurements for the deck, deep and mobile modems were -25, -29 and -34 dB re 1 V² respectively, not including KVS local transmissions which clipped the receivers. These results demonstrated a similar correlation as in earlier tests, with the contributions from vessel noise evident for those modems located at the mother ship.

Ambient noise measurements yielded results similar to previous trials and is shown in Figure B.8. The mobile node was found to exhibit the least amount of ambient noise in the frequencies used for communication. This was expected as it was the furthest from the vessel. However, high amounts of noise in the upper end of the spectrum were not expected. It is possible that electronic noise from the small boat may have contributed to this, however, this is uncertain.

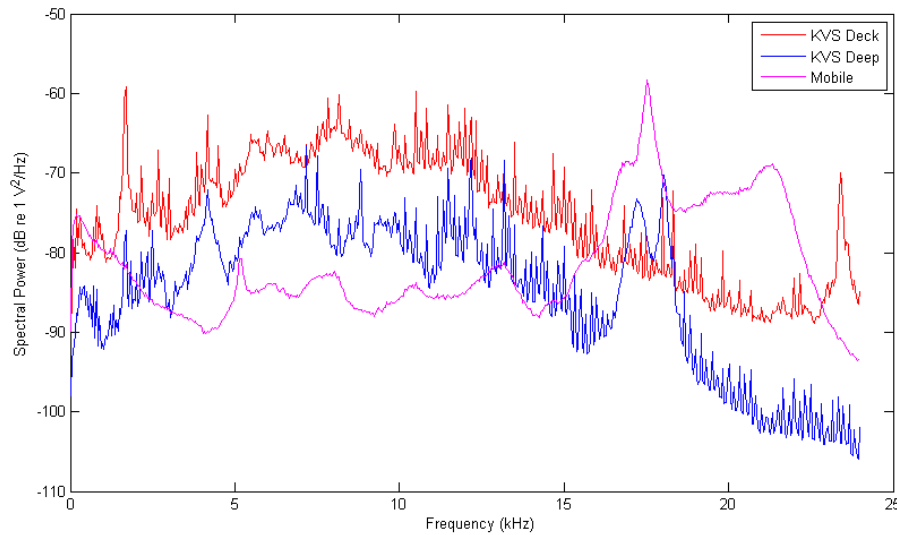


Figure B.8. Noise power spectrum measured during silence between modem communications. High amounts of electronic noise were exhibited at KVS deck. As expected, the mobile node exhibited the least amount of ambient noise over the frequencies of interest as it was the farthest from the vessel.

Both KVS deck and deep modems responded throughout the entire trial lasting an hour with an additional 30 minutes involving just the KVS local modems.

Unfortunately, for the purposes of statistics collected during this study, the overall response rate could not be correlated with channel quality as the ping requests at KVS would have certainly interfered with such investigation. In addition, the noise emitted from KVS was shown to create false positives at both the deck and deep receivers, preventing detection for up to 2 minutes at a time.

To best characterise the communication performance, data from the modems regarding the raw transmitted and received bytes were compared. The mobile modem was best suited to analyse the performance of communication in this way as the state of KVS deck and deep modems was not known to the same accuracy. For example, the probability of KVS deck being in the process of transmitting a ping command (which takes up to 8 s) was a confounding variable. Additionally, the low levels of noise at KVS mobile minimised the chances of false detections causing disruption to the receiver capability. Table B.3 summarises the values obtained by comparing transmitted packets to the number of times a packet of the same size was received by KVS mobile.

Table B.3. Detections statistics acquired during trials conducted in the Fjord nearby Longyearbyen. Only communication towards the mobile node was analysed. Vessel separation was approximately 2.5 km. Vertical separation between the KVS modems was approximately 70 m.

Link	Payload Size (Bytes)	Packets Transmitted	Packets Received	Percent Success	Total Success (%)
Deck - Mobile	< 10	53	40	75	81
	10 - 100	13	11	85	
	> 100	12	12	100	
Deep - Mobile	< 10	13	11	85	91
	10 - 100	7	6	86	
	> 100	12	12	100	

To determine the BER for the transmissions received by the mobile modem, the received packets were compared to those transmitted by both KVS deck and deep modems. Due to the difficulty in uniquely identifying each transmission, the modem time stamps were used as a matching guide and packets were required to mostly resemble an original transmission (> 50 %) as a whole before nibble (half a byte) comparison was performed. These criteria meant that only packets successfully synchronised to begin with were processed for BER analysis. As the synchronisation performance is also important for overall communication the results presented should only be considered tentative. However, from this analysis an average raw BER of 2.8 % and 0.5 % was calculated for transactions originating from the deck and deep modems respectively. The better statistics from the deep water modem are likely due to its location deeper in the water column.

For high speed mode analysis, the capacity to use a faster bit rate led to a subsequent increase in packet size. Only transmissions from the mobile modem to KVS deep are presented in Table B.4 as noise exhibited at the deck modem produced results unsuitable for BER analysis. Despite this, transmission between all three modems was found to be successful in high speed mode. Analysis of the high speed data also confirmed that when the modems had successfully acquired a signal, effective telemetry ensued. An overall BER of 2.2 % was achieved with most errors occurring with larger packets of up to 800 Bytes.

Table B.4. BER for high speed data packets following detection from KVS mobile to KVS deep. The data rate trialled here was 400 bps, 4 times the normal rate. (x) denotes the number of times the packet was received. Vessel separation was approximately 2.5 km.

Payload Size (Bytes)	Averaged BER (%)	Total BER (%)
75 (1)	0.7	2.2
143 (2)	0.0	
428 (2)	0.5	
817 (2)	3.6	

It was discovered that noise played a dominant role in the reception of data at KVS deck during the high speed trial. Analysis of the KVS deck modem recordings showed that interference not only prevented the detection of an acoustic stream, but also induced a high rate of false detections which further prevented the modem from operating effectively. The KVS deep modem located 100 m below KVS, however, received these signals with little difficulty.

Overall the results obtained in this trial confirmed that multipath propagation was not a major problem for deeper water channels, even at 200 m. Additionally, electronic and acoustic noise was shown to cause problems for KVS modems with the mobile modem exhibiting significantly less amounts of interference. High speed mode was found to work effectively during the trial with low BER measured. However, the major problem with the communication during this test, as with the previous tests, was false positives triggered by the large amounts of noise from the vessel. Despite this, communication was of high quality and data rates of 400 bps were obtained over 2.5 km with a BER of approximately 2.2 %.

B.5 Summary

The trials presented here demonstrated an effective underwater communication link in deep water over ranges up to 2.5 km. Despite logistical issues in testing at greater distances it was anticipated that communication over longer ranges could have been established, given the clarity of signals and high observed SNR in recordings.

The first trial established the link between the bathymetry and the nature of multipath interference for shorter range communication. This trial highlighted that a short burst of data transmitted within the delay difference of 0.7 s would not exhibit any significant ISI due to the path length difference. This difference alluded to the possibility of using much higher data rate systems without significant demand on receiver processing.

In the second trial, the impact of localised noise was highlighted as a contributing factor to errors in receiving data at KVS. Furthermore, it was possible that electronic noise picked up through the subsea cabling was interfering with the receiver close to the deck. The effects of noise only appeared to cause disruption to the detection and synchronisation of the signal. Once a packet was acquired, the subsequent decoding proved effective and low BER communication was achieved

The third trial demonstrated similar noise characterisation to previous trials. The use of the mobile modem was shown to be effective due to the isolation from noise. As in previous trials, the size of the packet only had a slight impact on the success rate of reception. This outcome also suggested the acquisition of a signal was more of a problem than its decoding following the successful synchronisation.

Overall, these trials highlighted several problems and promises for use of FSK based underwater acoustic communication as an effective means of retrieving data from sensors using interrogation techniques. The results reflected the robustness of FSK as communication was established in trying situations at a relatively low computational cost. With refinements in the technology and the application of the appropriate modulation and signal processing techniques, performance increases were expected as development continued.

Appendix C

Acoustic Tag Performance and Noise Measurements at Cockburn Sound

C.1 Introduction

The following investigation was performed in conjunction with a study by Department of Fisheries, Western Australia. During 2009, a series of experiments were conducted regarding the use of acoustic tags to monitor the movements of marine fauna. In acoustic monitoring, a surgically implanted or externally affixed acoustic device, periodically emitting coded pings, is used together with an array of receivers to uniquely identify and track marine life. The aim of this trial was to better understand the performance limitations and optimum configurations of the acoustic pingers and receivers, which operate at a relatively high carrier frequency of 69 kHz.

In order to achieve basic performance capability statistics, a long-term range test was conducted in conjunction with a deployment of two high frequency ambient noise recorders in Cockburn Sound, off the coast of Western Australia in November 2009. The test area comprised a sand seabed of relatively uniform bathymetry at a depth of approximately 8 m. To assess the performance of the tracking devices, one of the acoustic recorders was situated approximately 1 m horizontally from a mooring consisting of three acoustic pingers, each emitting a unique pulse modulated code. A diagram depicting the deployment configuration is shown in Figure C.1. Two of the acoustic tags were placed approximately 2 m above the seabed with another, more frequently transmitting tag, placed on the sea floor. The resulting range between the hydrophone and the first two tags was approximately 2.0 - 2.5 m whilst tag 3 was located within a metre. Purpose-built receivers were also positioned at ranges up to 297 m from the tags. An additional acoustic recorder was placed 100 m from the tags in order to help categorise the receiving capability at range.

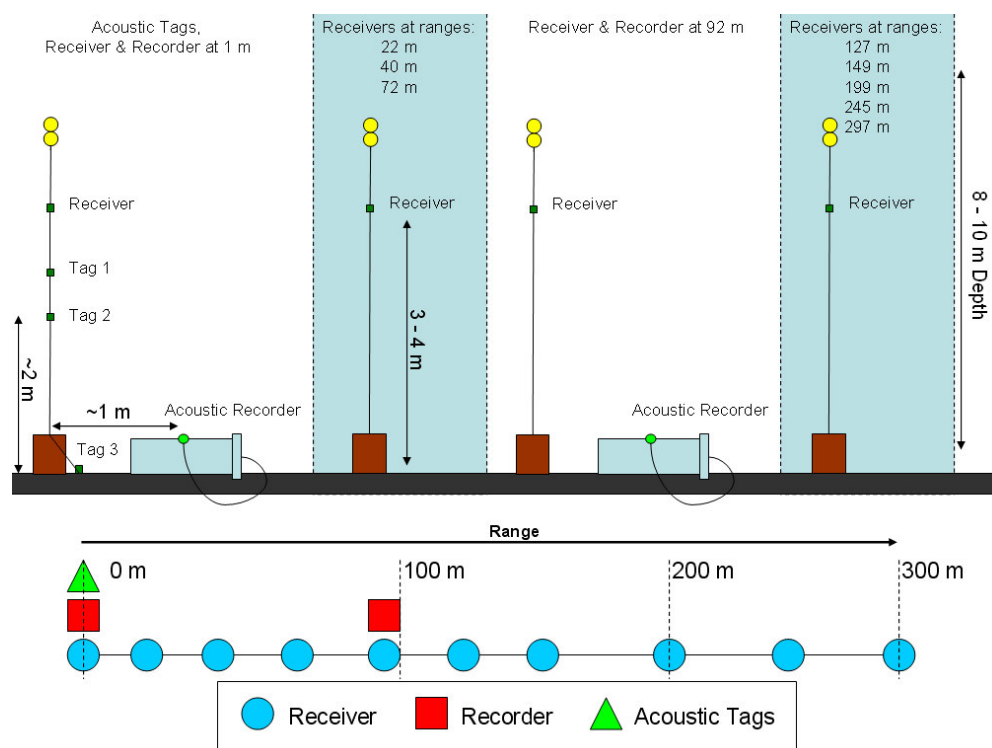


Figure C.1. Equipment layout used for the long-term deployment of acoustic tags and high frequency ambient noise recorders. Three acoustic tags were deployed with 10 matching receivers spread over a total distance of approximately 300 m. Additionally, 2 acoustic recorders were placed at ~1 and 92 m from the sources to measure ambient noise and incoming signals.

For this experiment the pinging tags operated independently of the acoustic recording components. The three pingers were configured to operate on separate schemes as shown in Table C.1. As well as emitting a distinct code, the configuration of the tags varied to separate both the intensity of the signal as well as the time between pings. This provided a diverse range of source levels for range testing, as well as allowing for the realistic possibility of overlapping pings interfering at the receiver.

Table C.1. Various configurations for the acoustic tags (pingers) used for the Cockburn Sound range trials.

Pinger Label	Unique Code	Source Level (dB re 1 μ Pa @ 1 m)	Ping Interval (s)	Average Ping Frequency (pings per day)	Ratio with lowest ping frequency
Tag 1 "V16-4H"	65430	158	700 – 1000	102	1.2
Tag 2 "V16-6L"	65445	153	900 - 1100	86	1
Tag 3 "V9-1H"	62729	147	80 - 200	617	7.2

As the pingers operated at 69 kHz, the high frequency capability of the ambient noise recorders was employed and configured to sample at 176.4 kHz. The deployment was considered to run long-term, lasting up to two weeks. Consequently, *PDALogger Skinny* was implemented on the PDA device with *ModCon* on the MCS operating in Deployment Mode B for adequate power saving. *ModCon* was configured to turn all hardware components on every 30 minutes with a forced shut-down limit of 10 minutes. However, *PDALogger Skinny* was expected to initiate a shut-down prior to this time limit, provided acoustic recording and data writing was complete. Figure C.2 represents the duty cycle of the recording system in this deployment.

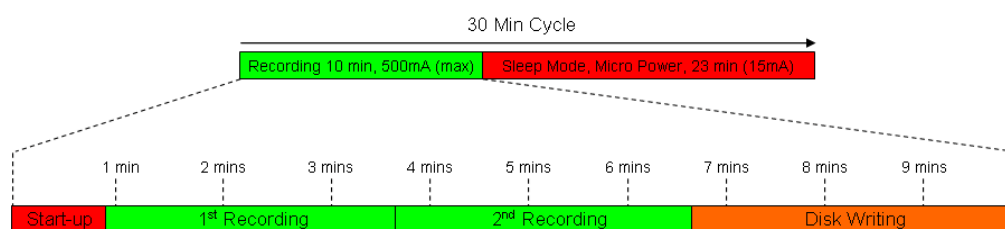


Figure C.2. Diagram depicting the duty cycles used for the high frequency underwater acoustic recordings in the Cockburn Sound range trial. A 30 minute cycle included a maximum of 10 minutes of high powered operation with four of these spent recording.

Due to the high data throughput associated with high frequency logging, the system was considered unstable for long-duration recording and data could not be reliably streamed direct to USB memory. In order to accommodate the faster data rate, each cycle of *PDALogger Skinny* included two successive 2 minute recordings. After completion of the second recording, the contents of the SD card was written directly to the USB disk, followed by a shut-down initiated via the MCS. This scheme optimised both the recording capacity and power consumption of the underwater acoustic recorder for a 12 day deployment. The recorder located at 98 m was capable of storing 32 GB of data on a USB flash disk. A previously deployed 16 GB USB flash drive was used at the source location to ensure successful recordings were made in case there was a problem associated with the new drives.

C.2 Receiver Ping Detection

The deployed acoustic tags were designed to operate in conjunction with an array of distributed receivers. In this trial, a straight line transect of approximately 300 m was occupied by purpose-built sensors for receiving the acoustic pings for range testing. These devices were capable of receiving and decoding the pulse modulated codes and storing them in internal memory for later recovery. Data from the tag receivers were provided by the Department of Fisheries, Western Australia. Analysis of the data provided an overview of the range capabilities of the acoustic tags as well as long-term performance statistics. The acoustic tags were programmed to emit at a random interval within a given time range, so the ping detection performance was best quantised by comparing detections at range with those detected at 1 m. Figure C.3 summarises the tag reception performance which demonstrates an overall decrease in tag detection with range.

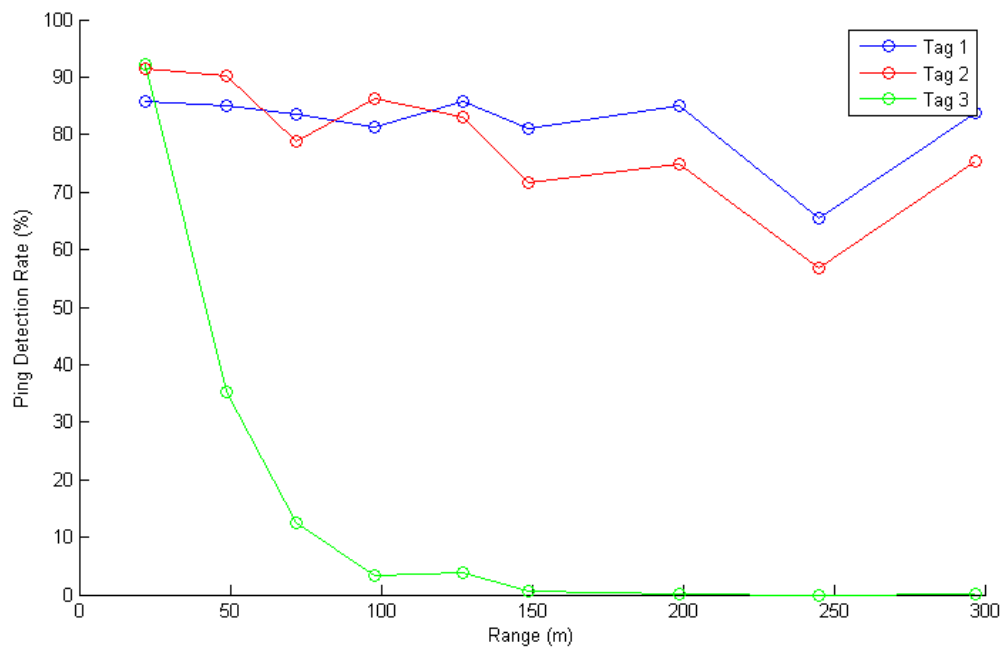


Figure C.3. Probability of ping detection versus range for the three acoustic tags deployed over the two week period. (Data courtesy of the Department of Fisheries, Western Australia)

The relationship between ping detections and separation distance for Tag 3 demonstrated a significant lack of range capability. This result is reflective of its low source power level (147 dB re 1 μPa^2 @ 1 m) compared to the other two tags, as well as possible complications due to its position on the seabed. The location of the second recorder was ideally suited to determine the signal characteristics at 100 m, as detection of Tag 3 had failed beyond this point. Analysis of the ambient noise recordings determined the existence of any signals from the acoustic tags and these results are shown later in Section C.4.

From the data, the receiver positioned 247 m from the acoustic tags was found to perform poorly overall, yielding a lesser number of detections than the receiver located at 297 m. As each of the receivers was deployed identically and in the same depth of water, this performance loss suggested other factors were preventing accurate detection. Possible causes include localised noise or even device malfunction. Another likely explanation would be possible directional sensitivity of the receivers.

In order to investigate the dependence of ping detections on the long-term environmental conditions, the number of detections for each tag code was grouped into four hour blocks. The detection rates were subsequently converted to a ratio with those measured at 0 m. Figure C.4 shows performance over the 16 day deployment period for all three tags. The starting point of the deployment was set at 12:00:00, 23rd November 2009. For ease of viewing, data from three ranges is included, accompanied by the average of all receivers. The average curve for Tag 3 only incorporated statistics from the first three receiver stations as others produced negligible detections as shown previously in Figure C.3.

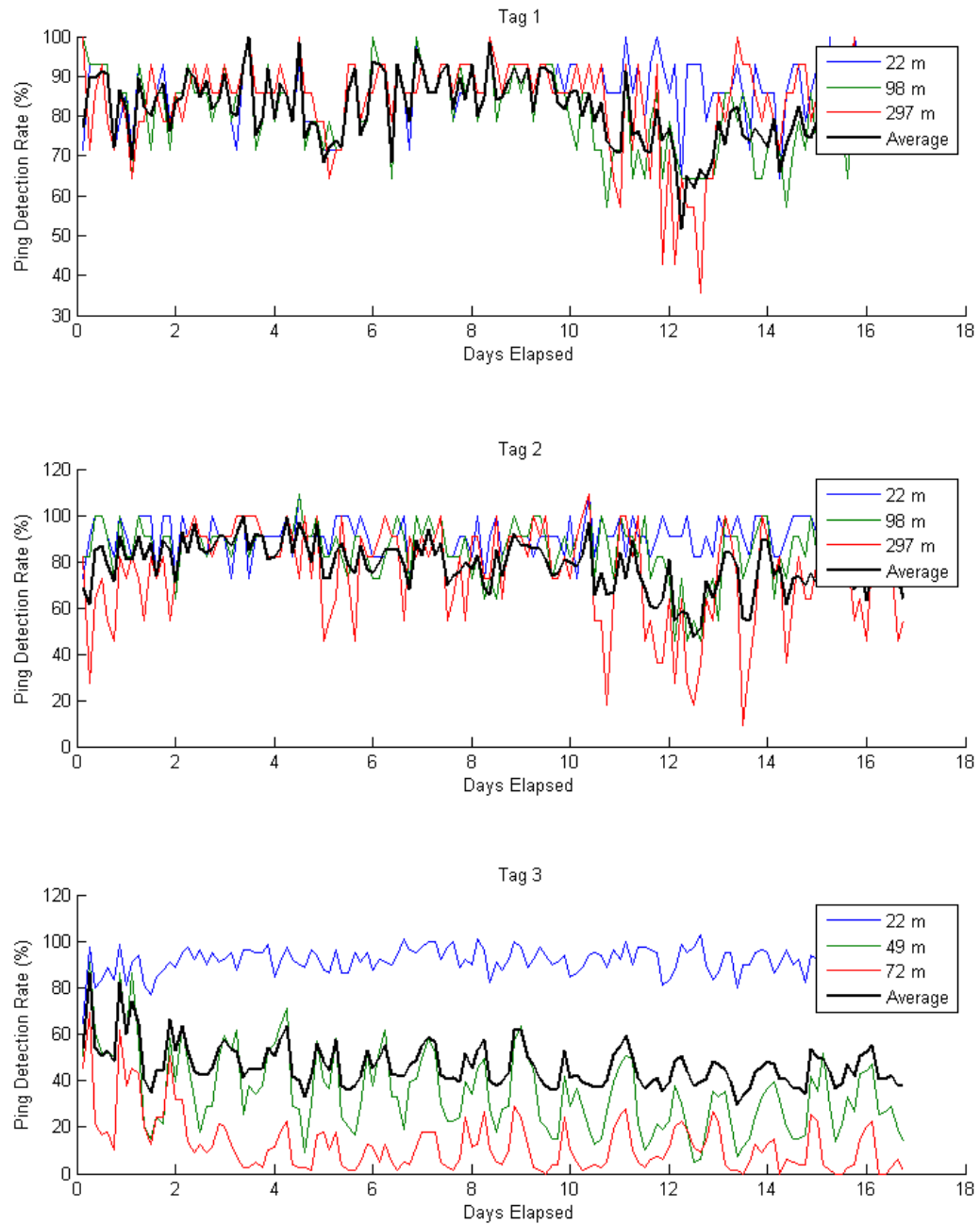


Figure C.4. Probability of ping detection versus time for the three acoustic tags deployed over the trial period. The graphs each include detections from various separation distances to indicate range dependency. Tag 3 (bottom) only included data from the closest three ranges as greater ranges yielded negligible detections.

Several areas of interest arose when investigating the temporal performance of the acoustic tag detection over the deployment period. A diurnal pattern was distinguishable in the detection rate for all sensors in the produced graphs. Furthermore, these fluctuations were more defined for the lower powered acoustic Tag 3, particularly for the receiver located 49 m from the source. These trends indicated a relationship existed between the detection probability and daily cycles of the environment such as noise contributions, wind and wave spectra and possibly vessel movement. However, at the shallow depth of the trial, it is unlikely that temperature variations would have significantly affected the propagation of the signal. For this deployment, the most likely cyclic influence was ambient noise originating at the surface such as wind and waves, and biological entities such as snapping shrimp.

When considering the higher powered acoustic tags, the influence of daily effects were reduced. Unfortunately, the relatively long time interval between pings for the higher powered tags restricted the resolution of the analysis. However, many periods of decreased performance were clearly observed for both tags. Approximately 10 days into the trial, the receivers were lowered by 1 m, to 3.0 m above the bottom. Additionally, the high powered tags were also lowered by 1 m, to 2.0 m and 2.4 m (tags 1 and 2 respectively) above the seabed. This repositioning was shown to have caused a negative performance affect at long ranges which is characterised by the general decrease in performance of tag 1 and 2 reception beyond 10 days (Figure C.4). The close-range receivers were relatively unaffected by the change, highlighted by little change in detections at 22 m.

C.3 Acoustic Noise Analysis

Ambient noise recordings by the logger located at the source continued for approximately 6 days before disk space limitations prevented further operation. The recorder located approximately 100 m from the tags operated for approximately 12 days before battery failure. Recordings from both devices involved two individual raw wave files for each half-hour period during the deployment. Unfortunately, data from the second recorder suffered from interference which resulted in approximately half of the data being unusable and the gain level uncertain. This error was likely due to inadequate grounding of the pre-amplifier input and other implications of this are shown later. Despite the loss of data, the recordings proved useful as only the first of two recordings was deemed unusable. As the corrupt recordings were interleaved with usable recordings over the trial, analysis over the full deployment period was still possible.

For measurements of the ambient noise, the recorder located at the source was used due to the higher reliability of the data. To calculate the ongoing noise spectrum each acoustic recording was analysed to detect any presence of ping energy, even if the probability of identification was small. This was done using a simple amplitude threshold with both recorders. The largest time period with no pings in each recording was then used to calculate the noise spectrum. A power spectral density (PSD) curve was calculated for each portion, giving an approximate frequency spacing of 350 Hz. As each file was time-stamped, a noise spectrogram could be established over the deployment time. For the recorder located at the source, two recordings were available for each half hour block. Making use of this redundancy, a weighted average PSD was calculated if pairs existed, factoring in the duration of the noise signal used for PSD calculation. The ambient noise spectrogram for the recorder located at the source is shown in Figure C.5. Additionally, a 1 kHz wide extract from the spectrogram at 69 kHz is presented, showing the ambient noise in the frequency band utilised by the acoustic tags. A clear diurnal cycle was discovered over a broad range of frequencies, indicating that the ambient noise was likely influenced by daily wind and wave fluctuations as well as snapping shrimp.

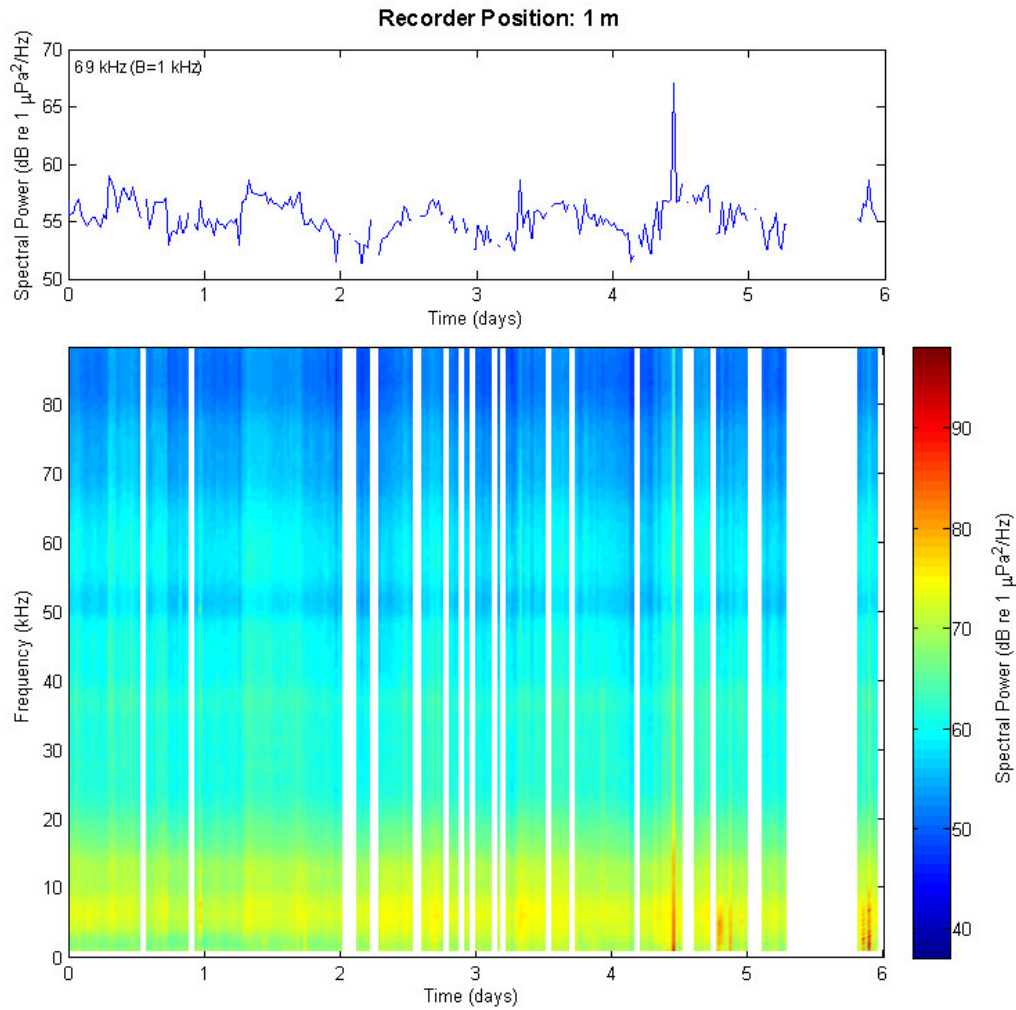


Figure C.5. Spectrogram (bottom) demonstrating the ambient noise over a period of approximately 5 days as observed by the acoustic recorder with the 69 kHz band extracted (top). The weighted average of the noise spectrum was produced from two recordings where available. Gaps indicate where the recording time was less than sufficient for noise analysis. Time elapsed is with reference to the trial starting point of mid-day.

A similar noise spectrum calculation was carried out for the longer range recorder, however, the gain of the system was found to be lower than expected due to the aforementioned fault in the pre-amplifier. To calibrate the values obtained from the recorder at 1 m, the ambient noise curves for three different periods were extracted for each location and compared, as shown in Figure C.6. Additional noise including electronic interference and an approximate gain discrepancy of 11 dB was discovered.

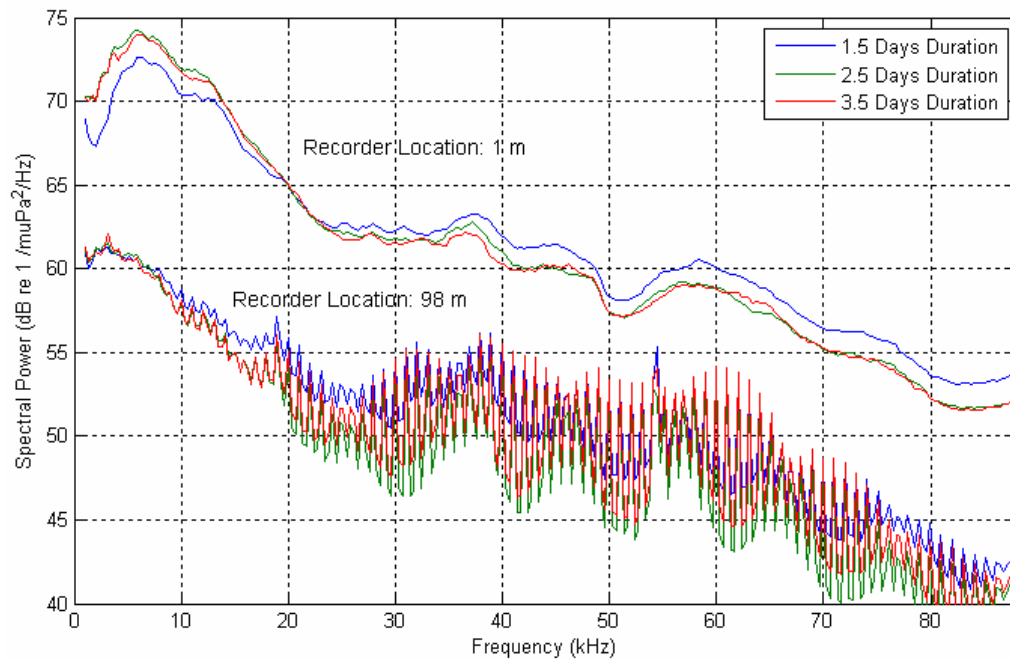


Figure C.6. Ambient noise power spectral density for a quiet period of the deployment (approximately 2 days elapsed) as observed by each acoustic recorder.

Recalibration of the longer range recorder was performed by applying the 11 dB discrepancy to the measured results. However, the overall integrity of the values obtained was somewhat questionable given the uncertainty in the cause of the interference and gain discrepancy. Additionally, electronic noise with a fundamental frequency of 1 kHz was shown to interfere with the recordings. Although the recording components were known to periodically cause interference in laboratory experiments at this frequency, the pre-amplifier shielding and metallic housing of the recorder was designed to minimise any electromagnetic interference. The presence of electronic interference suggested that the preamplifier was not adequately shielded from other electronic components. Additionally, the gain discrepancy supported a more likely explanation that the pre-amplifier was inadequately grounded which would also result in high electronic noise interference. Following application of the 11 dB offset, the ambient noise power over time was obtained for the recorder located 98 m from the tags and is shown in Figure C.7.

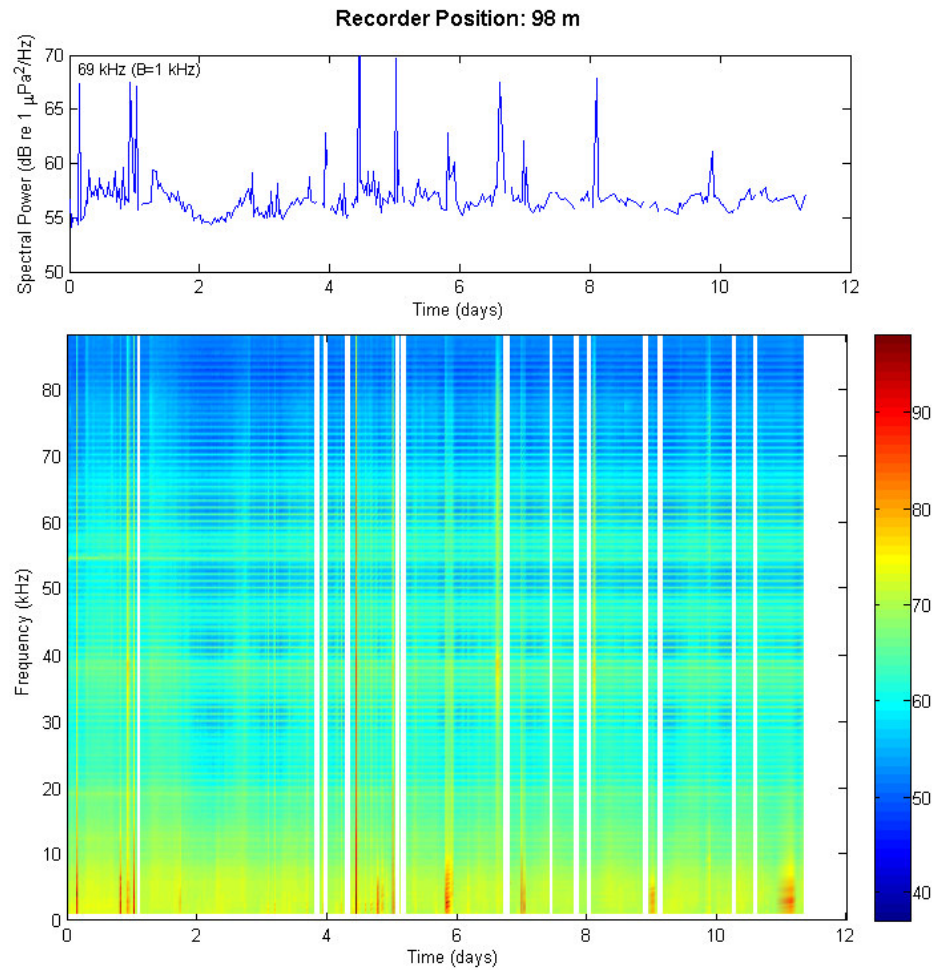


Figure C.7. Spectrogram (bottom) demonstrating the ambient noise over a period of approximately 5 days with the 69 kHz band extracted (top). These measurements were observed by the acoustic recorder 98 m from the acoustic tags include gain correction. Gaps indicate where the recording time was less than sufficient for noise analysis.

From the two noise spectrograms several key elements were present. Similarities visible in low frequencies, such as those at approximately 4.5 and 6 days were reflective of shipping noise which contributed unwanted energy to higher frequency bands. Additionally, the overall measured noise was shown to fluctuate with a diurnal cycle, likely caused by wind fluctuations and other daily events. Snapping shrimp were also a major contributor to broadband noise during this deployment as with others made off the Western Australian coast (Section 4.1). The effects of these high frequency noise components were of interest to the investigation, as the performance of the pingers was expected to depend on the SNR.

C.4 Acoustic Ping Detection

Ping detection was also performed using post-analysis of the ambient noise recordings at 0 and 98 m. Each pulse modulated ping was emitted at 69 kHz and with a pulse width of 10 ms. A 4th order Butterworth filter centred on the carrier frequency with a 100 Hz bandwidth was implemented to acquire the pinger signal for the detection algorithm. The mean power levels from each filter output were calculated over 2 ms blocks of data to obtain the envelope function for each recording. This result was then scaled using the sensitivity curve shown in Figure 3.1.3 and the gain of the acoustic recording hardware was applied. Figure C.8 shows the spectrogram and related filter output of one particular recording in which all three pingers were operating at close proximity to the recorder.

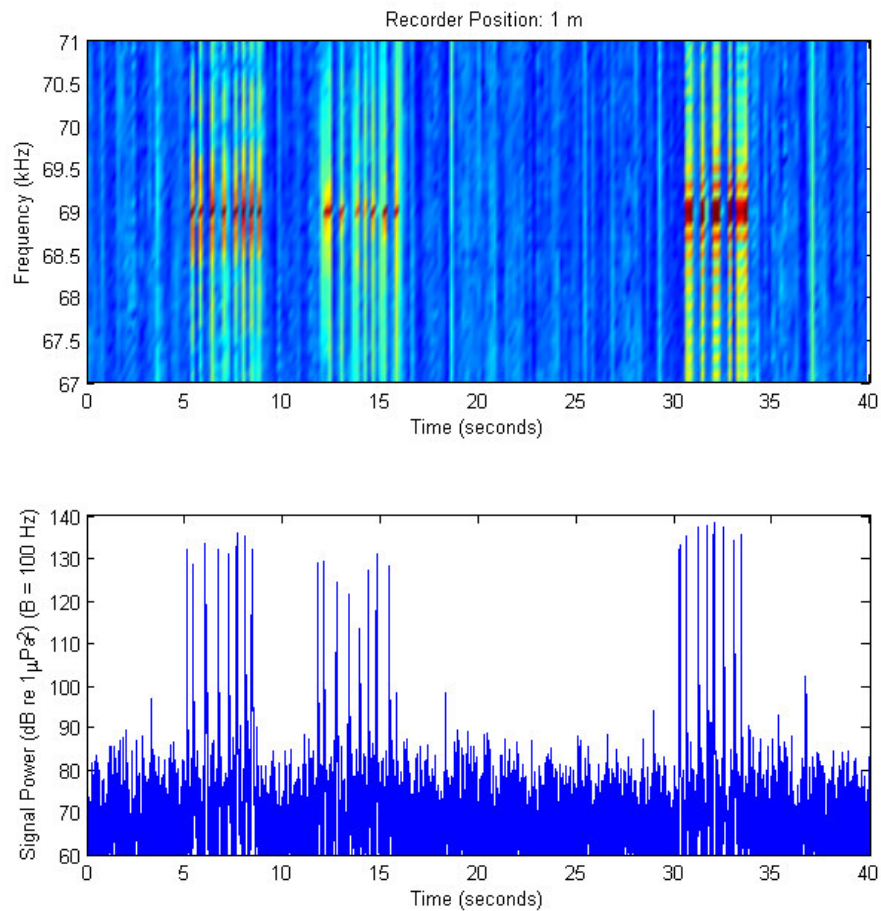


Figure C.8. Spectrogram of one recording using the recorder located at the source, demonstrating the reception of three separate and unique ping codes (top). Mean power versus time following filtering of the same recording (bottom).

The electronic noise of the long range recorder exhibited a fundamental frequency of 1 kHz which resulted in high levels of interference in the carrier band of 69 kHz. This is shown in Figure C.9 with a similar plot of three pings from the long range recorder. The modulation utilised by the acoustic tag was clearly shown to occupy the same frequency band as the electronic interference. The direct overlay of noise dramatically decreased the SNR and subsequent effectiveness of the detection algorithm for the recorder located at 98 m.

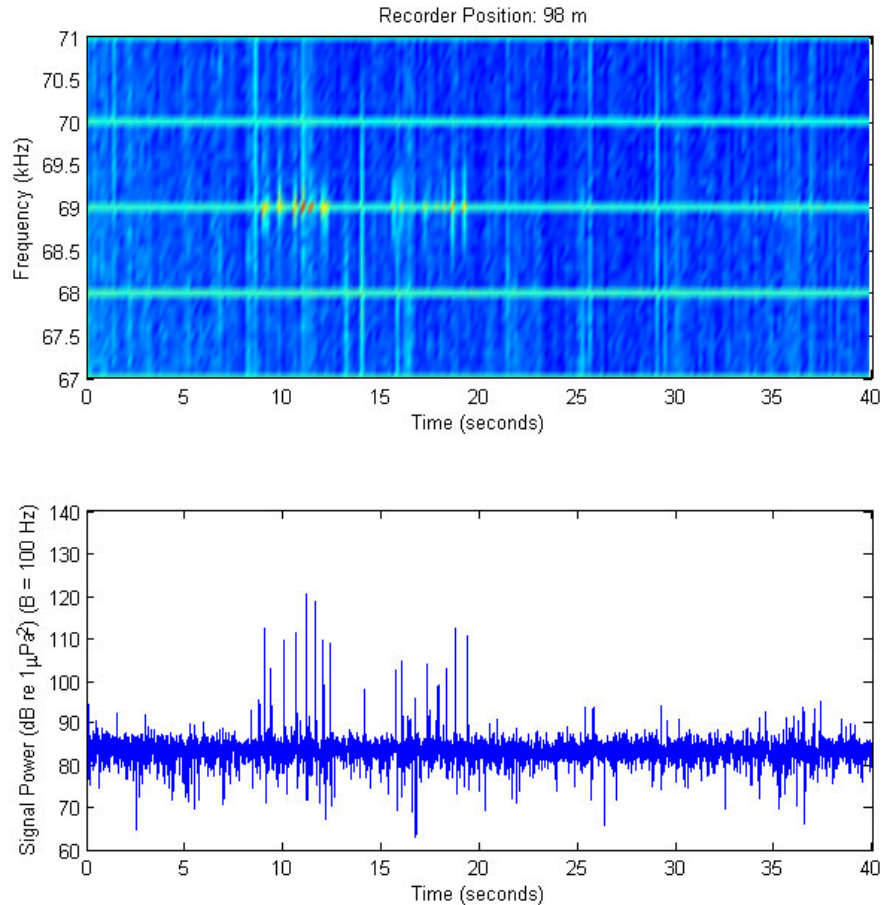


Figure C.9. Spectrogram of one recording using the recorder located 98 m from the acoustic tags, demonstrating the reception of three separate and unique ping codes (top). Mean power versus time following filtering of the same recording (bottom).

The transmission loss over 98 m resulted in a lack of reception for the third tag signal. In this particular recording the acoustic tags were shown to emit in the order of their output power, with the highest power first. Although the same order of pings appear in Figure C.9 the vertical discrepancy in tag positions resulted in unordered relative signal powers with the weakest tag located closest to the hydrophone.

After band-pass filtering and signal power calculation an envelope matched filter was applied. The envelope function for each of the three unique pingers was established by extracting measured data and using a threshold value to determine the location of each pulse. Reflections were then removed and a 10 ms pulse positioned accordingly, representing the template of the expected envelope function. Figure C.10 shows the three major steps from acquisition of the known pinger to the final representation of the template signal.

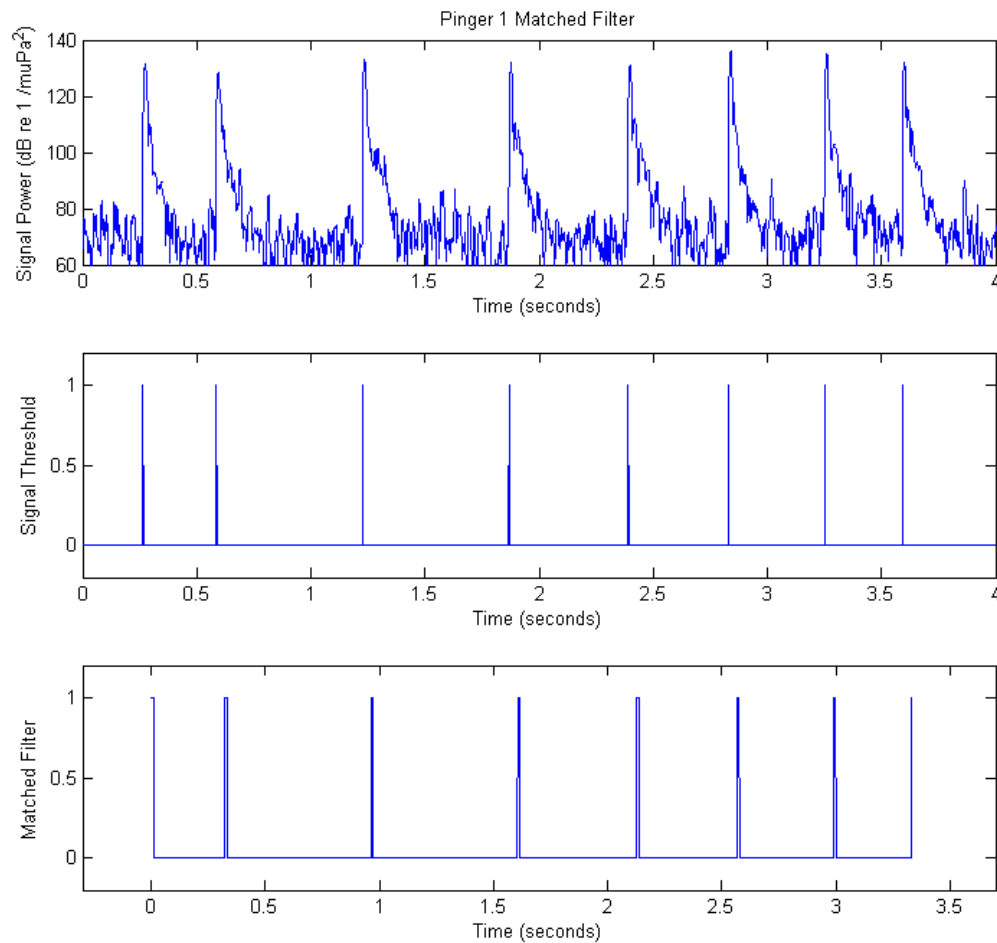


Figure C.10. Step-by-step construction of the matched filters used in the Cockburn Sound study. First, the known received signal is collected (top). Peaks are then distinguished using the gradient (middle). Finally, reflections are removed using reasonable thresholds to obtain an 8 pulse ping which is normalised and trimmed (bottom).

Following design, each template function was cross correlated with the band-pass filtered data. High pulses were produced when the templates for each ping code were aligned. An example is demonstrated in Figure C.11 which plots the matched filter output for the three different pinger codes on the recording shown in Figure C.10

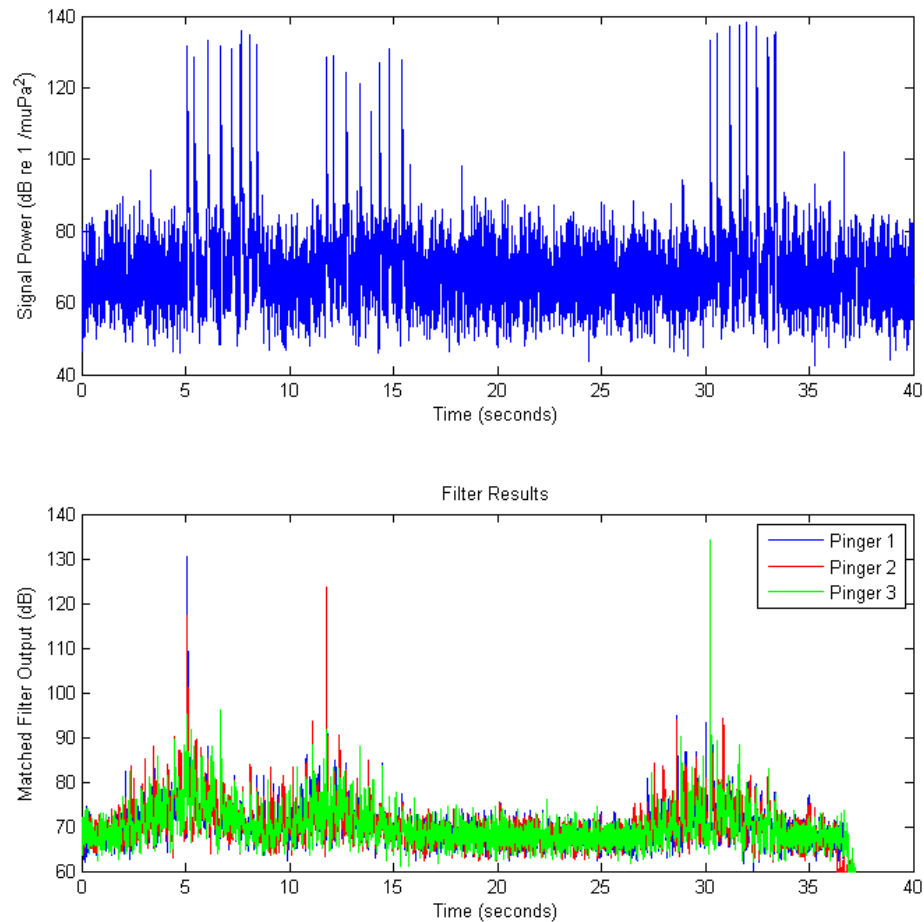


Figure C.11. Matched filter output showing pulses representing successful detection of the three unique tags in a single recording. The similarities between the ping codes resulted in a secondary peak for tag 2 at the location of the primary peak of tag 1.

An investigation of the effects of cross-talk between pingers was conducted by looking at a particular recording where cross-talk had occurred and analysing the output of the correlation. The detection algorithm was performed adequately when two tags were transmitting at the same time. This can be seen in Figure C.12 which shows the band pass filter output followed by the output of the envelope detector. However, the receiving devices designed for the tags likely utilised a different method for receiving pings.

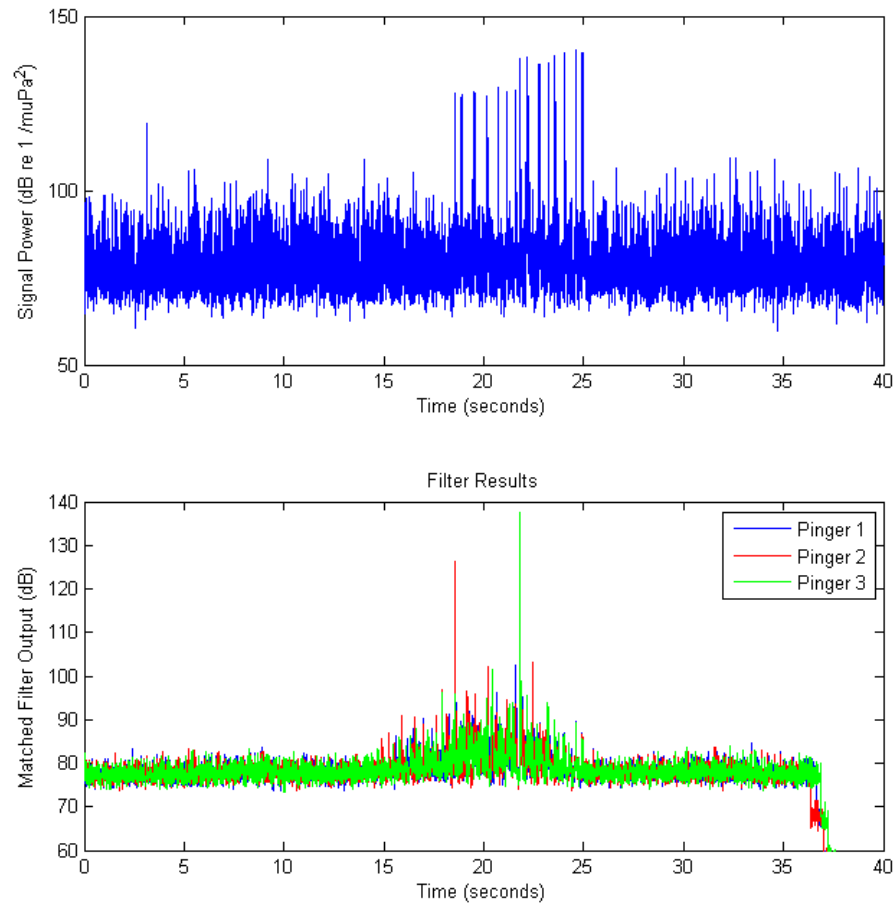


Figure C.12. Matched filter output showing pulses representing successful detection of two tags where pulse codes have overlapped. The two pings were successfully identified despite the respective codes crossing over.

Following the envelope detection, an algorithm was developed to make decisions of whether or not the correlation result corresponded to a ping. This was necessary due to the low probability of each recording containing all three pings. Additionally, the algorithm assumed that only one ping for each tag could occur over each recording given the time between emissions. First, the position of the maximum for each matched filter output over each recording was extracted. Where two or more peaks were located within a half of the width of the filter, the lower output was discarded as it was likely a secondary correlation with a similar code. By using the cross correlation peaks the decision algorithm was synchronised to the corresponding waveform in the band pass filter output. The height of the expected pulses in the original data was then extracted to obtain the median noise and then calculate a

suitable SNR. Using the minimum pulse height provided greater reliability in separating out false positives due to shrimp clicks and similarly coded pings. These unwanted detections likely involved one or more absent peaks in the code and were immediately separated out by the algorithm. The separation of filter peaks is shown in Figure C.13, highlighting regions of probable detections (top region) and null detections (bottom region). This separation is particularly evident for the recorder located closest to the tags at 1 m.

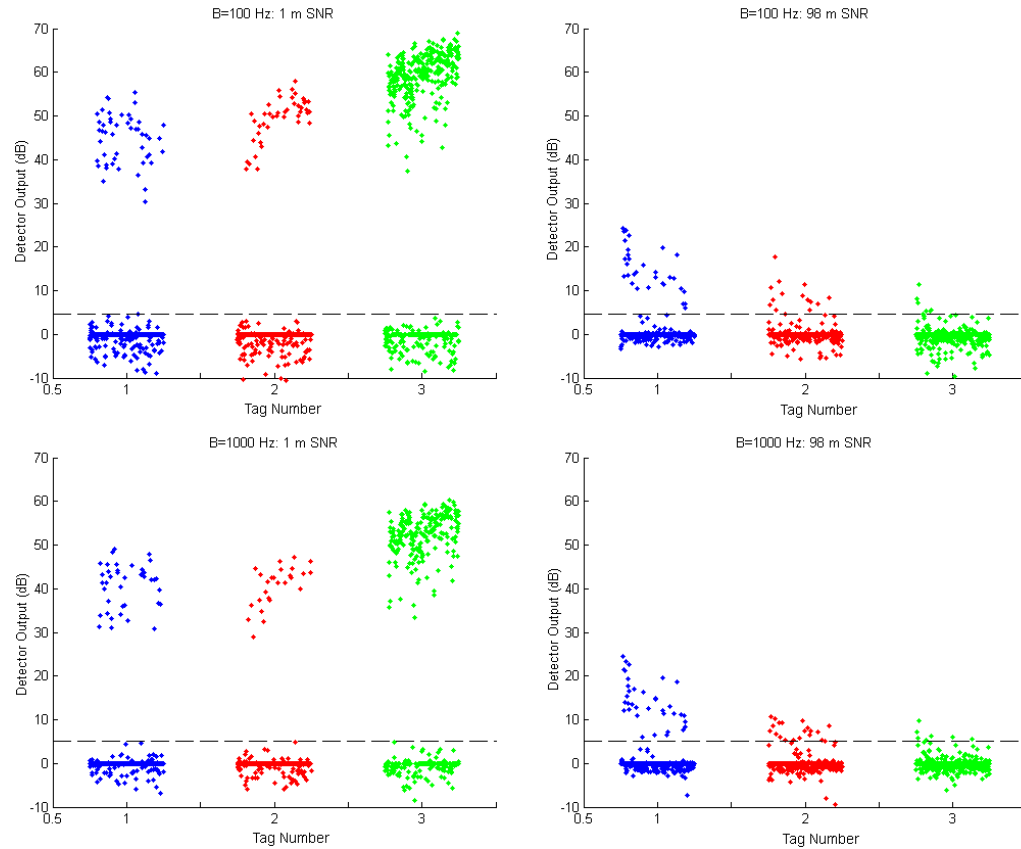


Figure C.13. Detection algorithm output (SNR of minimum amplitude pulse) which operated on each maximum of the matched filter (cross correlation) output. Blue, Red and Green markers denote Tags 1, 2 and 3 respectively. Analysis of recordings in close proximity to the tags demonstrates separation which distinguishes detections from the noise (left). When investigating recordings at 98 m, the same distinction is no longer apparent (right).

A detection threshold was calculated as the mean plus three times the standard deviation of the non-zero elements defined in the lower portion of the 1 m algorithm output. On closer analysis, any values above this threshold were found to be detections of the ping code at close range. Such a distinction between these decisions was not found in the recordings at 98 m due to the transmission loss over the

propagation path. It was not expected that the noise or propagation characteristics would have been distinctly different at either recording site. By assuming a similar environment for both recorders, the threshold obtained using the data at 1 m was used for the decisions in the filter output for 98 m. A summary of the results from this investigation is shown in Table C.2.

In an attempt to increase the separation of decisions and subsequent accuracy, the effect of modifying parameters of the detection algorithm was investigated. Whilst the optimum detection bandwidth in ideal conditions was 100 Hz, it was possible that deviations in tag frequency and Doppler effects may have influenced the output SNR. As a precaution, a similar investigation was performed using data from a band pass filter with a bandwidth of 1000 Hz.

Additionally, the results obtained using the SNR measurements alone were further optimised by factoring in the Standard Deviation (SD) of the peak levels during each pulse of each ping. The SNR was scaled by SD which represented the amplitude spread of peaks and subsequently the quality of the detections. By including the SD with the SNR, it was anticipated that further separation between detections and nulls could be established. The results of this improvement as well as the widened filter bandwidth are shown in Figure C.14.

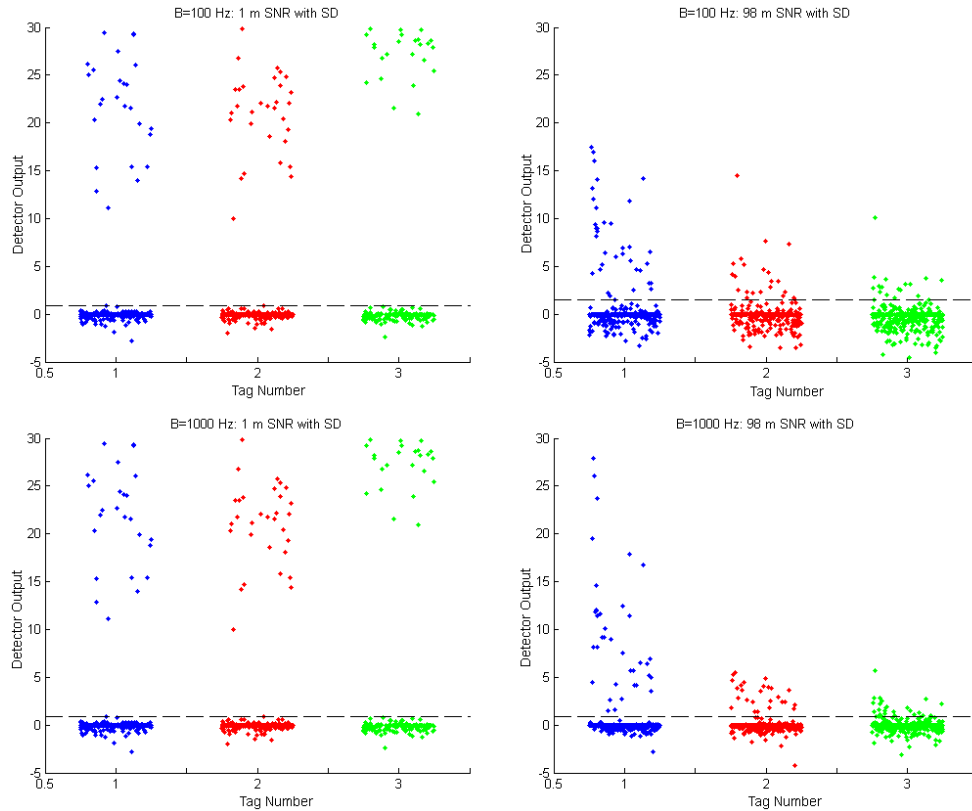


Figure C.14. Results of the improved detection algorithm which operated on each maximum of the matched filter (cross correlation) output. The minimum amplitude pulse SNR was divided by the mean SD of the pulse heights for each detection.

Data forming both sets of scatter plots demonstrated the difficulty in detecting pings from the third and weakest acoustic tag at 98 m. This difficulty reflected the negligible detection rate as recorded by the tag receiver at the same location. Whilst utilising the SNR alone produced a clear difference between detected pings and nulls at close range, the performance of the decision algorithm was improved by factoring in the deviation of the pulse heights and widening the bandwidth of the filter. Table C.2 demonstrates the performance improvement for each change to the algorithm. These results are compared to both the output parameters specified by the manufacturer of the tags, as well as the detections observable at 1 m by the recorder. The number of pings transmitted was unknown due to the uncertainty in ping timing. Regardless, data pertaining to the exact number of pings would be of no use for acoustic comparison as the total recording time for each recorder was unreliable. To best compare the results, the ratio between detections of different tags was compared.

Table C.2. Number of detections as observed by each recorder compared to the actual amount of pings transmitted by the tags. Also shown is the detection ratio with Tag 2 for comparison with the expected ratio shown in Table C.1.

Tag	Ratio of lowest ping frequency	Detections 1 m, 100 Hz SNR only (Ratio)	Detections 98 m, 100 Hz SNR only (Ratio)	Detections 98 m, 1000 Hz SNR only (Ratio)	Detections 98 m, 100 Hz SNR+SD (Ratio)	Detections 98 m, 1000 Hz SNR+SD (Ratio)
1	1.2	49 (1.2)	32 (2.2)	36 (1.8)	36 (1.6)	39 (1.5)
2	1.0	42 (1.0)	14 (1.0)	20 (1.0)	22 (1.0)	26 (1.0)
3	7.2	295 (7.0)	7 (0.5)	7 (0.4)	19 (0.9)	24 (0.9)

It was found during the analysis that the most efficient detection algorithm involved use of a higher filter bandwidth as well as factoring in the pulse height deviation. When the best results obtained at range were compared to those at the source, Tag 1 was shown to have a higher ratio of detections. This correlated with its stronger source level implying a relationship between the SNR and number of detections. Such a suggestion was supported by the much lower ratio of detections for Tag 3 where the overall lack of signal power reaching the receiver was shown to have a detrimental effect on the reception rate.

The maximum received signal levels were calculated for each of the three pingers. Calculations were based on the median of the five highest SNR measurements performed for each tag at both recorders. The results are shown in Table C.3

Table C.3. Recorded signal levels for each acoustic tag compared to the source level given in their description. (100 Hz Bandwidth)

Pinger Label	Source Level (specification) (dB re 1 μ Pa @ 1 m)	Received at 1 m (horizontal distance) (dB re 1 μ Pa)	Received at 98 m (horizontal distance) (dB re 1 μ Pa)
Tag 1 "V16-4H"	158	135	117
Tag 2 "V16-6L"	153	133	113
Tag 3 "V9-1H"	147	142	107

The received levels observed by the recorder at 1 m were greatly affected by the height of the sensors in the water column. As Tag 3 was situated on the sea floor with the hydrophone, the received levels were much higher. Received levels from the other two pingers located approximately 2 m away were subsequently lower. Due to the uncertainty in the absolute positions of the tags and receivers at close range, the observed levels could not be corrected to 1 m.

The levels received at 98 m correlated strongly with one other, exhibiting a common transmission loss of approximately 40 dB. A prediction of the attenuation over this path would involve a combination of spherical and cylindrical spreading and absorption into the water column and seabed. Assuming a direct path, the absorption of energy into the water column over 98 was calculated using Equation A.6 to be approximately 2.5 dB. The remaining TL was likely a mixture of spherical (Equation A.4) and cylindrical (Equation A.5) spreading which gives a contribution ranging between 20 – 40 dB.

Other factors not included in the detection analysis include possible timing problems. Given the temporal changes in the sea state, changes in the propagation characteristics may have caused the arrival times of the signals to vary slightly during reception. Given a 10 ms pulse with a strict matched filter template, a slight shift in the arrival time of acoustic energy during a ping lasting approximately 4 s may have resulted in no detection.

C.5 Reception Trends and Comparisons

The long-term trends regarding ambient noise and ping detections were compared to investigate any correlations between data sets. Firstly, the trends regarding the ambient noise were compared for each recorder. The average spectral energy within a bandwidth of approximately 300 Hz centred on 69.5 kHz was compared to the levels found overall as demonstrated in Figure C.15. The 500 Hz offset was applied to avoid the majority of spectral interference present at each 1 kHz interval. The effect of avoiding the electronic noise was demonstrated to enhance the clarity of the trends when compared to the broadband PSD.

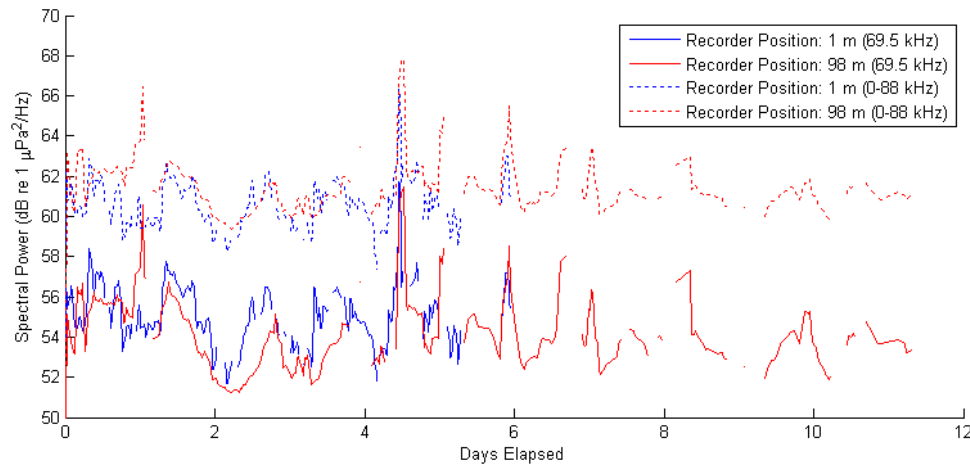


Figure C.15. Noise trends as measured by both ambient noise recorders showing measured narrowband and broadband energy.

Measured noise levels were significantly lower at the carrier frequency as expected, given the noise prediction curves and absorption characteristics of high frequencies. Diurnal fluctuations were observed at both recorders with noise peaks occurring over the middle of the night and the majority of troughs occurring at approximately 13:00 - 14:00 each day. These cycles were likely influenced by daily wind fluctuations; however, wind data was not available to confirm this. Due to the shallow and warm deployment environment, snapping shrimp were expected to contribute to the peaks exhibited during the evening as found in previous studies. Consistent with findings from Legg (2009) during a 24 hour study, the broadband noise was shown to exhibit two peaks at sunrise and sunset along with an overall increase in power during the evening.

The temporal resolution of the recorder detections prohibited a direct comparison with the overall success probability due to the large time between pings for the high powered tags. Whilst Tag 3 was likely to emit during one of the two recordings over each period, the overall lack of SNR prevented adequate detection throughout the majority of the trial. However, an investigation into the average received power over time was conducted. This analysis is shown in Figure C.16 which plots the measured signal power at each detection (SNR + SD). Received levels are given for a filter bandwidth of 1000 Hz where the best detection probability was obtained. The measurements were also compared to the overall power for each recording at 98 m of which a negligible amount contained pings. For the purposes of this study, this mean power measurement was considered the ambient noise floor as pings occupied a very small proportion of each recording.

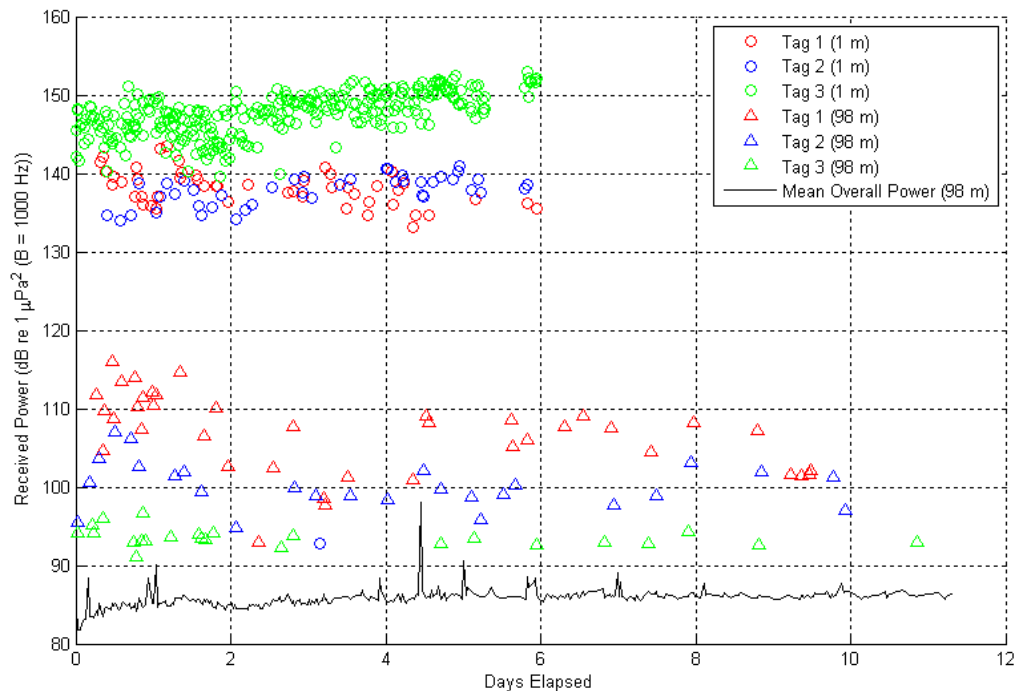


Figure C.16. Recorded signal power for ping detections made by the ambient noise recorders. The mean power for the recorder located at 98 m was considered the noise floor for this study as pings occupied a negligible fraction of the recordings.

When investigating the trends observed at 1 m, the pings emitted from Tag 3 were shown to yield a slight upward increase in detections over time. It is not known why this increase was observed. An upward trend in received intensity was also observed with the second closest pinger (Tag 2). When investigating the trends observed at 98 m, a large proportion of detections were made within the first two days of the deployment. The increase of detection rate was likely due to the lower observed narrowband noise during that time. This result suggested that electrical interference increased in amplitude during the first two days of the deployment, possibly due to the change in disk writing characteristics as the memory was written. The subsequent increase in ambient noise produced a lower detection rate throughout the rest of the deployment. However, the received signal strength was typically higher in the first days of the deployment than for the rest of the trial. The particular cause of this initial stronger signal strength (approximately 5 dB) was unknown.

Finally, a cross-comparison between the recorded ambient noise and the performance of the receivers was conducted. This investigation was performed to determine the effects of the ambient noise on ping detection over the deployment period. A close correlation was discovered between fluctuations in reception levels and the ambient noise. This comparison is shown in Figure C.17 which shows the detection failure rate compared with the ambient noise as measured over 5 days by the 1 m recorder. A similar correlation was found when comparing noise levels at the long range receiver as well as when using other receiver statistics. However, the recorder at 1 m exhibited significantly less electronic noise and was considered more suitable for this analysis. Additionally, the dynamic range of performance statistics was maximised with Tag 3 at 49 m from the receiver, yielding the most suitable resolution for a temporal investigation.

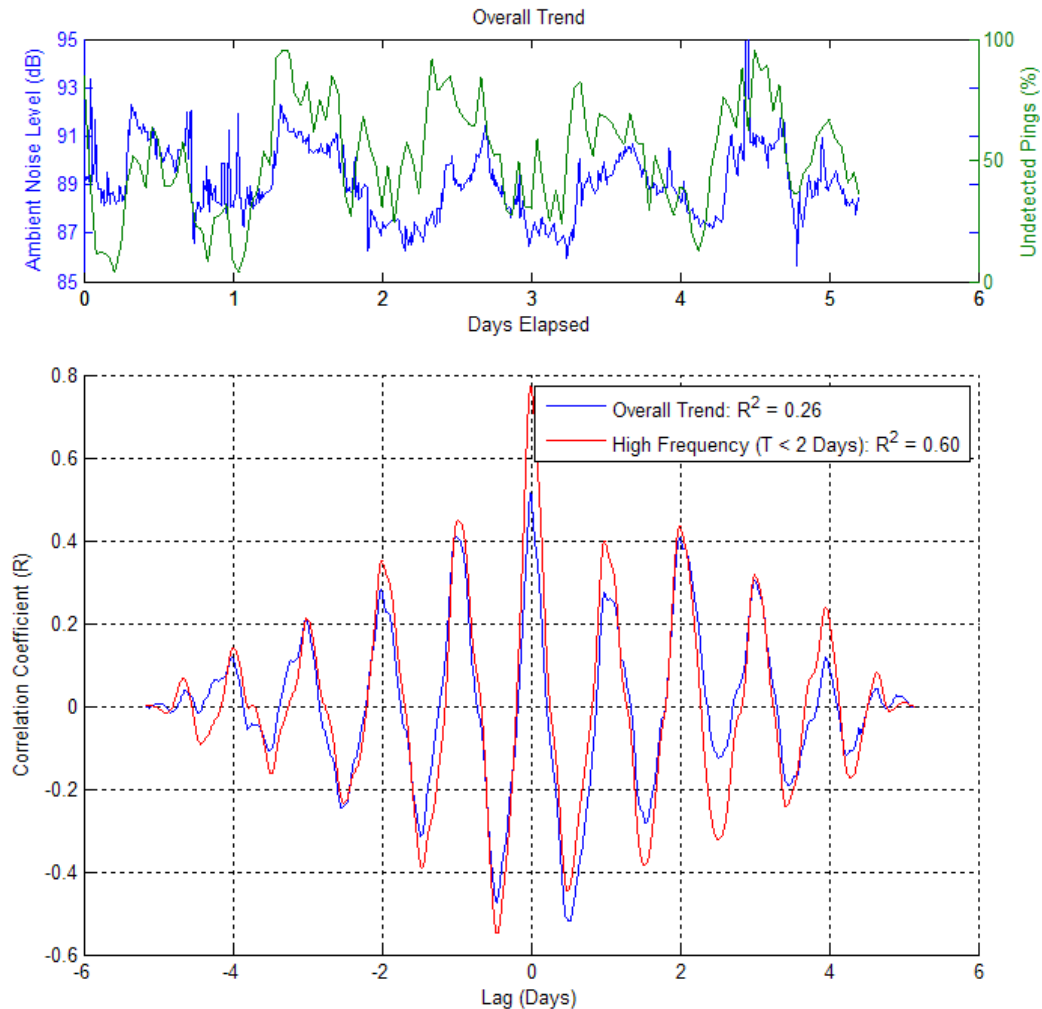


Figure C.17. Comparison and cross correlation of ambient noise power measured by the ambient noise recorder located at the source and the ping detection failure rate of the receiver located 49 m from the source.

A strong relationship was found between the ambient noise present in the channel and the detection failures as observed with Tag 3 at 49 m. The twin peaks (dusk and dawn) observed in the noise for each day was also present in the detection trend, suggesting a snapping shrimp influence on the detection probability. A notable period where the relationship was not as well correlated was found within the first two days of deployment. The overall statistics for Tag 3 during this period exhibited above average performance for ping detection with a significant offset. This performance change may have been due to changes in the orientation of the sensors which would have occurred as a consequence of changes in current. Another possible explanation for the above average performance of the receivers could be fluctuations

in the output power of the tags mid-way through the trial. This explanation would also account for the higher than average signal levels recorded at 98 m with the underwater acoustic recorder. Similar relationships were demonstrated with other tags and receivers when compared to the noise levels, confirming a strong correlation between the ambient noise and the detection probability.

C.6 *Summary*

This experiment was conducted to accompany the deployment of three acoustic pinging tags and help categorise their performance. Two of the tags were found to operate effectively over the full tested range whilst a lower powered third tag was ineffective beyond a distance of approximately 98 m. A decision algorithm applied to ambient noise recordings from this position performed similarly to a purpose built receiver. When investigating the ratio of received pings, the higher powered tags were adequately detected by the algorithm, whilst performance regarding Tag 3 was significantly limited. Approximately 10 days into the trial, the purpose built receivers were repositioned with the distance from the bottom changed from 4 m to 3 m. Additionally, the acoustic tags were moved from 2.4 m and 2.0 m to 1.4 m and 1.0 m from the bottom respectively. These changes had a negative effect on the performance of the receivers at long range, illustrating the dependence of operational depth on transmission characteristics. However, it is possible that only one of these modifications induced complications in receiving, suggesting further study is needed.

When investigating the long-term trends exhibited by the acoustic recorders, a correlation was found between the ambient noise levels and overall performance of the purpose built receivers. Statistics from both measurements were shown to fluctuate in a diurnal pattern. The dependence of performance on noise characteristics was established with the majority of noise likely due to snapping shrimp, typically increasing during the evenings.

Appendix D

Additional Equipment Information

D.1 Trialled Underwater Acoustic Modems

D.1.1 DSPComm: The AquaComm

For initial testing of the hardware, software and analysis techniques, a locally manufactured short range modem was used. The AquaComm modem, developed by DSPComm in Western Australia uses direct sequence spread spectrum (DSSS) over a bandwidth of 16 - 30 kHz to achieve ranges of up to 3 km in optimum conditions. Different modulation modes allow for speeds of either 100 or 480 bps depending on conditions with CRC16 error detection techniques. The AquaComm modem was unpackaged and provided by CSIRO as a stacked PCB component. The device was interfaced with the MCS using the alternative UART with power routed directly from the main power source. The MCS dimensions allowed for the direct attachment of the OEM AquaComm boards. The supplied transducer was 70 mm in diameter, 40 mm in height with an omnidirectional beam pattern.

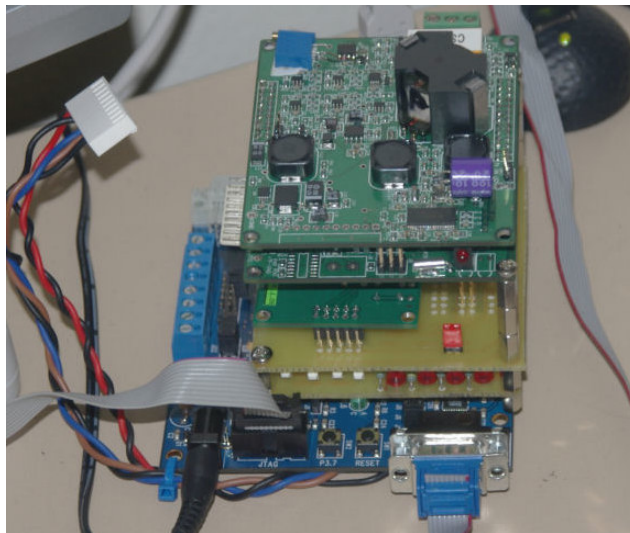


Figure D.1. Photo of assembled Modem Control Stack with attached AquaComm boards mounted as the two upper PCBs.

D.1.2 Aquatec Group Limited: The AQUAmodem

The primary modem used for evaluating the performance of underwater acoustic communications was a long range, low frequency modem. Developed by Aquatec Group Limited in the United Kingdom, the AQUAmodem operates using Frequency Shift Keying (FSK) based methods and Reed-Solomon (RS) encoding for error correction. The modem operates over a frequency range of 7 – 11 kHz and has a data transfer rate of 100 – 400 bps. The electronics were situated in a deep water metal housing, capable of depths up to 1000 m. A high powered transducer with a hemispherical beam pattern was utilised with the whole unit having a range capability of over 20 km.

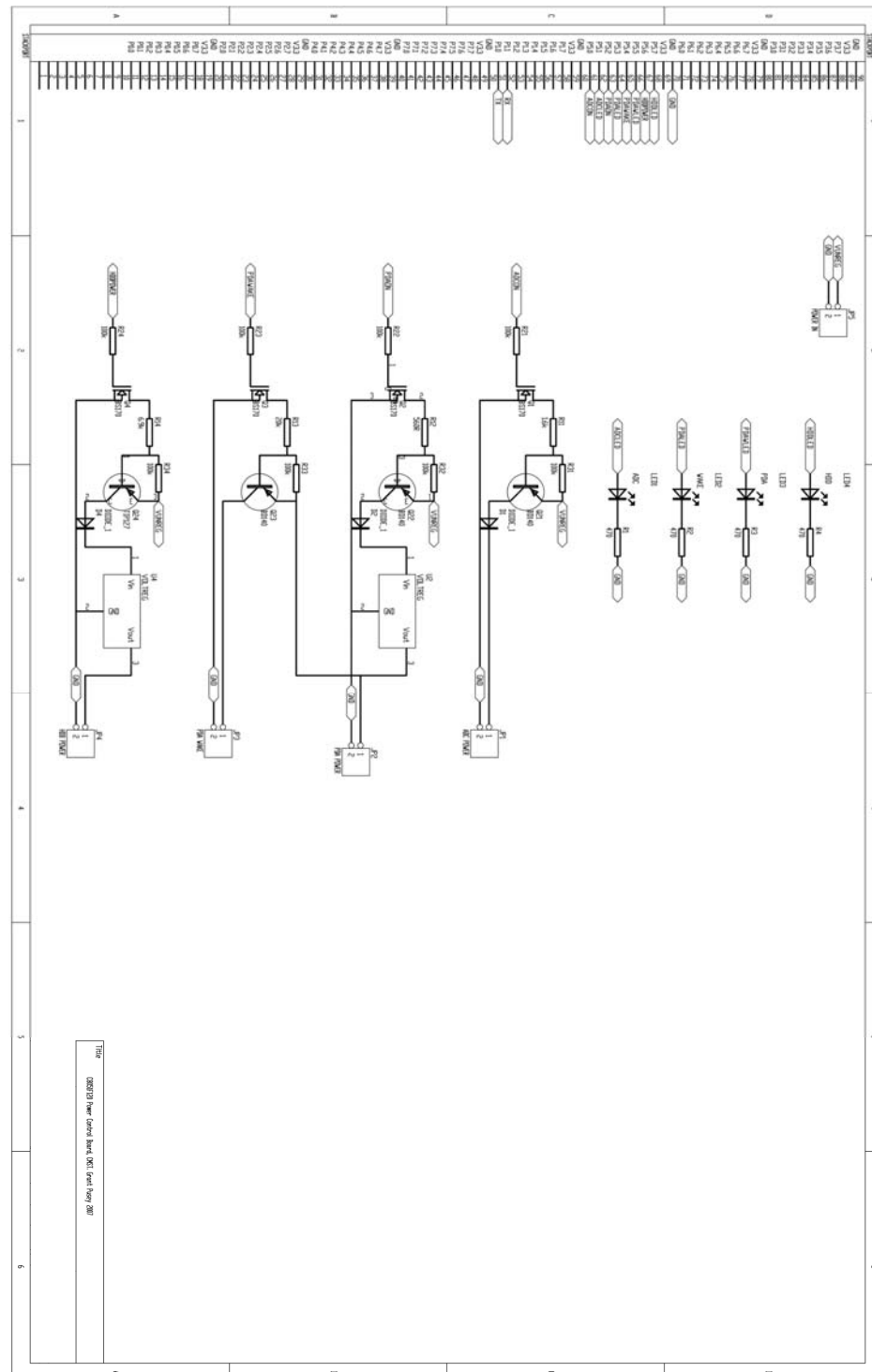
The AQUAmodem was designed for long-term deployment in Arctic waters for environmental monitoring in the DAMOCLES and ACOBAR projects. It has a low power sleep circuit which removed the need for the MCS to control its power consumption. Power and communication were routed using a subsea cable attached to an 8 pin locking connector. A cooperative relationship with the manufacturer of the AQUAmodem allowed customisation and updates of the modem hardware and software to better suit the needs of the trials. This also helped in obtaining alternative data sets and performing more experiments due to a mutual interest in the results.



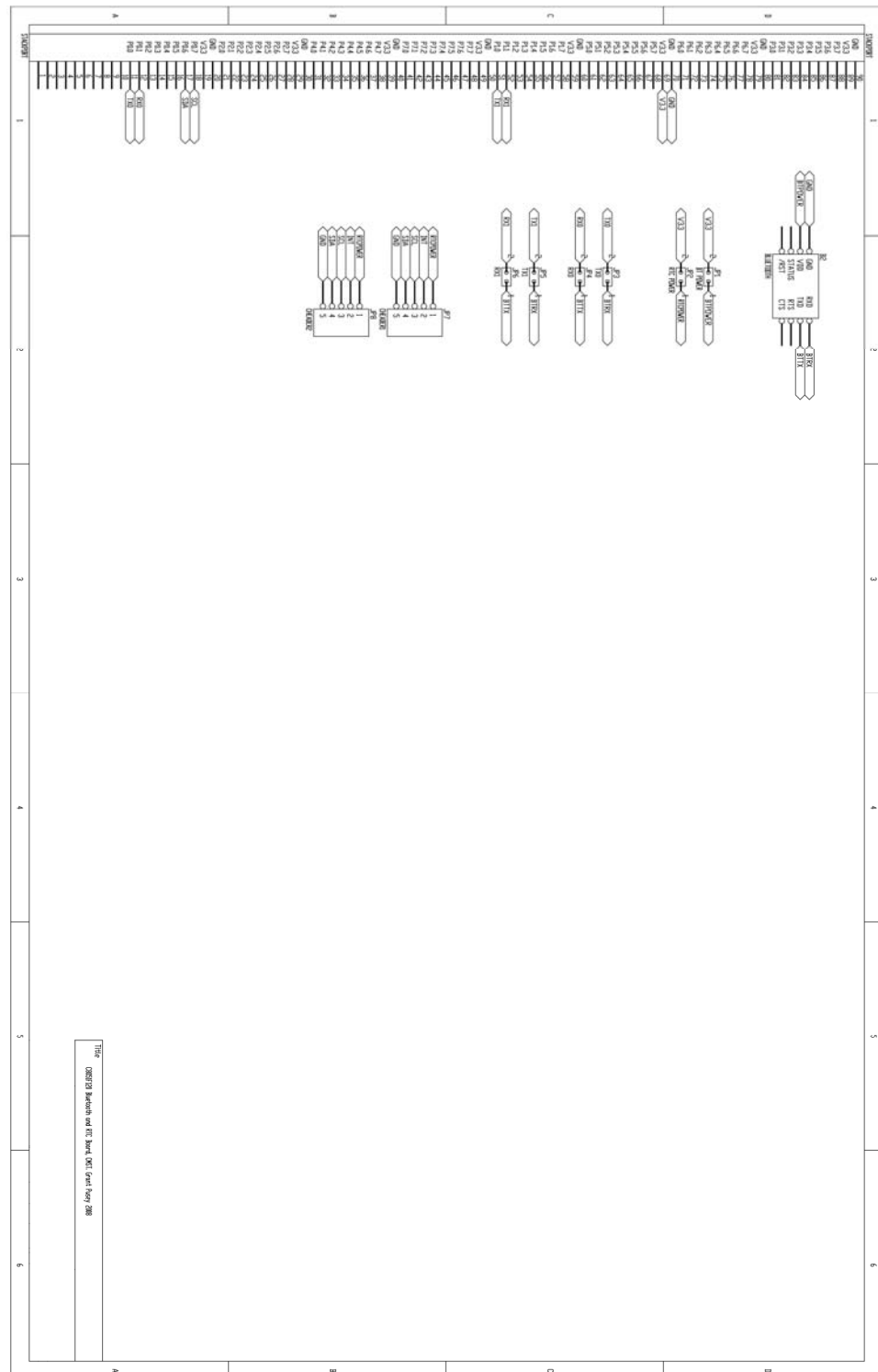
Figure D.2. Photo of the AQUAmodem fitted to the deep water housing for one of the experiments. A protective cage was attached to the transducer.

D.2 MCS Stackable Board Schematics

The following schematic describes the MCS power control board (Section 3.1.2). This board switched outputs of specific voltage ports based on the pin output from the interfaced C8051F120 microcontroller.

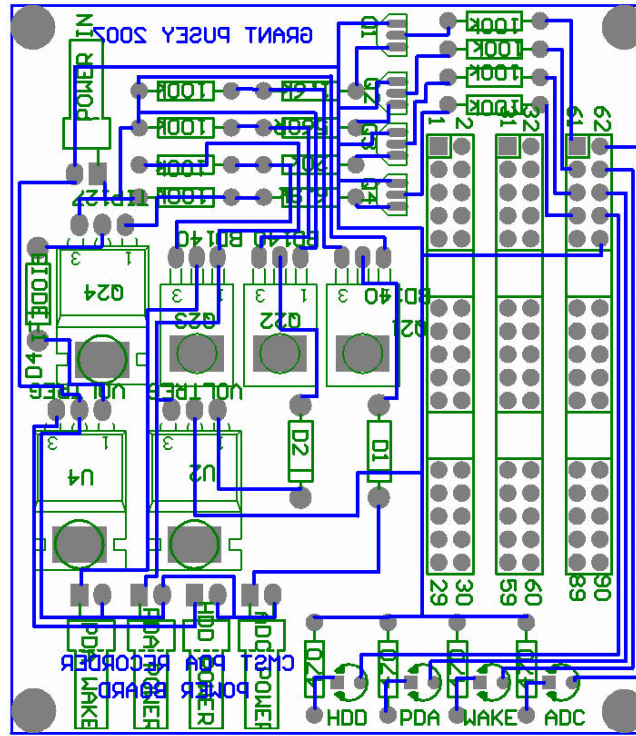


The following schematic describes the MCS communications board (Section 3.1.2). This board interfaced a Bluetooth module with either UART of the C8051F120 microcontroller. The RTC was also routed to the microcontroller SPI pins via this board.

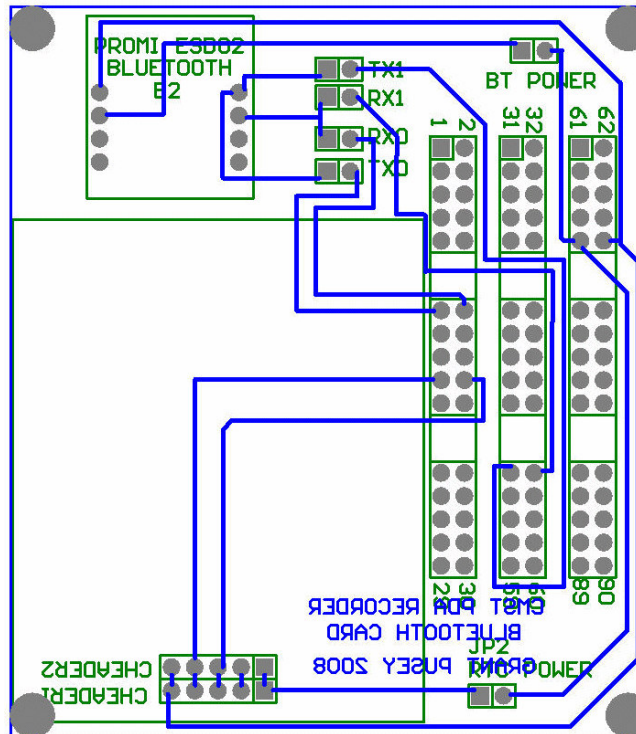


D.3 MCS PCB Designs

D.3.1 Power Control PCB Design



D.3.2 Communications and RTC PCB Design



D.4 *ModCon Routines*

The following routines were part of the MCS software package, *ModCon*, discussed in Section 3.2.1. For access to the source code, please contact the author.

Core Commands

<code>print2serial</code>	Takes a string array <code>c</code> and transfers it to the relevant serial port denoted by input <code>uart</code> which can be 0 or 1 on the microcontroller. <code>enter</code> specifies whether or not to send a linefeed after the transmission. A <code>uart</code> value of '9' corresponds to an internal function and no transmission will be made. A <code>uart</code> value of anything else will result in the string being transmitted on both ports.
<code>wait</code>	Halts the software for number of cycles denoted by input <code>towait</code> . Used to give suitable delay times to wait for external hardware to respond

Time and Schedule Commands

<code>do_comparison</code>	Used in deployment mode A. Compares the current date and time to the date and time set on the alarm. If there is a match, power is applied to all the devices and the PDA wakeup is initiated.
<code>LCDdate</code>	Prints the date to the LCD module from the current cursor position with the following format: <code>DD/MM/YY</code>
<code>LCDtime</code>	Prints the time to the LCD module from the current cursor position with the following format: <code>HH:MM:SS</code>
<code>printTime</code>	Returns the current date and time to the serial port the command was received from in the format: <code>DD/MM/YY, HH:MM:SS</code> This can be followed by a line feed, dependant on the

	newline input flag.
<i>do_quicktime</i>	Uses printTime to provide date and time information to the UART specified, followed by a line feed.
<i>do_gettime</i>	Employed to operate in deployment mode A. Provides the Date and Time. Following this is the internal alarm of the microcontroller used for direct comparison with the clock: Currently> DD/MM/YY HH:MM:SS Alarm> DD/MM/YY HH:MM:SS
<i>do_pushtime</i>	Sends the DATE_TIME_PUSH command to the PDALogger software followed by the date and time information currently on the RTC. This information synchronises the PDA clock with the RTC onboard the MCS.
<i>do_settime</i>	Assumes the input string cs in the format settime_DDMMYYHHMMSS and sets the RTC accordingly. Responds to the serial port to confirm the change
<i>do_alarmon</i>	Used for deployment mode A. Assumes the input string cs in the format alarmon_DDMMYYHHMMSS and sets an alarm for comparison. The PDA is then put into sleep mode using a command interpreted by PDALogger and an alarm flag, including a comparison into the main program loop.

Power Control Functions

<i>do_sleep</i>	Puts the C8051F120 Microcontroller into a “sleep” state as defined by the specification sheet
<i>do_idle</i>	Puts the C8051F120 Microcontroller into an “idle” state as defined by the specification sheet
<i>do_pda_on</i>	Activates output pin to power control board to supply power to the PDA.

<i>do_pda_off</i>	Deactivates output pin to power control board to remove power from the PDA.
<i>do_hdd_on</i>	Activates output pin to power control board to supply power to the HDD.
<i>do_hdd_off</i>	Deactivates output pin to power control board to remove power from the HDD.
<i>do_adc_on</i>	Activates output pin to power control board to supply power to the ADC.
<i>do_adc_off</i>	Deactivates output pin to power control board to remove power from the ADC.
<i>do_bt_on</i>	Activates the Bluetooth module on the communications board. Sets a security key and resets the module name. Useful for debugging, the response of the module is returned if the silent variable is set to zero.
<i>do_bt_off</i>	Turns the bluetooth module off, into a low power state. The response of the module is returned if the silent variable is set to zero.
<i>do_pda_wake</i>	Toggles the power board which outputs a short 5V pulse to the Activesync pin of the PDA. This will force the PDA to wake up if it is asleep.

User Interface and Statistics

<i>do_sending</i>	Used in deployment mode A when the modem has began transmitting. Statistics are updated to the internal logs and LCD module
<i>do_received</i>	Used in deployment mode A when a communication is received. Statistics are updated to the internal logs and LCD module
<i>do_sent</i>	Used in deployment mode A when a communication has successfully sent (reception of an acknowledgement). Statistics are updated to the internal logs and LCD module
<i>do_update1</i>	Interprets the command as the update of the local hard

	disk free space from the PDALogger Software and forwards this to the LCD Module
<i>do_updater</i>	Interprets the command as the update of the remote hard disk free space from the remote modem recorder and forwards this to the LCD Module
<i>do_ready</i>	Activated by the PDA, prompting the user to double check times and hard disk size for validation before commencing deployment. Then executes quicktime, presenting the current RTC time. Used in the first version of PDALogger for additional pre-deployment checks.
<i>do_mode_trans</i>	Deactivates command mode and moves to transparent mode. Here, any character received on one UART is immediately transferred to the other. <i>charProcess</i> is activated which searches for 'xxx' to return the software to command mode.
<i>charProcess</i>	Active when transparent mode is running. Every character cc received first passes through this command to determine whether or not three 'x' characters have been received. When 'xxx' has been received during transparent mode, the software switches over to command mode, which treats inputs line by line and deactivates <i>charProcess</i>
<i>do_led</i>	Toggles the LED located on the development board. Also sends a response to the serial port. This command is used for checking basic response of the software.
<i>do_hi</i>	Responds with a line of text with the software version number. Mostly used for checking microcontroller response.

DSPComm AquaComm Modem Related Functions

<i>do_readydsp</i>	Sends zeros to the DSPComm modem to prompt a return character, indicating it is ready for a command.
<i>do_break</i>	Sends the break signal to the DSPComm modem which is the only way to initiate it's configuration mode. This

	is done by slowing down the UART considerably, and sending a '?' symbol. Following this, the UART timers are set back to normal.
<i>do_dspsend</i>	This command responds to dsp>#### where #### represents a string to send via the DSPComm modem. This converts the input string into a suitable format and forwards the information to the modem for transmission.
<i>do_dspready</i>	Executes when the DSP modem has responded to the do_readydsp procedure. The do_readydsp function stops outputting zeros and indicates to the user that the modem is ready.
<i>do_dsptstat</i>	The result of a transmission made tstat by the local DSPComm modem is returned over the serial port. This command updates statistics based on the result.
<i>do_dsprstat</i>	Upon reception of a packet, the DSPComm modem will output 4 characters followed by the received string, cs . This command transfers the data to the PDALogger and updates statistics
<i>do_dspunknown</i>	When the DSPComm transmits information not immediately relevant (including signal strength details), this information is immediately transferred to PDALogger, cs for later usage

Aquatec Limited AQUAmodem Modem Related Functions

<i>hexConvert</i>	Converts a decimal number into a string containing it's hex representation.
<i>do_tecom</i>	The aquatec modem requires a checksum to be transmitted following any command for it to be recognised. This command responds to tec_#### where #### represents any command to be transmitted to the modem. This is transferred followed by the relevant checksum to the modem. This allows easy communication

	with the Aquamodem via the MCS without the need to calculate the checksum for every command.
<i>do_tecsend</i>	<p>This command reponds to</p> <p><i>tec>####</i></p> <p>where #### represents a string to send via the Aquatec Modem as a hex Data Block. The software runs the command necessary to transmit the data to the modem including the checksum needed to complete the command</p>
<i>do_tecshort</i>	<p>This command reponds to</p> <p><i>tec.####</i></p> <p>where #### represents a <16 character string to send via the Aquatec Modem as a hex SHORT Data Block (8 Bytes). The software runs the command necessary to transmit the data to the modem including the checksum needed to complete the command</p>
<i>do_tecreq</i>	<p>This command translates to the modem to request a specific number of blocks of memory data from the remote modem based on the cs character:</p> <p><i>1 - 0x08 - 8 Bytes - 2 Blocks of RS Encoded Data</i></p> <p><i>2 - 0x1E - 30 Bytes - 6 Blocks of RS Encoded Data</i></p> <p><i>3 - 0x3F - 63 Bytes - 10 Blocks of RS Encoded Data</i></p>
<i>do_setn</i>	<p>Sets the source and remote number of the modems to ModCon variables. When prompted, the Aquatec modem will provide the modem source number. This command saves the information locally and sets the remote modem number information accordingly. For example, if the modem source is presented as 1, then the remote modem number used for transmissions is 2, and vice versa.</p>
<i>do_tecr</i>	<p>If the Aquatec modem has recieved data, this will translate the information and forward it onto the PDALogger. Also, if it has detected that the data contains remote remaining disk space information, it will run the updater proceedure.</p>
<i>do_tecinit</i>	<p>Initialises (or wakes up) the Aquatec modem by requesting the modem number</p>

<i>do_tectstat</i>	The result of a transmission made by the local Aquatec modem is returned over the serial port. This command updates statistics based on the result.
--------------------	---

Cycle Related Commands

<i>services</i>	Used to constantly update the LCD module with date and time information as well as flash an LED to give indication that the software is operating.
<i>setupstages</i>	Used only for deployment mode B. Firstly transmits to the modem serial ports to initialise and wake them up. Obtains the current minutes value from the clock and sets up the duty cycle. Following the function, variables holding the minute intervals for the stage operations are validated.
<i>do_cycle</i>	Called on commencement of a deployment cycle. Calls setupstages for allocation of stage times and resets the power on and power off times.
<i>do_powerdown</i>	Initiates power down sequence for deployment mode B. Removes power from PDA, Storage and ADC. Turns Bluetooth off. Increments the minute interval for the next power down.
<i>do_cycleservice</i>	<p>This function runs as part of the main loop in Deployment Mode B. It makes constant comparisons between the stage time information stored by do_cycle command with the RTC to determine what stage the deployment is running at. When the time for a stage change is detected, the software will:</p> <ul style="list-style-type: none"> A) Power up the equipment if the first stage is about to begin B) Acoustically request a number of bytes from the remote modem C) Update PDALogger with the stage change, triggering a 40 second delay before next modem transmission D) Lift the flag, denoting the change is complete <p>Additionally, if the deployment stages are all complete, the software will notify PDALogger that it is</p>

	about to shut down, and initiates the power down sequence.
<code>do_cyclestatus</code>	Prints minute intervals for the next cycle to the user. The minute intervals in between represent each stage.

D.5 PDALogger Routines

The following routines were part of the PDA software package, *PDALogger*, discussed in Section 3.2.2. For access to the source code, please contact the author.

Core Functions

<code>OutPut</code>	A simple function which writes the handled detail to a textbox for the operator. Optionally, the information can be written to the serial port also.
<code>InitialiseSoftware</code>	Used to initialise the serial port and status flags. The recording software is stopped and the recording watchdog is also reset.
<code>Update_NonEssential</code>	Updates non-essential information which is performed only when the device is not recording. This includes hard disk and SD card disk space, communication status and power status. Also, a check is performed to determine if the hard disk has become full. If so, the PDA is put to sleep using function <code>Permanent_Sleep</code> .
<code>Update_Status</code>	Performs scheduling updates to determine the intended state of the software. Confirms or reconnects the serial connection (from sleep state). Calls the watchdog function. Updates the user interface with relevant information.
<code>ExitSoftware</code>	Kills PDALogger process
<code>Trim_Processes</code>	Kills all functions currently running except those critical to PDALogger functionality. This includes several Windows Mobile components that

	start automatically. This improves system stability
Prepfordeployment	Used before first deployment. Resets the power to the attached devices to ensure they respond. Synchronises the time. Sends “ready” prompt to <i>ModCon</i> to ensure connectivity.

Recording Related Commands

Record_Start	Power is applied to the ADC via Modcon commands. Watchdog counter is enabled. Live2496.exe is started. Schedule is updated.
Record_Stop	Live2496.exe is killed, power is removed from the ADC via Modcon, Schedule is updated.
Rec_WatchDog	Periodically checks on the recording media disk space. If it has not increased over time, the recording has stalled due to instability. The recording software is restarted and watchdog reset.

Disk Reading and Writing

HD_Sync	If a hard disk is connected, the SD card contents copied directly to the hard disk root directory and removed from the SD card.
HD_Wipe	If a hard disk is connected, each file is deleted from the root directory.
SD_Wipe	If an SD card is connected, each file is deleted from the root directory
SD_Info	The current status of the SD card contents is written to the serial port. This includes free space, number of files and filenames. Used for debugging
HD_Info	The current status of the Hard Disk contents is written to the serial port. This includes free space, number of files and filenames. Used for debugging

SD_Bleed	Called after every recording for high speed logging. This function determines if the next recording will fit on the SD card. If not, SD_CC is called to dump as much of the SD card contents to the hard disk before the next recording. If this is not possible, the next recording is cancelled and the process repeats.
SD_CC	This function writes each file from the SD card to the Hard Disk, deleting as it goes. Additionally, a check is performed to see how much time is left before the next schedule. If there is not enough time, the function returns.

Clock and External Schedule Functions

PushTime	This uses the settime function on ModCon to synchronise the MCS RTC.
Initiate_Sleep	Turns the ADC and Hard Disk off and sets an alarm via ModCon. ModCon then transmits a confirmation of alarm where the PDA goes to sleep mode using GoToSleep.
Permanent_Sleep	The same as Initiate_Sleep, except the alarm time is set to a date in the past (25/03/1985, Author's birth date). This results in a permanent sleep.
Time_Pull	Reciprical of PushTime, requests the time from ModCon which synchronises the PDA clock
GoToSleep	Calls the Windows routine to place the PDA into a low power suspended state. Upon wake, the software runs as it was before the sleep, however, the Bluetooth and other external devices need to be re-initialised.

Internal Scheduling Functions

Start_Stop_Run	If the schedule is currently not running, any old schedules are removed from the database and the schedule is started. Check_Schedule_List is
----------------	---

	called to determine the first course of action.
Schedule_Add_Time	Uses the input boxes and stores their corresponding date and time into the schedule database held in the list box. The list is then sorted chronologically.
Schedule_Add_Interval	Uses the input boxes as a single start date, and stores the information much the same as Schedule_Add_Time. The time is then incremented by the relevant input box and added to the schedule. This cycle repeats until the specified number of iterations is added.
Check_Schedule_List	This routine check determines the next state of the software. If there are no schedules in the system and scheduling is still enabled (ie. After the last recording) then scheduling is stopped. If there are more schedules to follow, the next alarm time is set via ModCon and the PDA is set to sleep mode provided power management is enabled.
Schedule_Info	Used for debugging. This returns the current schedule status to the serial port, including current schedules and recording status.
Schedule_Remove_Top	Removes the next schedule (located at the top of the list) from the database.
Schedule_Remove_All	Clears the schedule database
Update_Schedule	This updates Time_Start and Time_End variables holding the time (in seconds) before the start and ends of a recording respectively.
Comms_Add_Time	This is another method to set the schedule and used for debugging. A schedule can be added to the system without the use of the user interface. Instead, the date and time information can be passed through CommandCom and this function translates the information to a schedule. The schedule is then added and sorted as usual.
Comms_Add_Interval	As above. This command allows the addition of several schedules based on date, time, interval

	time and number of intervals. This information is passed through CommandCom via the serial port.
--	--

Command Interpreter

SerConnect	Sets the baud rate and other Bluetooth serial port settings then opens the port.
objPort_OnRead	Upon reception of a character over the serial port, each is stored in a cycling buffer until a return character is received. Once this occurs, the buffer is dumped to CommandCom and reset.
CommandCom	CommandCom compares the received string with a lookup table to determine the relevant response.
EnterTransparent	Sends "xxx" to ModCon to initiate transparent mode

D.6 PDALogger Skinny Routines

The following routines were part of the PDA software package, *PDALogger Skinny*, discussed in Section 3.2.3. For access to the source code, please contact the author.

Core Functions

OutPut	A simple function which writes the handled detail to a textbox for the operator. Optionally, the information can be written to the serial port also.
InitialiseSoftware	Used to initialise the serial port and status flags. The recording software is stopped and the recording watchdog is also reset.
Trim_Processes	Kills all functions currently running except those critical to PDALogger functionality. This includes several Windows Mobile components that start automatically. This improves system

	stability
killllive	Kills the Live2496 process and stops recording
killme	Kills PDALogger much more abruptly than a regular exit routine
CheckConnection	Check the status of the Bluetooth connection which allows for time synchronisation. If no connection is made within 20 seconds, set the PDA clock as an incremented number and start recording.
Log	Logs a specific string to PDA memory, including all modem transactions.
WritetoMCS	Takes an input string and writes it to the RS232 port, as well as calling Log().
StageAction	There are three stages of modem deployment. Each level transmits a different string using the attached modem.

Clock Functions

PushTime	This uses the settime function on ModCon to synchronise the MCS RTC. Used for setting up the system before deployment
Time_Pull	This is initiated upon startup by the MCS, synchronising the PDA clock with the RTC

High Frequency Recording Functions

Start_Second_Stage	Stops the current recording and starts a new one. Used for high frequency recordings where stability is a problem, this ensures recording continues in case there is a failure. If second stage has already been called previously, this signals the end of the recording period and recording stops to make way for SD_Dump.
SD_Dump	When a recording is finished, the free space of the SD card is checked. If files exist (high frequency recording writes to SD card) the files

	are copied to the hard disk. Following the copy, MCS is notified to shut off all power.
SD_Wipe	Wipes SD card memory.

Command Interpreter

SerConnect	Sets the baud rate and other Bluetooth serial port settings then opens the port.
objPort_OnRead	Upon reception of a character over the serial port, each is stored in a cycling buffer until a return character is received. Once this occurs, the buffer is dumped to CommandCom and reset.
CommandCom	CommandCom compares the received string with a lookup table to determine the relevant response.

Appendix E

List of Publications

Peer Reviewed Articles

Pusey, G., Duncan, A.J. (2009) "Development of a simple underwater acoustic channel simulator for analysis and prediction of horizontal data telemetry", Australian Acoustical Society, Proceedings of Acoustics 2009 Annual Conference, 23-25 November 2009, Adelaide, South Australia. ISBN 978-0-9757855-7-7.

Pusey, G., Duncan, A.J. (2008) "Characterisation of underwater acoustic modem performance for real-time horizontal data transmission", Annual Australian Acoustical Society, Proceedings of Acoustics 2008 Annual Conference, 24-26 November 2008, Geelong, Victoria, Australia,. ISBN 978-0-646-5040-0.

Published Papers / Abstracts

Pusey, G., Duncan, A.J. (2009) "An Investigation of Oceanographic Parameters Affecting Acoustic Modem Performance for Horizontal Data Transmission", Underwater Acoustic Measurements: Technologies & Results, 3rd International Conference and Exhibition, Nafplion, Greece, pp. 1303-1308, 21-26 June 2009. ISBN: 978-960-98883-0-1.

Pusey, G., Duncan, A.J., Smerdon, A.M. (2009) "Analysis of acoustic modem performance for long range horizontal data transmission", OCEANS 2009-EUROPE, 2009. OCEANS '09. , vol., no., pp.1-9, 11-14 May 2009 doi: 10.1109 / OCEANSE.2009.5278203

Pusey, G., Duncan, A.J. (2009) “A preliminary study of underwater acoustic communication over horizontal ranges”, Proceedings of the SUT Annual Conference 2009, Perth, Western Australia

Pusey, G., Duncan, A.J. (2008) “Analysis of shallow underwater acoustic data transmission in near horizontal channels”, Australian Institute of Physics Postgraduate Research Conference, 2008, Jarrahdale, Western Australia

Appendix F

Copyright Licenses

Figure 2.5.1 and Figure 2.5.2:

Acoustical Society of America License

License Number: 2585780534820

License date: Jan 11, 2011

Licensed content publisher: Acoustical Society of America

Licensed content publication: The Journal of the Acoustical Society of America

Licensed content title: Effects of ocean thermocline variability on noncoherent underwater acoustic communications

Licensed content author: Martin Siderius, Michael B. Porter, Paul Hursky, et al.

Figure 2.5.3:

Acoustical Society of America License

License Number: 2585780954112

License date: Jan 11, 2011

Licensed content publisher: Acoustical Society of America

Licensed content publication: The Journal of the Acoustical Society of America

Licensed content title: Impact of ocean variability on coherent underwater acoustic communications during the Kauai experiment (KauaiEx)

Licensed content author: Aijun Song, Mohsen Badiyeh, H. C. Song, William S. Hodgkiss, Michael B. Porter, the KauaiEx Group